QC
1
.U56
v.64A
no.6

Volume 64A

Number 6

Nov.–Dec. 1960

THE UNIVERSITY OF MICHIGAN
DEC 1 1960
LIBRARY

Journal of Research

of the

NATIONAL BUREAU OF STANDARDS

A. PHYSICS AND CHEMISTRY

Journal of Research
of the
National Bureau of Standards

A. Physics and Chemistry

NOV.–DEC. • 1960

VOLUME • 64A

NUMBER • 6

Editor: U. Fano

Associate Editors: L. M. Kushner
J. M. Richardson

Publication dates:
Feb. 1, Apr. 1, June 1, Aug. 1, Oct. 1, Dec. 1, 1960.

JOURNAL OF RESEARCH

The National Bureau of Standards Journal of Research reports research and development in the fields of activity shown at right. Also included from time to time are survey articles on topics closely related to the Bureau's scientific and technical program.

The Journal is published in four separate sections as follows:

A. Physics and Chemistry

Contains papers of interest primarily to scientists working in these fields. Issued six times a year. Annual subscription: domestic, $4.00; foreign, $4.75.

B. Mathematics and Mathematical Physics

Presents studies and compilations designed mainly for the mathematician and the theoretical physicist. Issued quarterly. Annual subscription: domestic, $2.25; foreign, $2.75.

C. Engineering and Instrumentation

Reports research and development results of interest chiefly to the engineer and the applied scientist. Issued quarterly. Annual subscription: domestic, $2.25; foreign, $2.75.

D. Radio Propagation

Reports work in radio propagation, upper atmospheric physics, and communications. Issued six times a year. Annual subscription: domestic, $4.00; foreign, $4.75.

U.S. DEPARTMENT OF COMMERCE
Frederick H. Mueller, Secretary

NATIONAL BUREAU OF STANDARDS
A. V. Astin, Director

Functions and Activities

The functions of the National Bureau of Standards are set forth in the Act of Congress, March 3, 1901, as amended. These include the development and maintenance of the national standards of measurement and the provision of means and methods for making measurements consistent with these standards; the determination of physical constants and properties of materials; the development of methods and instruments for testing materials, devices, and structures; advisory services to government agencies on scientific and technical problems; invention and development of devices to serve special needs of the Government; and the development of standard practices, codes, and specifications. The work includes basic and applied research, development, engineering, instrumentation testing, evaluation, calibration services, and various consultation and information services. The Bureau also serves as the Federal technical research center in a number of specialized fields. The scope of activities of the National Bureau of Standards is suggested in the following listing of the divisions and sections engaged in technical work.

Washington, D.C.

Electricity. Resistance and Reactance. **Electrochemistry.** Electrical Instruments. Magnetic Measurements. Dielectrics.

Metrology. Photometry and Colorimetry. Refractometry. Photographic Research. Length. Engineering Metrology. Mass and Scale. Volumetry and Densimetry.

Heat. Temperature Physics. Heat Measurement. **Cryogenic** Physics. Rheology. Molecular Kinetics. Free Radicals Research. Equation of State. Statistical Physics. Molecular Spectroscopy.

Radiation Physics. X-ray. Radioactivity. High Energy Radiation. Radiological Equipment. Nucleonic Instrumentation. Neutron Physics. Radiation Theory.

Chemistry. Surface Chemistry. Organic Chemistry. **Analytical** Chemistry. Inorganic Chemistry. Electrodeposition. Molecular Structure and Properties of Gases. Physical Chemistry. Thermochemistry. **Spectrochemistry.** Pure Substances.

Mechanics. Sound. Pressure and Vacuum. Fluid Mechanics. Engineering Mechanics. Combustion Controls.

Organic and Fibrous Materials. Rubber. **Textiles.** Paper. Leather. Testing and Specifications. Polymer Structure. **Plastics.** Dental Research.

Metallurgy. Thermal Metallurgy. Chemical **Metallurgy.** Mechanical Metallurgy. Corrosion. Metal Physics.

Mineral Products. Engineering Ceramics. **Glass. Refractories.** Enameled Metals. Constitution and Microstructure.

Building Technology. Structural Engineering. **Fire Protection.** Air Conditioning, Heating, and Refrigeration. Floor, Roof, and Wall Coverings. Codes and Safety Standards. Heat Transfer. Concreting **Materials.**

Applied Mathematics. Numerical Analysis Computation. Statistical Engineering. Mathematical Physics.

Data Processing Systems. SEAC Engineering Group. **Components** and Techniques. Digital Circuitry. Digital Systems. **Analog Systems.** Applications Engineering.

Atomic Physics. Spectroscopy. Radiometry. **Mass** Spectrometry. Solid State Physics. Electron Physics. Atomic Physics.

Instrumentation. Engineering Electronics. **Electron Devices.** Electronic Instrumentation. Mechanical Instruments. Basic Instrumentation.

• Office of Weights and Measures.

Boulder, Colorado

Cryogenic Engineering. Cryogenic Equipment. **Cryogenic Processes.** Properties of Materials. Gas Liquefaction.

Radio Propagation Physics. Upper Atmosphere **Research.** Ionosphere Research. Regular Prediction Services. Sun-Earth **Relationships.** VHF Research. Radio Warning Services. Airglow and **Aurora.** Radio Astronomy and Arctic Propagation.

Radio Propagation Engineering. Data Reduction **Instrumentation.** Radio Noise. Tropospheric Measurements. Tropospheric **Analysis.** Propagation-Terrain **Effects.** Radio-Meteorology. Lower Atmospheric **Physics.**

Radio Standards. High-Frequency Electrical Standards. Radio Broadcast Service. Radio and Microwave Materials. Electronic Calibration Center. Microwave Circuit Standards.

Radio Communication and Systems. Low Frequency and Very Low Frequency Research. High Frequency and Very High Frequency Research. Modulation Systems. Antenna Research. Navigation **Systems.** Systems Analysis. Field Operations.

Order all publications from the Superintendent of Documents,
U.S. Government Printing Office, Washington 25, D.C.

Use of funds for printing this publication approved by the Director of the Bureau of the Budget (June 24, 1958).

DEPOSITED BY THE
UNITED STATES OF AMERICA

JOURNAL OF RESEARCH of the National Bureau of Standards—A. Physics and Chemistry
Vol. 64A, No. 6, November–December 1960

The Spectrum of Singly Ionized Atomic Iodine (I II)

William C. Martin and Charles H. Corliss

(July 11, 1960)

The I II spectrum has been excited in electrodeless lamps and photographed from 655 A to 11084 A. Wavelengths and estimated intensities are given for almost 2,400 lines. A revision and extension of the earlier analyses of this spectrum has increased the number of known even levels from 43 to 124, and the number of odd levels from 55 to 190. New g_J-factors are given for 46 levels, and the previous designations of 40 levels are changed. Improved measurements in the vacuum ultraviolet region give a correction of 7.4 cm^{-1} to be subtracted from the values listed in *Atomic Energy Levels*, Vol. 3 (1958), for all levels above the ground configuration. The approximately 1,800 classified lines now include all of the strongest lines. The $^1S_0$ of the ground configuration $5s^25p^4$ has been found, and this configuration has been fitted to intermediate coupling theory. Magnetic dipole transitions between levels of the ground configuration, $^3P_2$—$^1D_2$ (7282 A) and $^3P_1$—$^1S_0$ (4460 A), have been observed and their nature confirmed by the Zeeman effect. The line $5p^4\ ^3P_2$—$^1D_2$ shows hyperfine structure which is in approximate agreement with a theoretical calculation of the expected structure. New levels have been found for almost all higher configurations. All previously known series have been extended and new ones found. From one of the new series, $5p^3(^4S^\circ)5\text{-}12g\ ^5G^\circ_6$, the principal ionization energy for I II (154304 ± 1 cm^{-1}) has been derived. The results of the analysis are compared with theoretical expectations in a number of cases.

1. Introduction

One of the purposes served by the systematic compilation of *Atomic Energy Levels* [1] [1] being carried out at NBS is to point out inadequacies in the existing analyses of atomic spectra. The work reported here was partly stimulated by the need revealed under the scrutiny of this program for new observations and analyses of the iodine and bromine spectra. Another reason for our interest in these particular spectra is that iodine and bromine are the halogens most frequently used in the electrodeless metal-halide lamps [2] developed in this laboratory. These lamps have proved to be excellent sources of metallic spectra. We have also found that the electrodeless lamp gives a strong pure iodine spectrum when used as described below. Since the spectrum of the halogen contained in a metal-halide lamp appears along with that of the metal, the user of these lamps needs a complete and accurate knowledge of the iodine and bromine spectra. The present or recently completed work of this laboratory includes new descriptions and analyses of the first and second spectra of both iodine and bromine.

The spectrum of singly ionized iodine has previously been analyzed by P. Lacroute [3] and by K. Murakawa [4]. The results of their work, together with some preliminary revisions and extensions made possible by the new observations reported here, are given in *Atomic Energy Levels* (AEL), Vol. III. Our observations are superior to earlier measurements in being more complete (particularly in the vacuum ultraviolet region) and more accurate. Also important is our ability to distinguish better between the first and second spectrum.

[1] Figures in brackets indicate the literature references on page 452.

2. Observations

The sources for the spectrum in the region 2000 to 11000 A were electrodeless lamps made from 5-mm i.d. quartz or vycor tubing about 10 cm long with a hemispherical window blown at one end and a side arm attached. These were thoroughly evacuated and outgassed, and a few crystals of iodine distilled into them before sealing off. The discharge was excited with the Raytheon Microtherm microwave generator which operates at 2,450 Mc with 125-w output. We made all observations with the lamp end-on except when Zeeman patterns were photographed. The spectra were dispersed with gratings having 30,000, 15,000, and 7,500 lines per inch, each mounted in parallel light to give stigmatic images. From 2000 to 2400 A the plate factor was 2.2 A/mm; from 2400 to 4400 A, 1.0 A/mm; from 4400 to 9000 A, 2.0 A/mm; from 9000 to 10400 A, 5 A/mm; and from 10400 to 11100 A, 10 A/mm.

Most of the wavelength values given in table 10.1, the line list (sec. 10, Appendix), are averages of measurements made on more than one plate. The intensities are visual estimates, meaningful only for lines in the same spectral region. Almost all of the stronger I II lines show hyperfine structure under high resolution. Where the structures were completely or partially resolved, we measured the individual components. With few exceptions, however, only the weighted average of the component wavelengths is given in table 10.1. The intensity given for such a line is the sum of the estimated component intensities. Murakawa [4, 5] has observed interferometrically the hyperfine structure of a number of I II lines.

Because of the line-broadening due to structure, the wavelength measurements here are not as

accurate as one might wish. However, the disagreement between the observed wavenumbers and the corresponding differences of the "best" values for the relevant energy levels is usually less than 0.1 cm^{-1} for lines in the region above 2500 A.

When the iodine in the side arm of the discharge tube was kept at 30° C, corresponding to about 1-mm vapor pressure, most lines of the first spectrum appeared in the discharge, with only the strongest lines of I II showing. As the temperature was lowered, the second spectrum increased in intensity until it became stronger than the first spectrum. The discharge ceased at about −28° C, when the pressure was between 10^{-2} and 10^{-3} mm Hg. We were able to assign most lines to the proper spectrum by including on every spectrogram these four spectra in juxtaposition: iron arc, "high" temperature (20 to 30° C) iodine spectrum, "low" temperature (≈−25 °C) iodine spectrum, and iron arc.

This procedure leaves the origin of some of the weaker lines doubtful for two reasons: the weaker I I lines appear in the low pressure discharge but not at the higher pressure, while the I III spectrum is also faintly excited at low pressures. The latter observation was surprising, but a comparison of the intensities in our list with those given by observers [3, 6, 7] of rather high energy discharges in iodine vapor leaves no doubt that our low pressure source gives the strongest I III lines weakly. However, we believe that by this comparison we have eliminated the I III lines from the list. Those unclassified lines above 5000 A which have intensity less than 50 comprise practically all the remaining lines of doubtful origin. These lines may belong to either the first or second spectrum.

We have observed the Zeeman effect in a field of about 37000 gauss for most of the strong I II lines in the region 4000 to 9000 A. The technique is described by Kiess and Corliss [8]. Zeeman patterns obtained from these observations are given in table 10.2.

The spectrum was dispersed in the region 584 to 2000 A by a 2-m radius concave grating of 30,000 lines per inch ruled directly on pyrex. This grating, which was ruled under the direction of R. W. Wood at Johns Hopkins, was originally mounted in a vacuum spectrograph by K. T. Compton and J. C. Boyce [9]. W. R. Bozman has designed a new housing for the grating and plateholder of the old instrument. It consists primarily of a cylindrical section of steel pipe 75 cm in diameter and 210 cm long fitted with aluminum end covers which are sealed to the main tube by means of O-ring flanges. The slit is contained in a side tube. The optical arrangement is essentially that of Compton and Boyce except that the angle of incidence has been decreased slightly to about 13.1° to give the normal spectrum at 1920 A. The plate factor is 4.26 A/mm at the normal and the plateholder covers the range 0 to 2570 A in the first order. The height of the plateholder is adjustable externally so that several different exposures may be made on one plate.

We mounted a glass discharge tube end-on to the slit housing by means of an O-ring seal. After a side tube was charged with iodine, the lamp was evacuated and excited as described above. The slit of the evacuated spectrograph was open directly to the light from the discharge. We used Eastman SWR plates below 1400 A and Ilford Q–2 plates in the region above 1400 A. The first order spectrum was measured from 500 to 2500 A; and from 800 to 1200 A all but the weaker lines were measured in the second order. Most lines were measured three or four times. Calculated wavelengths of lines in the I I spectrum [8] served as the principal standards in the region 1200 to 2060 A. Lines of helium, oxygen, nitrogen, and carbon also were used for standards. Some bands, due principally to carbon monoxide, appeared on the spectrograms.

Lines of bromine were found on all our vacuum region plates. The existing measurements of the bromine spectra were not complete enough for the elimination of these lines from our list. We have excited, photographed, and measured the Br I and Br II spectra in the vacuum ultraviolet. Analyses of these spectra are underway in this laboratory and will be reported later.

We have obtained averaged values of the I II $5p^4$ ground-configuration energy levels relative to the lower odd levels by using the measurements of lines from 1100 to 1300 A. These odd levels are known relative to each other with good accuracy from measurements above 2000 A. We then calculated the wavelengths of all singly-classified lines observed in the vacuum ultraviolet. Since these wavelengths are on a consistent scale and the I II spectrum is fairly rich below the I I limit (1200 A), we have thought it worthwhile to give these calculated wavelengths in table 10.1. Together with the I I wavelengths above 1200 A they comprise a consistent set of wavelengths over a large part of the vacuum region and should prove useful in reducing low- and medium-dispersion plates obtained with metal iodide lamp sources. An estimated uncertainty in the calculated I II wavelengths of ±0.005 A at 1100 A gives ±0.002 A at 665 A, where the first calculated lines occur. The new I II wavelengths in the vacuum ultraviolet region yield, for the energy levels above those of the ground configuration, values which are 7.4 cm^{-1} less than the corresponding values given in AEL.

3. Ground Configuration

The $5s^2\ 5p^4$ ground configuration of singly ionized iodine gives the Russell-Saunders terms ^3P, ^1D, and ^1S, as shown in table 1. The energy levels for these terms are listed in table 10.3, which includes all presently known even levels for I II. Lacroute's values for $^3P_1$, $^3P_0$, and $^1D_2$ are about 3 cm^{-1} too high relative to the ground state $^3P_2$. The level he designated $^1S_0$ is not real. In the three atoms for which the configuration $5p^4$ is known (Te I, I II, and Xe III) one finds good agreement with intermediate

TABLE 1. *Predicted terms of* I II

Configuration	Predicted terms				
$5s^2\,5p^4$	^3P ^1D ^1S				
$5s\,5p^5$	$^3P^\circ$ $^1P^\circ$				
	ns $n\geq 6$	np $n\geq 6$	nd $n\geq 5$	nf $n\geq 4$	ng $n\geq 5$
$5s^2\,5p^3(^4S^\circ)nx$	$^3S^\circ$ $^3S^\circ$	^5P ^3P	$^5D^\circ$ $^3D^\circ$	^5F ^3F	$^5G^\circ$ $^3G^\circ$
$5s^2\,5p^3(^2D^\circ)nx'$	$^3D^\circ$ $^1D^\circ$	^{3}(PDF) ^{1}(PDF)	^{3}(SPDFG)° ^{1}(SPDFG)°	^{3}(PDFGH) ^{1}(PDFGH)	^{3}(DFGHI)° ^{1}(DFGHI)°
$5s^2\,5p^3(^2P^\circ)nx''$	$^3P^\circ$ $^1P^\circ$	^{3}(SPD) ^{1}(SPD)	^{3}(PDF)° ^{1}(PDF)°	^{3}(DFG) ^{1}(DFG)	^{3}(FGH) ^{1}(FGH)

coupling theory. Robinson and Shortley [10] have calculated the coupling parameters for $5p^4$ in these atoms by making $^3P_1$, $^3P_2$, and ^1D—^3P_c exactly fit the theoretical curves given in Condon and Shortley [11], p. 301, and reproduced in figure 1. This method gives a good fit for all levels except $^1S_0$ which lies too high in all three cases. (The position for I II $5p^4$ $^1S_0$ in figure 1 of reference [10] must be corrected since only the incorrect value of Lacroute was available to Robinson and Shortley—this reduces the disagreement to about one third of its former value.) As Robinson and Shortley point out, this does not mean that $^1S_0$ is perturbed—an interaction would push the term *down*. We have

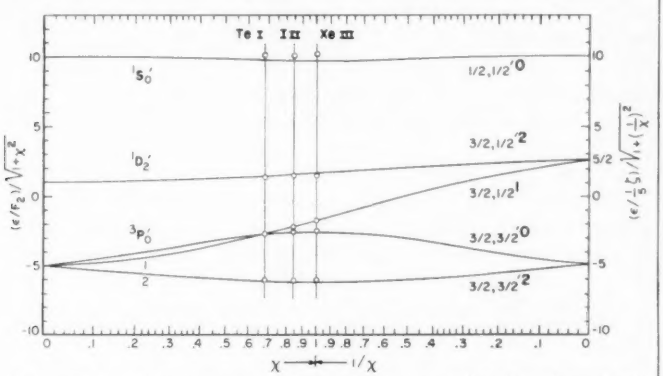

FIGURE 1. *The levels of* $5p^4$ *for three atoms fitted to theoretical intermediate-coupling curves.*

calculated the parameters by the method Condon and Shortley originally used for Te I, i.e., by making $^3P_1$, the mean of $^1D_2$ and $^3P_2$, and the mean of $^1S_0$ and $^3P_0$ fit exactly. This brings $^1S_0$ down to excellent agreement while leaving the value of $\chi=\frac{1}{5}\zeta_p/F_2$ (see Condon and Shortley for notation) essentially unchanged in all cases, but the agreement of the J=2 levels is not as good as in Robinson and Shortley. As a compromise we have averaged the values of the parameters obtained by these two methods. The results are given in table 2 and the corresponding values of the observed energy levels are plotted in figure 1, again making $^3P_1$ fit exactly. Since the Landé, Slater, and coupling ratios all are functions only of the parameter χ the good agreement obtained for them by Robinson and Shortley is retained here. The new ^1S term makes the agreement of the observed Slater ratio (^1S—^1D)/(^1D—^3P_c) in I II (1.481) with the theoretical value (1.365 for $\chi=0.844$) about the same as in Te I and better than in Xe III.

TABLE 2. *Intermediate-coupling parameters and predicted level positions for the* $5p^4$ *configuration in* Te I, I II, *and* Xe III

	Te I	I II	Xe III
$\chi=\frac{1}{5}\zeta_p/F_2$	0. 684	0. 844	1. 004
	cm^{-1}	cm^{-1}	cm^{-1}
$\zeta(5p)$	4090	5930	8180
$F_2(5p,5p)$	1195	1405	1630
$^3P_2$ pred.	−171	−220	−480
$^3P_2$ obs.	0	0	0
$^3P_1$ pred.	(4751)	(7087)	(9795)
$^3P_1$ obs.	4751	7087	9795
$^3P_0$ pred.	4697	6325	7878
$^3P_0$ obs.	4707	6448	8131
$^1D_2$ pred.	10708	13929	17580
$^1D_2$ obs.	10559	13727	17100
$^1S_0$ pred.	22731	28924	36162
$^1S_0$ obs.	23199	29501	37398

The eigenvectors of the two second-order energy matrices for p^4 in intermediate coupling, for J=0 and J=2, respectively, are functions of χ only. By calculating these eigenvectors and squaring the elements of each, one obtains the percentage composition of each level of a given J in terms of the pure Russell-Saunders levels of that J. The results of this calculation for $\chi=0.844$ (I II $5p^4$) are that $^1D_2$ and $^3P_2$ have 90.3 percent Russell-Saunders purity (i.e., they are 9.7% mixed), while the purity for $^1S_0$ and $^3P_0$ is 83.5 percent. Hence the *LS* designations assigned these levels are not without some meaning.

4. Magnetic Dipole Transitions

"Forbidden" transitions between pairs of levels belonging to the p^4 configuration have been observed in laboratory sources of the spectra O I (the aurora line at 5577 A, $^1S_0$—$^1D_2$), Se I [12], Te I [13], Xe III [14], and Po I [15]. We have found two such transitions in I II: $5p^4\,^3P_1$—$^1S_0$ (4460.185 A) and $5p^4\,^3P_2$—$^1D_2$ (7282.83 A). A diagram of the ground configuration levels showing these transitions is given in figure 2. The observed wavenumber of each line is that predicted by the separation of the relevant levels as determined from lines in the vacuum ultraviolet. The transition probabilities as derived from magnetic dipole strengths tabulated against χ by Shortley et al. [16] are 99 sec^{-1} for the line at 4460 A, and 9.1 sec^{-1} for the line 7282 A ($\chi=0.844$; both lines have zero transition probability in pure Russell-Saunders coupling, where $\chi=0$). Of course the observed intensities in table 10.1 have no absolute meaning, and for these two lines in different spectral regions do not give even relative experimental intensities. Both transitions appear much stronger

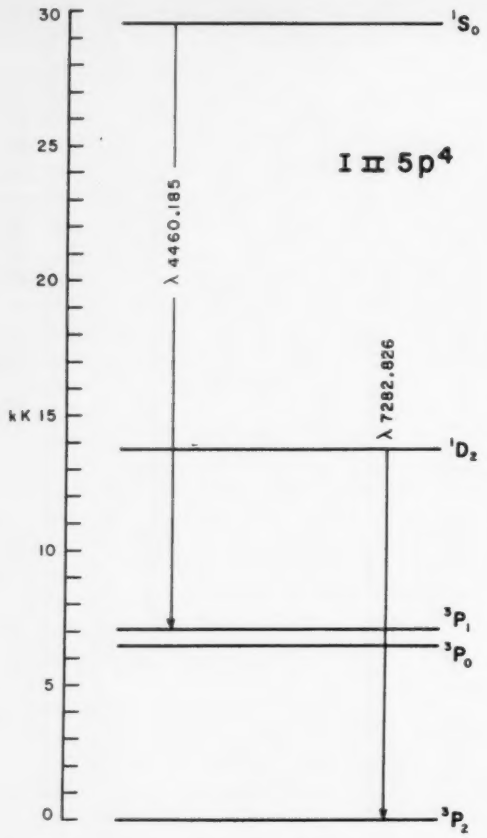

FIGURE 2. *Two magnetic dipole transitions observed in* I II.

in the high pressure (I I) discharge than with low pressure (I II) excitation. This first spectrum character is not surprising since these transitions occur between levels which are series limits for the I I spectrum. The levels lie about 100,000 cm^{-1} above the I I ground state, while the excitation energy for any I II line in this region is almost twice that amount. In his note on the xenon spectra, Edlén [14] mentioned that such lines were at first experimentally referred to the next lower ionization than that to which they actually belonged.

The line at 4460 A is pure magnetic dipole radiation, and its classification was made certain by the transverse Zeeman effect observation shown in figure 3. After the line had been classified, a search through the Zeeman data of Kiess and Corliss yielded this pattern. In a field of about 37,000 gauss the line splits into a triplet with separation of 1.51 Lorentz units (L.U.). But the unshifted perpendicularly polarized component and the symmetrically displaced parallel components form a pattern that is the inverse of the other triplets appearing in the figure, and can arise only from a magnetic dipole transition. The derived g_J-value for $5p^4\ ^3P_1$ is, of course, 1.51. By observing the Zeeman effect for the analogous transition in Pb I, $6p^2\ ^3P_1$—$^1S_0$ at 4618A, H. Niewodniczanski [17] gave the first definite experimental proof for the occurrence of magnetic dipole radiation in atomic spectra.

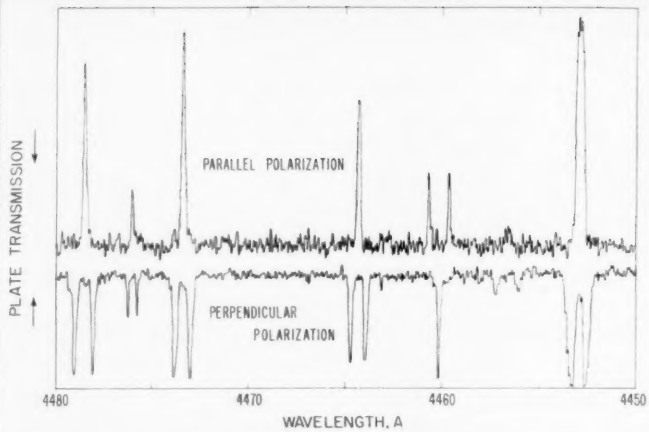

FIGURE 3. *Microphotometer traces of an iodine spectrogram showing the transverse Zeeman effect in the region near 4460 A.*

The "upside-down" Lorentz triplet observed for the I II line at 4460.185 A is definite proof of its magnetic-dipole character.

The resolution obtained in the first order spectrum with a grating of 30,000 lines per inch was sufficient to resolve partly the hyperfine structure of the line $5p^4\ ^3P_2$—$^1D_2$ (7282 A), as shown in figure 4. There seem to be three or four components on our plates, though only one is well resolved from the rest. In order to compare the observed structure of this line with theory, we have calculated the hyperfine splittings of the $5p^4\ ^3P_2$ and $5p^4\ ^1D_2$ levels in I^{127} II. The required constants were taken as follows: nuclear spin=5/2, nuclear magnetic moment=2.81 n.m., nuclear electric quadrupole moment=-0.62×10^{-24} cm^2 [18]. The formulas of Goudsmit [19] and Casimir [20] give the magnetic splitting factors, A(J), and the electric quadrupole factors, B(J), respectively. Trees [21] has published convenient general expressions for evaluating these formulas. We have also taken the effects of intermediate coupling into account. The calculated splittings are $A(^3P_2)=0.033$ cm^{-1}, $B(^3P_2)=-0.00017$ cm^{-1}, $A(^1D_2)$

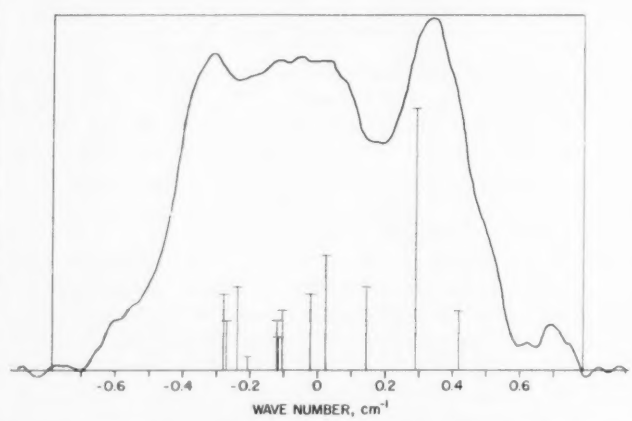

FIGURE 4. *Microphotometer trace showing the hyperfine structure of the forbidden line* $5p^4\ ^3P_2$—$^1D_2$ *at 7282 A.*

The theoretical relative intensities and calculated positions of the components of this pattern are also indicated. The position of the trace with respect to the zero of the wavenumber scale is arbitrary.

$=0.078\ cm^{-1}$, $B(^1D_2)=0.00042\ cm^{-1}$. If it is assumed that $5p^4\ ^3P_2$—$^1D_2$ is predominately a magnetic dipole transition, the same intensity ratios as for electric dipole radiation should apply to the hyperfine components [22, 23]. The "theoretical" hyperfine pattern in figure 4 is based on this assumption and the calculated splittings. In view of the approximations made in the theory, the agreement of the calculated and observed patterns seems satisfactory and may be regarded as a confirmation of the suggested origin of this line.

Since the Zeeman effect for a forbidden line showing hyperfine structure has rarely been observed, three separate several-hour exposures were made especially to obtain the magnetic splitting of the line 7282 A in a field of 35,500 gauss. A microphotometer tracing of one of the Zeeman patterns obtained is shown in figure 5. Assuming the calculated intermediate coupling g_J-values of 1.451 for $5p^4\ ^3P_2$ and 1.049 for $5p^4\ ^1D_2$, one obtains the calculated Zeeman-component positions given in table 3. The observed values, which are averages for measurements of the three patterns, are also given. The agreement of calculated and observed positions and the reversal of the respective polarizations from those expected for an electric dipole transition are definite proof of the origin of this line. The average values of the g_J-factors derived from the measured patterns are 1.457 for $^3P_2$ and 1.046 for $^1D_2$.

TABLE 3. *Zeeman effect for the forbidden line at 7282 A*

The observed component positions are average values from 3 patterns obtained with a magnetic field of about 35,500 gauss. Only half the pattern is given since the centers of gravity of any two corresponding components were, within the errors of observation, located symmetrically with respect to the zero of the magnetic displacement scale in figure 5.

π-components $M_J(^1D_2) \rightarrow M'_J(^3P_2)$	Theoretical relative intensity	Calculated position	Observed position	Calculated total width
2→1	2	0. 647 L.U.		0. 615 cm^{-1}
1→0	3	1. 049	1. 042 L.U.	. 390
0→1	3	1. 451	1. 459	. 165
1→2	2	1. 853	1. 860	. 060
σ-components				
1→1	2	0. 402 L.U.	0. 393 L.U.	0. 225 cm^{-1}
2→2	8	. 804	. 808	. 450

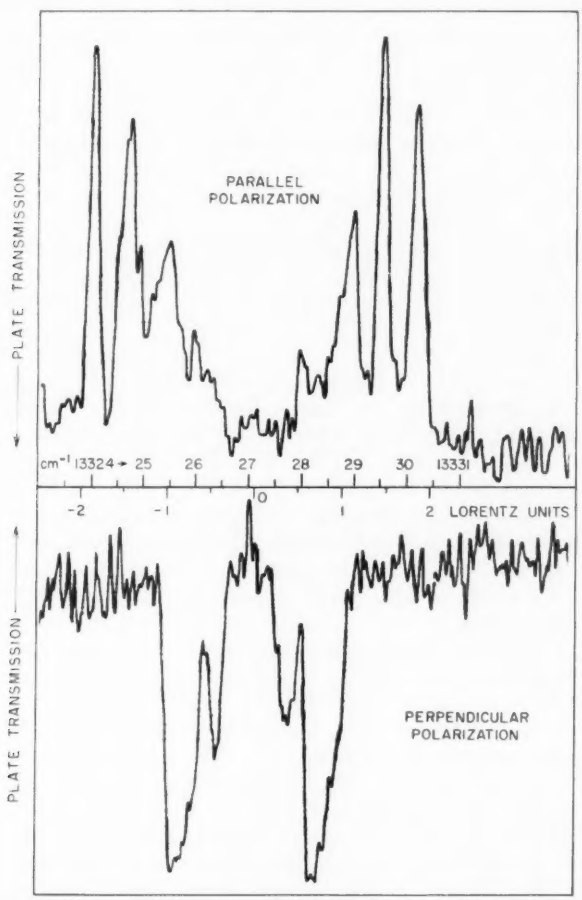

FIGURE 5. *Microphotometer traces of the transverse Zeeman pattern for the line at 7282 A.*

The spectrogram from which these traces have been made was obtained with the source in a field of 35,500 gauss. In order to locate the Zeeman components with respect to the undisplaced hyperfine pattern, an exposure with the source in zero magnetic field was also made on this spectrogram (not shown). The zero of the above Lorentz unit scale is taken at the same position, relative to the observed hyperfine pattern of figure 4, as the zero of the wavenumber scale in figure 4.

A broadening due to unresolved hyperfine structure is apparent for most of the components in figure 5. Since the splitting of either level by the external magnetic field is here several times larger than the zero-field hyperfine splitting, the formula for the Back-Goudsmit case [24] should give a fair approximation for the total energy of each magnetic-hyperfine state. This formula predicts a splitting of each Zeeman component into $2I+1=6$ equally spaced hyperfine components. The expected overall width of a given Zeeman component due to this structure can be obtained from the previously calculated values of the hyperfine splitting factors for the two levels (see above) and the standard formula for the Back-Goudsmit effect [24]. These calculated widths are given in table 3. Neglecting for a moment the observed asymmetries, one can see that the general features of the pattern are in accord with these widths. In particular, what might at first be taken as large deviations from the predicted relative intensities of table 3 can probably for the most part be explained as effects due to the different widths. For example, the appearance of the distinct and relatively narrow π-components at ± 1.85 L.U., as contrasted with the barely observable structures at ± 0.65 L.U.—where components with the same total intensities as those at ± 1.85 L.U. should occur—is, no doubt, due principally to the fact that the predicted overall width of the innermost components is 10 times that of the outermost components. Since the additional broadening of all components due to Doppler and instrumental effects has not been considered, the calculated widths of

table 3 should be taken only as indicative. Previous experience with uncooled electrodeless lamps excited as described above indicates effective gas temperatures of 4,000 to 8,000 °C when the lamp is in a strong magnetic field. At these temperatures the Doppler width of each transition contributing to one of the Zeeman components of 7282 A is comparable to the "total width" of table 3 for the narrowest components (0.06 cm^{-1}).

The asymmetries, with respect to total width and peak intensity, observed between members of the symmetrically positioned pairs of components in figure 5 are confirmed on the other two Zeeman spectrograms of this pattern. The complete Back-Goudsmit effect would divide each Zeeman component into six equally intense components without altering the overall symmetry of the usual Zeeman pattern. It seems likely that the asymmetries are caused more by deviations from the intensity rule for the Back-Goudsmit case than by the remaining asymmetries in the level positions. With the present resolution, no significant asymmetries in the positions of the centers-of-gravity of corresponding components are observed.

The line $^3P_2$—$^1D_2$ is allowed in electric quadrupole radiation as well as in magnetic dipole radiation. Although it is certain that 7282 A is almost pure magnetic dipole in character, it might be possible to deduce from a symmetric Zeeman pattern a slight admixture of electric quadrupole radiation in the line. This was done for a similar transition, $6p^2$ $^3P_1$—$^1D_2$ in Pb I, by Jenkins and Mrozowski [25]. These investigators also were able to confirm an interesting "interference" effect [23] between the magnetic dipole and electric quadrupole radiation in this line. An application of this type of analysis to the pattern in figure 5 does not appear feasible because of the asymmetries due to hyperfine structure. It is possible that a detailed calculation of this pattern by use of the formulas for the "intermediate field" case would be worthwhile.

5. Higher Even Terms

The higher terms of I II are of three types, according to whether the parent term in I III is $5p^3$ $^4S°$, $^2D°$, or $^2P°$. As shown in table 1, these are denoted by affixing to the valence electron no prime, one prime, or two primes, respectively. No meaningful analysis exists for I III, but one can estimate the positions of $5p^3$ ^2D and $5p^3$ ^2P from their positions in Sb I and Te II. The result is that the $^2D_{1½,2½}$ levels should lie about 12,000 and 15,000 cm^{-1}, respectively, above ^4S, and the $^2P_{½,1½}$ at approximately 25,000 and 30,000 cm^{-1}, respectively.

We have indicated in our discussion of $5p^4$ the extent to which Russell-Saunders designations are meaningful for that configuration. For many of the higher levels such designations have considerably less meaning. The overlapping of the "terms" belonging to a given configuration and parentage signifies the usual heavy-atom departure from Russell-Saunders coupling, and makes the L-S naming of some of these higher levels little more than a convenient accounting system. With the reader thus warned we shall, however, use this notation.

Earlier investigators found the levels of the even groups $(^4S°)6p$, $(^2D°)6p'$, and $(^4S°)4f$. Transitions from these levels to lower odd levels are responsible for the strongest I II lines in the air region. The intensities of the $5d$—$4f$ transitions indicate that the strong line at 2993.866 A is due to $5d$ $^3D_1°$—$4f$ $^3F_2$. This requires that the designations of the levels previously called $5d$ $^3D_1°$ and $6s'$ $^3D_1°$ be interchanged, as well as those of $4f$ $^3F_2$ and $6p''$ $^3D_2$. Murakawa [4] noted that the $^3D_1°$ levels were almost indistinguishable, and Lacroute [3] mentioned "l'analogie" of the J=2 levels involved. Neither of these authors had available a complete line list with a uniform intensity scale. We unfortunately did not notice Murakawa's incorrect designation of the $4f$ levels as $5f$—an error retained by Lacroute—until after the publication of AEL, Vol. III. Our measurement of these strong multiplets has resulted in some designation changes. While some configuration mixing undoubtedly takes place for each of these pairs, the intensities of most of the other combinations of these levels confirm our changes. In the next section it will be shown that the present choice of $6s'$ $^3D_1°$ is supported by theory. The relative position of the level here designated $4f$ $^3F_2$ is supported by the position of $^3F_2$ in the newly-found $5f$ configuration. Also on the basis of our intensities and g-values, we have reversed Murakawa's designations of the pairs $6p'$ $^3F_3$, $^3D_3$ and $6p'$ $^1P_1$, $^3D_1$.

The $7p$ $^{5,3}P$ levels, all of which have been found, overlap the $4f$ levels but do not make as strong combinations. The level $7p$ $^5P_2$ was previously known.

The terms of $(^2P°)6p''$ are now complete. Lacroute gave five of these levels correctly, although the level he designated $6p''$ y_1 has a J-value of 2. As noted above, his $6p''$ $^3D_2$ fits better in the $4f$ configuration. We assign his $6p''$ $^3P_2$ to $6p''$ $^1D_2$. The $6p''$ group overlaps both the $4f$ and $7p$ levels. From the line intensities it appears that the $4f$ levels and $7p$ $^5P_3$ are relatively pure, while most of the remaining levels of $7p$ and $6p''$ are configuration-mixed.

The analysis has yielded all but two of the levels arising from $4f'$ and $7p'$. Since these groups overlap and mix, any individual assignment to configuration and Russell-Saunders designation at best represents only the principal contribution to a complete description of a given level. Lacroute found five of these levels, assigning them to $7p'$. We have assigned all but one of these to $4f'$. Four other levels listed by Lacroute for $7p'$ are not real.

All the levels of the complete $5f$ configuration are new except $^3F_3$, which was given by Lacroute as $7p'$ $^1P_1$. Most of the levels of nf are now known through $n=8$. Four levels are assigned to $9f$—three of them tentatively—on the basis of series regularity.

The level given in table 10.3 as $8p$ $^3P_2$ was erroneously assigned a J-value of 3 in the AEL table, while $8p$ $^3P_1$ was given by Lacroute as $7p'$ $^3D_2$. The $8p$ levels fall amongst those of $4f'$ and $7p'$, but the

present designations seem most likely on the basis of combination intensities and series considerations.

A group of 13 higher even levels which may belong to any of four configurations, as shown in table 10.3, have been given only numerical designations.

6. Odd-Parity Configurations

Table 10.4 is a complete list of the presently known odd levels in I II. The terms of $5s5p^5$, $5p^3(^4S°)6s$, $(^4S°)5d$, and $(^2D°)6s'$ were previously known. The $5p^5$, $6s$, and $5d$ configurations are probably mixed, but the new intensities leave no doubt that Lacroute's designations for $5p^5\ ^3P°_0$ and $5d\ ^5D°_0$ must be reversed. The resulting new position of $5d\ ^5D°_0$ is confirmed in the $6d$ configuration.

A comparison of the predictions of intermediate coupling theory for p^5s with the experimental results for a number of rare-gas type atoms is made in the book of Condon and Shortley ([11], p. 304). It seems of interest to make this comparison for the known examples of sp^5 which exhibit intermediate coupling to a significant extent. There are only three of these, and the results for them are shown in table 4 and figure 6. The levels for Kr III $4s\ 4p^5$ and Xe III $5s\ 5p^5$ were fitted to the intermediate coupling formulas in Condon and Shortley by the method used

TABLE 4. *Intermediate-coupling parameters and predicted level positions for the configuration* sp^5 *in three atoms*

	Kr III $4s4p^5$	I II $5s5p^5$	Xe III $5s5p^5$
$\chi=\frac{3}{4}\zeta_p/G_1$	0. 236	1. 000	1. 240
$\zeta(np)$	3741 cm^{-1}	5900 cm^{-1}	9621 cm^{-1}
$G_1(ns,np)$	11890	4425	5819
$^3P°_2$ pred.	(115932) cm^{-1}	81555 cm^{-1}	(98263) cm^{-1}
$^3P°_2$ obs.	115932	81908	98263
$^3P°_1$ pred.	119358	85296	103686
$^3P°_1$ obs.	119381	84222	103569
$^3P°_0$ pred.	(121544)	(90405)	(112694)
$^3P°_0$ obs.	121544	90405	112694
$^1P°_1$ pred.	141899	95514	118909
$^1P°_1$ obs.	141876	95956	119026

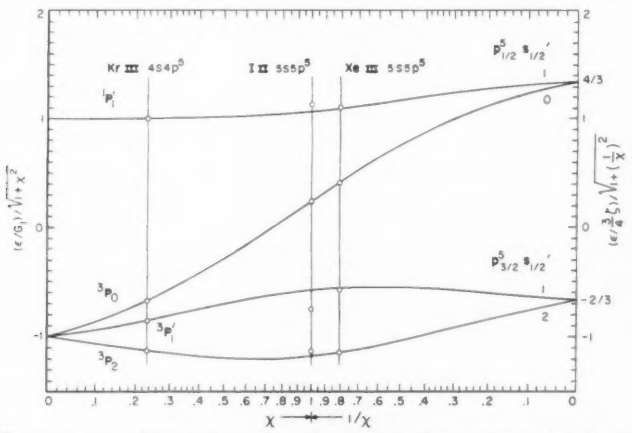

FIGURE 6. *Observed levels of* sp^5 *for three atoms fitted to intermediate-coupling curves.*

there: the parameter χ is chosen so that the levels J=0,2, and the mean of the two levels of J=1, fit the theory exactly. The value of χ chosen for I II $5s\ 5p^5$ gives a somewhat better fit than is obtained by the Condon and Shortley method. Still, the fit for I II is not as good as for the other two atoms. Interaction with either $5d\ ^3D°_1$ or $6s'\ ^3D°_1$, or with both, probably causes the apparent depression of $5p^5\ ^3P°_1$ in I II. In any case this calculation definitely supports the designation change for $5d\ ^5D°_0$ and $5p^5\ ^3P°_0$ mentioned above. The other known cases of sp^5, in Cl II through Sc VI of the S I isoelectronic sequence, are quite close to L–S coupling ($\chi<0.1$).

The level adopted here for $5p^5\ ^3P°_0$ in Xe III is listed as $5d\ ^5D°_0$ in AEL, Vol. III. The analogy with I II and Kr III leaves little doubt that our change should be made. The three combinations [26] on which the level is based were not sufficient to determine its configuration unambiguously. Humphreys' [26] level for $5p^5\ ^3P°_0$ in Xe III would seem questionable; it is far lower than the expected position of $5d\ ^5D°_0$, the only other possible designation. The known levels $5d\ ^5D°_{3,2,1}$ of Xe III agree with the order found in I II.

A diagonalization of the energy matrix in intermediate coupling for the configuration $5p^3\ 6s$ in I II has increased our confidence in the configuration and parentage assignments made here for all the known odd levels based on $5p^3\ ^2D°$ and $5p^3\ ^2P°$ parents. The matrices of the electrostatic and spin-orbit interactions for sp^3 are given on pages 199 and 268, respectively, of Condon and Shortley [11]. The value of $F_2(5p,5p)$ used in our calculation, 1425 cm^{-1}, was obtained from the relation $6F_2=^3P°_0-^3D°_3$ for sp^3. It is supported by the value of F_2 for the $5p^4$ configuration given above, 1405 cm^{-1}. If one knows F_2 and the levels of either J=2 or J=1, the value of $G_1(6s,5p)$ may be obtained from the diagonal-sum rule. At the time the value of G_1 adopted here (1000 cm^{-1}) was chosen, however, it was based on values obtained from the equation $5p^3(^4S°)6s\ (^3S°_1-{}^5S°_2)=4G_1$. This gives $G_1=952$ cm^{-1} for I II and $G_1=1035$ cm^{-1} for Xe III. By carrying out the calculation for $G_1=500$, 1000, and 1500 cm^{-1} we have assured ourselves that the intermediate value is very close to the "best" value for fitting the observed levels. The other parameter needed for the calculation, ζ_p, was taken to be 5930 cm^{-1}, as in the $5p^4$ configuration.

The calculated energies and g_J-values for the levels of $5p^36s$ are given in table 5, together with the observed values. An exact fit is assumed for the $^3D°_0$ and $^3P°_0$ levels. The average deviation of the predicted and observed values, 322 cm^{-1}, seems reasonable for a calculation neglecting configuration mixing. Table 6 gives the calculated composition of the levels of J=1 and J=2 in terms of pure Russel-Saunders states.

It will be seen that the aforementioned designation of the level at 94825 cm^{-1} as $6s'\ ^3D°_1$, instead of the level at 92133 cm^{-1}, is supported by this calculation. The indicated perturbation of $6s'\ ^3D°_1$ is in the direction to be expected if it is caused mainly by inter-

TABLE 5. *Predictions of intermediate-coupling calculation for* I II $5p^3$ 6s *compared with observation*

The parameters were taken as follows: $\zeta(5p) = 5930$ cm^{-1}, $F_2(5p,5p) = 1425$ cm^{-1} and $G_1(6s,5p) = 1000$ cm^{-1}.

Designation	Predicted position	Observed position	Difference	Predicted g_J	Observed g_J
6s $^5S^\circ_2$	81176 cm^{-1}	81033 cm^{-1}	143 cm^{-1}	1.954	1.95
6s $^3S^\circ_1$	84862	84843	19	1.877	1.753
6s′ $^3D^\circ_1$	94096	94825	−729	0.703	0.653
6s′ $^3D^\circ_2$	94103	93691	412	1.235	1.16
6s′ $^3D^\circ_3$	(96651)	96651	0	1.333	1.36
6s′ $^1D^\circ_2$	98035	97701	334	1.048	0.996
6s″ $^3P^\circ_0$	(105201)	105201	0		
6s″ $^3P^\circ_1$	105749	106103	−354	1.383	
6s″ $^3P^\circ_2$	110015	110459	−444	1.430	1.36
6s″ $^3P^\circ_1$	111173	111962	−789	1.037	

TABLE 6. *Calculated percentage compositions for the levels of* I II $5p^3$ 6s

The composition of each level is given in the column under its assigned designation.

	6s $^5S^\circ_2$	6s′ $^3D^\circ_2$	6s′ $^1D^\circ_2$	6s″ $^3P^\circ_2$
	%	%	%	%
6s $^5S^\circ_2$	91.7	4.5	0.3	3.6
6s′ $^3D^\circ_2$	0.8	65.6	22.5	11.1
6s′ $^1D^\circ_2$	0.4	13.7	75.6	10.2
6s″ $^3P^\circ_2$	7.1	16.2	1.6	75.1
	6s $^3S^\circ_1$	6s′ $^3D^\circ_1$	6s″ $^3P^\circ_1$	6s″ $^1P^\circ_1$
	%	%	%	%
6s $^3S^\circ_1$	87.4	7.9	0.2	4.6
6s′ $^3D^\circ_1$	3.0	80.1	0.8	16.0
6s″ $^3P^\circ_1$	3.6	4.9	77.1	14.4
6s″ $^1P^\circ_1$	6.0	7.1	21.9	65.0

action with 5*d* $^3D^\circ_1$. The other ambiguities resolved by this calculation were between the 5*d*′ and 5*d*″ levels on the one hand and those belonging to 6*s*″ on the other. As between the 5*d*′ and 6*s*″ groups, the present assignments are in general supported by the relative intensities of combinations of levels belonging to these configurations with levels of the distinct 6*p*′ and 6*p*″ groups.

The intensities would not have served, however, to distinguish the 6*s*″ levels from those of 5*d*″. The assignments of the two levels 5*d*″ $^1D^\circ_2$ and 5*d*″ $^3D^\circ_3$ may be considered questionable, since the former is well below a level of J=2 assigned to 5*d*′ and the latter is near the level designated 5*d*′ $^1F^\circ_3$. However, these assignements fit in with the other levels of J=2 and J=3 within each parentage group better than any other arrangement. The 5*d*′ group is now known except for one level of J=5, and only $^3F^\circ_4$ is lacking in the 5*d*″ group.

The sorting-out of these lower odd levels, together with an approximate knowledge of the various series limit positions which they approach, have enabled us to assign definite configuration and parentage designations to the complex group of 91 odd levels between 118074 cm^{-1} (5*d*′ $^3P^\circ_1$) and 145837 cm^{-1} ($20^\circ_{2,1}$). Only eight of the levels expected in this region are missing, four of them from 9*d* $^{5,3}D^\circ$. The levels of 6*d* $^{5,3}D^\circ$ and 7*s* $^{5,3}S^\circ$ were previously known and correctly identified. About 15 other previously listed higher odd levels are included in this analysis, usually with a changed designation or a new assignment to a definite configuration.

It is interesting to note that the smallness of the $^3D^\circ_1$—$^3D^\circ_2$ intervals in the 7*s*′ and 8*s*′ terms (2.37 and 36.12 cm^{-1}, respectively) is in accord with the theoretical predictions for the corresponding levels of 6*s*′. In table 5 the predicted positions of 6*s*′ $^3D^\circ_1$ and $^3D^\circ_2$ are both very near 94100 cm^{-1}. The large observed separation of these levels, 1134 cm^{-1}, is apparently due to perturbations in opposite directions for the two levels.

We have assigned 15 levels to the 6*d*′ group, but there is really no good basis for giving them term designations; hence they are listed numerically. The Russell-Saunders designations given the 5*d*′ and 5*d*″ levels probably should not be taken as more than suggestive, but the names given here fit the observed combinations better than any other arrangement.

The levels of the newly-found ($^4S^\circ$)*ng* $^{5,3}G^\circ$ terms in table 10.4 are based on combinations with 4*f* $^{5,3}F$ and, in the case of the higher series members, with 5*f* $^{5,3}F$. Although we have assigned multiplicities to the *ng* levels on the basis of these transitions—intercombinations are definitely weaker than intrasystem transitions—it is clear from figure 7 that these levels

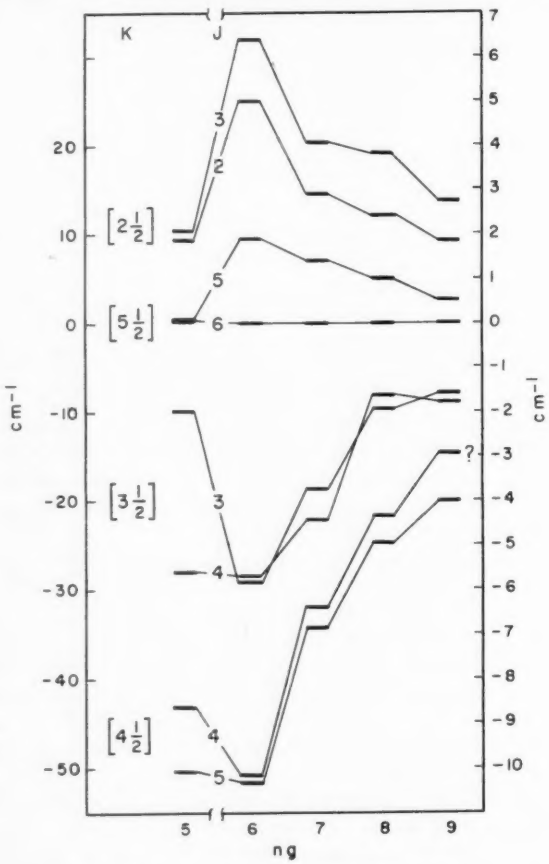

FIGURE 7. *Levels of the* ($^4S^\circ$)ng *groups.*

The ordinate scale on the left applies to the 5*g* levels, the higher levels being plotted according to the scale on the right. The Russell-Saunders designations for these levels may be obtained by comparing this figure with the level values given in table 10.4.

do not fall into the triplet-quintet pattern of Russell-Saunders coupling. The numbers under "K" in this figure refer to pair-coupling [27]; they are the four possible results of adding the orbital angular momentum of a g-electron to the J of the parent $^4S^\circ_{1\frac{1}{2}}$ level. While these levels certainly do not show good pair-coupling, it seems probable that this notation describes the observed structures better than the L-S scheme in table 10.4.

Each ng triplet level is paired with a quintet level in the three higher "pairs" of figure 7. In the known I II terms of the type $(^4S^\circ)nl\ ^5L, ^3L$, where $l=p, d, f$, or g, a characteristic partial inversion of levels occurs except in $np\ ^5P$. (Both of the known terms $6p, 7p, ^5P$ show large deviations from the Landé interval rule in the direction of partial inversion.) However, this deviation from Russell-Saunders structure is compounded by overlapping of the triplet and quintent terms only in the $(^4S^\circ)ng$ groups. Even the $(^4S^\circ)nf\ ^3F$ terms are well above the corresponding quintets.

It would seem from figure 7 that some of the ng levels are perturbed by amounts comparable to the (small) level separations. The position of the $5g$ $[5\frac{1}{2}]_5$ level and the crossing-over behavior of the $[3\frac{1}{2}]_{3,4}$ pair with each increase in n are probably the most obvious examples. Perhaps the best overall description of the grouping observed for these ng levels would be "frustrated pair-coupling."

In addition to the identified series members based on the $5p^3(^4S^\circ)$ parent, the higher group of odd levels beginning with $20^\circ_{1,2}$ at 145837.7 cm^{-1} probably contains levels belonging to each of the designations $6d''$, $7d'$, $7s''$, $8s'$, and $5g'$. We have given only numerical designations to these levels, no attempt having been made to assign them to definite parents and configurations.

7. Series and the Ionization Energy

In a singly-ionized atom, the Rydberg denominator n^* for a series member is defined by the equation $4T=R/(n^*)^2$; where 4T is the position of the level measured from the series limit, and R is the Rydberg constant. (The quantity T is the "reduced" absolute term value. For convenience in using the Rydberg Interpolation Table [28], the value of R was taken as 109737.4 cm^{-1} in the series calculations reported here.) Many unperturbed series obey quite closely the Ritz formula $n^*=n+\mu+\alpha T$, where n runs through the successive integers for the series and μ and α are constants for a given series. Since the fraction by which n^* exceeds an integer is a linear function of T for such a series, the position of the series limit is taken as that value which gives the "best" straight line when these successive fractions are plotted against the corresponding values of T.

Figure 8 shows two such plots for the new $(^4S^\circ)ng\ ^5G^\circ_6$ series, $n=5$ through 12. The approximately straight line is obtained by taking the $5p^3\ ^4S^\circ$ limit, the ground state of I III, to lie 154304 cm^{-1} above the $5p^4\ ^3P_2$ ground level of I II. The curved line, representing a very unlikely behavior for this series, results from assuming the limit to be only 4 cm^{-1} above the straight-line value. It is seen that the Rydberg denominator fractions for the higher series members become increasingly sensitive to the limit chosen or, equivalently, to the series level values as n increases. The last point on the left in the straight-line plot, for $n=12$, would fall on the straight line if the position of $12g\ ^5G^\circ_6$ were raised by 0.2 cm^{-1}. Since this level is based on two weak lines—transitions to $4f\ ^5F_5$ and $5f\ ^5F_5$—the observational uncertainty in its position is about 0.1 cm^{-1}. In any case a series of this regularity leaves small doubt about the reality of any of its members.

Another example of a fairly regular series, $ns\ ^5S^\circ$, is shown in figure 9, along with the perturbed $ns\ ^3S^\circ$

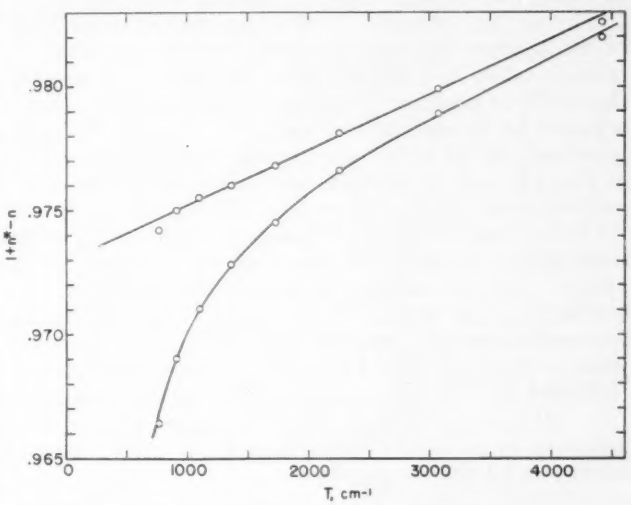

FIGURE 8. *The* $(^4S^\circ)ng\ ^5G^\circ_6$ *series plotted for two different limit values, 154304 cm*$^{-1}$ *(straight line) and 154308 cm*$^{-1}$ *(curved line).*

The series runs from $n=5$, at the right, through $n=12$.

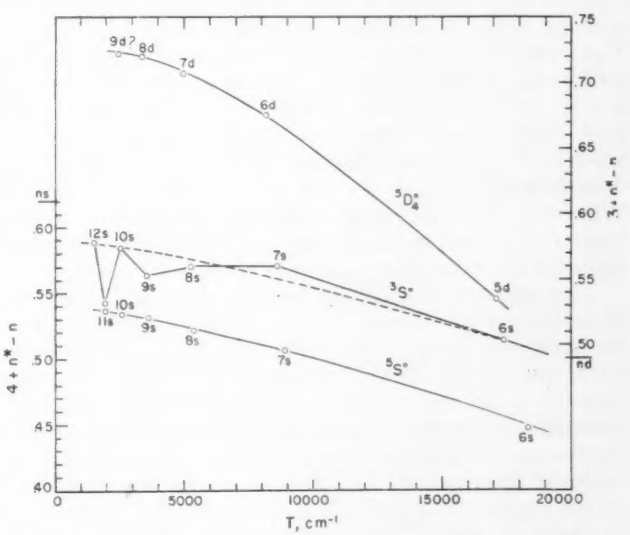

FIGURE 9. *Three series in* I II *based on the* I III $5p^3\ ^4S^\circ$ *limit at 154304 cm*$^{-1}$ *above the ground level of* I II.

series. The behavior of the latter series is certainly too irregular to be caused by a single perturbing level. By analogy with the $^5S^\circ$ series, one might guess that the dashed line shown in figure 9 approximates a hypothesized "unperturbed" behavior of the $^3S^\circ$ series. The fact that $9s\ ^3S^\circ_1$ combines strongly with $5p^4\ ^1D_2$, whereas the analogous transition for the other $ns\ ^3S^\circ$ levels does not occur or is quite weak, suggests that the level $6d'\ 15^\circ_1$ is mainly responsible for the depression of $9s\ ^3S^\circ_1$. This 15°_1 level, only 375 cm^{-1} above $9s\ ^3S^\circ_1$, combines with $5p^4\ ^1D_2$ in a transition just twice as strong as the $5p^4\ ^1D_2$—$9s\ ^3S^\circ_1$ line. Similarly, an interaction probably exists between $11s\ ^3S^\circ_1$ and either or both of the slightly higher levels 25°_1 and 29°_1. The perturbations of the $^3S^\circ$ series are actually not very large. For example, the perturbation required to remove the point for $11s\ ^3S^\circ$ from the dashed line to the position shown is only 90 cm^{-1} (a change of 22 cm^{-1} in the reduced term value).

The $nd\ ^5D^\circ_4$ series is shown in figure 9 as an example of an apparently regular series which nevertheless fails to obey the simple Ritz formula. It is clear that a limit position determined by assuming such a series to be Ritzian will be too low. A previous value reported [29] by us for the principal ionization energy of I II, 19.12 ev, corresponds to a limt of 154260 cm^{-1} derived from the $ns\ ^5S^\circ_2$ and $nd\ ^5D^\circ_4$ series.

On the basis of the $ng\ ^5G^\circ_6$ series in figure 8, it seems reasonable to take the position of I III $5p^3\ ^4S^\circ$ as 154304 ± 1 cm^{-1} above the ground level of I II. By combining this result with a recent value [30] for the conversion factor, (wavenumber)/(energy in electron-volts) $= 8066.03 \pm 0.14$ cm^{-1} ev^{-1}, we obtain 19.1301 ± 0.0004 ev for the principal ionization energy of I II. If the conversion factor adopted in the AEL volumes is applied to our new limit, the resulting energy is 19.126 ev.

8. Conclusion

The earlier analyses of the I II spectrum, which yielded 43 even and 55 odd levels, have been revised and extended to include 124 even and 190 odd levels. The revisions include changed designations for over 40 levels, improved values for all previously known levels, and new Landé g_J factors for 46 levels. All previously known series have been extended and new ones found. The ionization potential of I II is well determined by one of the new series, $(^4S^\circ)ng\ ^5G^\circ_6$. Wherever feasible, the results of the analysis have been compared with theory and with experimental findings for homologous and isoelectronic atoms.

This improved analysis was made possible by the observation of almost 2400 I II lines excited in an electrodeless lamp. We have measured the Zeeman patterns of 83 lines. About 1800 lines are now classified, as compared to approximately 500 lines classified in previous analyses. None of the remaining unclassified lines is very strong. The present list includes approximately 300 lines in the vacuum ultraviolet region, 655 to 2000 A, and extends to 11085 A in the infrared. The measurement of the vacuum ultraviolet spectrum has yielded an accurate value for the connection between the higher levels and those of the ground configuration.

We have observed two magnetic dipole transitions among levels of the $5p^4$ ground configuration and verified their nature by the Zeeman effect.

This work was begun at the suggestion of Dr. C. C. Kiess, who measured most of the Zeeman patterns in connection with the investigation of the first spectrum of iodine. Charlotte Moore compiled most of the new g_J values and prepared a preliminary line list for the region above 2000 A. Mrs. Ruth Peterson has very accurately carried out the hand calculations needed for a new I II square array. She also punched the input cards used in calculations made at the Bureau IBM 704 installation.

The observed wavelengths in air were reduced to vacuum wavenumbers on the 704 with a code devised by Charles DeW. Coleman and William R. Bozman. In addition, an energy level search program written by Coleman and Bozman for the computer can be credited with finding a good number of the higher levels. Mr. Bozman has generously devoted many hours to assisting us with the computer work.

The numerical computations involved in an intermediate-coupling calculation for the $5p^36s$ configuration were carried out on the 704 by Dr. Richard E. Trees, using a code written by him. Dr. Trees has also been of help in some of the other theoretical calculations.

Together with Mrs. Agnes Rhodes, who typed and proofread the manuscript, each of these colleagues deserves our sincere thanks for assisting in this work.

9. References

[1] C. E. Moore, Atomic energy levels, NBS Cir. 467, Vol. I (1949), Vol. II (1952), Vol. III (1958).
[2] C. H. Corliss, W. R. Bozman, and F. O. Westfall, J. Opt. Soc. Am. **43,** 398 (1953).
[3] P. Lacroute, Ann. Phys. (11) **3,** 5 (1935); Ann. Astrophys. **2,** 318 (1939). References to Lacroute's earlier work and to the previous observations of others are given in these papers.
[4] K. Murakawa, Z. Phys. **109,** 162 (1938). Contains references to previous work.
[5] K. Murakawa, Z. Phys. **112,** 234 (1939).
[6] L. Bloch and E. Bloch, Ann. Phys. (10) **11,** 141 (1929).
[7] L. Bloch, E. Bloch, and N. Felici, J. Phys. Radium **8,** 355 (1937).
[8] C. C. Kiess and C. H. Corliss, J. Research NBS **63A,** 1 (1959).
[9] K. T. Compton and J. C. Boyce, Rev. Sci. Instr. **5,** 218 (1934).
[10] H. A. Robinson and G. H. Shortley, Phys. Rev. **52,** 713 (1937).
[11] E. U. Condon and G. H. Shortley, Theory of atomic spectra (Cambridge University Press, Cambridge, England, 1951).
[12] J. E. Ruedy and R. C. Gibbs, Phys. Rev. **46,** 880 (1934).
[13] H. Niewodniczanski and F. Lipinski, Nature **142,** 1160 (1938).
[14] Bengt Edlén, Phys. Rev. **65,** 248 (1944).
[15] S. Mrozowski, J. Opt. Soc. Am. **46,** 663 (1956).
[16] G. H. Shortley, L. H. Aller, J. G. Baker, and D. H. Menzel, Ap. J. **93,** 178 (1941).

[17] H. Niewodniczanski, Acta Phys. Polon. **3,** 285 (1934).
[18] K. Murakawa, J. Phys. Soc. Japan **13,** 484 (1958).
[19] S. Goudsmit, Phys. Rev. **37,** 663 (1931).
[20] H. B. G. Casimir, Verhandel, Teyler's Tweede Genootschap, Haarlem (1936).
[21] R. E. Trees, Phys. Rev. **92,** 308 (1953).
[22] S. Mrozowski, Phys. Rev. **58,** 1086 (1940).
[23] E. Gerjuoy, Phys. Rev. **60,** 233 (1941).
[24] H. E. White, Introduction to Atomic Spectra. ch. 18, sec. 10 (McGraw-Hill Book Co., Inc., New York, N.Y., 1934).
[25] F. A. Jenkins and S. Mrozowski, Phys. Rev. **60,** 225 (1941).
[26] C. J. Humphreys, J. Research NBS **16,** 639 (1936) RP 898.
[27] G. Racah, Phys. Rev. **61,** 537 (L) (1942).
[28] Rydberg interpolation table (published by Depts. of Physics and Astronomy, Princeton University, Princeton, N. J., 1934).
[29] W. C. Martin and C. H. Corliss, J. Opt. Soc. Am. **48,** 865 (A) (1958).
[30] J. W. M. DuMond and E. R. Cohen, Handbook of Physics, pt. 7, ch. 10, p. 170 (ed. by E. U. Condon and H. Odishaw, McGraw-Hill Book Co., Inc., New York, N.Y., 1958).

10. Appendix

TABLE 10.1. *Observed lines of* I II

λ(vac) observed	λ(vac) calculated	Intensity	Observed wavenumber, cm^{-1}	Classification
655. 804		2	152484. 6	
657. 029		1	152200. 3	$5p^4\ ^3P_2$— $51^\circ_{1,\ 2,\ 3}$
659. 004		6	151744. 1	$5p^4\ ^3P_2$— $49^\circ_{1,\ 2}$
661. 412		1	151191. 7	$5p^4\ ^3P_2$—$14d\ ^3D^\circ_3$
663. 977		8	150607. 6	$5p^4\ ^3P_2$—$13d\ ^3D^\circ_3$
664. 031		3	150595. 4	$5p^4\ ^3P_2$— $48^\circ_{1,\ 2}$
664. 520	. 512	8	150484. 6	$5p^4\ ^3P_2$— $47^\circ_{1,\ 2}$
665. 055	. 041	8	150363. 5	$5p^4\ ^3P_2$— 46°_2
665. 135	. 132	5	150345. 4	$5p^4\ ^3P_2$— $45^\circ_{1,\ 2}$
665. 699	. 695	150	150218. 0	$5p^4\ ^3P_2$— $43^\circ_{1,\ 2}$
666. 660	. 653	150	150001. 5	$5p^4\ ^3P_2$— 42°_2
667. 270		100	149864. 4	$5p^4\ ^3P_2$— $41^\circ_{1,\ 2,\ 3}$
668. 264	. 250	15	149641. 4	$5p^4\ ^3P_2$—$12d\ ^3D^\circ_3$
668. 976	. 981	25	149482. 2	$5p^4\ ^3P_2$— 40°_3
672. 505	. 491	40	148697. 8	$5p^4\ ^3P_2$—$11d\ ^3D^\circ_3$
674. 063		4	148354. 1	$5p^4\ ^3P_2$—$12s\ ^3S^\circ_1$
675. 748	. 732	1	147984. 2	$5p^4\ ^3P_2$— 34°_2
676. 493	. 480	80	147821. 2	$5p^4\ ^3P_2$— 33°_3
678. 856	. 853	200	147306. 6	$5p^4\ ^3P_2$—$10d\ ^3D^\circ_3$
679. 155	. 152	5	147241. 8	$5p^4\ ^3P_2$— 30°_2
679. 618	. 616	50	147141. 5	$5p^4\ ^3P_2$—$10d\ ^3D^\circ_2$
680. 971	. 967	15	146849. 2	$5p^4\ ^3P_2$— 26°_3
681. 266	. 269	6	146785. 5	$5p^4\ ^3P_2$— $25^\circ_{1,\ 2}$
682. 180	. 179	25	146588. 9	$5p^4\ ^3P_2$—$11s\ ^3S^\circ_1$
682. 685	. 682	40	146480. 4	$5p^4\ ^3P_2$— $24^\circ_{1,\ 2}$
683. 414		1	146324. 2	
683. 569	. 565	80	146291. 0	$5p^4\ ^3P_2$— 21°_1
685. 685	. 694	1	145839. 6	$5p^4\ ^3P_2$— $20^\circ_{1,\ 2}$
689. 294		15	145076. 0	
689. 817	. 822	250	144966. 0	$5p^4\ ^3P_2$— $9d\ ^3D^\circ_3$
690. 082		5	144910. 3	
690. 272		3	144870. 4	
690. 453	. 455	80	144832. 4	$5p^4\ ^3P_2$— $9d\ ^3D^\circ_2$
691. 194	. 193	15	144677. 2	$5p^4\ ^3P_2$— $8s'\ ^3D^\circ_2$
691. 295		5	144656. 0	$5p^4\ ^3P_1$— $49^\circ_{1,\ 2}$
693. 567	. 566	40	144182. 2	$5p^4\ ^3P_2$—$10s\ ^3S^\circ_1$
696. 630		1	143548. 2	
696. 840		1	143505. 0	$5p^4\ ^3P_1$— $48^\circ_{1,\ 2}$
697. 358	. 353	1*h*	143398. 4	$5p^4\ ^3P_1$— $47^\circ_{1,\ 2}$
697. 606		10	143347. 4	
697. 940	. 936	5	143278. 8	$5p^4\ ^3P_1$— 46°_2
698. 032	. 036	3	143259. 9	$5p^4\ ^3P_1$— $45^\circ_{1,2}$
698. 650	. 656	8	143133. 2	$5p^4\ ^3P_1$— $43^\circ_{1,2}$
699. 697	. 712	1	142919. 0	$5p^4\ ^3P_1$— 42°_2

TABLE 10.1. *Observed lines of* I II—Continued

λ(vac) observed	λ(vac) calculated	Intensity	Observed wavenumber, cm^{-1}	Classification
701. 007		1	142651. 9	
701. 909		40	142468. 6	
706. 055	. 044	400	141632. 0	$5p^4\ ^3P_2$— $8d\ ^3D^\circ_3$
706. 319		10	141579. 1	
706. 622	. 611	3	141518. 4	$5p^4\ ^3P_2$— $8d\ ^3D^\circ_1$
706. 901	. 898	150	141462. 5	$5p^4\ ^3P_2$— $8d\ ^3D^\circ_2$
707. 136	. 133	100	141415. 5	$5p^4\ ^3P_0$— 33.5°_1
708. 122	. 113	7	141218. 6	$5p^4\ ^3P_1$— 36°_2
709. 733	. 720	50*w*	140898. 0	$5p^4\ ^3P_1$— 34°_2
709. 856	. 871	1	140873. 6	$5p^4\ ^3P_2$— $8d\ ^5D^\circ_2$
711. 746	. 742	6	140499. 6	$5p^4\ ^3P_2$— $6d'\ 15^\circ_1$
712. 918	. 914	200	140268. 6	$5p^4\ ^3P_1$— 31°_0
713. 152		2	140222. 6	
713. 502	. 493	25	140153. 8	$5p^4\ ^3P_1$— 30°_2
713. 557	. 565	10	140143. 0	$5p^4\ ^3P_0$—$11s\ ^3S^\circ_1$
713. 654	. 645	100	140123. 9	$5p^4\ ^3P_2$— $9s\ ^3S^\circ_1$
715. 832	. 830	150	139697. 6	$5p^4\ ^3P_1$— $25^\circ_{1,2}$
716. 161	. 157	10	139633. 4	$5p^4\ ^3P_2$— $6d'\ 14^\circ_3$
716. 583	. 580	150	139551. 2	$5p^4\ ^3P_2$— $6d'\ 13^\circ_{1,2}$
717. 388	. 390	80	139394. 6	$5p^4\ ^3P_1$— $24^\circ_{1,2}$
718. 360	. 365	1	139206. 0	$5p^4\ ^3P_1$— 21°_1
719. 546	. 539	1000	138976. 5	$5p^4\ ^3P_2$— $6d'\ 12^\circ_1$
722. 169		15	138471. 7	$5p^4\ ^1D_2$— $51^\circ_{1,2,3}$
722. 980	. 980	1000	138316. 4	$5p^4\ ^3P_2$— $6d'\ 10^\circ_2$
724. 550		2	138016. 7	$5p^4\ ^1D_2$— $49^\circ_{1,2}$
725. 432		10	137848. 9	
725. 976	. 979	4	137745. 6	$5p^4\ ^3P_1$— $9d\ ^3D^\circ_2$
726. 019	. 035	2	137737. 4	$5p^4\ ^3P_0$—$10s\ ^3S^\circ_1$
726. 798	. 794	3	137589. 8	$5p^4\ ^3P_1$— $8s'\ ^3D^\circ_2$
726. 987	. 985	10	137554. 0	$5p^4\ ^3P_1$— $8s'\ ^3D^\circ_1$
727. 246	. 246	800	137505. 1	$5p^4\ ^3P_2$— $6d'\ 9^\circ_3$
730. 423		1	136907. 0	
731. 005	. 002	7	136798. 0	$5p^4\ ^3P_0$— $7s''\ ^3P^\circ_1$
731. 169		5	136767. 3	
731. 216	. 213	7	136758. 5	$5p^4\ ^1D_2$— $47^\circ_{1,2}$
731. 860	. 853	20	136638. 2	$5p^4\ ^1D_2$— 46°_2
731. 961	. 964	25	136619. 3	$5p^4\ ^1D_2$— $45^\circ_{1,2}$
732. 092	. 081	50	136594. 9	$5p^4\ ^1D_2$— $44^\circ_{2,3}$
732. 276	. 269	15	136560. 5	$5p^4\ ^3P_2$— $6d'\ 7^\circ_{1,2}$
732. 910	. 905	5	136442. 4	$5p^4\ ^3P_2$— $6d'\ 6^\circ_{1,2}$
734. 430	. 433	1	136160. 0	$5p^4\ ^3P_1$— $7s''\ ^3P^\circ_1$
735. 402	. 401	2	135980. 0	$5p^4\ ^3P_1$— $7s''\ ^3P^\circ_0$
737. 546	. 545	500	135584. 8	$5p^4\ ^3P_2$— $7d\ ^3D^\circ_3$
740. 342	. 343	25	135072. 7	$5p^4\ ^3P_0$— $8d\ ^3D^\circ_1$
740. 950	. 959	300	134961. 9	$5p^4\ ^3P_2$— $7d\ ^3D^\circ_2$
741. 131	. 129	6	134928. 9	$5p^4\ ^1D_2$— 37°_2
741. 207	. 213	6	134915. 1	$5p^4\ ^3P_2$— $6d'\ 5^\circ_1$
743. 054	. 052	20	134579. 7	$5p^4\ ^1D_2$— 36°_2
743. 848		60	134436. 1	$5p^4\ ^3P_1$— $8d\ ^3D^\circ_1$ $5p^4\ ^3P_0$— $8d\ ^5D^\circ_1$
744. 188	. 180	40	134374. 6	$5p^4\ ^3P_1$— $8d\ ^3D^\circ_2$
744. 822	. 821	20	134260. 3	$5p^4\ ^1D_2$— 34°_2
746. 143	. 136	1	134022. 6	$5p^4\ ^3P_2$— $6d'\ 3^\circ_3$
746. 523	. 517	15	133954. 3	$5p^4\ ^3P_2$— $6d'\ 2^\circ_3$
748. 781	. 780	800	133550. 4	$5p^4\ ^3P_2$— $7s'\ ^3D^\circ_3$
748. 978	. 978	7	133515. 3	$5p^4\ ^1D_2$— 30°_2
749. 552	. 550	15	133413. 0	$5p^4\ ^3P_1$— $6d'\ 15^\circ_1$
750. 197		250	133298. 3	$5p^4\ ^3P_2$— $8s\ ^3S^\circ_1$
751. 187	. 185	25	133122. 6	$5p^4\ ^3P_2$— $6d'\ 1^\circ_2$ $5p^4\ ^1D_2$— 26°_3

TABLE 10.1. *Observed lines of* I II—Continued

λ(vac) observed	λ(vac) calculated	Intensity	Observed wavenumber, cm^{-1}	Classification
752. 656	. 660	6	132862. 8	$5p^4\ ^1D_2$—$11s\ \ ^3S^\circ_1$
752. 798	. 801	7	132837. 8	$5p^4\ ^3P_2$— $8s\ \ ^5S^\circ_2$
753. 263	. 273	40	132755. 8	$5p^4\ ^1D_2$— $24^\circ_{1,\ 2}$
753. 364	. 381	3	132738. 0	$5p^4\ ^3P_2$— $5d''\ ^3P^\circ_1$
754. 342	. 348	1	132565. 9	$5p^4\ ^1D_2$— 21°_1
754 540	. 546	8	132531. 1	$5p^4\ ^3P_0$— $6d'\ 12^\circ_1$
754. 913	. 918	35	132465. 6	$5p^4\ ^3P_1$— $6d'\ 13^\circ_{1,\ 2}$
756. 935	. 942	2	132111. 7	$5p^4\ ^1D_2$— $20^\circ_{1,\ 2}$
758. 201	. 203	25	131891. 1	$5p^4\ ^3P_1$— $6d'\ 12^\circ_1$
761. 739	. 747	120	131278. 6	$5p^4\ ^3P_1$— $6d'\ 11^\circ_0$
763. 644	. 649	12	130951. 1	$5p^4\ ^1D_2$— $8s'\ \ ^3D^\circ_2$
765. 594		600	130617. 5	$5p^4\ ^3P_2$— $7s'\ \ ^3D^\circ_2$
				$5p^4\ ^3P_2$— $7s'\ \ ^3D^\circ_1$
770. 771	. 777	300	129746. 2	$5p^4\ ^3P_0$— $7d\ \ ^3D^\circ_1$
772. 078	. 086	1	129520. 6	$5p^4\ ^1D_2$— $7s''\ ^3P^\circ_1$
772. 344	. 351	400	129476. 0	$5p^4\ ^3P_1$— $6d'\ \ 7^\circ_{1,\ 2}$
773. 055	. 058	500	129356. 9	$5p^4\ ^3P_1$— $6d'\ \ 6^\circ_{1,\ 2}$
786. 413	. 409	15	127159. 6	$5p^4\ ^1D_2$— $8d\ \ ^3D^\circ_1$
786. 460		20	127152. 0	$5p^4\ ^3P_1$— $6d'\ \ 4^\circ_0$
				$5p^4\ ^1D_2$— $8d\ \ ^3D^\circ_3$
788. 329	. 338	3	126850. 6	$5p^4\ ^3P_0$— $8s\ \ ^3S^\circ_1$
788. 815	. 811	700	126772. 4	$5p^4\ ^1D_2$— $6d'\ 15^\circ_1$
791. 147	. 149	350	126398. 8	$5p^4\ ^1D_2$— $9s\ \ ^3S^\circ_1$
791. 851	. 847	7	126286. 4	$5p^4\ ^3P_0$— $5d''\ ^3P^\circ_1$
791. 967		15	126267. 9	
792. 313		70	126212. 7	$5p^4\ ^3P_1$— $6d'\ \ 1^\circ_2$
				$5p^4\ ^3P_1$— $8s\ \ ^3S^\circ_1$
794. 237	. 238	500	125907. 0	$5p^4\ ^1D_2$— $6d'\ 14^\circ_3$
794. 757	. 758	400	125824. 6	$5p^4\ ^1D_2$— $6d'\ 13^\circ_{1,\ 2}$
797. 819	. 836	2	125341. 7	$5p^4\ ^3P_2$— $6d\ \ ^3D^\circ_1$
798. 158	. 159	1000	125288. 5	$5p^4\ ^3P_2$— $6d\ \ ^3D^\circ_3$
798. 427	. 419	400	125246. 3	$5p^4\ ^3P_2$— $6d\ \ ^3D^\circ_2$
802. 618	. 637	1	124592. 3	$5p^4\ ^1D_2$— $6d'\ 10^\circ_2$
805. 361	. 365	5	124167. 9	$5p^4\ ^3P_0$— $7s'\ \ ^3D^\circ_1$
809. 188	. 192	60	123580. 7	$5p^4\ ^3P_2$— $5d''\ ^1F^\circ_3$
809. 523		150	123529. 5	$5p^4\ ^3P_1$— $7s'\ \ ^3D^\circ_2$
				$5p^4\ ^3P_1$— $7s'\ \ ^3D^\circ_1$
814. 094	. 103	50	122835. 9	$5p^4\ ^1D_2$— $6d'\ 7^\circ_{1,\ 2}$
814. 459	. 476	3	122780. 9	$5p^4\ ^3P_2$— $5d''\ ^3F^\circ_2$
814. 880	. 888	12	122717. 4	$5p^4\ ^1D_2$— $6d'\ 6^\circ_{1,\ 2}$
818. 047	. 039	700	122242. 4	$5p^4\ ^3P_2$— $6d\ \ ^5D^\circ_1$
820. 884	. 892	150	121819. 9	$5p^4\ ^3P_2$— $6d\ \ ^5D^\circ_2$
821. 159	. 164	30	121779. 1	$5p^4\ ^3P_2$— $6d\ \ ^5D^\circ_3$
823. 426	. 436	170	121443. 8	$5p^4\ ^3P_0$— $5d''\ ^1P^\circ_1$
824. 841	. 858	1	121235. 5	$5p^4\ ^1D_2$— $7d\ \ ^3D^\circ_2$
825. 122	. 113	500	121194. 2	$5p^4\ ^3P_2$— $5d''\ ^3F^\circ_3$
825. 934	. 929	300	121075. 0	$5p^4\ ^3P_2$— $5d''\ ^3D^\circ_1$
827. 797	. 792	400	120802. 6	$5p^4\ ^3P_1$— $5d''\ ^1P^\circ_1$
828. 888	. 897	1	120643. 6	$5p^4\ ^1D_2$— $7d\ \ ^5D^\circ_2$
831. 168	. 187	300	120312. 6	$5p^4\ ^1D_2$— $7s'\ \ ^1D^\circ_2$
831. 270	. 278	150	120297. 8	$5p^4\ ^1D_2$— $6d'\ \ 3^\circ_3$
834. 095	. 106	1200	119890. 4	$5p^4\ ^3P_2$— $7s\ \ ^3S^\circ_1$
838. 070	. 075	700	119321. 8	$5p^4\ ^3P_2$— $5d''\ ^3D^\circ_3$
840. 259	. 282	3	119010. 9	$5p^4\ ^1D_2$— $5d''\ ^3P^\circ_1$
841. 097	. 106	700	118892. 4	$5p^4\ ^3P_0$— $6d\ \ ^3D^\circ_1$
843. 113	. 116	600	118608. 1	$5p^4\ ^3P_2$— $7s\ \ ^5S^\circ_2$
845. 638	. 652	25	118253. 9	$5p^4\ ^3P_1$— $6d\ \ ^3D^\circ_1$
846. 295	. 306	900	118162. 1	$5p^4\ ^3P_1$— $6d\ \ ^3D^\circ_2$
847. 796		600	117952. 9	$5p^4\ ^3P_1$— $5d''\ ^3P^\circ_0$?
847. 926	. 922	1000	117934. 8	$5p^4\ ^3P_2$— $5d''\ ^3P^\circ_2$

TABLE 10.1. *Observed lines of* I II—Continued

λ(vac) observed	λ(vac) calculated	Intensity	Observed wavenumber, cm^{-1}	Classification
855. 494	. 502	400	116891. 5	$5p^4\ {}^1D_2$— $7s'\ {}^3D^\circ_3$
863. 590	. 590	600	115795. 7	$5p^4\ {}^3P_0$— $6d\ {}^5D^\circ_1$
868. 380	. 383	750	115157. 0	$5p^4\ {}^3P_1$— $6d\ {}^5D^\circ_1$
870. 343	. 341	900	114897. 2	$5p^4\ {}^3P_2$— $5d'\ {}^1P^\circ_1$
871. 596	. 599	30	114732. 0	$5p^4\ {}^3P_1$— $6d\ {}^5D^\circ_2$
872. 391	. 388	800	114627. 5	$5p^4\ {}^3P_0$— $5d''\ {}^3D^\circ_1$
873. 489	. 495	1500	114483. 4	$5p^4\ {}^3P_2$— $5d'\ {}^3P^\circ_2$
875. 941	. 940	1000	114162. 9	$5p^4\ {}^1D_2$— $5d''\ {}^1P^\circ_1$
877. 276	. 279	800	113989. 2	$5p^4\ {}^3P_1$— $5d''\ {}^3D^\circ_1$
879. 844	. 847	2000	113656. 5	$5p^4\ {}^3P_2$— $5d''\ {}^3D^\circ_3$
881. 881	. 889	1500	113394. 0	$5p^4\ {}^3P_2$— $5d'\ {}^1F^\circ_3$
886. 492	. 511	30	112804. 2	$5p^4\ {}^3P_1$— $7s\ {}^3S^\circ_1$
890. 995	. 995	1000	112234. 1	$5p^4\ {}^3P_1$— $5d''\ {}^3D^\circ_2$
893. 167	. 163	1000	111961. 1	$5p^4\ {}^3P_2$— $6s''\ {}^1P^\circ_1$
895. 844	. 847	400	111626. 6	$5p^4\ {}^3P_0$— $5d'\ {}^3P^\circ_1$
895. 957	. 963	200	111612. 5	$5p^4\ {}^1D_2$— $6d\ {}^3D^\circ_1$
896. 376	. 370	400	111560. 3	$5p^4\ {}^1D_2$— $6d\ {}^3D^\circ_3$
896. 692		400	111521. 0	$5p^4\ {}^1D_2$— $6d\ {}^3D^\circ_2$ / $5p^4\ {}^3P_1$— $7s\ {}^5S^\circ_2$
901. 004	. 006	200	110987. 3	$5p^4\ {}^3P_1$— $5d'\ {}^3P^\circ_1$
902. 130	. 133	400	110848. 8	$5p^4\ {}^3P_1$— $5d''\ {}^3P^\circ_2$
905. 313	. 314	100	110459. 0	$5p^4\ {}^3P_2$— $6s''\ {}^3P^\circ_2$
910. 309	. 309	400	109852. 8	$5p^4\ {}^1D_2$— $5d''\ {}^1F^\circ_3$
914. 957	. 951	200	109294. 8	$5p^4\ {}^3P_2$— $5d'\ {}^3S^\circ_1$
917. 007	. 001	300	109050. 4	$5p^4\ {}^1D_2$— $5d''\ {}^3F^\circ_2$
921. 343	. 340	400	108537. 2	$5p^4\ {}^3P_2$— $5d'\ {}^1D^\circ_2$
922. 085	. 088	100	108449. 9	$5p^4\ {}^3P_0$— $5d'\ {}^1P^\circ_1$
925. 119	. 142	1	108094. 2	$5p^4\ {}^1D_2$— $6d\ {}^5D^\circ_2$
925. 477	. 488	15	108052. 4	$5p^4\ {}^1D_2$— $6d\ {}^5D^\circ_3$
929. 143	. 144	800	107626. 0	$5p^4\ {}^3P_2$— $5d'\ {}^3G^\circ_3$
930. 133	. 131	100	107511. 5	$5p^4\ {}^3P_2$— $5d'\ {}^3F^\circ_2$
930. 506	. 506	150	107468. 4	$5p^4\ {}^1D_2$— $5d''\ {}^3F^\circ_2$
931. 139	. 137	100	107395. 4	$5p^4\ {}^3P_1$— $5d'\ {}^3P^\circ_2$
937. 322	. 332	20	106686. 9	$5p^4\ {}^1S_0$— $7d\ {}^3D^\circ_1$
940. 904	. 902	200	106280. 8	$5p^4\ {}^3P_1$— $5d''\ {}^1D^\circ_2$
941. 936	. 960	2	106164. 3	$5p\ {}^1D_2$— $7s\ {}^3S^\circ_1$
942. 472	. 478	40	106103. 9	$5p^4\ {}^3P_2$— $6s''\ {}^3P^\circ_1$
947. 023	. 024	100	105594. 0	$5p^4\ {}^1D_2$— $5d''\ {}^3D^\circ_2$
947. 749	. 744	15	105513. 2	$5p^4\ {}^3P_0$— $6s''\ {}^1P^\circ_1$
948. 658	. 653	80	105412. 1	$5p^4\ {}^1S_0$— $6d'\ 5^\circ_1$
953. 199		8	104909. 9	
953. 489		30*d*	104878. 0	$5p^4\ {}^3P_1$— $6s''\ {}^1P^\circ_1$ / $5p^4\ {}^1D_2$— $7s\ {}^5S^\circ_2$
956. 503	. 515	10	104547. 5	$5p^4\ {}^3P_2$— $5d'\ {}^3D^\circ_1$
958. 333	. 342	25	104347. 9	$5p^4\ {}^1D_2$— $5d'\ {}^3P^\circ_1$
959. 619	. 617	100	104208. 0	$5p^4\ {}^1D_2$— $5d''\ {}^3P^\circ_2$
961. 979	. 982	70	103952. 4	$5p^4\ {}^3P_1$— $5d'\ {}^1S^\circ_0$
963. 415	. 430	4	103797. 4	$5p^5\ {}^1S_0$— $8s\ {}^3S^\circ_1$
967. 378	. 381	700	103372. 2	$5p^4\ {}^3P_1$— $6s''\ {}^3P^\circ_2$
968. 670	. 677	100	103234. 3	$5p^4\ {}^1S_0$— $5d''\ {}^3P^\circ_1$
972. 292	. 313	10	102849. 8	$5p^4\ {}^3P_0$— $5d'\ {}^3S^\circ_1$
978. 394	. 393	300	102208. 3	$5p^4\ {}^3P_1$— $5d'\ {}^3S^\circ_1$
988. 434	. 433	200	101170. 1	$5p^4\ {}^1D_2$— $5d'\ {}^1P^\circ_1$
992. 508	. 503	150	100754. 8	$5p^4\ {}^1D_2$— $5d'\ {}^3P^\circ_2$
995. 768	. 770	700	100425. 0	$5p^4\ {}^3P_1$— $5d'\ {}^3F^\circ_2$
1000. 572	. 569	1200	99942. 8	$5p^4\ {}^3P_2$— $5d'\ {}^3F^\circ_3$
1000. 701	. 711	80	99929. 9	$5p^4\ {}^1D_2$— $5d''\ {}^3D^\circ_3$
1003. 350	. 354	1000	99666. 1	$5p^4\ {}^1D_2$— $5d'\ {}^1F^\circ_3$
1003. 457	. 458	500	99655. 5	$5p^4\ {}^3P_0$— $6s''\ {}^3P^\circ_1$

TABLE 10.1. *Observed lines of* I II—Continued

λ(vac) observed	λ(vac) calculated	Intensity	Observed wavenumber, cm^{-1}	Classification
1003. 612	. 605	300	99640. 1	$5p^4\ ^1D_2$— $5d''\ ^1D_2^\circ$
1009. 936	. 935	700	99016. 2	$5p^4\ ^3P_1$— $6s''\ ^3P_1^\circ$
1016. 381	. 375	20	98388. 3	$5p^4\ ^1S_0$— $5d''\ ^1P_1^\circ$
1017. 977	. 973	200	98234. 0	$5p'\ ^1D_2$— $6s''\ ^1P_1^\circ$
1018. 583	. 581	4000	98175. 6	$5p^4\ ^3P_2$— $5d'\ ^3D_3^\circ$
1019. 230	. 223	400	98113. 3	$5p^4\ ^3P_1$— $6s''\ ^3P_0^\circ$
1019. 400	. 386	800	98096. 9	$5p^4\ ^3P_0$— $5d'\ ^3D_1^\circ$
1023. 544	. 533	200	97699. 8	$5p^4\ ^3P_2$— $6s'\ ^1D_2^\circ$
1026. 065	. 070	350	97459. 7	$5p^4\ ^3P_1$— $5d'\ ^3D_1^\circ$
1030. 047	. 043	800	97082. 9	$5p^4\ ^3P_2$— $5d'\ ^3D_2^\circ$
1033. 801	. 787	400	96730. 4	$5p^4\ ^1D_2$— $6s''\ ^3P_2^\circ$
1034. 655	. 655	10000	96650. 6	$5p^4\ ^3P_2$— $6s'\ ^3D_3^\circ$
1042. 154	. 146	100	95955. 1	$5p'\ ^3P_2$— $5p^5\ ^1P_1^\circ$
1043. 430	. 431	2	95837. 8	$5p\ \ ^1S_0$— $6d\ \ ^3D_1^\circ$
1046. 373	. 373	200	95568. 2	$5p^4\ ^1D_2$— $5d'\ ^3S_1^\circ$
1054. 582	. 571	150	94824. 3	$5p^4\ ^3P_2$— $6s'\ ^3D_1^\circ$
1054. 742	. 738	1500	94809. 9	$5p^4\ ^1D_2$— $5d'\ ^1D_2^\circ$
1064. 981	. 977	60	93898. 4	$5p^4\ ^1D_2$— $5d'\ ^3G_3^\circ$
1066. 273	. 273	250	93784. 6	$5p^4\ ^1D_2$— $5d'\ ^3F_2^\circ$
1067. 341	. 334	2000	93690. 8	$5p^4\ ^3P_2$— $6s'\ ^3D_2^\circ$
1075. 210	. 200	3000	93005. 1	$5p^4\ ^3P_2$— $5d\ \ ^3D_3^\circ$
1082. 540	. 531	400	92375. 3	$5p^4\ ^1D_2$— $6s''\ ^3P_1^\circ$
1085. 405	. 405	700	92131. 5	$5p^4\ ^3P_2$— $5d\ \ ^3D_2^\circ$
1101. 099	. 091	30	90818. 4	$5p^4\ ^1D_2$— $5d'\ ^3D_1^\circ$
1101. 239	. 232	400	90806. 8	$5p^4\ ^3P_1$— $5d'\ ^3P_0^\circ$
1103. 590	. 584	800	90613. 4	$5p^4\ ^3P_1$— $6s'\ ^1D_2^\circ$
1105. 000	4. 993	5000	90497. 7	$5p^4\ ^3P_2$— $5d\ \ ^3D_2^\circ$
1111. 165	. 157	2500	89995. 6	$5p^4\ ^3P_1$— $5d'\ ^3D_2^\circ$
1117. 219	. 219	1500	89508. 0	$5p^4\ ^3P_0$— $5p^5\ ^1P_1^\circ$
1125. 251	. 254	3500	88869. 1	$5p^4\ ^3P_1$— $5p^5\ ^1P_1^\circ$
1131. 504	. 511	2000	88378. 0	$5p^4\ ^3P_0$— $6s'\ ^3D_1^\circ$
1139. 752	. 753	1200	87738. 4	$5p^4\ ^3P_1$— $6s'\ ^3D_1^\circ$
1139. 805	. 808	10000	87734. 3	$5p^4\ ^3P_2$— $5d\ \ ^5D_1^\circ$
1154. 668	. 676	1500	86605. 0	$5p^4\ ^3P_1$— $6s'\ ^3D_2^\circ$
1159. 871	. 879	1000	86216. 5	$5p^4\ ^1D_2$— $5d'\ ^3F_3^\circ$
1160. 562	. 565	10000	86165. 2	$5p^4\ ^3P_2$— $5d\ \ ^5D_2^\circ$
1166. 482	. 480	20000	85727. 9	$5p^4\ ^3P_2$— $5d\ \ ^5D_3^\circ$
1167. 054	. 069	1500	85685. 8	$5p^4\ ^3P_0$— $5d\ \ ^3D_1^\circ$
1171. 007	. 014	50	85396. 6	$5p^4\ ^1S_0$— $5d'\ ^1P_1^\circ$
1175. 841	. 840	5000	85045. 5	$5p^4\ ^3P_1$— $5d\ \ ^3D_1^\circ$
1178. 650	. 649	10000	84842. 8	$5p^4\ ^3P_2$— $6s\ \ ^3S_1^\circ$
1184. 156	. 153	200	84448. 3	$5p^4\ ^1D_2$— $5d'\ ^3D_3^\circ$
1187. 338	. 335	15000	84222. 0	$5p^4\ ^3P_2$— $5p^5\ ^3P_1^\circ$
1190. 853	. 850	10000	83973. 4	$5p^4\ ^1D_2$— $6s'\ ^1D_2^\circ$
1198. 884	. 878	5000	83410. 9	$5p^4\ ^3P_1$— $5d\ \ ^3D_2^\circ$
1199. 677	. 672	1000	83355. 8	$5p^4\ ^1D_2$— $5d'\ ^3D_2^\circ$
1200. 223	. 221	7000	83317. 8	$5p^4\ ^3P_1$— $5p^5\ ^3P_0^\circ$
1205. 931	. 933	2000	82923. 5	$5p^4\ ^1D_2$— $6s'\ ^3D_3^\circ$
1216. 125	. 121	3000	82228. 4	$5p^4\ ^1D_2$— $5p^5\ ^1P_1^\circ$
1220. 887	. 885	20000	81907. 7	$5p^4\ ^3P_2$— $5p^5\ ^3P_2^\circ$
1230. 222	. 221	600	81286. 1	$5p^4\ ^3P_0$— $5d\ \ ^5D_1^\circ$
1233. 069	. 074	100	81098. 5	$5p^4\ ^1D_2$— $6s'\ ^3D_1^\circ$
1234. 063	. 070	20000	81033. 1	$5p^4\ ^3P_2$— $6s\ \ ^5S_2^\circ$
1239. 969	. 970	80	80647. 2	$5p^4\ ^3P_1$— $5d\ \ ^5D_1^\circ$
1250. 559	. 560	700	79964. 2	$5p^4\ ^1D_2$— $6s'\ ^3D_2^\circ$
1264. 580	. 576	20	79077. 6	$5p^4\ ^3P_1$— $5d\ \ ^5D_2^\circ$
1275. 424	. 422	2000	78405. 3	$5p^4\ ^1D_2$— $5d\ \ ^3D_1^\circ$
1275. 596	. 592	1000	78394. 7	$5p^4\ ^3P_0$— $6s\ \ ^3S_1^\circ$
1277. 190	. 186	2500	78296. 9	$5p^4\ ^3P_1$— $5d\ \ ^5D_0^\circ$
1285. 782	. 772	1500	77773. 7	$5p^4\ ^3P_0$— $5p^5\ ^3P_1^\circ$

TABLE 10.1. *Observed lines of* I II—Continued

λ(vac) observed	λ(vac) calculated	Intensity	Observed wavenumber, cm^{-1}	Classification
1286. 084	. 076	4000	77755. 4	$5p^4\ {}^3P_1$— $6s\ {}^3S_1^\circ$
1296. 416	. 425	3000	77135. 7	$5p^4\ {}^3P_1$— $5p^5\ {}^3P_1^\circ$
1302. 580	. 573	150	76770. 7	$5p^4\ {}^1D_2$— $5d\ {}^3D_3^\circ$
1332. 533	. 536	12	75045. 0	$5p^4\ {}^1S_0$— $5d'\ {}^3D_1^\circ$
1336. 517	. 527	20000	74821. 3	$5p^4\ {}^3P_1$— $5p^5\ {}^3P_2^\circ$
1351. 219	. 225	20	74007. 2	$5p'\ {}^1D_2$— $5d\ {}^5D_1^\circ$
1380. 501	. 497	500	72437. 5	$5p^4\ {}^1D_2$— $5d\ {}^5D_2^\circ$
1406. 138	. 159	10	71116. 8	$5p^4\ {}^1D_2$— $6s\ {}^3S_1^\circ$
1418. 539	. 540	25	70495. 1	$5p^4\ {}^1D_2$— $5p^5\ {}^3P_1^\circ$
1466. 673	. 693	1000	68181. 5	$5p^4\ {}^1D_2$— $5p^5\ {}^3P_2^\circ$
1485. 734	. 763	30	67306. 8	$5p^4\ {}^1D_2$— $6s\ {}^5S_2^\circ$
1504. 761	. 788	10	66455. 7	$5p^4\ {}^1S_0$— $5p^5\ {}^1P_1^\circ$
1521. 068		15	65743. 3	
1700. 529		2	58805. 2	
1825. 049	. 059	2	54793. 0	$5p^5\ {}^3P_2^\circ$— $8p\ {}^3P_2$
1826. 705		10	54743. 4	
1828. 550		3	54688. 1	
1828. 729		3	54682. 8	
1859. 466		3	53778. 9	
1961. 837	. 839	2	50972. 6	$5d\ {}^5D_3^\circ$— $8p\ {}^3P_2$
1964. 631	. 636	3	50900. 1	$5d\ {}^3D_2^\circ$— $6f\ {}^3F_2$
1978. 816	. 799	2	50535. 3	$5d\ {}^5D_2^\circ$— $8p\ {}^3P_2$
1981. 360		3	50470. 4	
1990. 944		3	50227. 4	

TABLE 10.1. *Observed lines of* I II—Continued

λ(air)	Intensity	Wave number	Classification	λ(air)	Intensity	Wave number	Classification
2014. 178	1	49632. 00	$5p^5\ {}^3P_0^\circ$— $4f'\ {}^3D_1$	2125. 156	1	47040. 50	
2023. 100	8	49413. 17	$5d\ {}^5D_3^\circ$— $5f\ {}^5F_4$	2132. 921	1	46869. 27	$6s'\ {}^3D_2^\circ$— $4f'\ {}^1P_1$
2024. 580	2	49377. 05	$5d'\ {}^3D_2^\circ$— $1_{2,3}$	2140. 992	2	46692. 61	$6s'\ {}^3D_2^\circ$— $7p'\ {}^3F_3$
2026. 155	1	49338. 67		2141. 338	1*h*	46685. 06	$5d\ {}^3D_3^\circ$— $4f'\ {}^3G_3$
2034. 068	15	49146. 76	$5d\ {}^5D_4^\circ$— $5f\ {}^5F_5$	2143. 876	1	46629. 80	
2035. 812	1	49104. 66	$5d\ {}^5D_4^\circ$— $5f\ {}^5F_4$	2150. 143	3	46493. 90	
2037. 806	2	49056. 62	$5d\ {}^5D_2^\circ$— $5f\ {}^5F_2$	2171. 863	2	46028. 99	
2038. 561	1	49038. 46		2172. 223	5	46021. 36	
2041. 256	4	48973. 72	$5d\ {}^5D_2^\circ$— $5f\ {}^5F_3$	2177. 480	4	45910. 26	$5d\ {}^3D_2^\circ$— $8p\ {}^3P_1$
2048. 816	1	48793. 04	$5d\ {}^5D_1^\circ$— $4f'\ {}^3F_2$	2203. 313	8*h*	45372. 04	
2053. 160	1	48689. 82		2208. 736	1	45260. 65	$6p\ {}^5P_2$— $9d\ {}^5D_3^\circ$
2053. 802	1	48674. 60	$5d\ {}^5D_1^\circ$— $8p\ {}^3P_1$				$5d\ {}^3D_1^\circ$— $4f'\ {}^3P_1$
2060. 167	2	48524. 24		2210. 358	3	45227. 44	$5d\ {}^3D_2^\circ$— $5f\ {}^3F_2$
2091. 300	3	47801. 95		2210. 876	2	45216. 85	
2096. 797	7	47676. 65	$5d'\ {}^3F_4^\circ$— $8f\ {}^3F_3$; $6p\ {}^5P_3^\circ$— $35_{2,3}^\circ$	2211. 135	1	45211. 55	$6s'\ {}^3D_1^\circ$— $4f'\ {}^3D_1$
				2211. 533	1	45203. 42	$6s\ {}^5S_2^\circ$— $7p\ {}^3P_1$
2103. 562	1*h*	47523. 34	$5p^5\ {}^3P_2^\circ$— $6p''\ {}^3D_3$	2217. 279	2	45086. 28	$6s'\ {}^3D_1^\circ$— $7p'\ {}^3F_2$
2105. 120	1	47488. 17	$5d'\ {}^3G_4^\circ$— $4_{3,4}$	2227. 385	1	44881. 74	$5d\ {}^3D_1^\circ$— $4f'\ {}^3D_2$
2114. 745	6	47272. 06		2229. 246	30	44844. 28	$5d\ {}^3D_2^\circ$— $5f\ {}^3F_3$
2116. 970	1	47222. 38	$5p^5\ {}^3P_1^\circ$— $6p''\ {}^1D_2$	2230. 393	2	44821. 22	
2117. 767	1	47204. 61		2231. 371	1	44801. 58	
2118. 690	1*h*	47184. 05		2236. 618	1	44696. 48	$6p\ {}^5P_2$—$10s\ {}^5S_2^\circ$
2119. 858	2*h*	47158. 06	$5d\ {}^3D_3^\circ$— $7p'\ {}^1F_3$	2236. 762	1	44693. 60	$6p\ {}^3P_2$—$10d\ {}^3D_3^\circ$
2122. 086	8	47108. 55		2239. 433	3	44640. 30	$5d\ {}^3D_2^\circ$— $5f\ {}^5F_3$
2122. 252	1	47104. 87		2239. 714	1*h*	44634. 70	
2122. 372	1	47102. 20	$5d\ {}^3D_3^\circ$— $7p'\ {}^3F_4$	2244. 666	5	44536. 24	

TABLE 10.1. *Observed lines of* I II—Continued

λ(air)	Intensity	Wave number	Classification
2246. 675	2*h*	44496. 42	$5p^5\ {}^3P_2^\circ$— $7p\ {}^3P_2$
2255. 206	1*h*	44328. 12	$5p^5\ {}^3P_2^\circ$— $7p\ {}^3P_1$
2256. 674	3*h*	44299. 28	
2260. 035	20	44233. 41	$5p^5\ {}^1P_1^\circ$— $7p'\ {}^1D_2$
2261. 700	4	44200. 85	
2262. 032	2*h*	44194. 36	$6s\ {}^5S_2^\circ$— $4f\ {}^3F_3$
2262. 533	1*h*	44184. 58	
2267. 855	2*h*	44080. 90	$5p^5\ {}^1P_1^\circ$— $4f'\ {}^3D_1$
2274. 322	3	43955. 57	$5p^5\ {}^1P_1^\circ$— $7p'\ {}^3F_2$
2276. 270	1*h*	43917. 95	
2286. 564	4	43720. 26	$6s\ {}^3S_1^\circ$— $6p''\ {}^3S_1$
2287. 060	1	43710. 77	$5d\ {}^5D_1^\circ$— $6p''\ {}^1D_2$
2287. 903	15	43694. 67	$5d\ {}^3D_3^\circ$— $8p\ {}^3P_2$
2288. 569	1	43681. 96	
2288. 693	2	43679. 59	
2291. 767	2	43621. 01	$6p\ {}^5P_3$— $10s\ {}^5S_2^\circ$
2293. 226	25	43593. 26	$5d\ {}^3D_1^\circ$— $5f\ {}^3F_2$
2302. 945	1	43409. 30	
2310. 139	5	43274. 13	
2310. 551	2	43266. 41	$5d\ {}^5D_2^\circ$— $6p''\ {}^3D_3$
2311. 205	1*h*	43254. 17	$5p^5\ {}^3P_2^\circ$— $6p''\ {}^3P_1$
2314. 761	2	43187. 73	$6p\ {}^3P_1$— $9d\ {}^3D_2^\circ$
2315. 638	4	43171. 38	
2319. 150	1	43106. 00	$5d'\ {}^3D_2^\circ$— $7p'\ {}^1D_2$
2319. 968	2	43090. 81	$5d\ {}^3D_3^\circ$— $4f'\ {}^3F_3$
2320. 329	10	43084. 10	$5d\ {}^3D_3^\circ$— $4f'\ {}^3G_4$
2322. 532	2*c*	43043. 24	
2327. 395	1	42953. 31	$5d'\ {}^3D_2^\circ$— $4f'\ {}^3D_1$
2331. 650	3*c*	42874. 93	
2333. 076	1	42848. 73	
2334. 203	20	42828. 04	$5d'\ {}^3D_2^\circ$— $7p'\ {}^3F_2$
2335. 502	10*c*	42804. 22	$5p^5\ {}^3P_2^\circ$— $4f\ {}^5F_3$
2336. 188	1	42791. 66	$6s'\ {}^1D_2^\circ$— $4f'\ {}^1D_2$
2339. 831	1	42725. 04	
2340. 072	1	42720. 64	
2340. 277	3	42716. 90	$6s'\ {}^3D_2^\circ$— $8p\ {}^3P_1$
2340. 778	3	42707. 75	$5d'\ {}^3F_2^\circ$— $10_{2,3}$
2341. 947	1	42686. 44	$6s'\ {}^1D_2^\circ$— $4f'\ {}^1F_3$
2342. 402	50	42678. 15	$5d\ {}^3D_3^\circ$— $5f\ {}^3F_4$
2343. 067	3	42666. 03	$5d'\ {}^3P_0^\circ$— $4f'\ {}^1P_1$
2344. 303	1	42643. 54	
2345. 301	4	42625. 40	$5d'\ {}^3G_3^\circ$— $11_{3,4}$
2346. 266	15	42607. 86	$5d'\ {}^3D_2^\circ$— $4f'\ {}^3G_3$
2347. 044	4	42593. 74	$5d'\ {}^3G_3^\circ$— $10_{2,3}$
2348. 485	5	42567. 61	$6s'\ {}^3D_1^\circ$— $4f'\ {}^3P_1$
2349. 180	1	42555. 02	
2350. 115	1	42538. 09	$6p\ {}^3P_1$—$10s\ {}^3S_1^\circ$
2352. 860	3	42488. 46	$6s'\ {}^1D_2^\circ$— $7p'\ {}^1D_2$
2354. 286	8	42462. 73	$6s'\ {}^1D_2^\circ$— $7p'\ {}^1F_3$
2357. 473	3	42405. 33	$6s'\ {}^3D_2^\circ$— $4f'\ {}^3F_3$
2359. 965	2	42360. 56	$5d'\ {}^3P_0^\circ$— $7p'\ {}^1P_1$
2360. 474	7	42351. 42	$6p\ {}^3P_2$— $9d\ {}^3D_3^\circ$
2361. 174	10	42338. 87	$6s\ {}^3S_1^\circ$— $7p\ {}^3P_0$
2361. 303	4	42336. 56	$5d\ {}^3D_3^\circ$— $5f\ {}^3F_3$
2362. 399	4	42316. 92	
2362. 946	1	42307. 12	$6p\ {}^5P_2$— $8d\ {}^3D_3^\circ$
2363. 303	1	42300. 73	$6p\ {}^5P_1$— $8d\ {}^3D_1^\circ$
2367. 224	3	42230. 67	$5d\ {}^3D_1^\circ$— $6p''\ {}^1S_0$
2367. 930	1	42218. 08	
2368. 332	7*c*	42210. 92	
2369. 574	20	42188. 79	
2369. 960	10	42181. 92	$5p^5\ {}^3P_1^\circ$— $7p\ {}^3P_2$
2371. 622	1	42152. 36	$5d'\ {}^3F_4^\circ$— $6f\ {}^3F_4$
2372. 192	15	42142. 24	$5d'\ {}^3P_0^\circ$— $4f'\ {}^3D_1$
2372. 596	3	42135. 06	$5d\ {}^3D_3^\circ$— $5f\ {}^5F_4$
2378. 034	10	42038. 72	$5d\ {}^5D_1^\circ$— $6p''\ {}^3P_2$
2379. 463	5	42013. 47	$5d'\ {}^3D_3^\circ$— $7p'\ {}^1D_2$
2380. 761	1	41990. 57	$6s'\ {}^1D_2^\circ$— $4f'\ {}^3G_3$
2380. 917	2	41987. 82	$5d'\ {}^3D_3^\circ$— $7p'\ {}^1F_3$
2384. 069	20	41932. 31	$5d'\ {}^3D_3^\circ$— $7p'\ {}^3F_4$
2395. 244	25*c*	41736. 69	
2397. 260	25	41701. 59	$6s'\ {}^3D_1^\circ$— $4f'\ {}^3F_2$
2397. 753	3	41693. 02	$5d'\ {}^3F_3^\circ$— $7_{2,3}$
2398. 225	10*d*	41684. 81	$5p^5\ {}^1P_1^\circ$— $4f'\ {}^3P_2$
2398. 370	4	41682. 29	$5d'\ {}^1D_2^\circ$— $10_{2,3}$
2399. 209	4	41667. 72	$6p\ {}^5P_1$— $8d\ {}^5D_1^\circ$
2400. 166	6	41651. 11	$6p\ {}^5P_1$— $8d\ {}^5D_2^\circ$
2400. 588	3	41643. 79	$6p\ {}^5P_1$— $8d\ {}^5D_0^\circ$
2400. 974	1	41637. 09	$6p\ {}^3P_0$— $8s'\ {}^3D_1^\circ$
2403. 863	1	41587. 06	$5d'\ {}^3F_3^\circ$— $6f\ {}^3F_4$
2404. 090	20	41583. 13	$6s'\ {}^3D_1^\circ$— $8p\ {}^3P_1$
2404. 926	2	41568. 67	$6p\ {}^3P_2$—$10s\ {}^3S_1^\circ$
2405. 384	3*d*	41560. 76	$6p\ {}^5P_2$— $8d\ {}^5D_1^\circ$
2405. 887	20	41552. 07	$6p\ {}^5P_2$— $8d\ {}^5D_3^\circ$
2406. 393	10	41543. 33	$5d'\ {}^3D_3^\circ$— $4f''\ {}^1G_4$ $6p\ {}^5P_2$— $8d\ {}^5D_2^\circ$
2408. 008	100	41515. 48	$5d'\ {}^3D_3^\circ$— $4f''\ {}^3G_3$
2411. 967	1	41447. 34	$6s'\ {}^3D_2^\circ$— $5f\ {}^5F_3$
2412. 570	40*d*	41436. 98	
2414. 154	1	41409. 79	
2415. 117	3	41393. 28	
2415. 732	2	41382. 74	
2417. 853	3	41346. 44	$5d'\ {}^3G_3^\circ$— $6_{2,3,4}$
2419. 176	100	41323. 83	$5d'\ {}^3D_3^\circ$— $4f'\ {}^3F_4$
2434. 830	4	41058. 18	
2437. 087	1	41020. 15	$5d'\ {}^3G_3^\circ$— $4_{3,4}$
2437. 710	5	41009. 67	$5d'\ {}^3F_4^\circ$— $4f'\ {}^1F_3$
2437. 901	20	41006. 46	$5d'\ {}^3F_4^\circ$— $7p'\ {}^3F_3$
2438. 285	25	41000. 00	$5p^5\ {}^3P_1^\circ$— $6p''\ {}^3D_2$
2441. 484	3	40946. 28	$5d\ {}^3D_3^\circ$— $6p''\ {}^1D_2$
2441. 872	2	40939. 78	$5p^5\ {}^3P_1^\circ$— $6p''\ {}^3P_1$
2444. 220	40	40900. 45	$6s'\ {}^3D_1^\circ$— $5f\ {}^3F_2$
2446. 516	3	40862. 07	$5p^5\ {}^3P_1^\circ$— $7p\ {}^5P_2$
2448. 496	30	40829. 03	$5d\ {}^5D_1^\circ$— $6p''\ {}^3S_1$
2451. 075	4	40786. 08	$5d'\ {}^3F_4^\circ$— $7p'\ {}^1F_3$
2451. 194	5	40784. 10	$5p^5\ {}^3P_1^\circ$— $6p''\ {}^3P_0$
2453. 952	5	40738. 26	$6p\ {}^5P_1$— $9s\ {}^5S_2^\circ$
2454. 434	2	40730. 26	
2454. 533	30	40728. 62	$5p^5\ {}^3P_1^\circ$— $7p\ {}^5P_1$
2454. 958	3	40721. 57	
2456. 046	1*h*	40703. 53	
2457. 367	2	40681. 65	$6s\ {}^3S_1^\circ$— $4f\ {}^5F_2$
2457. 703	6	40676. 09	$5d\ {}^5D_3^\circ$— $7p\ {}^3P_2$
2458. 239	5*h*	40667. 22	$5d'\ {}^1D_2^\circ$— $7_{2,3}$
2459. 005	2	40654. 55	
2460. 444	8	40630. 78	$6p\ {}^5P_2$— $9s\ {}^5S_2^\circ$
2461. 126	30	40619. 52	$5p^5\ {}^3P_1^\circ$— $4f\ {}^5F_1$
2464. 085	15*c*	40570. 74	
2464. 684	80	40560. 89	$5p^5\ {}^3P_1^\circ$— $4f\ {}^5F_2$
2466. 249	1	40535. 15	
2469. 167	20	40487. 25	$6p\ {}^5P_3$— $8d\ {}^5D_4^\circ$

TABLE 10.1. *Observed lines of* I II—Continued

λ(air)	Intensity	Wave number	Classification
2469.824	6	40476.48	$6p\ {}^5P_3 - 8d\ {}^5D^\circ_3$
2470.369	1	40467.55	$6p\ {}^5P_3 - 8d\ {}^5D^\circ_2$
2471.295	25*d*	40452.39	
2471.664	2	40446.35	
2473.272	2	40420.06	$5p^5\ {}^3P^\circ_0 - 6p''\ {}^1P_1$
2475.766	1	40379.34	$6s\ {}^3S^\circ_1 - 6p''\ {}^3D_2$
2476.213	2	40372.05	$5d'\ {}^3G^\circ_4 - 6f\ {}^3F_4$
2476.738	1	40363.50	
2478.073	5*c*	40341.75	$5d'\ {}^3F^\circ_4 - 4f'\ {}^1G_4$
2478.994	2	40326.76	$5d\ {}^3D^\circ_2 - 6p''\ {}^1P_1$
2479.467	3	40319.07	$6s\ {}^3S^\circ_1 - 6p''\ {}^3P_1$
2479.797	6	40313.71	$5d'\ {}^3F^\circ_4 - 4f'\ {}^3G_3$
2480.029	2	40309.94	
2480.486	1	40302.51	
2481.103	25	40292.49	$5d'\ {}^1D^\circ_2 - 5_{2,3}$
2481.289	1	40289.47	
2481.689	2	40282.98	
2482.058	25	40276.98	$5d'\ {}^3D^\circ_2 - 7p'\ {}^3D_3$
2483.261	1	40257.48	
2483.520	3*c*	40253.28	$5p^5\ {}^1P^\circ_1 - 7p'\ {}^3D_1$
2483.951	1	40246.29	$5d'\ {}^3F^\circ_3 - 7p'\ {}^1D_2$
2484.246	1	40241.52	$6s\ {}^3S^\circ_1 - 7p\ {}^5P_2$
2484.387	2	40239.23	$5d\ {}^5D^\circ_2 - 7p\ {}^5P_2$
2487.027	10	40196.52	
2489.065	10*c*	40163.61	$6s\ {}^3S^\circ_1 - 6p''\ {}^3P_0$
2491.638	50	40122.14	$5d'\ {}^3F^\circ_4 - 4f'\ {}^3F_4$
2492.514	8	40108.04	$6s\ {}^3S^\circ_1 - 7p\ {}^5P_1$
2493.458	3	40092.86	
2494.738	100	40072.29	$5d'\ {}^3F^\circ_4 - 4f'\ {}^3G_5$
2496.123	2*c*	40050.05	$6s'\ {}^3D^\circ_3 - 8p\ {}^3P_2$
2497.984	1	40020.22	
2499.316	30	39998.89	$6s\ {}^3S^\circ_1 - 4f\ {}^5F_1$
2502.981	70	39940.32	$6s\ {}^3S^\circ_1 - 4f\ {}^5F_2$
2503.560	10	39931.09	$5d'\ {}^3D^\circ_2 - 4f'\ {}^3D_2$ $5d'\ {}^3G^\circ_4 - 6f\ {}^5F_5$
2506.999	6	39876.32	$6s'\ {}^3D^\circ_3 - 4f'\ {}^3F_2$ $6p\ {}^3P_1 - 8d\ {}^3D^\circ_1$
2508.941	1	39845.45	
2510.612	8	39818.94	$6p\ {}^3P_1 - 8d\ {}^3D^\circ_2$
2513.199	20	39777.95	$5d\ {}^5D^\circ_0 - 6p''\ {}^3P_1$
2514.617	10	39755.52	$5d\ {}^5D^\circ_3 - 7p\ {}^5P_3$
2515.022	10	39749.12	$5d\ {}^5D^\circ_3 - 4f\ {}^3F_4$
2519.494	5	39678.57	
2519.898	1	39672.21	$6s'\ {}^1D^\circ_2 - 7p'\ {}^3P_2$
2521.989	1	39639.32	
2525.206	3	39588.82	
2525.988	4	39576.57	$5d'\ {}^3D^\circ_2 - 7p'\ {}^3P_1$
2526.612	8	39566.79	$5d\ {}^5D^\circ_0 - 7p\ {}^5P_1$
2527.350	10	39555.24	$6p\ {}^5P_3 - 9s\ {}^5S^\circ_2$
2530.974	50	39498.61	$5d'\ {}^3P^\circ_0 - 4f'\ {}^3P_1$
2533.372	5	39461.22	$5d'\ {}^3F^\circ_2 - 2_{2,3}$
2533.605	100	39457.59	$5d\ {}^5D^\circ_0 - 4f\ {}^5F_1$
2534.272	200	39447.21	$5d\ {}^5D^\circ_4 - 7p\ {}^5P_3$
2534.505	40	39443.58	$5d'\ {}^3D^\circ_2 - 4f'\ {}^3F_2$
2535.708	2	39424.87	
2535.846	2	39422.73	$5d'\ {}^3F^\circ_2 - 8f\ {}^5F_3$
2536.994	4	39404.89	$5d'\ {}^1D^\circ_2 - 3_{2,3}$
2537.583	2	39395.74	
2540.126	40	39356.31	$5d\ {}^5D^\circ_3 - 7p\ {}^5P_2$
2542.140	60*d*	39325.13	$5d'\ {}^3D^\circ_2 - 8p\ {}^3P_1$
2542.557	3	39318.68	$5d\ {}^5D^\circ_2 - 7p\ {}^5P_3$
2542.976	1	39312.20	$5d\ {}^3D^\circ_1 - 6p''\ {}^1D_2$
2545.416	20	39274.52	$5d\ {}^3D^\circ_2 - 6p''\ {}^3P_2$
2548.342	15*c*	39229.43	$5d'\ {}^3G^\circ_4 - 4f'\ {}^1F_3$
2548.556	25*c*	39226.13	$5d'\ {}^3G^\circ_4 - 7p'\ {}^3F_3$ $6p\ {}^3P_1 - 8d\ {}^5D^\circ_2$
2550.426	4	39197.37	$5d'\ {}^3D^\circ_3 - 7p'\ {}^3P_2$
2551.258	6	39184.59	$5d'\ {}^3D^\circ_3 - 7p'\ {}^3D_3$
2552.448	1	39166.32	
2557.699	50	39085.92	$5d'\ {}^3D^\circ_2 - 4f'\ {}^3D_3$
2559.258	25	39062.11	$5d\ {}^5D^\circ_2 - 4f\ {}^3F_3$
2559.571	10	39057.34	$5d\ {}^5D^\circ_2 - 6p''\ {}^3D_2$
2559.708	20	39055.25	$5d\ {}^5D^\circ_3 - 4f\ {}^5F_2$
2561.132	5*c*	39033.53	$6s'\ {}^3D^\circ_3 - 5f\ {}^3F_4$
2561.977	30	39020.66	$6p\ {}^3P_2 - 8d\ {}^3D^\circ_3$
2562.451	300*c*	39013.44	$5d'\ {}^3D^\circ_2 - 4f'\ {}^3F_3$
2562.701	2	39009.64	
2562.945	2	39005.92	$5d'\ {}^3G^\circ_4 - 7p'\ {}^1F_3$
2563.350	10*c*	38999.76	$6s'\ {}^1D^\circ_2 - 8p\ {}^3P_2$
2563.518	15	38997.20	$5d\ {}^5D^\circ_3 - 6p''\ {}^3P_1$
2564.386	200	38984.00	$5d\ {}^5D^\circ_3 - 4f\ {}^5F_3$
2566.242	1000	38955.81	$5d\ {}^5D^\circ_3 - 4f\ {}^5F_4$
2566.604	2	38950.32	$5d'\ {}^3G^\circ_4 - 7p'\ {}^3F_4$
2566.712	3	38948.68	$5d'\ {}^3F^\circ_2 - 1_{2,3}$
2567.529	3	38936.29	
2568.642	8	38919.42	$5d\ {}^5D^\circ_2 - 7p\ {}^5P_2$
2572.956	5	38854.16	
2573.253	5	38849.68	$6p\ {}^3P_2 - 8d\ {}^3D^\circ_2$
2573.992	5	38838.53	$5d'\ {}^3D^\circ_3 - 4f'\ {}^3D_2$
2574.256	1	38834.54	$5d'\ {}^3G^\circ_3 - 1_{2,3}$
2574.817	1	38826.08	$6s'\ {}^1D^\circ_2 - 4f'\ {}^3F_2$
2577.473	1	38786.08	$5d\ {}^5D^\circ_2 - 7p\ {}^5P_1$
2577.652	2	38783.38	
2580.145	5*c*	38745.91	$6s''\ {}^3P^\circ_2 - 7_{2,3}$
2582.794	2000	38706.18	$5d\ {}^5D^\circ_4 - 4f\ {}^5F_5$
2583.710	2	38692.46	$5d\ {}^3D^\circ_1 - 6p''\ {}^1P_1$
2584.746	10	38676.95	$5d\ {}^5D^\circ_2 - 4f\ {}^5F_1$
2584.837	8	38675.59	$5d\ {}^5D^\circ_4 - 4f\ {}^5F_3$
2585.202	5	38670.12	$5d\ {}^5D^\circ_1 - 7p\ {}^3P_2$
2585.407	2*c*	38667.06	
2586.721	100	38647.42	$5d\ {}^5D^\circ_4 - 4f\ {}^5F_4$
2587.052	4*c*	38642.48	$5d'\ {}^3D^\circ_2 - 5f\ {}^3F_2$
2588.132	8*d*	38626.35	$5d'\ {}^3D^\circ_3 - 4f'\ {}^3H_4$
2588.670	150	38618.32	$5d\ {}^5D^\circ_2 - 4f\ {}^5F_2$
2592.010	2*h*	38568.56	$6p'\ {}^3F_2 - 4l_{1,2,3}$
2592.490	3*c*	38561.42	$5d'\ {}^3G^\circ_4 - 4f'\ {}^1G_4$
2593.458	300	38547.03	$5d\ {}^5D^\circ_2 - 4f\ {}^5F_3$
2594.376	4	38533.39	$5d'\ {}^3G^\circ_4 - 4f'\ {}^3G_3$
2594.954	20*c*	38524.81	$5d'\ {}^3D^\circ_3 - 8p\ {}^3P_2$
2595.518	8	38516.44	$6p\ {}^3P_0 - 8d\ {}^3D^\circ_1$
2596.063	4*h*	38508.35	$6s'\ {}^1D^\circ_2 - 7p'\ {}^3D_1$
2596.500	6	38501.87	$5d\ {}^5D^\circ_1 - 7p\ {}^3P_1$
2597.878	6	38481.45	$6p\ {}^2P_1 - 9s\ {}^3S^\circ_1$

TABLE 10.1. *Observed lines of* I II—Continued

λ(air)	Intensity	Wave number	Classification	λ(air)	Intensity	Wave number	Classification
2598. 397	4	38473. 77		2694. 056	25	37107. 74	$5d\ {}^5D_1^\circ$— $4f\ {}^5F_1$
2598. 765	4	38468. 32	$6s'\ {}^1D_2^\circ$— $4f''\ {}^3D_3$	2694. 593	1*c*	37100. 35	
2600. 757	1	38438. 86	$5d\ {}^3D_3^\circ$— $6p''\ {}^1D_2$	2696. 702	6	37071. 33	$5d'\ {}^3F_3^\circ$— $4f'\ {}^3D_2$
2600. 989	2	38435. 43		2697. 375	2	37062. 08	$5d'\ {}^1G_4^\circ$— $7p'\ {}^1F_3$
2602. 890	10*c*	38407. 36	$5p^5\ {}^1P_1^\circ$— $6p''\ {}^1S_0$	2698. 319	50	37049. 12	$5d\ {}^5D_1^\circ$— $4f\ {}^5F_2$
2603. 658	8*h*	38396. 03	$6s'\ {}^1D_2^\circ$— $4f'\ {}^3F_3$	2700. 419	3	37020. 31	$6p\ {}^3P_2$— $6d'\ 14_3^\circ$
2605. 340	3	38371. 24	$6s''\ {}^3P_2^\circ$— $5_{2,3}$	2701. 431	50	37006. 44	$5d'\ {}^1G_4^\circ$— $7p'\ {}^3F_4$
2606. 703	2	38351. 18	$5d'\ {}^3D_3^\circ$— $4f'\ {}^3F_2$	2704. 257	1	36967. 77	
2607. 347	30	38341. 71	$5d'\ {}^3G_4^\circ$— $4f'\ {}^3F_4$	2704. 424	2*c*	36965. 49	
2608. 442	1	38325. 62		2704. 522	20*c*	36964. 15	
2609. 175	1	38314. 85	$5d'\ {}^3P_0^\circ$— $7p'\ {}^3D_1$	2706. 320	3*c*	36939. 59	
2610. 740	150	38291. 88	$5d'\ {}^3G_4^\circ$— $4f'\ {}^3G_5$	2707. 400	3	36924. 86	$5d'\ {}^3D_1^\circ$— $6f\ {}^3F_2$
2612. 524	1	38265. 74	$6p\ {}^3P_2$— $8d\ {}^5D_3^\circ$	2708. 159	50	36914. 51	
2612. 963	20	38259. 31	$5d'\ {}^3D_3^\circ$— $5f\ {}^3F_4$	2709. 708	1	36893. 41	
2619. 890	30	38158. 16	$5p^5\ {}^3P_0^\circ$— $6p''\ {}^3S_1$	2710. 206	1	36886. 63	$5d'\ {}^1F_3^\circ$— $12_{1,2}$?
2621. 362	4*c*	38136. 73	$5d\ {}^5D_0^\circ$— $6p''\ {}^3D_1$	2710. 857	1	36877. 77	
2621. 858	3	38129. 52		2712. 236	150	36859. 02	$5d'\ {}^3F_3^\circ$— $4f'\ {}^3H_4$
2626. 309	2	38064. 90	$5d\ {}^3D_2^\circ$— $6p''\ {}^3S_1$	2713. 108	1	36847. 18	$6p'\ {}^3F_3^\circ$— 39_4°
2626. 974	8	38055. 26	$5d'\ {}^3D_3^\circ$— $5f\ {}^5F_3$	2715. 784	4	36810. 87	
2627. 334	8	38050. 05	$6s\ {}^5S_2^\circ$— $6p'\ {}^1D_2$	2719. 726	20	36757. 52	$5d'\ {}^3F_3^\circ$— $8p\ {}^3P_2$
2631. 983	15	37982. 84	$5d'\ {}^3F_4^\circ$— $7p'\ {}^3D_3$	2722. 542	2*c*	36719. 50	$6p'\ {}^3D_2$— 38_1°
2632. 756	1	37971. 69	$5d'\ {}^1G_4^\circ$— $6f\ {}^5F_4$	2723. 041	40*c*	36712. 77	$5d'\ {}^3F_4^\circ$— $4f'\ {}^3G_4$
2635. 298	1	37935. 07		2726. 649	2	36664. 20	
2636. 270	20*w*	37921. 08	$5d'\ {}^3D_3^\circ$— $4f'\ {}^3F_3$	2728. 749	6	36635. 98	
2636. 729	150*w*	37914. 48	$5d'\ {}^3D_3^\circ$— $4f'\ {}^3G_4$	2730. 124	500	36617. 53	$5d'\ {}^1G_4^\circ$— $4f'\ {}^1G_4$
2638. 644	1	37886. 96	$6p\ {}^3P_2$— $6d'\ 15_1^\circ$	2731. 788	20	36595. 23	$6s''\ {}^3P_2^\circ$— $8f\ {}^3F_3$
2641. 302	20	37848. 84					$5d''\ {}^3D_3^\circ$— $11_{3,4}$
2645. 375	2	37790. 57	$5d\ {}^5D_1^\circ$— $4f\ {}^3F_2$	2732. 200	5	36589. 71	$5d'\ {}^1G_4^\circ$— $4f'\ {}^3G_3$
2651. 301	1	37706. 11		2732. 735	10	36582. 55	$6p'\ {}^3D_1$—$11s\ {}^3S_1^\circ$
2651. 874	1*h*	37697. 96	$5d'\ {}^3F_3^\circ$— $4f'\ {}^3P_2$	2734. 137	3	36563. 79	$6p'\ {}^3F_4$— $50_{3,4}^\circ$
2652. 636	1*h*	37687. 13	$6p'\ {}^3D_2$— $41_{1,2,3}^\circ$	2734. 877	1	36553. 90	$6p'\ {}^1P_1$— 46_2°
2655. 829	10*c*	37641. 82	$6s'\ {}^1D_2^\circ$— $5f\ {}^3F_3$	2736. 410	1	36533. 42	$6p'\ {}^1P_1$— $45_{1,2}^\circ$
2660. 396	1	37577. 21		2736. 938	1	36526. 37	
2665. 014	5	37512. 10	$6p\ {}^3P_2$— $9s\ {}^3S_1^\circ$	2744. 533	20	36425. 30	$5d\ {}^3D_3^\circ$— $6p''\ {}^3D_3$
2665. 284	20	37508. 30	$5d'\ {}^3D_3^\circ$— $5f\ {}^3F_4$	2746. 590	8	36398. 02	$5d'\ {}^1G_4^\circ$— $4f'\ {}^3F_4$
2666. 141	1	37496. 24	$6p\ {}^3P_0$— $6d'\ 15_1^\circ$	2747. 502	4	36385. 94	
2667. 049	3	37483. 48	$6s''\ {}^3P_2^\circ$— $3_{2,3}$	2749. 133	1*c*	36364. 35	$6p\ {}^3P_2$— $6d'\ 12_1^\circ$
2667. 624	1	37475. 40		2749. 884	2*c*	36354. 42	
2670. 304	4*d*	37437. 79	$6s'\ {}^1D_2^\circ$— $5f\ {}^5F_3$	2750. 362	2*c*	36348. 10	$5d'\ {}^1G_4^\circ$— $4f'\ {}^3G_5$
2670. 854	4	37430. 08	$5d'\ {}^3F_3^\circ$— $7p'\ {}^3P_2$	2753. 502	10*d*	36306. 66	$5d'\ {}^3F_4^\circ$— $5f\ {}^3F_4$
2671. 008	5	37427. 92	$5d\ {}^5D_1^\circ$— $6p''\ {}^3P_1$	2754. 745	1	36290. 28	
2671. 239	6	37424. 69	$5d'\ {}^3F_4^\circ$— $4f''\ {}^3H_4$	2755. 128	5	36285. 23	$6p'\ {}^3D_1$— 21_1°
2671. 770	1	37417. 25	$5d'\ {}^3F_3^\circ$— $7p'\ {}^3D_3$	2757. 213	7	36257. 79	$6p\ {}^5P_2$— $7d\ {}^3D_3^\circ$
2674. 795	150	37374. 94	$5d'\ {}^3F_4^\circ$— $4f'\ {}^3H_5$	2758. 702	1	36238. 22	
2676. 150	3*c*	37356. 01	$5d\ {}^5D_2^\circ$— $6p''\ {}^3D_1$	2759. 624	8	36226. 12	$5d'\ {}^3F_3^\circ$— $4f'\ {}^3D_3$
2676. 562	10	37350. 26	$5d\ {}^5D_1^\circ$— $7p\ {}^5P_2$	2761. 431	15	36202. 41	$5d'\ {}^3G_4^\circ$— $7p'\ {}^3D_3$
2676. 983	1	37344. 39	$6p\ {}^3P_2$— $9s\ {}^5S_2^\circ$	2761. 930	1*c*	36195. 87	
2681. 203	10	37285. 62	$5d'\ {}^1G_4^\circ$— $4f'\ {}^1F_3$	2764. 142	4*c*	36166. 91	$6p'\ {}^1F_3$— $44_{2,3}^\circ$
2681. 597	10	37280. 14	$5d''\ {}^1D_2^\circ$— $13_{2,3}$	2764. 250	2	36165. 50	$5d'\ {}^3P_2^\circ$— $13_{2,3}$
2682. 160	15	37272. 31	$5d\ {}^5D_1^\circ$— $6p''\ {}^3P_0$	2765. 149	20	36153. 74	$5d'\ {}^3F_3^\circ$— $4f'\ {}^3F_3$
2683. 392	3	37255. 20	$5d'\ {}^1F_3^\circ$— $13_{2,3}$	2765. 660	200	36147. 06	$5d'\ {}^3F_3^\circ$— $4f'\ {}^3G_4$
2685. 160	2*c*	37230. 67		2769. 734	2*c*	36093. 89	
2686. 154	20	37216. 90	$5d\ {}^5D_1^\circ$— $7p\ {}^5P_1$	2770. 695	20	36081. 37	$6s'\ {}^3D_2^\circ$— $6p''\ {}^3P_2$
2687. 164	1*c*	37202. 91		2775. 306	1*h*	36021. 43	
2688. 536	5	37183. 92		2775. 613	1	36017. 45	
2688. 981	200*c*	37177. 77		2775. 856	4	36014. 29	$5d'\ {}^3D_1^\circ$— $4f'\ {}^1P_1$
2689. 192	30*c*	37174. 85	$5p^5\ {}^3P_2^\circ$— $6p'\ {}^1D_2$	2776. 241	2	36009. 30	$6p'\ {}^3F_2$—$10d\ {}^3D_3^\circ$
2689. 722	1*c*	37167. 53		2776. 990	4*c*	35999. 59	$6s'\ {}^3D_1^\circ$— $6p''\ {}^1P_1$
2691. 652	1	37140. 88		2781. 129	10*d*	35946. 01	$5d'\ {}^3D_1^\circ$— $4f'\ {}^1D_2$
2693. 040	1*h*	37121. 74	$6p\ {}^3P_0$— $9s\ {}^3S_1^\circ$	2782. 793	1*h*	35924. 52	

TABLE 10.1. *Observed lines of* I II—Continued

λ(air)	Intensity	Wave number	Classification
2783. 290	8*c*	35918. 11	
2784. 243	10	35905. 81	$5d\ ^3D^o_2$— $7p\ ^3P_2$
2788. 236	1*c*	35854. 40	
2788. 696	1*h*	35848. 48	
2788. 911	5*c*	35845. 72	$6p'\ ^1F_3$— 42^o_3
2789. 056	10	35843. 85	$6p'\ ^3F_2$—$10d\ ^3D^o_2$
2789. 601	30*c*	35836. 85	$5d''\ ^1D^o_2$— $7_{2,3}$
2790. 060	10	35830. 96	$6p'\ ^3D_1$— $20^o_{1,2}$
2790. 573	1*c*	35824. 37	
2790. 994	1*h*	35818. 97	
2791. 524	2*c*	35812. 17	
2792. 724	6	35796. 78	$5d'\ ^3P^o_2$— $12_{1,2}$
2793. 933	6*c*	35781. 29	
2797. 089	10:	35740. 92	$5d'\ ^3F^o_3$— $5f\ ^3F_4$
2797. 367	20*c*	35737. 37	
2799. 632	6*c*	35708. 46	
2804. 766	8	35643. 10	$5d'\ ^3D^o_1$— $7p'\ ^1D_2$
2805. 564	4	35632. 96	$6p\ ^5P_2$— $7d\ ^3D^o_2$
2808. 594	200	35594. 52	$5d'\ ^3G^o_4$— $4f'\ ^3H_5$
2809. 789	10	35579. 38	$5d'\ ^1F^o_3$— $6_{2,3,4}$
2811. 927	1*c*	35552. 33	
2812. 210	4*c*	35548. 75	$5d''\ ^3D^o_3$— $7_{2,3}$
2812. 692	2	35542. 66	
2815. 118	3	35512. 03	
2816. 821	15	35490. 56	$5d'\ ^3D^o_1$— $4f'\ ^3D_1$
2817. 090	1*c*	35487. 18	$6p'\ ^1F_3$—$12d\ ^3D^o_3$
2817. 909	1	35476. 86	
2819. 086	25	35462. 05	$5d''\ ^1D^o_2$— $5_{2,3}$
2823. 629	1*c*	35405. 00	$6p'\ ^3F_3$— 33^o_3
2824. 060	10	35399. 60	$5d'\ ^3F^o_3$— $5f\ ^3F_3$
2825. 461	4	35382. 04	$5d'\ ^1P^o_1$— $12_{1,2}$
2826. 004	3	35375. 24	
2826. 814	30	35365. 11	$5d'\ ^3D^o_1$— $7p'\ ^3F_2$
2829. 338	1	35333. 56	
2829. 837	8*c*	35327. 33	$6p\ ^5P_1$— $7d\ ^5D^o_1$
2830. 110	30	35323. 92	$6p'\ ^1F_3$— 40^o_3
2830. 735	100	35316. 12	$5d''\ ^3D^o_3$— $6_{2,3,4}$
2832. 494	1	35294. 19	
2832. 736	3	35291. 18	$6p'\ ^3F_2$—$11s\ ^3S^o_1$
2833. 495	20	35281. 73	$6p\ ^5P_1$— $7d\ ^5D^o_0$
2836. 768	10	35241. 02	
2838. 482	1*h*	35219. 74	$6p\ ^5P_2$— $7d\ ^5D^o_1$
2840. 236	6	35197. 99	$5d'\ ^3F^o_3$— $5f\ ^5F_4$
2840. 438	6	35195. 49	$5d'\ ^3F^o_3$— $5f\ ^5F_3$
2840. 970	25	35188. 90	
2841. 444	20	35183. 03	$6p'\ ^3F_2$— $24^o_{1,2}$
2841. 920	1	35177. 14	
2842. 175	7	35173. 98	$5d''\ ^3D^o_3$— $5_{2,3}$
2844. 121	25	35149. 92	$6p\ ^5P_1$— $7d\ ^5D^o_2$
2846. 986	50	35114. 54	$6p\ ^5P_2$— $7d\ ^5D^o_3$
2847. 442	20	35108. 92	$6p'\ ^1F_3$— 39^o_3
2848. 272	1	35098. 69	$6p'\ ^3D_3$— 46^o_3
2849. 671	10	35081. 46	
2851. 170	1*c*	35063. 02	$6p'\ ^3D_2$— 30^o_3
2851. 723	7	35056. 22	$6p'\ ^3D_3$— $44^o_{2,3}$
2852. 060	20*c*	35052. 08	$6s\ ^5S^o_2$— $6p'\ ^3P_1$
2852. 290	8	35049. 25	$5d\ ^3D^o_1$— $7p\ ^3P_0$
2852. 852	25	35042. 35	$6p\ ^5P_3$— $7d\ ^5D^o_2$
2854. 168	80	35026. 19	$5d\ ^3D^o_2$— $4f\ ^3F_2$
2854. 964	4	35016. 42	$6p\ ^5P_1$— $6d'\ 4^o_0$
2856. 798	8	34993. 95	$6p'\ ^3F_2$— 21^o_1
2857. 132	15*c*	34989. 86	$5d''\ ^3D^o_3$— $4_{3,4}$
2857. 515	35	34985. 17	$5d\ ^3D^o_2$— $7p\ ^5P_3$
2859. 376	20	34962. 40	$6p'\ ^3D_2$—$10d\ ^3D^o_2$
2860. 602	35	34947. 41	$6s'\ ^3D^o_1$— $6p''\ ^3P_2$
2861. 290	3	34939. 01	$5d'\ ^3G^o_4$— $4f'\ ^3F_3$
2861. 838	40	34932. 32	$5d'\ ^3G^o_4$— $4f'\ ^3G_4$
2865. 184	6	34891. 53	$6p\ ^3P_2$— $6d'\ 9^o_3$
2865. 458	4	34888. 19	$6p'\ ^3F_3$—$10d\ ^3D^o_3$
2865. 766	5*d*	34884. 44	$5d'\ ^3P^o_2$— $8_{1,2}$
2867. 021	20*c*	34869. 17	$5p^5\ ^1P^o_1$— $6p''\ ^1P_1$
2867. 704	1*c*	34860. 87	
2867. 970	2*c*	34857. 64	
2869. 767	7	34835. 81	$6s''\ ^3P^o_0$— $4f'\ ^3D_1$
2870. 635	2	34825. 28	$6p'\ ^3D_1$— $9d\ ^3D^o_2$
2871. 416	1	34815. 80	
2872. 788	7	34799. 18	$6p\ ^3P_1$— $6d'\ 6^o_{1,2}$
2873. 208	5*c*	34794. 09	$6s'\ ^3D^o_3$— $6p''\ ^1D_2$
2873. 667	1	34788. 53	
2874. 281	1	34781. 10	
2874. 550	1	34777. 85	$6p'\ ^3P_2$— $47^o_{1,2}$
2875. 738	2	34763. 48	
2876. 262	5	34757. 15	$5p^5\ ^3P^o_0$— $6p''\ ^3P_1$
2877. 212	2*c*	34745. 67	
2878. 632	1500	34728. 54	$5d\ ^3D^o_2$— $4f\ ^3F_3$
2879. 021	30	34723. 84	$5d\ ^2D^o_2$— $6p''\ ^3D_2$
2879. 172	8*h*	34722. 02	
2883. 019	60	34675. 69	$6s\ ^5S^o_2$— $6p'\ ^3P_2$
2883. 440	10	34670. 63	$6p'\ ^3D_1$— $8s'\ ^3D^o_2$
2883. 996	1	34663. 94	$6p'\ ^3D_2$— 26^o_3
2885. 949	1	34640. 49	
2886. 446	10	34634. 52	$6p'\ ^3D_1$— $8s'\ ^3D^o_1$
2886. 961	3	34628. 35	$6p\ ^5P_2$— $6d'\ 2^o_3$
2888. 024	1	34615. 60	$6p'\ ^3P_2$— $44^o_{2,3}$
2888. 874	2	34605. 42	$6p'\ ^3D_2$— $25^o_{1,2}$
2890. 137	1	34590. 29	
2890. 498	10	34585. 97	$5d\ ^3D^o_2$— $7p\ ^5P_2$
2891. 462	7	34574. 44	$5d''\ ^1D^o_2$— $3_{2,3}$
2892. 878	3	34557. 52	$6p\ ^5P_3$— $7d\ ^3D^o_2$
2893. 566	1*c*	34549. 30	
2893. 847	7	34545. 95	$5p^5\ ^3P^o_0$— $7p\ ^5P_1$
2894. 114	10	34542. 76	$6p\ ^3P_1$— $7d\ ^3D^o_1$
2894. 377	8	34539. 62	$6p'\ ^3F_2$— $20^o_{1,2}$
2895. 354	3	34527. 97	$5d'\ ^3F^o_2$— $7p'\ ^3D_2$
2895. 498	15	34526. 25	$5d'\ ^3G^o_4$— $5f\ ^3F_4$
2896. 813	10	34510. 58	$6p'\ ^3P_2$— $43^o_{1,2}$
2897. 909	10	34497. 53	
2900. 253	15*c*	34469. 65	$5d'\ ^1P^o_1$— $8_{1,2}$
2903. 015	10	34436. 86	$5p^5\ ^3P^o_0$— $4f\ ^5F_1$
2903. 488	1	34431. 25	$6p'\ ^3F_3$— 26^o_3
2906. 004	2	34401. 44	$6p'\ ^3P_1$— $47^o_{1,2}$
2909. 390	5*c*	34361. 40	$5d'\ ^3D^o_2$— $6p''\ ^1D_2$
2910. 567	8	34347. 51	$5d'\ ^3P^o_2$— $5_{2,3}$
2910. 906	1	34343. 51	$5d\ ^3D^o_2$— $4f\ ^5F_1$
2914. 458	20	34301. 65	$6p'\ ^3D_2$— $24^o_{1,2}$
2915. 061	15*c*	34294. 56	$6p'\ ^3P_2$— 42^o_2
2915. 762	3*c*	34286. 31	$5d''\ ^3D^o_3$— $3_{2,3}$
2915. 881	10	34284. 91	$5d\ ^3D^o_2$— $4f\ ^5F_2$
2916. 146	4	34281. 80	$6p'\ ^3P_1$— 46^o_2
2917. 740	8	34263. 07	$6p'\ ^3P_0$— 38^o_1

TABLE 10.1. *Observed lines of* I II—Continued

λ(air)	Intensity	Wave number	Classification	λ(air)	Intensity	Wave number	Classification
2917. 911	2	34261. 06	$6p'\ ^3P_1$— $45^\circ_{1,2}$	2990. 484	20*c*	33429. 65	$6p'\ ^1P_1$— 30°_2
2919. 715	6*c*	34239. 90	$6s\ ^2S^\circ_{\frac{1}{2}}$— $6p'\ ^1D_2$	2992. 391	2*c*	33408. 35	
2920. 122	10	34235. 12	$6s\ ^5S^\circ_2$— $6p'\ ^3D_3$	2993. 866	1000	33391. 89	$5d\ ^3D^\circ_1$— $4f\ ^3F_2$
2921. 134	6*c*	34223. 26	$6p\ ^5P_2$— $7s'\ ^3D^\circ_3$	2994. 991	20	33379. 35	$6p'\ ^3F_2$— $8s'\ ^3D^\circ_2$
2921. 686	8*c*	34216. 80		2996. 734	100*c*	33359. 94	$5p^5\ ^3P^\circ_2$— $6p'\ ^3D_3$
2921. 982	50	34213. 33	$6p'\ ^3D_3$— 40°_2	2997. 189	25*c*	33354. 87	$5d\ ^5D^\circ_3$— $6p'\ ^1D_2$
2925. 087	80*c*	34177. 02	$5p^5\ ^3P^\circ_2$— $6p'\ ^3P_1$	2998. 229	10*d*	33343. 30	$6p'\ ^3F_2$— $8s'\ ^3D^\circ_1$
2926. 769	3*c*	34157. 38		2999. 498	20*c*	33329. 20	$6p'\ ^1P_1$—$10d\ ^3D^\circ_2$
2927. 388	2*c*	34150. 15	$6p'\ ^1F_3$— 36°_2	3000. 694	40	33315. 91	$6p\ ^3P_1$— $7d\ ^3D^\circ_2$
2927. 664	1*c*	34146. 93		3004. 858	8	33269. 75	$6p\ ^3P_1$— $6d'\ 5^\circ_1$
2927. 850	30	34144. 76		3007. 318	15*c*	33242. 53	
2928. 758	4*c*	34134. 18	$6p'\ ^3P_1$— $43^\circ_{1,2}$	3010. 480	7*c*	33207. 62	$6p'\ ^1P_1$— 29°_1
2929. 112	60	34130. 05		3012. 712	20	33183. 02	$6p\ ^3P_0$— $7d\ ^3D^\circ_1$
2930. 627	2	34112. 41	$6p'\ ^3D_2$— 21°_1	3018. 042	30*c*	33124. 42	$6s\ ^5S^\circ_2$— $6p'\ ^1F_3$
2931. 720	200	34099. 69	$6p\ ^5P_3$— $7d\ ^5D^\circ_4$	3018. 249	20*c*	33122. 14	$6s'\ ^3D^\circ_3$— $6p''\ ^3P_2$
2932. 911	10*c*	34085. 85	$6s''\ ^3P^\circ_1$— $7p'\ ^1D_2$	3018. 826	15*c*	33115. 81	$5p^5\ ^3P^\circ_2$— $6p''\ ^3D_1$
2933. 394	1	34080. 24	$6p\ ^5P_1$— $6d'\ 1^\circ_2$	3020. 751	35*c*	33094. 71	$5d'\ ^3D^\circ_1$— $4f'\ ^3P_2$
2933. 638	5	34077. 40	$6p\ ^5P_1$— $8s\ ^3S^\circ_1$	3020. 950	7*d*	33092. 53	$5d''\ ^1D^\circ_2$— $1_{2,3}$
2934. 963	25	34062. 02	$6p'\ ^3F_3$— $24^\circ_{1,2}$	3021. 214	100	33089. 64	$5d\ ^3D^\circ_1$— $6p''\ ^3D_2$
2936. 954	40	34038. 93	$6p\ ^5P_3$— $7d\ ^5D^\circ_3$	3023. 211	1*h*	33067. 78	$5d'\ ^1G^\circ_4$— $4f'\ ^3D_3$
2938. 155	6	34025. 01	$5d'\ ^3G^\circ_4$— $5f\ ^5F_5$	3024. 948	15*c*	33048. 80	$5d'\ ^3F^\circ_2$— $4f'\ ^1P_1$
2940. 471	40	33998. 22	$6p'\ ^3D_3$— 39°_4	3031. 204	30*c*	32980. 59	$5d'\ ^3F^\circ_2$— $4f'\ ^1D_2$
2941. 778	4	33983. 11	$5d'\ ^3G^\circ_4$— $5f\ ^5F_4$	3032. 039	80*c*	32971. 51	$6p\ ^3P_2$— $7d\ ^3D^\circ_3$
2942. 429	60	33975. 59		3033. 856	35	32951. 76	$5d\ ^3D^\circ_1$— $7p\ ^5P_2$
2942. 923	10	33969. 89	$6p\ ^5P_2$— $8s\ ^3S^\circ_1$	3035. 807	40	32930. 59	$5d'\ ^3P^\circ_0$— $6p''\ ^1P_1$
2943. 192	15	33966. 79	$6p\ ^5P_3$— $7d\ ^5D^\circ_2$	3036. 973	4*c*	32917. 94	$5d\ ^5D^\circ_2$— $6p'\ ^1D_2$
2943. 267	1	33965. 92		3040. 888	15*c*	32875. 56	$5d'\ ^3F^\circ_2$— $4f'\ ^1F_3$
2943. 842	2	33959. 29	$5d'\ ^3F^\circ_2$— $6f\ ^3F_2$	3041. 207	1*c*	32872. 12	$5d'\ ^3F^\circ_2$— $7p'\ ^3F_3$
2945. 857	10*c*	33936. 06	$6p'\ ^3P_2$—$12d\ ^3D^\circ_3$	3041. 735	15*c*	32866. 41	$5d'\ ^3G^\circ_3$— $4f'\ ^1D_2$
2946. 081	8*c*	33933. 48	$6s''\ ^3P^\circ_1$— $4f'\ ^3D_1$	3042. 243	3*d*	32860. 92	$5d'\ ^1D^\circ_2$— $6f\ ^3F_3$
2947. 055	10	33922. 26	$6p'\ ^1F_3$— $35^\circ_{2,3}$	3043. 530	8*d*	32847. 03	
2947. 927	40	33912. 23	$6p'\ ^3F_4$— 39°_4	3045. 391	30	32826. 96	$5d'\ ^3D^\circ_1$— $7p'\ ^3P_2$
2948. 642	25	33904. 01	$5d'\ ^3G^\circ_3$— $6f\ ^3F_4$	3049. 691	80*c*	32780. 67	$6s'\ ^3D^\circ_3$— $6p''\ ^3D_3$
2950. 152	6	33886. 66	$5d'\ ^3F^\circ_2$— $6f\ ^3F_3$	3051. 188	2	32764. 59	$6p'\ ^1P_1$—$11s\ ^5S^\circ_2$
2953. 773	5	33845. 12	$5d'\ ^3G^\circ_3$— $6f\ ^3F_2$	3051. 792	40*c*	32758. 11	$5d'\ ^3G^\circ_3$— $7p'\ ^3F_3$
2955. 086	20*c*	33830. 08		3053. 072	3	32744. 37	$5d'\ ^3S^\circ_1$— $7p'\ ^3D_2$
2955. 795	1*h*	33821. 96		3053. 177	25	32743. 25	$5d'\ ^3F^\circ_2$— $7p'\ ^1P_1$
2956. 236	100*c*	33816. 92	$5p^5\ ^1P^\circ_1$— $6p''\ ^3P_2$	3055. 365	50	32719. 80	$6p'\ ^3D_3$— 34°_2
2957. 008	5*c*	33808. 09	$6s''\ ^3P^\circ_1$— $7p'\ ^3F_2$	3056. 005	90*c*	32712. 95	$6s'\ ^3D^\circ_3$— $7p\ ^3P_2$
2957. 658	200*c*	33800. 66	$5p^5\ ^3P^\circ_2$— $6p'\ ^3P_2$	3059. 322	50	32677. 48	$5d'\ ^3F^\circ_2$— $7p'\ ^1D_2$
2959. 796	15	33776. 25		3061. 716	20	32651. 93	$5d'\ ^3F^\circ_2$— $7p'\ ^1F_3$
2960. 113	1	33772. 63	$6p'\ ^3P_2$— 40°_3	3064. 603	2	32621. 17	
2962. 632	10*c*	33743. 92	$6s'\ ^1D^\circ_2$— $6p''\ ^1D_2$	3065. 902	60*c*	32607. 35	$5p^5\ ^1P^\circ_1$— $6p''\ ^3S_1$
2962. 819	1	33741. 78	$5d'\ ^3D^\circ_2$— $6p''\ ^1P_1$	3067. 346	1	32592. 00	
2967. 350	5	33690. 27	$5d'\ ^3D^\circ_1$— $4f'\ ^3P_0$	3070. 042	35	32563. 38	$5d'\ ^3G^\circ_3$— $7p'\ ^1D_2$
2969. 413	25	33666. 86	$6p'\ ^1F_3$— 33°_3	3070. 705	30*c*	32556. 35	$6p'\ ^3D_3$— 33°_3
2970. 694	7	33652. 34		3071. 046	2	32552. 74	
2970. 819	30*c*	33650. 93	$5d'\ ^1G^\circ_4$— $4f'\ ^2H_5$	3072. 456	80	32537. 80	$5d'\ ^3G^\circ_3$— $7p'\ ^1F_3$
2971. 895	2	33638. 74		3073. 658	7*c*	32525. 07	$5d'\ ^3F^\circ_2$— $4f'\ ^3D_1$
2973. 766	40	33617. 58	$6p\ ^5P_1$— $8s\ ^5S^\circ_2$	3074. 132	3	32520. 06	
2974. 880	20*c*	33604. 99	$5d''\ ^1D^\circ_2$— $2_{2,3}$	3074. 255	8	32518. 76	$5d\ ^3D^\circ_3$— $4f\ ^3F_2$
2977. 656	4	33573. 66	$6p\ ^3P_2$— $7d\ ^3D^\circ_1$	3075. 678	4	32503. 71	
2978. 287	4*c*	33566. 55	$5d''\ ^1D^\circ_2$— $8f\ ^5F_3$	3076. 210	20	32498. 09	$6p'\ ^3D_2$— $8s'\ ^3D^\circ_2$
2979. 044	25*c*	33558. 02		3077. 708	40*c*	32482. 28	$5d'\ ^3G^\circ_3$— $7p'\ ^3F_4$
2979. 487	2	33553. 03	$6p\ ^5P_3$— $6d'\ 2^\circ_3$	3078. 754	5000	32471. 24	$5d\ ^3D^\circ_3$— $4f\ ^3F_4$
2980. 322	7*c*	33543. 63	$6p'\ ^1P_1$— 31°_0	3079. 641	20	32461. 89	$6p'\ ^3D_2$— $8s'\ ^3D^\circ_1$
2981. 162	2*c*	33534. 18		3082. 229	60	32434. 63	$6p\ ^5P_3$— $8s\ ^5S^\circ_2$
2983. 312	50	33510. 02	$6p\ ^5P_2$— $8s\ ^5S^\circ_2$	3083. 315	4	32423. 21	
2986. 011	4	33479. 73		3084. 278	6*c*	32413. 09	$6p'\ ^3F_3$— $9d\ ^3D^\circ_2$
2987. 789	6	33459. 80	$5d'\ ^3P^\circ_2$— $3_{2,3}$	3085. 509	60*c*	32400. 16	

TABLE 10.1. *Observed lines of* I II—Continued

λ(air)	Intensity	Wave number	Classification
3086. 446	3	32390. 32	
3086. 989	4	32384. 62	$6p'\ {}^3P_0$— 29°_1
3089. 652	20*d*	32356. 71	$6s'\ {}^3D^\circ_1$— $7p\ {}^3P_0$
3090. 476	10*c*	32348. 08	$5d'\ {}^3D^\circ_2$— $6p''\ {}^3D_3$
3090. 609	25	32346. 69	$6p\ {}^3P_2$— $7d\ {}^3D^\circ_2$
3092. 698	15*c*	32324. 84	
3094. 035	1	32310. 88	
3096. 384	15*c*	32286. 36	
3096. 459	10	32285. 58	$5d'\ {}^3G^\circ_3$— $7p'\ {}^3F_2$
3097. 075	1*h*	32279. 16	$6p'\ {}^3P_2$— 34°_2
3099. 064	35	32258. 45	$6p'\ {}^3F_3$— $8s'\ {}^3D^\circ_2$
3099. 925	60*c*	32249. 49	$5p^5\ {}^3P^\circ_2$— $6p'\ {}^1F_3$
3101. 067	3*c*	32237. 61	
3102. 663	60	32221. 03	$5d\ {}^3D^\circ_3$— $4f\ {}^3F_3$
3104. 171	10	32205. 38	$5d'\ {}^3P^\circ_1$— $12^\circ_{1,2}$
3106. 665	40	32179. 52	$5d'\ {}^3F^\circ_2$— $4f'\ {}^3G_3$
3112. 838	30*c*	32115. 71	$6p'\ {}^3P_2$— 33°_3
3113. 026	10	32113. 77	$5d'\ {}^3D^\circ_1$— $7p'\ {}^3P_1$
3116. 441	8	32078. 58	$5d\ {}^3D^\circ_3$— $7p\ {}^5P_2$
3117. 071	30*c*	32072. 10	$6s'\ {}^1D^\circ_2$— $6p''\ {}^3P_2$
3117. 718	40*c*	32065. 44	$5d'\ {}^3G^\circ_3$— $4f'\ {}^3G_3$
3119. 878	5	32043. 24	
3121. 648	15*c*	32025. 08	$6p'\ {}^1P_1$— $20^\circ_{1,2}$
3125. 976	50	31980. 74	$5d'\ {}^3D^\circ_1$— $4f'\ {}^3F_2$
3128. 507	35*c*	31954. 87	$5d'\ {}^1D^\circ_2$— $4f'\ {}^1D_2$
3128. 638	10	31953. 53	$6p'\ {}^3P_0$—$11s\ {}^3S^\circ_1$
3132. 910	25*c*	31909. 96	$6p\ {}^3P_0$— $6d'\ 5^\circ_1$
3133. 397	50*c*	31905. 00	$5p^5\ {}^3P^\circ_2$— $6p'\ {}^1P_1$
3133. 618	10*c*	31902. 75	$6p'\ {}^3P_1$— 34°_2
3136. 473	100*d*	31873. 71	$5d'\ {}^3G^\circ_3$— $4f'\ {}^3F_4$
3137. 604	60	31862. 22	$5d'\ {}^3D^\circ_1$— $8p\ {}^3P_1$
3138. 830	90*c*	31849. 78	$5d'\ {}^1D^\circ_2$— $4f'\ {}^1F_3$
3140. 946	8	31828. 32	$6p\ {}^3P_2$— $7d\ {}^5D^\circ_3$
3144. 212	1	31795. 26	
3144. 997	1	31787. 33	
3145. 346	2	31783. 80	
3148. 089	8	31756. 10	$6p\ {}^3P_2$— $7d\ {}^5D^\circ_2$
3149. 636	8	31740. 51	
3151. 915	2	31717. 56	$5d\ {}^1D^\circ_2$— $7p'\ {}^1P_1$
3153. 078	5*c*	31705. 86	$5d\ {}^3D^\circ_3$— $4f\ {}^5F_3$
3155. 573	1	31680. 79	$6p'\ {}^1F_3$— $20^\circ_{1,2}$
3155. 864	10	31677. 87	$5d\ {}^3D^\circ_3$— $4f\ {}^5F_4$
3157. 337	3	31663. 09	$5d'\ {}^3D^\circ_1$— $7p'\ {}^3D_1$
3158. 080	20	31655. 64	$6p\ {}^3P_1$— $6d'\ 1^\circ_2$
3158. 357	20	31652. 87	$6p\ {}^3P_1$— $8s\ {}^3S^\circ_1$
3158. 466	40	31651. 78	$5d'\ {}^1D^\circ_2$— $7p'\ {}^1D_2$
3159. 175	1	31644. 67	
3161. 027	200	31626. 13	$5d'\ {}^1D^\circ_2$— $7p'\ {}^1F_3$
3163. 935	40*c*	31597. 07	$5d'\ {}^3D^\circ_3$— $6p''\ {}^3P_2$
3169. 882	15*c*	31537. 79	$6s''\ {}^3P^\circ_1$— $4f'\ {}^3P_2$
3173. 509	3*c*	31501. 75	
3173. 752	5*c*	31499. 34	$5d'\ {}^1D^\circ_2$— $4f'\ {}^3D_1$
3175. 066	1000	31486. 30	$5p^5\ {}^3P^\circ_1$— $6p'\ {}^3P_2$
3176. 630	15*c*	31470. 80	$6s'\ {}^3D^\circ_2$— $6p''\ {}^3P_1$
3177. 828	10	31458. 94	$6s''\ {}^3P^\circ_0$— $7p'\ {}^3P_1$
3178. 064	1	31456. 60	$6p'\ {}^3D_1$— $8d\ {}^3D^\circ_2$
3180. 575	10*c*	31431. 76	$5d''\ {}^3P^\circ_2$— $8_{1,2}$
3182. 602	2	31411. 75	
3182. 709	10*d*	31410. 69	$6s'\ {}^3D^\circ_1$— $7p\ {}^3P_1$
3184. 489	4*c*	31393. 13	$6s'\ {}^3D^\circ_2$— $7p\ {}^5P_2$
3186. 440	20	31373. 91	$5d'\ {}^1D^\circ_2$— $7p'\ {}^3F_2$
3189. 680	20	31342. 05	$6p\ {}^3P_2$— $6d'\ 2^\circ_3$
3194. 682	35	31292. 98	$5d'\ {}^3P^\circ_1$— $8_{1,2}$
3195. 610	6*c*	31283. 89	$6p'\ {}^1D_2$— 46°_2
3197. 074	40*d*	31269. 56	$5d''\ {}^3P^\circ_2$— $7_{2,3}$
3197. 514	2*c*	31265. 26	$5d'\ {}^3S^\circ_1$— $4f'\ {}^1P_1$
3197. 711	2*c*	31263. 33	$6p'\ {}^1D_2$— $45^\circ_{1,2}$
3198. 069	2*c*	31259. 83	
3199. 891	60	31242. 04	$6s\ {}^3S^\circ_1$— $6p'\ {}^3P_1$
3201. 547	3*c*	31225. 88	$5p^5\ {}^1P^\circ_1$— $7p\ {}^3P_0$
3204. 517	5*c*	31196. 94	$5d'\ {}^3S^\circ_1$— $4f'\ {}^1D_2$
3204. 894	2	31193. 27	$6p\ {}^3P_1$— $8s\ {}^5S^\circ_2$
3208. 946	25	31153. 88	$5d'\ {}^1D^\circ_2$— $4f'\ {}^3G_3$
3209. 664	30*c*	31146. 91	$6s\ {}^5S^\circ_2$— $6p'\ {}^3D_2$
3221. 493	3	31032. 55	$5d'\ {}^3S^\circ_1$— $7p'\ {}^3P_0$
3229. 081	4	30959. 63	$5d'\ {}^3S^\circ_1$— $7p'\ {}^1P_1$
3231. 433	2*c*	30937. 09	$6p\ {}^3P_2$— $7s'\ {}^3D^\circ_3$
3235. 951	5	30893. 90	$5d'\ {}^3S^\circ_1$— $7p'\ {}^1D_2$
3238. 909	25*c*	30865. 69	$6s\ {}^3S^\circ_1$— $6p'\ {}^3P_2$
3239. 245	20*c*	30862. 48	$6s'\ {}^1D^\circ_2$— $6p''\ {}^3S_1$
3252. 008	3	30741. 36	$5d'\ {}^3S^\circ_1$— $4f'\ {}^3D_1$
3256. 460	100*c*	30699. 34	$6s'\ {}^3D^\circ_1$— $4f\ {}^3F_2$
3257. 814	2	30686. 58	
3258. 125	20	30683. 65	$6p\ {}^3P_2$— $8s\ {}^3S^\circ_1$
3265. 309	1	30616. 15	$5d'\ {}^3S^\circ_1$— $7p'\ {}^3F_2$
3267. 320	5*c*	30597. 30	$6s''\ {}^3P^\circ_1$— $8p\ {}^3P_2$
3270. 440	4	30568. 12	
3271. 534	1	30557. 89	
3276. 536	30*c*	30511. 24	$5p^5\ {}^3P^\circ_2$— $6p'\ {}^3F_3$
3278. 418	1*d*	30493. 73	$6p'\ {}^3D_1$— $6d'\ 15^\circ_1$
3279. 256	2*c*	30485. 94	
3288. 860	100*c*	30396. 92	$6s'\ {}^3D^\circ_1$— $6p''\ {}^3D_2$
3296. 368	3*c*	30327. 68	$5d'\ {}^3P^\circ_2$— $7f\ {}^3F_3$
3300. 133	10	30293. 09	$6p\ {}^3P_0$— $8s\ {}^3S^\circ_1$
3301. 538	20*c*	30280. 20	$5p^5\ {}^1P^\circ_1$— $7p\ {}^3P_1$
3302. 457	150*c*	30271. 77	$5p^5\ {}^3P^\circ_2$— $6p'\ {}^3D_2$
3303. 841	15	30259. 09	$6s'\ {}^3D^\circ_1$— $7p\ {}^5P_2$
3307. 701	10	30223. 78	$6p\ {}^3P_2$— $8s\ {}^5S^\circ_2$
3309. 502	1	30207. 33	
3312. 374	10*d*	30181. 14	$6s'\ {}^3D^\circ_1$— $6p''\ {}^3P_0$
3313. 825	1	30167. 93	
3314. 478	3	30161. 98	
3315. 326	2*c*	30154. 27	
3318. 088	40	30129. 17	$5d'\ {}^3F^\circ_2$— $4f'\ {}^3P_2$ $6p'\ {}^3P_2$— $20^\circ_{1,2}$
3319. 210	2	30118. 98	$6p'\ {}^3D_1$— $9s\ {}^3S^\circ_1$
3321. 099	1	30101. 85	
3321. 641	1	30096. 94	
3323. 700	2	30078. 30	$6s''\ {}^1P^\circ_1$— $7p'\ {}^3D_2$
3326. 405	50*c*	30053. 84	$5d'\ {}^3F^\circ_4$— $6p''\ {}^3D_3$
3327. 256	1*c*	30046. 15	
3330. 708	2*c*	30015. 01	$5d'\ {}^3G^\circ_3$— $4f'\ {}^3P_2$
3331. 585	6	30007. 11	$5d''\ {}^3P^\circ_2$— $3_{2,3}$
3331. 754	8	30005. 59	$6p'\ {}^3P_0$— $8s'\ {}^3D^\circ_1$
3334. 536	2*c*	29980. 56	$5d\ {}^5D^\circ_3$— $6p'\ {}^3P_2$
3340. 351	3*c*	29928. 37	$6s''\ {}^3P^\circ_2$— $4f'\ {}^1F_3$
3341. 289	100	29919. 97	$5d\ {}^5D^\circ_2$— $6p'\ {}^3P_1$
3345. 342	25*c*	29883. 72	$5d''\ {}^3D^\circ_2$— $7_{2,3}$
3345. 607	3*c*	29881. 35	$5d'\ {}^3F^\circ_2$— $4f'\ {}^3P_1$
3346. 219	2*c*	29875. 89	
3347. 857	40*c*	29861. 27	$5d'\ {}^3F^\circ_2$— $7p'\ {}^3P_2$

TABLE 10.1. *Observed lines of* I II—Continued

λ(air)	Intensity	Wave number	Classification	λ(air)	Intensity	Wave number	Classification
3349. 286	20	29848. 53	$5d'\ ^3F^o_2$— $7p'\ ^3D_3$	3464. 540	4c	28855. 60	$5d'\ ^1D^o_2$— $4f'\ ^3P_1$
3351. 394	30	29829. 76	$5d'\ ^3F^o_3$— $6p''\ ^3P_2$	3466. 953	10	28835. 51	$5d'\ ^1D^o_2$— $7p'\ ^3P_2$
3352. 823	10c	29817. 04	$5d'\ ^3D^o_1$— $6p''\ ^1S_0$	3467. 261	5c	28832. 95	$6s'\ ^3D^o_3$— $7p\ ^3P_3$
3352. 928	2	29816. 11	$6p'\ ^1D_2$— 38^o_1	3468. 046	30c	28826. 43	$6s'\ ^3D^o_3$— $4f\ ^3F_4$
3355. 531	300	29792. 98	$6s\ ^3S^o_1$— $6p'\ ^3P_0$	3468. 486	20	28822. 77	$5d'\ ^1D^o_2$— $7p'\ ^3D_3$
3359. 961	150c	29753. 70	$6s'\ ^3D^o_3$— $7p\ ^3P_2$	3469. 342	1	28815. 66	
3360. 699	8c	29747. 17	$5d'\ ^3G^o_3$— $7p'\ ^3P_2$	3470. 131	6	28809. 11	
3362. 137	7	29734. 44	$5d'\ ^3G^o_3$— $7p'\ ^3D_3$	3478. 279	3c	28741. 62	
3362. 598	20c	29730. 37	$6s''\ ^3P^o_2$— $7p'\ ^1D_2$	3481. 569	1	28714. 46	
3363. 367	2	29723. 57		3482. 917	1	28703. 35	$6s'\ ^1D^o_2$— $7p\ ^3P_2$
3365. 500	20c	29704. 73	$6s''\ ^3P^o_2$— $7p'\ ^1F_3$	3483. 706	5	28696. 85	
3366. 575	7d	29695. 25		3483. 894	60c	28695. 30	$6s'\ ^3D^o_1$— $6p''\ ^3D_1$
3374. 457	100c	29625. 89	$5d\ ^5D^o_3$— $6p'\ ^3F_4$	3488. 509	15	28657. 34	$5d'\ ^3F^o_2$— $4f'\ ^3D_3$
3378. 475	6c	29590. 66	$5p^5\ ^3P^o_1$— $6p'\ ^1P_1$	3489. 100	2	28652. 49	
3380. 983	30c	29568. 71	$5p^5\ ^1P^o_1$— $4f\ ^3F_2$	3489. 561	4	28648. 70	
3382. 711	2	29553. 60		3490. 488	1	28641. 09	
3383. 858	80c	29543. 58	$5d\ ^5D^o_2$— $6p'\ ^3P_2$	3491. 273	1	28634. 65	
3386. 377	4c	29521. 61	$5d'\ ^1S^o_0$— $4f'\ ^1P_1$	3492. 916	4	28621. 18	$5d''\ ^3D^o_2$— $3_{2,3}$
3390. 214	15c	29488. 20	$5d'\ ^3F^o_3$— $6p''\ ^3D_3$	3495. 624	1c	28599. 01	$6s''\ ^1P^o_1$— $4f'\ ^1P_1$
3391. 360	7c	29478. 23	$7s\ ^3S^o_1$— $8_{1,2}$	3496. 408	5	28592. 60	$6p'\ ^3P_1$— $8s'\ ^3D^o_2$
3394. 192	7c	29453. 64		3497. 406	300c	28584. 44	$5d\ ^3D^o_2$— $6p'\ ^1D_2$
3399. 537	8	29407. 33		3498. 372	2	28576. 55	
3400. 316	5	29400. 59		3498. 500	1	28575. 50	
3401. 500	50c	29390. 36	$5p^5\ ^3P^o_2$— $6p'\ ^3F_2$	3498. 985	25c	28571. 54	$6s'\ ^3D^o_3$— $6p''\ ^3D_2$
3402. 587	4c	29380. 97		3500. 824	2	28556. 53	$6p'\ ^3P_1$— $8s'\ ^3D^o_1$
3409. 138	2c	29324. 52		3502. 457	2	28543. 22	$5d'\ ^3G^o_3$— $4f'\ ^3D_3$
3409. 692	7c	29319. 75		3503. 459	35c	28535. 06	$6s'\ ^1D^o_2$— $7p\ ^3P_1$
3409. 938	30c	29317. 64	$5d\ ^5D^o_4$— $6p'\ ^3F_4$	3503. 996	30c	28530. 68	$6s''\ ^1P^o_1$— $4f'\ ^1D_2$
3411. 173	1	29307. 02		3504. 729	1c	28524. 72	
3415. 911	30c	29266. 37	$5p^5\ ^1P^o_1$— $6p''\ ^3D_2$	3510. 630	10	28476. 77	$5d'\ ^1D^o_2$— $4f'\ ^3D_2$
3416. 759	5	29259. 11		3511. 357	20	28470. 88	$5d'\ ^3G^o_3$— $4f'\ ^3F_3$
3417. 606	5	29251. 86		3512. 177	100	28464. 23	$5d'\ ^3G^o_3$— $4f'\ ^3G_4$
3421. 805	7	29215. 96	$5d'\ ^1S^o_0$— $7p'\ ^1P_1$	3513. 304	2	28455. 10	
3421. 987	3	29214. 41		3513. 971	2	28449. 70	
3422. 948	20c	29206. 21	$5p^5\ ^1P^o_1$— $6p''\ ^3P_1$	3514. 319	1	28446. 88	$7s\ ^5S^o_2$— $8f\ ^3F_3$
3424. 993	250c	29188. 77	$5d'\ ^3F^o_2$— $8p\ ^3P_2$	3514. 757	2	28443. 34	
3426. 461	20	29176. 26	$5d'\ ^3G^o_3$— $4f'\ ^3H_4$	3515. 021	15	28441. 20	$5d'\ ^3D^o_2$— $4f\ ^3F_2$
3429. 784	7d	29148. 00	$5d'\ ^3F^o_2$— $7p'\ ^3P_1$	3515. 661	3	28436. 02	
3432. 080	25c	29128. 50	$5p^5\ ^1P^o_1$— $7p\ ^5P_2$	3516. 504	50c	28429. 20	$5d\ ^5D^o_3$— $6p'\ ^1F_3$
3433. 277	4c	29118. 34	$6s''\ ^3P^o_1$— $5f\ ^5F_2$	3517. 822	3h	28418. 55	$5d'\ ^3G^o_3$— $8p\ ^5P_2$?
3435. 093	80c	29102. 95	$5d\ ^5D^o_2$— $6p'\ ^3D_3$	3518. 688	1	28411. 56	
3436. 712	3	29089. 24		3519. 105	3	28408. 19	
3438. 434	20w	29074. 67	$5d'\ ^3G^o_3$— $8p\ ^3P_2$	3520. 089	5c	28400. 25	$5d'\ ^3D^o_2$— $7p\ ^5P_2$
3438. 792	3	29071. 65		3522. 007	2	28384. 79	
3440. 510	2	29057. 13		3523. 646	2	28371. 58	
3441. 290	25c	29050. 54	$5p^5\ ^1P^o_1$— $6p''\ ^3P_0$	3523. 886	1	28369. 65	
3442. 819	7	29037. 64	$5d''\ ^3P^o_2$— $2_{2,3}$	3524. 095	2	28367. 97	
3444. 433	1	29024. 04	$5d''\ ^3F^o_3$— $10_{2,3}$	3524. 292	15	28366. 38	$6s''\ ^1P^o_1$— $7p'\ ^3P_0$
3446. 365	1	29007. 77		3525. 403	2	28357. 44	$6p'\ ^3D_1$— $6d'\ 11^o_0$
3447. 683	35c	28996. 68	$6p'\ ^1D_2$— $35^o_{2,3}$	3525. 798	1	28354. 27	
3447. 872	10c	28995. 09	$5p^5\ ^1P^o_1$— $7p\ ^5P_1$	3526. 223	60d	28350. 85	$5d\ ^5D^o_1$— $6p'\ ^3P_1$
3450. 764	8c	28970. 79		3526. 904	500	28345. 38	$5d'\ ^3S^o_1$— $4f'\ ^3P_2$
3454. 191	4	28942. 05		3527. 385	4	28341. 51	$5d'\ ^3P^o_0$— $7p\ ^3P_1$
3455. 886	1	28927. 85		3528. 062	2	28336. 07	$6p'\ ^3F_2$— $6d'\ 14^o_3$
3458. 654	20	28904. 70	$6p'\ ^1D_2$— 34^o_2	3528. 574	2	28331. 96	
3459. 108	10	28900. 91	$5d'\ ^3G^o_3$— $4f'\ ^3F_2$	3528. 810	1	28330. 07	
3459. 626	3	28896. 58	$5d'\ ^3F^o_2$— $8p\ ^3P_1$	3529. 316	2h	28326. 00	
3461. 812	1	28878. 34		3529. 540	1	28324. 21	
3462. 097	1	28875. 96		3531. 331	5h	28309. 84	$6p'\ ^3D_1$— $6d'\ 10^o_2$
3462. 332	2c	28874. 00	$6s'\ ^3D^o_3$— $4f\ ^3F_2$	3533. 379	60	28293. 43	$6s''\ ^1P^o_1$— $7p'\ ^1P_1$

TABLE 10.1. *Observed lines of* I II—Continued

λ(air)	Intensity	Wave number	Classification
3533.648	10	28291.28	$5d''\ ^3D_1^\circ$— $8_{1,2}$
3535.876	70	28273.45	$5d'\ ^3G_4^\circ$— $6p''\ ^3D_3$
3537.561	10*c*	28259.99	$6s''\ ^3P_1^\circ$— $6p''\ ^1S_0$
3538.334	1*h*	28253.81	$6p'\ ^3F_2$— $6d'\ 12_{1,2}^\circ$
3539.628	1	28243.48	
3541.605	100	28227.72	$6s''\ ^1P_1^\circ$— $7p'\ ^1D_2$
3543.319	1	28214.06	$5d'\ ^3F_2^\circ$— $5f\ ^3F_2$
3547.170	1	28183.44	
3549.734	2	28163.08	$5d'\ ^1D_2^\circ$— $8p\ ^3P_2$
3552.196	100*c*	28143.56	$5d'\ ^3D_2^\circ$— $4f\ ^3F_3$
3552.782	20	28138.92	$5d'\ ^3D_2^\circ$— $6p''\ ^3D_2$
3553.034	8*c*	28136.92	$5d'\ ^1F_3^\circ$— $6f\ ^3F_4$
3553.843	1	28130.52	
3554.873	5	28122.37	$5d'\ ^1D_2^\circ$— $7p'\ ^3P_1$
3555.039	2*c*	28121.05	$5d\ ^5D_3^\circ$— $6p'\ ^1F_3$
3555.576	2	28116.81	
3558.008	50	28097.59	$5d'\ ^3S_1^\circ$— $4f'\ ^3P_1$
3560.542	200	28077.59	$5d'\ ^3S_1^\circ$— $7p'\ ^3P_2$
3563.001	5	28058.22	$5d'\ ^3G_3^\circ$— $5f\ ^3F_4$
3566.158	2	28033.38	$6s'\ ^3D_3^\circ$— $4f\ ^5F_4$
3569.696	1	28005.59	
3569.888	6	28004.09	$6p\ ^3P_2$— $7s'\ ^3D_2^\circ$
3570.278	10*c*	28001.03	$5d'\ ^3D_2^\circ$— $7p\ ^5P_2$
3571.386	10*c*	27992.34	$5d\ ^5D_2^\circ$— $6p'\ ^1F_3$
3571.769	10*d*	27989.34	$5d'\ ^1D_2^\circ$— $4f'\ ^3F_2$
3573.680	200*c*	27974.37	$5d\ ^5D_1^\circ$— $6p'\ ^3P_2$
3575.861	70	27957.31	$5p^5\ ^3P_1^\circ$— $6p'\ ^3D_2$
3576.826	1	27949.77	$6s''\ ^1P_1^\circ$— $7p'\ ^3F_2$
3579.477	1	27929.07	
3586.568	3*c*	27873.85	$5d''\ ^3D_3^\circ$— $6f\ ^3F_4$
3586.946	10	27870.92	$5d'\ ^1D_2^\circ$— $8p\ ^3P_1$
3587.105	1	27869.68	$5d''\ ^3F_2^\circ$— $13_{2,3}$
3587.363	3*c*	27867.68	$5d'\ ^3D_2^\circ$— $7p\ ^5P_1$
3588.505	4	27858.81	
3592.110	15	27830.85	$5d'\ ^3F_2^\circ$— $5f\ ^3F_3$
3592.738	4	27825.98	
3593.030	1*h*	27823.72	$6s'\ ^1D_2^\circ$— $4f\ ^3F_2$
3594.691	2	27810.87	
3596.204	1	27799.17	
3597.133	4	27791.99	
3598.012	3	27785.20	
3606.902	1	27716.72	$5d'\ ^3G_3^\circ$— $5f\ ^3F_3$
3611.680	8*h*	27680.05	$5d'\ ^1F_3^\circ$— $6f\ ^5F_4$
3612.769	2	27671.71	$5d'\ ^1D_2^\circ$— $7p'\ ^3D_1$
3615.372	3	27651.78	$5d''\ ^3D_2^\circ$— $2_{2,3}$
3615.868	20*d*	27647.99	$5d\ ^5D_2^\circ$— $6p'\ ^1P_1$
3617.136	1	27638.30	
3618.014	6	27631.59	$5d'\ ^1D_2^\circ$— $4f'\ ^3D_3$
3618.652	6	27626.72	$5d'\ ^3F_2^\circ$— $5f\ ^5F_3$
3620.408	1	27613.32	$5d''\ ^3D_2^\circ$— $8f\ ^5F_3$
3620.691	1	27611.16	$6p\ ^3P_0$— $7s'\ ^3D_1^\circ$
3626.755	20*c*	27565.00	$5p^5\ ^1P_1^\circ$— $6p''\ ^3D_1$
3627.507	15	27559.28	$5d'\ ^1D_2^\circ$— $4f'\ ^3F_3$
3627.785	3	27557.17	$5d'\ ^3P_2^\circ$— $7p'\ ^3D_2$
3631.880	6*c*	27526.10	$6s'\ ^1D_2^\circ$— $4f\ ^3F_3$
3632.500	10	27521.40	$6s'\ ^1D_2^\circ$— $6p''\ ^3D_2$
3633.665	1	27512.58	$5d'\ ^3G_3^\circ$— $5f\ ^5F_3$
3640.432	1*c*	27461.44	
3641.130	1	27456.18	
3648.812	2*h*	27398.37	$6p'\ ^1D_2$— $24_{1,2}^\circ$
3649.144	3*h*	27395.88	
3650.800	20*c*	27383.46	$6s'\ ^1D_2^\circ$— $7p\ ^5P_2$
3652.299	4	27372.22	$6p'\ ^3D_2$— $6d'\ 13_{1,2}^\circ$
3653.355	15	27364.30	$5d'\ ^3S_1^\circ$— $7p'\ ^3P_1$
3655.423	5*h*	27348.82	$5d'\ ^3D_3^\circ$— $4f\ ^3F_2$
3657.060	100	27336.58	$6s\ ^3S_1^\circ$— $6p'\ ^3D_2$
3661.792	50*c*	27301.26	$5d'\ ^3D_3^\circ$— $4f\ ^3F_4$
3662.816	2	27293.62	
3671.889	1	27226.19	
3677.874	3*c*	27181.88	$6s''\ ^3P_2^\circ$— $4f'\ ^3P_2$
3685.694	3*c*	27124.21	$5d''\ ^1D_2^\circ$— $4f'\ ^1D_2$
3692.266	5*c*	27075.93	$5p^5\ ^3P_1^\circ$— $6p'\ ^3F_2$
3695.633	1*c*	27051.26	$5d'\ ^3D_3^\circ$— $4f\ ^3F_3$
3696.292	15*c*	27046.44	$5d'\ ^3D_3^\circ$— $6p''\ ^3D_2$
3700.027	1	27019.14	$5d''\ ^1D_2^\circ$— $4f'\ ^1F_3$
3700.703	1	27014.21	
3703.426	5*c*	26994.34	$5d'\ ^1F_3^\circ$— $4f'\ ^1F_3$
3709.498	40*c*	26950.16	$5d\ ^3D_1^\circ$— $6p'\ ^1D_2$
3714.466	1*c*	26914.11	$6s''\ ^3P_2^\circ$— $7p'\ ^3P_2$
3715.233	5*c*	26908.56	$5d'\ ^3D_3^\circ$— $7p\ ^5P_2$
3716.170	50	26901.77	$5d\ ^5D_1^\circ$— $6p'\ ^3P_0$
3725.274	1	26836.03	$5d''\ ^3D_3^\circ$— $4f'\ ^1D_2$
3727.200	2	26822.16	$5d'\ ^3P_1^\circ$— $7f\ ^3F_2$
3727.330	10	26821.23	$5d''\ ^1D_2^\circ$— $7p'\ ^1D_2$
3729.580	1	26805.05	$5d'\ ^1D_2^\circ$— $5f\ ^3F_3$
3730.890	25	26795.64	$5d''\ ^1D_2^\circ$— $7p'\ ^1F_3$
3734.366	60*c*	26770.70	$5d'\ ^1F_3^\circ$— $7p'\ ^1F_3$
3739.327	2	26735.18	$6d\ ^5D_3^\circ$— $9f\ ^5F_4$?
3740.358	4*c*	26727.81	$5d''\ ^3D_3^\circ$— $7p'\ ^3F_3$
3740.900	2	26723.94	
3742.138	200	26715.10	$5d'\ ^1F_3^\circ$— $7p'\ ^3F_4$
3744.138	1	26700.83	$6d\ ^5D_2^\circ$— $9f\ ^5F_3$?
3745.553	6*c*	26690.74	$4f\ ^3F_3$— $50_{3,4}^\circ$ $6d\ ^5D_4^\circ$— $9f\ ^5F_5$?
3746.008	3*c*	26687.50	$6p'\ ^1P_1$— $6d'\ 15_1^\circ$ $6d\ ^5D_4^\circ$— $9f\ ^5F_4$?
3748.299	4*c*	26671.19	$5d''\ ^1F_3^\circ$— $11_{3,4}$
3764.694	2	26555.04	$6p'\ ^3D_1$— $6d'\ 7_{1,2}^\circ$
3766.364	3	26543.26	$5d''\ ^1D_2^\circ$— $7p'\ ^3F_2$
3767.804	4*c*	26533.12	$5d''\ ^3D_3^\circ$— $7p'\ ^1D_2$
3769.287	1	26522.68	
3769.891	5	26518.43	$5d'\ ^1F_3^\circ$— $7p'\ ^3F_2$
3771.453	10	26507.45	$5d''\ ^3D_3^\circ$— $7p'\ ^1F_3$
3772.506	1	26500.05	$4f\ ^5F_5$—$12g\ ^5G_6^\circ$
3778.068	2	26461.04	$5d'\ ^3F_3^\circ$— $7p\ ^3P_2$
3778.913	10*c*	26455.12	$6s\ ^3S_1^\circ$— $6p'\ ^3F_2$
3779.374	25	26451.90	$5d''\ ^3D_3^\circ$— $7p'\ ^3F_4$
3781.442	20*c*	26437.43	$5d'\ ^3D_2^\circ$— $6p''\ ^3D_1$
3787.772	1	26393.25	$4f\ ^3F_2$— $50_{3,4}^\circ$
3789.289	5	26382.68	$5d\ ^5D_4^\circ$— $6p'\ ^3F_3$
3792.147	1	2€362.80	
3793.419	10	26353.96	$5d'\ ^1S_0^\circ$— $4f'\ ^3P_1$
3800.176	2	26307.10	
3801.073	2	26300.89	
3801.453	5*d*?	26298.26	$5d'\ ^1F_3^\circ$— $4f'\ ^3G_3$
3804.274	1	26278.76	$5d'\ ^3D_1^\circ$— $6p''\ ^1P_1$
3804.720	1	26275.68	
3804.843	6	26274.83	$6s''\ ^1P_1^\circ$— $4f'\ ^3P_0$
3807.840	10	26254.16	$5d\ ^5D_2^\circ$— $6p'\ ^3F_3$
3809.651	5*c*	26241.68	$6s''\ ^3P_2^\circ$— $8p\ ^3P_2$
3815.519	1*c*	26200.82	$6s''\ ^3P_2^\circ$— $7p'\ ^3P_1$

TABLE 10.1. *Observed lines of* I II—Continued

λ(air)	Intensity	Wave number	Classification	λ(air)	Intensity	Wave number	Classification
3818. 597	2	26180. 20	$6p'\ ^3D_1$— $7d\ ^3D_1^\circ$	4086. 888	1	24461. 59	
3826. 022	1	26129. 39		4089. 598	3	24445. 38	$5d\ ^5D_1^\circ$— $6p'\ ^3D_2$
3829. 355	1	26106. 65	$5d'\ ^1F_3^\circ$— $4f'\ ^3F_4$	4094. 310	1	24417. 25	$6p'\ ^3P_2$— $9s\ ^3S_1^\circ$
3833. 736	35*c*	26076. 82	$5d\ ^3D_3^\circ$— $6p'\ ^1D_2$	4094. 598	5	24415. 53	$6p'\ ^3P_1$— $6d'\ 15_1^\circ$
3842. 914	25	26014. 54	$5d\ ^5D_2^\circ$— $6p'\ ^3D_2$	4095. 232	1*c*	24411. 75	
3848. 808	1	25974. 70		4100. 186	2	24382. 26	$6p'\ ^3D_2$— $6d'\ 7_{1,2}^\circ$
3850. 818	8	25961. 15	$6p\ ^5P_2$— $6d\ ^3D_3^\circ$	4102. 895	6	24366. 16	$6p'\ ^3D_3$— $6d'\ 14_3^\circ$
3851. 243	1	25958. 28		4103. 463	1	24362. 78	$6p'\ ^3D_1$— $7d\ ^5D_2^\circ$
3857. 334	1	25917. 29	$4f\ ^5F_5$—$11g\ ^5G_6^\circ$	4107. 818	3	24336. 96	
3870. 276	1	25830. 63		4109. 658	2	24326. 06	
3871. 878	3	25819. 94	$6s'\ ^1D_2^\circ$— $6p''\ ^3D_1$	4111. 646	3	24314. 30	$6p'\ ^3F_3$— $6d'\ 8_4^\circ$
3877. 198	25	25784. 51	$5p^5\ ^3P_1^\circ$— $6p'\ ^3D_1$	4115. 615	3	24290. 85	
3879. 028	5	25772. 35	$5d'\ ^3P_2^\circ$— $7p'\ ^1P_1$	4116. 294	6	24286. 84	$6p'\ ^3F_2$— $7d\ ^3D_3^\circ$
3884. 064	4	25738. 94	$6p'\ ^1P_1$— $6d'\ 13_{1,2}^\circ$	4116. 438	1	24286. 00	
3893. 000	70*c*	25679. 85	$5p^5\ ^3P_0^\circ$— $6p'\ ^3P_1$	4116. 823	3	24283. 72	$6p'\ ^3D_3$— $6d'\ 13_{1,2}^\circ$?
3895. 547	10*c*	25663. 06	$5d'\ ^1P_1^\circ$— $4f'\ ^1P_1$	4117. 892	3	24277. 42	
3901. 118	20*c*	25626. 42	$5d'\ ^3P_0^\circ$— $6p''\ ^3D_1$	4118. 813	1	24271. 99	$6p''\ ^3D_1$— 32_1°
3904. 896	1	25601. 62		4119. 599	1	24267. 36	
3905. 917	3*c*	25594. 93	$5d'\ ^1P_1^\circ$— $4f'\ ^1D_2$	4120. 190	8	24263. 88	$6p'\ ^3D_2$— $6d'\ 6_{1,2}^\circ$
3907. 201	100	25586. 52	$5d\ ^3D_2^\circ$— $6p'\ ^3P_1$	4121. 281	3*c*	24257. 46	$6s'\ ^3D_1^\circ$— $6p'\ ^1D_2$
3908. 940	1	25575. 14	$5d''\ ^3D_3^\circ$— $7f\ ^3F_2$	4122. 931	4	24247. 75	$6s''\ ^1P_1^\circ$— $7p'\ ^3D_1$
3909. 708	1	25570. 12	$5d\ ^5D_3^\circ$— $6p'\ ^3F_2$	4124. 536	2	24238. 31	
3910. 678	2	25563. 77		4126. 093	10	24229. 17	$6p'\ ^3D_1$— $6d'\ 4_0^\circ$
3915. 234	30	25534. 03	$5d'\ ^3F_3^\circ$— $4f\ ^3F_4$	4135. 723	1	24172. 75	$4f\ ^5F_4$— $9g\ ^3G_5^\circ$
3924. 018	2*c*	25476. 87	$6p'\ ^1F_3$— $6d'\ 14_3^\circ$	4136. 482	2	24168. 32	$4f\ ^5F_4$— $9g\ ^5G_5^\circ$
3931. 169	10*c*	25430. 53	$5d'\ ^1P_1^\circ$— $7p'\ ^3P_0$	4138. 030	5*c*	24159. 28	$6p'\ ^1F_3$— $6d'\ 10_2^\circ$
3931. 442	15	25428. 76	$5d'\ ^3P_2^\circ$— $7p'\ ^3F_2$	4139. 702	1	24149. 52	
3937. 222	60*c*	25391. 43	$6s'\ ^3D_3^\circ$— $6p'\ ^1D_2$	4142. 014	2	24136. 04	
3942. 476	20*d*	25357. 59	$5d'\ ^1P_1^\circ$— $7p'\ ^1P_1$	4145. 865	3	24113. 62	$4f\ ^5F_5$— $9g\ ^5G_6^\circ$
3944. 019	1	25347. 67		4153. 136	2	24071. 40	$4f\ ^5F_2$— $9g\ ^5G_3^\circ$
3945. 000	2*c*	25341. 37	$6s''\ ^3P_1^\circ$— $6p''\ ^1D_2$	4158. 425	3	24040. 79	$6p'\ ^3P_1$— $9s\ ^3S_1^\circ$
3952. 724	2*w*	25291. 85	$5d'\ ^1P_1^\circ$— $7p'\ ^1D_2$	4160. 646	4*c*	24027. 96	$6d\ ^3D_1^\circ$— $8_{1,2}$
3953. 978	2	25283. 83	$5d'\ ^3F_3^\circ$— $4f\ ^3F_3$	4162. 565	1	24016. 88	$5d'\ ^3D_1^\circ$— $6p''\ ^3S_1$
3960. 504	1	25242. 17		4162. 689	1	24016. 16	$4f\ ^5F_1$— $9g\ ^5G_2^\circ$
3961. 538	1	25235. 58	$6d\ ^5D_2^\circ$— $8f\ ^3F_3$	4166. 838	2	23992. 25	$5d''\ ^1D_2^\circ$— $7p'\ ^3D_3$
3962. 959	15*d*	25226. 53	$5d'\ ^3D_1^\circ$— $6p''\ ^3P_2$	4171. 155	1*c*	23967. 42	$5d'\ ^1F_3^\circ$— $7p'\ ^3D_3$
3965. 544	50*c*	25210. 09	$5d\ ^3D_2^\circ$— $6p'\ ^3P_2$	4173. 810	40*c*, *Z*	23952. 17	$5d\ ^3D_1^\circ$— $6p'\ ^3P_1$
3965. 772	10	25208. 64	$5d'\ ^3P_2^\circ$— $4f'\ ^3G_3$	4177. 179	4	23932. 86	$5d'\ ^3F_2^\circ$— $6p''\ ^1D_2$
3972. 839	30	25163. 80	$6s\ ^3S_1^\circ$— $6p'\ ^3D_1$	4178. 440	1	23925. 63	$6p'\ ^3P_2$— $6d'\ 14_3^\circ$
3973. 481	3	25159. 73	$6d\ ^5D_3^\circ$— $8f\ ^5F_4$	4179. 928	1	23917. 12	
3974. 067	1	25156. 02	$6d\ ^5D_3^\circ$— $8f\ ^5F_3$	4183. 035	1	23899. 35	
3974. 953	1	25150. 42	$4f\ ^5F_5$—$10g\ ^5G_6^\circ$	4183. 516	2	23896. 60	
3977. 968	1	25131. 35	$6d\ ^5D_2^\circ$— $8f\ ^5F_2$	4192. 862	1	23843. 34	$6p'\ ^3P_2$— $6d'\ 13_{1,2}^\circ$
3980. 433	2	25115. 79	$6d\ ^5D_2^\circ$— $8f\ ^5F_3$	4197. 190	2	23818. 75	$5d'\ ^3G_3^\circ$— $6p''\ ^1D_2$
3981. 043	1	25111. 94	$6d\ ^5D_4^\circ$— $8f\ ^5F_4$	4206. 534	1	23765. 84	
3983. 574	4	25095. 99	$6d\ ^5D_4^\circ$— $8f\ ^5F_5$	4217. 476	3*h*	23704. 19	$5d''\ ^3D_3^\circ$— $7p'\ ^3D_3$
3988. 076	15	25067. 66	$5d'\ ^3S_1^\circ$— $6p''\ ^1S_0$	4219. 138	10	23694. 85	$6p\ ^3P_1$— $6d\ ^3D_1^\circ$
3990. 835	1	25050. 33		4224. 993	10	23662. 01	$6p'\ ^3F_2$— $7d\ ^3D_2^\circ$
3996. 642	5	25013. 93	$5d'\ ^1P_1^\circ$— $7p'\ ^3F_2$	4225. 542	50*c*, *Z*	23658. 94	$5d\ ^3D_2^\circ$— $6p'\ ^1F_3$
4006. 349	6	24953. 33	$6p'\ ^3D_1$— $7d\ ^3D_2^\circ$	4231. 185	1	23627. 39	$4f\ ^3F_3$— $9g\ ^3G_4^\circ$
4013. 765	4	24907. 22	$6p'\ ^3D_1$— $6d'\ 5_1^\circ$	4233. 249	2	23615. 87	$6p'\ ^3F_2$— $6d'\ 5_1^\circ$
4017. 235	2*c*	24885. 71	$6p\ ^5P_3$— $6d\ ^3D_3^\circ$	4235. 511	30*Z*	23603. 26	$6p\ ^3P_1$— $6d\ ^3D_2^\circ$
4019. 310	1	24872. 86		4240. 441	15*c*	23575. 82	$5d\ ^3D_1^\circ$— $6p'\ ^3P_2$
4036. 092	50*c*	24769. 44	$5d\ ^3D_2^\circ$— $6p'\ ^3D_3$	4242. 545	1	23564. 12	$5d\ ^5D_1^\circ$— $6p'\ ^3F_2$
4043. 893	20*c*	24721. 66	$6s''\ ^3P_1^\circ$— $6p''\ ^1P_1$	4248. 287	1	23532. 27	
4060. 184	2	24622. 47	$5d\ ^5D_0^\circ$— $6p'\ ^3D_1$	4249. 711	1*w*	23524. 39	
4077. 366	1	24518. 72		4254. 193	1	23499. 61	$6p''\ ^3D_1$— 29_1°
4078. 556	1	24511. 56		4254. 282	1	23499. 11	
4079. 877	1	24503. 62	$6p'\ ^1P_1$— $6d'\ 10_2^\circ$	4256. 129	2	23488. 92	
4081. 378	5	24494. 61	$6p'\ ^3D_1$— $7d\ ^5D_0^\circ$	4257. 606	1*w*	23480. 77	

TABLE 10.1. *Observed lines of* I II—Continued

λ(air)	Intensity	Wave number	Classification
4260. 128	3*c*	23466. 87	$6p'\ {}^3P_1$— $6d'\ 13^\circ_{1,2}$
4265. 801	2	23435. 66	
4266. 925	1	23429. 49	$4f\ {}^3F_3$— 37°_2
4271. 310	6	23405. 43	$6p'\ {}^3D_2$— $7d\ {}^3D^\circ_3$
4276. 015	1	23379. 68	$4f\ {}^3F_4$— $9g\ {}^3G^\circ_5$
4279. 188	4*c*	23362. 35	$6s''\ {}^3P^\circ_0$— $6p''\ {}^3S_1$
4281. 834	5*c*	23347. 91	$6p'\ {}^1F_3$— $6d'\ 9^\circ_3$
4282. 912	4	23342. 03	
4287. 924	2	23314. 75	$5d\ {}^3D^\circ_2$— $6p'\ {}^1P_1$
4288. 215	6	23313. 17	$5d'\ {}^3F^\circ_2$— $6p''\ {}^1P_1$
4291. 923	30	23293. 03	$6p'\ {}^3D_1$— $6d'\ 1^\circ_2$
4296. 286	10	23269. 37	$6p'\ {}^3P_2$— $6d'\ 12^\circ_1$
4315. 481	10	23165. 87	$6p'\ {}^3F_3$— $7d\ {}^3D^\circ_3$
4316. 897	5*c*	23158. 28	$5d'\ {}^3P^\circ_2$— $4f'\ {}^3P_2$
4319. 623	1*w*	23143. 66	$6p'\ {}^3F_2$— $7d\ {}^5D^\circ_3$
4322. 756	50	23126. 89	$5p^5\ {}^1P^\circ_1$— $6p'\ {}^1D_2$
4333. 159	2*c*	23071. 36	$6p'\ {}^3F_2$— $7d\ {}^5D^\circ_2$
4334. 246	2	23065. 58	
4337. 427	2	23048. 66	$6p'\ {}^3D_3$— $6d'\ 10^\circ_2$
4338. 224	1*c*	23044. 43	$5d''\ {}^3D^\circ_3$— $8p\ {}^3P_2$
4342. 078	20*Z*	23023. 98	$6p\ {}^5P_1$— $6d\ {}^5D^\circ_1$
4355. 036	1	22955. 47	
4362. 456	10	22916. 43	$6p\ {}^5P_2$— $6d\ {}^5D^\circ_1$
4364. 224	5	22907. 14	$5d'\ {}^1D^\circ_2$— $6p''\ {}^1D_2$
4368. 247	2	22886. 05	
4369. 834	2	22877. 74	$5d'\ {}^3P^\circ_2$— $7p'\ {}^3D_3$
4371. 722	1*c*	22867. 86	
4373. 686	3	22857. 59	$6p''\ {}^3P_0$— $33.\ 5^\circ_1$
4374. 760	3	22851. 98	$6d\ {}^5D^\circ_3$— $7f\ {}^5F_3$
4376. 139	100*Z*	22844. 78	
4376. 745	8	22841. 61	$6d\ {}^5D^\circ_3$— $7f\ {}^5F_4$
4379. 048	2	22829. 60	
4382. 489	5	22811. 68	$6d\ {}^5D^\circ_2$— $7f\ {}^5F_3$
4383. 998	15	22803. 82	$6d\ {}^5D^\circ_4$— $7f\ {}^5F_5$
4385. 904	2	22793. 91	$6d\ {}^5D^\circ_4$— $7f\ {}^5F_4$
4388. 458	10	22780. 65	$6p'\ {}^3D_2$— $7d\ {}^3D^\circ_2$
4390. 278	20*c*	22771. 20	$6p''\ {}^3D_1$— 21°_1
4394. 555	6*c*	22749. 04	$6p'\ {}^1P_1$— $6d'\ 7^\circ_{1,2}$
4398. 585	10	22728. 20	$6p'\ {}^3D_1$— $5d''\ {}^3P^\circ_1$
4399. 037	60*c*	22725. 86	$6p'\ {}^3F_2$— $6d'\ 3^\circ_3$
4399. 592	1	22722. 99	$4f\ {}^5F_4$— $8g\ {}^3G^\circ_5$
4400. 741	4*c*	22717. 06	$4f\ {}^5F_4$— $8g\ {}^5G^\circ_5$
4403. 566	60*c*, *Z*	22702. 49	$5d\ {}^3D^\circ_3$— $6p'\ {}^3P_2$
4404. 580	7*d*	22697. 26	$5d'\ {}^1F^\circ_3$— $4f''\ {}^3G_4$
4405. 577	1	22692. 12	$4f\ {}^5F_3$— $8g\ {}^3G^\circ_4$
4406. 097	3	22689. 45	$4f\ {}^5F_3$— $8g\ {}^5G^\circ_4$
4408. 954	60*Z*	22674. 74	$6p\ {}^3P_2$— $6d\ {}^3D^\circ_3$
4411. 198	5	22663. 21	$4f\ {}^5F_5$— $8g\ {}^5G^\circ_6$
4412. 333	50*Z*	22657. 38	$6p'\ {}^3F_2$— $6d'\ 2^\circ_3$
4416. 569	10	22635. 65	$5d'\ {}^3D^\circ_1$— $7p\ {}^3P_0$
4416. 890	10	22634. 00	$6p\ {}^3P_2$— $6d\ {}^3D^\circ_2$
4417. 567	10*c*	22630. 54	$6p'\ {}^1P_1$— $6d'\ 6^\circ_{1,2}$ $6p''\ {}^3P_1$— 32°_1
4419. 496	2	22620. 66	$4f\ {}^5F_2$— $8g\ {}^5G^\circ_3$
4421. 965	30*c*	22608. 03	$6p'\ {}^3P_2$— $6d'\ 10^\circ_2$
4423. 725	100*c*, *Z*	22599. 03	$6p\ {}^5P_1$— $6d\ {}^5D^\circ_2$
4428. 195	50*d*, *Z*	22576. 22	$6p'\ {}^1F_3$— $6d'\ 8^\circ_4$
4430. 130	2	22566. 36	$4f\ {}^5F_1$— $8g\ {}^5G^\circ_2$
4435. 104	5	22541. 05	$6p'\ {}^3F_3$— $7d\ {}^3D^\circ_2$ $5d''\ {}^3D^\circ_3$— $8p\ {}^5P_3$?
4436. 937	3	22531. 74	$5d'\ {}^3P^\circ_2$— $4f'\ {}^3D_2$
4442. 562	200*Z*	22503. 21	$5d\ {}^3D^\circ_1$— $6p'\ {}^3P_0$
4444. 873	150*Z*	22491. 51	$6p\ {}^5P_2$— $6d\ {}^5D^\circ_3$
4445. 872	3*c*	22486. 46	$5d'\ {}^3P^\circ_1$— $4f'\ {}^1P_1$
4446. 742	40*Z*	22482. 06	$6p\ {}^5P_1$— $6d\ {}^5D^\circ_0$
4451. 149	25*c*	22459. 80	$6s''\ {}^3P^\circ_1$— $6p''\ {}^3S_1$
4452. 858	300*Z*	22451. 18	$6p\ {}^5P_2$— $6d\ {}^5D^\circ_3$
4456. 250	10*c*	22434. 10	$5d''\ {}^3D^\circ_3$— $4f'\ {}^3G_4$
4456. 625	100*c*, *Z*	22432. 20	$6s'\ {}^3D^\circ_3$— $6p'\ {}^1D_2$
4457. 643	5	22427. 08	
4458. 474	20*c*	22422. 90	$6p'\ {}^1F_3$— $5g\ {}^5G^\circ_4$
4460. 185	30*Z*	22414. 30	$5p^4\ {}^4P_1$— $5p^4\ {}^1S_0$
4461. 928	2	22405. 54	$7p\ {}^5P_1$— 31°_0
4462. 708	100	22401. 63	$6s''\ {}^1P^\circ_1$— $6p''\ {}^1S_0$
4464. 338	150*c*, *Z*	22393. 45	$6s'\ {}^3D^\circ_2$— $6p'\ {}^3P_1$
4468. 167	3*c*	22374. 26	$6p'\ {}^1P_1$— $7d\ {}^3D^\circ_1$
4473. 412	100*c*, *Z*	22348. 03	$5d\ {}^3D^\circ_3$— $6p'\ {}^3F_4$
4476. 037	10*Z*	22334. 92	$6p\ {}^3P_0$— $6d\ {}^3D^\circ_1$
4479. 656	30	22316. 88	$6p''\ {}^3D_1$— $20^\circ_{1,2}$
4483. 730	1	22296. 60	$7p\ {}^3P_2$—$11d\ {}^3D^\circ_3$
4484. 829	2*w*	22291. 14	$5d'\ {}^1F^\circ_3$— $5f\ {}^3F_4$
4487. 234	7	22279. 19	$6p'\ {}^3P_1$— $6d'\ 11^\circ_0$
4488. 552	40*Z*	22272. 65	$5d\ {}^5D^\circ_1$— $6p'\ {}^3D_1$
4490. 652	4	22262. 23	$6p'\ {}^3D_2$— $7d\ {}^5D^\circ_3$
4490. 912	3	22260. 94	$5d'_3\ {}^3F^\circ_2$— $6p''\ {}^3P_2$
4492. 352	3	22253. 81	$5d'\ {}^3P^\circ_1$— $7p'\ {}^3P_0$
4492. 649	1*w*	22252. 34	$6p'\ {}^3F_2$— $7s'\ {}^3D^\circ_3$
4495. 698	15*c*	22237. 24	$6p'\ {}^3D_3$— $6d'\ 9^\circ_3$
4496. 815	1	22231. 72	$6p'\ {}^3P_1$— $6d'\ 10^\circ_2$
4497. 535	7	22228. 16	$5d''\ {}^3P^\circ_2$— $7p'\ {}^1F_3$
4497. 708	10	22227. 31	
4498. 586	1	22222. 97	$7p\ {}^5P_2$—$10d\ {}^3D^\circ_3$
4499. 604	20*c*	22217. 94	$5d'\ {}^3P^\circ_2$— $8p\ {}^3P_2$
4504. 375	1	22194. 41	$6p''\ {}^3P_1$— 31°_0
4505. 072	6	22190. 97	$7p\ {}^5P_1$—$10d\ {}^3D^\circ_2$
4505. 265	5	22190. 02	$6p'\ {}^3D_2$— $7d\ {}^5D^\circ_2$
4506. 772	1	22182. 60	$4f\ {}^3F_3$— $8g\ {}^3G^\circ_3$
4507. 129	2	22180. 85	$5d'\ {}^3P^\circ_1$— $7p'\ {}^1P_1$
4507. 866	10	22177. 22	$5d'\ {}^3P^\circ_2$— $7p'\ {}^3P_1$ $4f\ {}^3F_3$— $8g\ {}^3G^\circ_4$
4508. 441	1	22174. 39	$4f\ {}^3F_3$— $8g\ {}^5G^\circ_4$
4513. 170	8*c*	22151. 16	$6p'\ {}^3F_4$— $6d'\ 9^\circ_3$ $7s\ {}^3S^\circ_1$— $7p'\ {}^3D_2$
4513. 508	8*c*	22149. 50	
4514. 064	20*c*	22146. 77	$5d'\ {}^3G^\circ_3$— $6p''\ {}^3P_2$
4519. 910	1	22118. 13	$7p\ {}^3P_1$—$12s\ {}^3S^\circ_1$?
4520. 528	4	22115. 10	$5d'\ {}^3P^\circ_1$— $7p'\ {}^1D_2$
4526. 672	2	22085. 09	$6p''\ {}^3D_2$—$10d\ {}^3D^\circ_3$
4527. 024	10	22083. 37	$6p'\ {}^3F_3$— $7d\ {}^5D^\circ_4$
4529. 898	1	22069. 36	$7p\ {}^5P_1$— 29°_1
4532. 296	1	22057. 68	$7p\ {}^5P_2$—$10d\ {}^3D^\circ_2$
4535. 046	5	22044. 31	$5d'\ {}^3P^\circ_2$— $4f'\ {}^3F_2$
4537. 599	5	22031. 90	$5d''\ {}^3F^\circ_2$— $7f\ {}^3F_3$
4538. 411	3*w*	22027. 96	$5d''\ {}^3D^\circ_3$— $5f\ {}^3F_4$
4540. 644	40*Z*	22017. 13	$6s'\ {}^3D^\circ_2$— $6p'\ {}^3P_2$
4541. 306	8	22013. 92	$6p''\ {}^3P_0$— 29°_1
4543. 833	25	22001. 68	$6p'\ {}^3F_2$— $6d'\ 1^\circ_2$
4544. 272	50	21999. 55	$5d'\ {}^3D^\circ_2$— $6p'\ {}^1D_2$
4544. 339	20	21999. 23	
4548. 342	7	21979. 87	$6p''\ {}^3P_1$—$10d\ {}^3D^\circ_2$
4549. 071	4	21976. 35	
4549. 437	1	21974. 58	$5d''\ {}^1D^\circ_2$— $5f\ {}^3F_3$
4556. 012	1*w*	21942. 87	
4558. 758	4	21929. 65	$4f\ {}^3F_4$— $8g\ {}^3G^\circ_5$

TABLE 10.1. *Observed lines of* I II—Continued

λ(air)	Intensity	Wave number	Classification	λ(air)	Intensity	Wave number	Classification
4559. 545	8*w*	21925. 86	$5d'\ {}^3P^\circ_2$— $8p\ {}^3P_1$	4687. 890	20	21325. 59	$4f\ {}^3F_2$— 26°_3
4559. 999	1	21923. 68	$4f\ {}^3F_4$— $8g\ {}^5G^\circ_5$	4702. 468	25	21259. 48	$6s'\ {}^3D^\circ_1$— $6p'\ {}^3P_1$
4560. 612	15*Z*	21920. 73	$5d\ {}^3D^\circ_2$— $6p'\ {}^3F_3$	4702. 594	7	21258. 91	$6p''\ {}^3D_2$— $24^\circ_{1,2}$
4560. 880	10	21919. 45	$5d'\ {}^3F^\circ_2$— $6p''\ {}^3D_3$	4706. 453	1*w*	21241. 48	$6p'\ {}^3F_4$— $5g\ {}^3G^\circ_4$
4568. 068	3	21884. 95	$4f\ {}^3F_2$— $8g\ {}^3G^\circ_3$	4707. 842	40	21235. 21	$5d'\ {}^1D^\circ_2$— $6p''\ {}^3P_2$
4571. 517	12	21868. 44	$6p\ {}^5P_2$— $5d''\ {}^3F^\circ_3$	4709. 844	20*c*	21226. 18	$6p'\ {}^3F_4$— $5g\ {}^5G^\circ_4$
4573. 543	2	21858. 76	$6d\ {}^3D^\circ_3$— $8f\ {}^3F_4$	4711. 430	25*c*	21219. 04	$6p'\ {}^3F_4$— $5g\ {}^5G^\circ_5$
4573. 718	5	21857. 92	$5d'\ {}^3D^\circ_1$— $7p\ {}^3P_2$	4712. 498	1	21214. 23	
4574. 090	20*Z*	21856. 14	$6p\ {}^5P_1$— $5d''\ {}^3D^\circ_1$	4713. 988	1*w*	21207. 52	$7p\ {}^5P_2$— 21°_1
4576. 550	40*Z*	21844. 39	$6p'\ {}^3D_2$— $6d'\ 3^\circ_3$	4722. 102	12*c*	21171. 08	$5d''\ {}^3D^\circ_2$— $4f'\ {}^1D_2$
4578. 017	1	21837. 39	$5d'\ {}^3P^\circ_1$— $7p'\ {}^3F_2$	4726. 535	20*c*	21151. 23	$5d\ {}^3D^\circ_3$— $6p'\ {}^1F_3$
4578. 710	7	21834. 09	$7p\ {}^5P_1$— $25^\circ_{1,2}$	4730. 366	25	21134. 10	$6p\ {}^3P_1$— $5d''\ {}^3F^\circ_2$
4584. 457	1	21806. 72	$6d\ {}^3D^\circ_2$— $8f\ {}^3F_3$	4730. 958	20*c*	21131. 45	$6p'\ {}^3F_3$— $7s'\ {}^3D^\circ_3$
4584. 752	2	21805. 32	$5d'\ {}^3G^\circ_3$— $6p''\ {}^3D_3$	4731. 316	8	21129. 85	$6p''\ {}^3P_1$— 21°_1
4586. 582	20	21796. 62	$6p'\ {}^3P_2$— $6d'\ 9^\circ_3$	4733. 414	6	21120. 49	$6p'\ {}^3D_2$— $6d'\ 1^\circ_2$
4589. 495	1	21782. 78	$4f\ {}^3F_2$—$10d\ {}^3D^\circ_3$	4737. 544	2	21102. 08	
4590. 764	25	21776. 76		4737. 691	2	21101. 42	
4590. 930	20*Z*	21775. 97	$6p'\ {}^3D_2$— $6d'\ 2^\circ_3$	4737. 828	4	21100. 81	
4593. 066	7	21765. 85	$6d\ {}^3D^\circ_3$— $8f\ {}^3F_3$	4739. 388	1	21093. 87	$7p\ {}^5P_3$—$11s\ {}^5S^\circ_2$
4596. 720	6	21748. 54	$6p\ {}^5P_2$— $5d''\ {}^3D^\circ_1$	4742. 810	50*c*	21078. 65	$6s''\ {}^3P^\circ_1$— $7p\ {}^3P_0$
4599. 769	200*Z*	21734. 13		4744. 797	3	21069. 82	$6p''\ {}^3D_2$— 21°_1
4600. 365	1*w*	21731. 31		4748. 978	20	21051. 27	$5d'\ {}^3F^\circ_2$— $6p''\ {}^3S_1$
4604. 309	1*c*	21712. 70		4750. 846	1*c*	21042. 99	$6p'\ {}^1D_2$— $9s\ {}^3S^\circ_1$
4605. 924	1	21705. 09		4751. 798	4	21038. 78	
4609. 191	1	21689. 71		4752. 676	60	21034. 89	$6s''\ {}^3P^\circ_0$— $7p\ {}^3P_1$
4611. 224	40*c*, *Z*	21680. 14	$5d\ {}^3D^\circ_1$— $6p'\ {}^1P_1$	4753. 825	1	21029. 81	
4612. 265	1	21675. 25	$7p\ {}^3P_2$— $35^\circ_{2,3}$	4763. 820	60	20985. 68	$6s''\ {}^3P^\circ_2$— $6p''\ {}^1D_2$
4614. 102	1	21666. 62		4765. 519	30	20978. 20	$5d'\ {}^3D^\circ_1$— $4f\ {}^3F_2$
4621. 854	100*Z*	21630. 28		4768. 193	15	20966. 44	$6p\ {}^3P_2$— $5d''\ {}^1F^\circ_3$
4622. 172	7	21628. 79		4770. 456	5	20956. 49	$4f\ {}^3F_2$— $24^\circ_{1,2}$
4622. 347	20	21627. 97	$6p''\ {}^3D_2$— 26°_3	4770. 857	1	20954. 73	
4623. 417	8	21622. 96	$6p''\ {}^3P_1$— $25^\circ_{1,2}$	4772. 841	1	20946. 02	
4624. 603	1	21617. 42	$4f\ {}^3F_2$—$10d\ {}^3D^\circ_2$	4775. 674	10	20933. 60	
4625. 288	5	21614. 22	$5d'\ {}^3P^\circ_2$— $4f'\ {}^3F_3$	4782. 000	6	20905. 90	$7p\ {}^3P_1$—$10d\ {}^3D^\circ_2$
4627. 292	5	21604. 86	$6p'\ {}^3F_3$— $6d'\ 3^\circ_3$	4782. 658	5	20903. 03	$7p\ {}^3P_2$—$10d\ {}^3D^\circ_3$
4632. 446	300*c*, *Z*	21580. 82	$6s\ {}^5S^\circ_2$— $6p\ {}^3P_2$	4784. 798	50	20893. 68	$5d'\ {}^1D^\circ_2$— $6p''\ {}^3D_3$
4633. 365	50	21576. 54	$6s'\ {}^3D^\circ_2$— $6p'\ {}^3D_3$	4786. 389	2*c*	20886. 73	$7p\ {}^5P_1$— $20^\circ_{1,2}$
4638. 810	8	21551. 21	$6p'\ {}^3P_0$— $7d\ {}^3D^\circ_1$	4787. 228	50*c*	20883. 07	$6s'\ {}^3D^\circ_1$— $6p'\ {}^3P_2$
4640. 831	150	21541. 83		4787. 776	3	20880. 68	$6p'\ {}^3F_3$— $6d'\ 1^\circ_2$
4641. 142	7	21540. 38		4790. 690	30	20867. 98	$5d''\ {}^3D^\circ_2$— $7p'\ {}^1D_2$
4641. 984	30	21536. 48	$6p'\ {}^3F_3$— $6d'\ 2^\circ_3$	4792. 522	1*w*	20860. 01	$5d'\ {}^3P^\circ_2$— $5f\ {}^3F_3$
4643. 843	1	21527. 86		4796. 576	25	20842. 38	$5d''\ {}^3D^\circ_2$— $7p'\ {}^1F_3$
4647. 472	1	21511. 05	$5d'\ {}^1P^\circ_1$— $8p\ {}^3P_1$	4805. 662	4*c*	20802. 97	$6p'\ {}^1F_3$— $7d\ {}^3D^\circ_2$
4649. 114	1	21503. 45		4806. 402	75*Z*	20799. 77	$5d\ {}^3D^\circ_2$— $6p'\ {}^3F_2$
4651. 324	1	21493. 23	$7p\ {}^5P_2$—$11s\ {}^5S^\circ_2$	4807. 320	3	20795. 79	
4654. 492	3	21478. 60		4807. 998	20	20792. 86	$6p\ {}^5P_3$— $5d''\ {}^3F^\circ_3$
4657. 302	30	21465. 65	$6p'\ {}^3D_3$— $6d'\ 8^\circ_4$	4812. 106	1*w*	20775. 11	
4663. 560	1*c*	21436. 84	$6p'\ {}^3F_2$— $5d''\ {}^3P^\circ_1$	4813. 902	2	20767. 36	$4f\ {}^3F_2$— 21°_1
4665. 537	10*c*	21427. 76	$6p'\ {}^1F_3$— $7d\ {}^3D^\circ_3$	4825. 452	1	20717. 65	
4666. 484	500*d*?	21423. 41	$6p\ {}^5P_3$— $6d\ {}^5D^\circ_4$	4828. 252	70*c*, *Z*	20705. 64	$5p^5\ {}^3P^\circ_2$— $6p\ {}^3P_2$
4668. 116	20	21415. 92	$6p\ {}^5P_3$— $6d\ {}^5D^\circ_2$	4831. 600	1	20691. 29	
4672. 280	2	21396. 83	$7p\ {}^5P_2$— $24^\circ_{1,2}$	4832. 238	5*c*	20688. 56	$6p'\ {}^1P_1$— $7d\ {}^5D^\circ_0$
4675. 530	1000*Z*	21381. 96	$6s'\ {}^1D^\circ_2$— $6p'\ {}^1D_2$	4833. 747	3	20682. 10	$7p\ {}^3P_0$— 33.5°_1
4676. 080	20	21379. 45	$6p'\ {}^3F_4$— $6d'\ 8^\circ_4$	4835. 178	40	20675. 98	$5d'\ {}^3D^\circ_1$— $6p''\ {}^3D_2$
4676. 902	75	21375. 69	$6p\ {}^5P_3$— $6d\ {}^5D^\circ_3$	4849. 308	4*w*	20615. 74	$5d'\ {}^3D^\circ_1$— $6p''\ {}^3P_1$
4677. 909	20*c*	21371. 09	$6p'\ {}^3D_2$— $7s'\ {}^3D^\circ_3$	4850. 303 [a]	60*c*	20611. 51	$6s\ {}^5S^\circ_2$— $6p\ {}^3P_1$
4684. 507	1*w*	21340. 99	$7p\ {}^5P_1$— 21°_1	4851. 017	20	20608. 47	$6p'\ {}^3D_1$— $7s'\ {}^3D^\circ_1$
4684. 928	2*w*	21339. 07	$5d''\ {}^1F^\circ_3$— $7f\ {}^3F_4$	4851. 292	3	20607. 31	$4f\ {}^5F_4$— $7g\ {}^3G^\circ_5$
4685. 349	1*w*	21337. 15		4853. 174	15*d*	20599. 32	$6p\ {}^3P_1$— $6d\ {}^5D^\circ_1$ $4f\ {}^5F_4$— $7g\ {}^5G^\circ_4$
4687. 468	5*c*	21327. 51	$6p'\ {}^3D_3$— $5g\ {}^3G^\circ_4$	4853. 254	15	20598. 98	$4f\ {}^5F_4$— $7g\ {}^5G^\circ_5$

TABLE 10.1. *Observed lines of* I II—Continued

λ(air)	Intensity	Wave number	Classification	λ(air)	Intensity	Wave number	Classification
4859. 150	1	20573. 98	$4f\ ^5F_3$— $7g\ ^5G^\circ_3$	5063. 37	15	19744. 19	$6p''\ ^3S_1$— 36°_2
4859. 341	1	20573. 18	$4f\ ^5F_3$— $7g\ ^3G^\circ_4$	5065. 37	400*c*, *Z*	19736. 39	$5p^5\ ^3P^\circ_2$— $6p\ ^3P_1$
4859. 786	15	20571. 29	$4f\ ^5F_3$— $7g\ ^5G^\circ_4$	5068. 08	20*c*	19725. 84	$6p''\ ^3D_1$— $7s''\ ^3P^\circ_1$
4864. 513	60	20551. 30	$6p'\ ^1D_2$— $6d'\ 14^\circ_3$ $6p''\ ^3P_2$— $44^\circ_{2,3}$	5069. 93	2	19718. 64	
				5092. 60	30	19630. 86	$6d\ ^3D^\circ_3$— $7f\ ^3F_4$
4865. 029	2	20549. 12	$7p\ ^3P_1$— $25^\circ_{1,2}$	5100. 16	8	19601. 77	$5p^5\ ^3P^\circ_0$— $6p'\ ^3D_1$
4865. 500	20	20547. 13	$4f\ ^5F_5$— $7g\ ^5G^\circ_6$	5110. 36	8	19562. 64	$6d\ ^3D^\circ_2$— $7f\ ^3F_3$
4867. 649	20	20538. 06	$5d'\ ^3D^\circ_1$— $7p\ ^5P_2$	5111. 79	6	19557. 17	$6d\ ^3D^\circ_1$— $7f\ ^3F_2$
4874. 200	2	20510. 45	$4f\ ^5F_2$— $7g\ ^3G^\circ_3$	5114. 56	20*c*	19546. 58	$6p''\ ^3D_1$— $7s''\ ^3P^\circ_0$
4874. 473	2*d*	20509. 31	$4f\ ^5F_2$— $7g\ ^5G^\circ_2$	5115. 89	2	19541. 50	$6p''\ ^1P_1$— 46°_2
4876. 051	10*c*	20502. 67	$4f\ ^5F_2$— $7g\ ^5G^\circ_3$	5124. 57	40	19508. 40	$5d\ ^3D^\circ_2$— $6p'\ ^3D_1$
4881. 185	4*h*	20481. 10		5125. 87	5	19503. 45	$7p\ ^5P_2$— $9d\ ^5D^\circ_3$
4882. 127	40*c*	20477. 15	$5d'\ ^3S^\circ_1$— $6p''\ ^3P_2$ $6p'\ ^3P_1$— $6d'\ 7^\circ_{1,2}$	5126. 58	2	19500. 75	
				5130. 20	10*c*	19486. 99	$6p'\ ^1P_1$— $6d'\ 1^\circ_2$
4884. 083	40*c*	20468. 95	$6p'\ ^1D_2$— $6d'\ 13^\circ_{1,2}$	5131. 24	50	19483. 04	$6s''\ ^1P^\circ_1$— $6p''\ ^1D_2$
4884. 828	80*c*, *Z*	20465. 83	$6s'\ ^3D^\circ_2$— $6p'\ ^1F_3$	5135. 79	100*d*	19465. 78	$5d'\ ^1P^\circ_1$— $6p''\ ^1S_0$
4886. 182	5	20460. 16	$5d'\ ^3D^\circ_1$— $6p''\ ^3P_0$	5143. 01	10	19438. 45	
4888. 423	4	20450. 78	$4f\ ^5F_1$— $7g\ ^5G^\circ_2$	5147. 55	100*c*	19421. 31	$6s''\ ^3P^\circ_1$— $4f\ ^3F_2$
4891. 224	2	20439. 07	$7s\ ^3S^\circ_1$— $7p'\ ^3P_0$	5149. 73	200	19413. 09	$5d\ ^3D^\circ_3$— $6p'\ ^3F_3$
4895. 037	10*c*	20423. 15	$6p'\ ^1P_1$— $6d'\ 4^\circ_0$	5154. 97	50	19393. 35	$6p'\ ^1F_3$— $7s'\ ^3D^\circ_3$
4899. 465	3	20404. 69	$5d'\ ^3D^\circ_1$— $7p\ ^5P_1$	5156. 41	100*Z*	19387. 94	$6p\ ^5P_1$— $7s\ ^5S^\circ_2$
4908. 755	25*c*	20366. 07	$7s\ ^3S^\circ_1$— $7p'\ ^1P_1$ $6s''\ ^3P^\circ_2$— $6p''\ ^1P_1$	5161. 20	3000*c*, *Z*	19369. 94	$6s\ ^5S^\circ_2$— $6p\ ^5P_3$
				5174. 70	50	19319. 41	$6p'\ ^3F_2$— $7s'\ ^3D^\circ_2$
4910. 579	10	20358. 51	$6p'\ ^3P_1$— $6d'\ 6^\circ_{1,2}$	5175. 32	40*d*	19317. 10	$6p'\ ^3F_2$— $7s'\ ^3D^\circ_1$
4911. 454	1	20354. 88		5176. 19	300	19313. 85	$6s''\ ^3P^\circ_2$— $6p''\ ^3P_2$
4920. 587	6*c*	20317. 10	$6p'\ ^3D_3$— $7d\ ^3D^\circ_3$	5179. 22	12	19302. 55	$6d\ ^5D^\circ_3$— $6f\ ^5F_3$
4924. 546	40*c*	20300. 77	$6s''\ ^3P^\circ_1$— $7p\ ^3P_2$	5181. 29	30	19294. 84	$6d\ ^5D^\circ_3$— $6f\ ^5F_4$
4930. 049	6	20278. 11	$6p'\ ^3P_0$— $6d'\ 5^\circ_1$	5183. 21	10	19287. 69	
4941. 533	3*c*	20230. 98	$6p'\ ^3F_4$— $7d\ ^3D^\circ_3$	5185. 17	200	19280. 40	$6p\ ^5P_2$— $7s\ ^5S^\circ_2$
4943. 163	30*c*	20224. 31	$6p'\ ^1P_1$— $7s'\ ^1D^\circ_2$	5188. 62	20	19267. 58	$5d'\ ^3S^\circ_1$— $6p''\ ^3S_1$
4957. 756	10	20164. 78	$6p\ ^3P_2$— $5d''\ ^3F^\circ_2$	5189. 90	50	19262. 83	$6d\ ^5D^\circ_4$— $6f\ ^5F_5$
4959. 992	1	20155. 69		5190. 06	20	19262. 24	$6d\ ^5D^\circ_2$— $6f\ ^5F_3$
4965. 687	50*c*	20132. 58	$6s''\ ^3P^\circ_1$— $7p\ ^3P_1$	5192. 89	4*c*	19251. 74	$6p'\ ^3P_2$— $7d\ ^3D^\circ_2$
4968. 431	80	20121. 46	$6s'\ ^3D^\circ_2$— $6p'\ ^1P_1$	5194. 15	8	19247. 07	$6d\ ^5D^\circ_4$— $6f\ ^5F_4$
4980. 773	1*c*	20071. 60	$6p''\ ^3D_2$— $7g\ ^3G^\circ_3$	5198. 89	6	19229. 52	$6p''\ ^3S_1$— 32°_1
4981. 960	1	20066. 82	$4f\ ^3F_3$— $7g\ ^3G^\circ_3$	5205. 48	20	19205. 18	$6p\ ^3P_2$— $6d\ ^5D^\circ_2$
4982. 796	3	20063. 45		5209. 26	2*c*	19191. 24	
4984. 083	15*c*	20058. 27	$4f\ ^3F_3$— $7g\ ^3G^\circ_4$	5210. 06	2*c*	19188. 29	$5d''\ ^3F^\circ_3$— $7p'\ ^3F_3$
4984. 265	5*c*	20057. 54	$6p\ ^3P_1$— $6d\ ^5D^\circ_0$	5214. 08	200*Z*	19173. 50	$5d\ ^3D^\circ_3$— $6p'\ ^3D_2$
4984. 562	3*c*	20056. 34	$4f\ ^3F_3$— $7g\ ^5G^\circ_4$	5216. 27	600*Z*	19165. 45	$5d\ ^3D^\circ_1$— $6p'\ ^3F_2$
4985. 351	2	20053. 17		5221. 76	4*d*	19145. 30	
4986. 922	1000*Z*	20046. 85	$5d\ ^3D^\circ_1$— $6p'\ ^3D_2$	5222. 51	3*c*	19142. 55	$6p'\ ^1F_3$— $6d'\ 1^\circ_2$
4990. 949	4	20030. 68	$7s'\ ^3D^\circ_2$— $13^\circ_{2,3}$	5223. 28	1*c*	19139. 73	$5d'\ ^3F^\circ_3$— $6p'\ ^1D_2$
4992. 223	50	20025. 57	$5d'\ ^1D^\circ_2$— $6p''\ ^3S_1$	5228. 97	500*d*	19118. 90	$6s''\ ^3P^\circ_1$— $6p''\ ^3D_2$
4994. 976	6*c*	20014. 53		5230. 47	1*c*	19113. 42	$5d''\ ^3D^\circ_1$— $7p'\ ^1D_2$
5000. 12	5	19993. 94	$6p\ ^5P_2$— $5d''\ ^3D^\circ_2$	5232. 00	5	19107. 83	$7p\ ^5P_3$— $9d\ ^5D^\circ_4$?
5002. 02	5*c*	19986. 35		5232. 98	3	19104. 25	$7p\ ^5P_3$— $9d\ ^5D^\circ_3$
5008. 36	100	19961. 05	$6s''\ ^3P^\circ_0$— $6p''\ ^3P_1$	5241. 64	2	19072. 69	$7p\ ^5P_1$—$10s\ ^5S^\circ_2$
5028. 82	30*c*	19879. 84	$6p'\ ^1F_3$— $7s'\ ^1D^\circ_2$	5242. 01	3	19071. 34	
5029. 39	4	19877. 58	$5d''\ ^3F^\circ_3$— $6f\ ^5F_4$	5243. 50	1*c*	19065. 92	
5029. 67	15*c*	19876. 48	$6p'\ ^3P_2$— $7d\ ^3D^\circ_3$	5245. 71	3000*c*, *Z*	19057. 89	$6s'\ ^3D^\circ_3$— $6p'\ ^3P_2$
5032. 15	6*c*	19866. 68	$6p'\ ^1F_3$— $6d'\ 3^\circ_3$	5256. 19	1*c*	19019. 89	
5040. 23	15*w*	19834. 83	$6p''\ ^3D_3$— 39°_4	5259. 34	2	19008. 50	
5045. 55	25	19813. 92	$4f\ ^3F_4$— $7g\ ^3G^\circ_5$	5261. 27	15*c*	19001. 53	$5d'\ ^3D^\circ_2$— $6p'\ ^3P_1$
5046. 43	150*Z*	19810. 47	$6s'\ ^3D^\circ_1$— $6p'\ ^3P_0$	5263. 47	2	18993. 59	$5d''\ ^3F^\circ_3$— $7p'\ ^1D_2$
5048. 16	10*c*	19803. 68		5265. 16	150*c*, *Z*	18987. 49	$6s'\ ^3D^\circ_1$— $6p'\ ^1P_1$
5049. 52	5*c*	19798. 34	$6p'\ ^1F_3$— $6d'\ 2^\circ_3$	5266. 96	100*c*	18981. 00	$6s''\ ^3P^\circ_1$— $7p\ ^5P_2$
5052. 70	6	19785. 88	$5d'\ ^1S^\circ_0$— $6p''\ ^1P_1$	5269. 36	500	18972. 36	$6s''\ ^3P^\circ_2$— $6p''\ ^3D_3$
5057. 00	3	19769. 06	$4f\ ^3F_2$— $7g\ ^3G^\circ_3$	5270. 58	2	18967. 97	$5d''\ ^3F^\circ_3$— $7p'\ ^1F_3$
5061. 91	150	19749. 88	$6s''\ ^3P^\circ_0$— $7p\ ^5P_1$	5272. 52	5	18960. 99	$5d''\ ^3D^\circ_1$— $4f'\ ^3D_1$

TABLE 10.1. *Observed lines of* I II—Continued

λ(air)	Intensity	Wave number	Classification	λ(air)	Intensity	Wave number	Classification
5278. 57	4	18939. 25	$7p\ {}^5P_2$—$10s\ {}^5S_2^\circ$	5491. 50	800*Z*	18204. 90	$6p\ {}^5P_3$— $7s\ {}^5S_2^\circ$
5286. 09	8*c*	18912. 31	$5d''\ {}^3F_3^\circ$— $7p'\ {}^3F_4$	5492. 31	5	18202. 22	
5288. 68	200*c*	18903. 05	$6s''\ {}^3P_1^\circ$— $6p''\ {}^3P_0$	5493. 43	400	18198. 51	$6p'\ {}^3F_3$— $7s'\ {}^3D_2^\circ$
5291. 68	8	18892. 33	$5d'\ {}^3F_2^\circ$— $7p\ {}^3P_2$	5494. 00	400*c*	18196. 62	$6p'\ {}^3F_4$— $7s'\ {}^3D_3^\circ$
				5496. 94	1000*c*	18186. 89	$6s\ {}^5S_2^\circ$— $6p\ {}^5P_1$
5293. 65	4	18885. 30					
5294. 11	10	18883. 66	$6p''\ {}^3P_2$— 37_2°	5497. 65	300	18184. 54	$5d'\ {}^3D_2^\circ$— $6p'\ {}^3D_3$
5296. 24	50	18876. 07	$6p''\ {}^3D_3$— 36_3°	5504. 72	1000*Z*	18161. 18	$6s\ {}^3S_1^\circ$— $6p\ {}^3P_0$
5296. 45	20	18875. 32	$6p'\ {}^3P_1$— $7d\ {}^3D_2^\circ$	5510. 50	2	18142. 13	
5299. 78	400	18863. 46	$6s''\ {}^1P_1^\circ$— $6p''\ {}^1P_1$	5517. 23	2	18120. 00	
				5518. 38	8	18116. 23	$7p\ {}^5P_1$— $7s''\ {}^3P_0^\circ$
5303. 42	4	18850. 51	$6d\ {}^5D_1^\circ$— $6f\ {}^5F_2$?				
5304. 25	60*c*	18847. 56	$6s''\ {}^3P_1^\circ$— $7p\ {}^5P_1$	5522. 06	600*c*	18104. 16	$6s''\ {}^3P_2^\circ$— $6p''\ {}^3S_1$
5305. 87	5*c*	18841. 81		5523. 60	8	18099. 11	$6p'\ {}^3P_0$— $5d''\ {}^3P_1^\circ$
5306. 56	2	18839. 36		5525. 44	12	18093. 08	$7s\ {}^5S_2^\circ$— $8p\ {}^3P_2$
5307. 63	10*c*	18835. 56	$5d''\ {}^3D_1^\circ$— $7p'\ {}^3F_2$	5525. 92	5*c*	18091. 51	
				5527. 88	6	18085. 09	
5309. 44	20	18829. 14	$6p'\ {}^3P_1$— $6d'\ 5_1^\circ$				
5322. 80	400*Z*	18781. 88	$5p^5\ {}^3P_1^\circ$— $6p\ {}^3P_0$	5528. 09	6	18084. 41	$6p''\ {}^3P_1$— $7s''\ {}^3P_1^\circ$
5323. 83	80	18778. 25	$5d'\ {}^3G_3^\circ$— $7p\ {}^3P_2$	5528. 19	2	18084. 08	
5326. 39	100*c*	18769. 22	$6p'\ {}^3D_3$— $7s'\ {}^1D_2^\circ$	5531. 96	2	18071. 76	$6p\ {}^3P_0$— $5d''\ {}^3D_1^\circ$
5327. 54	15	18765. 17	$5d''\ {}^3P_2^\circ$— $8p\ {}^3P_2$	5538. 08	6*c*	18051. 79	$5d'\ {}^1F_3^\circ$— $6p''\ {}^1D_2$ $5d''\ {}^3D_2^\circ$— $7p'\ {}^3P_2$
5330. 13	8*c*	18756. 05	$6p'\ {}^3D_3$— $6d'\ 3_3^\circ$	5541. 52	4	18040. 58	
5337. 13	15	18731. 45					
5338. 22	10000*Z*	18727. 63	$6s'\ {}^3D_2^\circ$— $6p'\ {}^3F_3$	5541. 96	8	18039. 15	$5d''\ {}^3D_2^\circ$— $7p'\ {}^3D_3$
5345. 15	5000*c*, *Z*	18703. 35	$6s'\ {}^3D_3^\circ$— $6p'\ {}^3F_4$	5544. 17	10*c*	18031. 96	$6p'\ {}^3D_3$— $6d'\ 1_2^\circ$
5349. 61	50*c*	18687. 75	$6p'\ {}^3D_3$— $6d'\ 2_3^\circ$	5546. 55	30*w*	18024. 22	$6p''\ {}^3D_2$— $7s''\ {}^3P_1^\circ$
				5550. 08	50	18012. 76	$5d'\ {}^3F_2^\circ$— $4f\ {}^3F_2$
5351. 85	75*c*	18679. 93	$5p^5\ {}^1P_1^\circ$— $6p'\ {}^3P_0$ $6p''\ {}^3S_1$— 30_2°	5550. 51	2	18011. 36	$6d\ {}^5D_1^\circ$— $7p'\ {}^1P_1$
5354. 71	8*c*	18669. 96		5551. 65	400	18007. 66	$6s'\ {}^1D_2^\circ$— $6p'\ {}^3P_2$
5367. 60	150*c*	18625. 12	$5d'\ {}^3D_2^\circ$— $6p'\ {}^3P_2$	5568. 80	20*c*	17952. 21	$6p'\ {}^3P_1$— $7s'\ {}^1D_2^\circ$
5369. 10	15*c*	18619. 92	$5d''\ {}^3F_2^\circ$— $6f\ {}^3F_3$	5569. 56	6	17949. 76	$5d''\ {}^1F_3^\circ$— $6f\ {}^3F_4$
5369. 86	1000*c*	18617. 28	$6s'\ {}^3D_3^\circ$— $6p'\ {}^3D_3$	5570. 60	2	17946. 40	$7p\ {}^3P_1$— $10s\ {}^3S_1^\circ$
				5575. 78	3	17929. 73	
5372. 49	30	18608. 17	$6p\ {}^5P_2$— $5d''\ {}^3P_2^\circ$				
5373. 27	6*c*	18605. 47	$6d\ {}^5D_3^\circ$— $7p'\ {}^3F_3$	5583. 44	25	17905. 13	$6p''\ {}^3P_1$— $7s''\ {}^3P_0^\circ$
5374. 38	30*c*	18601. 63	$6p'\ {}^3F_4$— $6d'\ 2_3^\circ$	5584. 04	20	17903. 21	
5376. 04	4	18595. 88		5585. 48	4	17898. 59	$5d'\ {}^3G_3^\circ$— $4f\ {}^3F_2$
5378. 99	3	18585. 68	$5d'\ {}^3P_1^\circ$— $7p'\ {}^3P_1$	5587. 88	4	17890. 91	$5d''\ {}^1F_3^\circ$— $6f\ {}^3F_2$
				5589. 29	80	17886. 39	$5d'\ {}^3S_1^\circ$— $7p\ {}^3P_0$
5380. 04	60	18582. 06	$6p\ {}^3P_2$— $5d''\ {}^3F_3^\circ$				
5386. 23	20	18560. 70	$7p\ {}^3P_2$— $9d\ {}^3D_3^\circ$	5590. 20	8	17883. 48	$6p'\ {}^3D_1$— $5d''\ {}^1P_1^\circ$
5387. 56	4*c*	18556. 12	$6p''\ {}^3D_3$— 34_3°	5593. 12	300*Z*	17874. 15	$5d\ {}^3D_1^\circ$— $6p'\ {}^3D_1$
5392. 27	12	18539. 91	$7p\ {}^5P_3$—$10s\ {}^5S_2^\circ$	5595. 47	4*w*	17866. 64	$5d'\ {}^1D_2^\circ$— $7p\ {}^3P_2$
5393. 39	10	18536. 06		5598. 52	600*c*	17856. 91	$5p^5\ {}^1P_1^\circ$— $6p'\ {}^1P_1$
				5600. 32	1000	17851. 17	$5d'\ {}^3G_3^\circ$— $4f\ {}^3F_4$
5393. 86	8	18534. 45	$6p''\ {}^3P_2$— 36_2°				
5399. 53	3	18514. 98		5601. 94	4	17846. 00	
5405. 42	800*c*, *Z*	18494. 81	$5p^5\ {}^3P_2^\circ$— $6p\ {}^5P_3$	5603. 16	80	17842. 12	$6p'\ {}^3P_2$— $7s'\ {}^3D_3^\circ$
5407. 36	800*c*	18488. 17	$6s'\ {}^3D_3^\circ$— $6p'\ {}^3D_2$	5606. 52	15	17831. 43	$6p''\ {}^1P_1$— 37_2°
5414. 96	15	18462. 23	$6p\ {}^3P_2$— $5d''\ {}^3D_1^\circ$ $6p'\ {}^3P_1$— $7d\ {}^5D_1^\circ$	5608. 41	4	17825. 42	
				5612. 89	1500	17811. 19	$6s''\ {}^1P_1^\circ$— $6p''\ {}^3P_2$ $6p''\ {}^3D_3$— 30_2°
5422. 05	100	18438. 08	$6p'\ {}^3D_2$— $7s'\ {}^3D_2^\circ$				
5422. 74	100	18435. 74	$6p'\ {}^3D_2$— $7s'\ {}^3D_1^\circ$	5616. 77	10	17798. 89	
5425. 06	4*d*	18427. 85	$7p\ {}^3P_2$— $9d\ {}^3D_2^\circ$	5618. 28	6	17794. 10	
5435. 83	3000	18391. 34	$5p^5\ {}^3P_1^\circ$— $6p\ {}^3P_2$	5618. 57	5	17793. 18	$6d\ {}^5D_1^\circ$— $4f'\ {}^3D_1$
5438. 00	1000*Z*	18384. 00	$6s'\ {}^1D_2^\circ$— $6p'\ {}^3P_1$	5620. 02	10*c*	17788. 59	$5d''\ {}^3D_3^\circ$— $6p''\ {}^1D_2$
				5623. 30	12	17778. 22	$7p\ {}^3P_2$—$10s\ {}^3S_1^\circ$
5448. 80	10	18347. 57	$7s\ {}^3S_1^\circ$— $4f'\ {}^3P_0$				
5454. 43	8*d*	18328. 63	$6f'\ {}^3P_2$— $7s'\ {}^1D_2^\circ$	5625. 69	10000*Z*	17770. 67	$6s\ {}^3S_1^\circ$— $6p\ {}^3P_2$
5457. 06	200*c*	18319. 79	$6s''\ {}^3P_0^\circ$— $6p''\ {}^3D_1$ $5d''\ {}^3D_2^\circ$— $4f'\ {}^3P_2$	5638. 91	1	17729. 00	$6p''\ {}^3S_1$— 21_1°
				5639. 78	1	17726. 27	
5458. 36	15*c*	18315. 43	$6p'\ {}^3P_2$— $6d'\ 3_3^\circ$	5641. 10	20*c*	17722. 12	$4f\ {}^3F_2$— $7s''\ {}^3P_1^\circ$
5464. 62	2000*c*	18294. 45	$6s\ {}^5S_2^\circ$— $6p\ {}^5P_2$	5643. 32	100	17715. 15	$5d'\ {}^3F_2^\circ$— $4f\ {}^3F_3$
5467. 52	15	18284. 75	$6p'\ {}^3P_1$— $7d\ {}^5D_2^\circ$	5643. 67	5*c*	17714. 05	$5d''\ {}^3F_2^\circ$— $4f'\ {}^1D_2$
5468. 12	50	18282. 74	$6p'\ {}^3D_3$— $7s'\ {}^3D_3^\circ$	5648. 66	15*c*	17698. 40	$5d'\ {}^1D_2^\circ$— $7p\ {}^3P_1$
5478. 80	2*w*	18247. 10	$6p'\ {}^3P_2$— $6d'\ 2_3^\circ$	5649. 06	2	17697. 15	
5479. 56	60	18244. 57	$6p\ {}^3P_1$— $7s\ {}^3S_1^\circ$	5655. 10	10	17678. 25	
5480. 84	10*c*	18240. 31	$6p''\ {}^3P_0$— $7s''\ {}^3P_1^\circ$	5655. 52	5*w*	17676. 93	$6p\ {}^3P_1$— $5d''\ {}^3D_2^\circ$

TABLE 10.1. *Observed lines of* I II—Continued

λ(air)	Intensity	Wave number	Classification	λ(air)	Intensity	Wave number	Classification
5658. 46	8*c*	17667. 75	$6d\ {}^5D_1^\circ$— $7p'\ {}^3F_2$	5812. 31	4*c*	17200. 09	$5d'\ {}^3F_2^\circ$— $4f\ {}^5F_3$
5663. 63	25	17651. 62	$5d'\ {}^3P_1^\circ$— $5f\ {}^3F_2$	5815. 06	40	17191. 96	$4f\ {}^5F_1$— $6g\ {}^5G_2^\circ$
5665. 71	6	17645. 14		5819. 71	80*c*	17178. 22	$5d'\ {}^3D_3^\circ$— $6p'\ {}^3F_4$
5676. 70	7	17610. 98		5821. 97	30*w*	17171. 56	
5678. 08	1000*Z*	17606. 70	$6s'\ {}^3D_2^\circ$— $6p'\ {}^3F_2$	5823. 54	3*c*	17166. 93	
5678. 88	1*c*	17604. 22		5823. 71	10	17166. 43	
5679. 92	50	17601. 00	$5d'\ {}^3G_3^\circ$— $4f\ {}^3F_3$	5824. 19	20	17165. 01	
5682. 64	15	17592. 57		5825. 69	6	17160. 59	$5d''\ {}^3D_1^\circ$— $4f'\ {}^3P_0$
5683. 83	2	17588. 89	$6p'\ {}^3P_2$— $8s\ {}^3S_1^\circ$	5827. 74	4	17154. 55	
5688. 21	30	17575. 35		5830. 79	4*c*	17145. 58	
5690. 91	2000*c*, *Z*	17567. 01	$6s'\ {}^1D_2^\circ$— $6p'\ {}^3D_3$	5832. 86	15	17139. 50	
5692. 68	10	17561. 55	$7s\ {}^5S_2^\circ$— $4f'\ {}^3D_3$	5834. 78	8*c*	17133. 86	
5698. 97	2	17542. 16		5835. 06	10	17133. 04	$5d''\ {}^3F_2^\circ$— $7p'\ {}^3F_2$
5702. 05	500*Z*	17532. 69	$5d'\ {}^3D_3^\circ$— $6p'\ {}^3P_2$	5838. 57	8	17122. 74	
5704. 87	20	17524. 02	$5d'\ {}^1S_0^\circ$— $6p''\ {}^3S_1$	5839. 88	2	17118. 89	
5710. 53	4000*c*, *Z*	17506. 65	$6s'\ {}^3D_3^\circ$— $6p'\ {}^1F_3$	5843. 38	50	17108. 64	$5d'\ {}^3S_1^\circ$— $7p\ {}^3P_2$
5715. 57	40	17491. 22		5845. 04	6	17103. 78	
5716. 34	3	17488. 86		5849. 03	20	17092. 11	$5d'\ {}^3D_3^\circ$— $6p'\ {}^3D_3$
5717. 58	1*c*	17485. 07		5851. 76	20	17084. 14	
5717. 85	5	17484. 24	$7s\ {}^3S_1^\circ$— $7p'\ {}^3P_2$	5855. 26	10*d*	17073. 93	$5d'\ {}^3D_2^\circ$— $6p'\ {}^1F_3$
5726. 76	15	17457. 04		5863. 07	5	17051. 19	
5733. 46	20	17436. 64	$7s\ {}^5S_2^\circ$— $8p\ {}^5P_2$?	5868. 64	5	17035. 00	
5735. 69	12	17429. 86		5873. 12	3	17022. 01	
5735. 87	15	17429. 31		5893. 06	20	16964. 41	
5738. 27	1000*Z*	17422. 02	$5p^5\ {}^3P_1^\circ$— $6p\ {}^3P_1$	5899. 47	8*c*	16945. 98	$5d'\ {}^1D_2^\circ$— $7p\ {}^5P_3$
5738. 83	40	17420. 32		5901. 41	60	16940. 41	$5d'\ {}^3S_1^\circ$— $7p\ {}^3P_1$
5738. 89	70	17420. 14		5906. 04	10	16927. 13	
5739. 01	100	17419. 78	$5p^5\ {}^3P_2^\circ$— $6p\ {}^5P_2$	5910. 42	20	16914. 58	
5739. 18	150	17419. 26		5911. 18	20	16912. 41	$5d''\ {}^1F_3^\circ$— $4f'\ {}^1D_2$
5739. 40	200	17418. 59		5911. 78	12	16910. 69	
5739. 59	150	17418. 02		5911. 96	60	16910. 18	
5739. 77	200	17417. 47	$6s''\ {}^3P_1^\circ$— $6p''\ {}^3D_1$	5913. 40	10	16906. 06	
5739. 88	70	17417. 14		5913. 67	50	16905. 29	
5739. 95	40	17416. 92		5918. 10	12	16892. 63	
5741. 94	3	17410. 89	$5d''\ {}^3F_2^\circ$— $7p'\ {}^1D_2$	5920. 59	200*Z*	16885. 53	$5d\ {}^5D_3^\circ$— $6p\ {}^3P_2$
5743. 06	30	17407. 49		5920. 87	40	16884. 73	$6p\ {}^3P_0$— $7s\ {}^3S_1^\circ$
5749. 04	5	17389. 39		5928. 63	20	16862. 63	$6p''\ {}^1D_2$— 36_2°
5750. 41	50	17385. 24	$5d''\ {}^3F_2^\circ$— $7p'\ {}^1F_3$	5934. 96	10	16844. 65	
5752. 35	25*c*	17379. 38	$5d''\ {}^3D_2^\circ$— $8p\ {}^3P_2$	5938. 35	10	16835. 03	
5757. 22	6*c*	17364. 68		5939. 69[c]	100	16831. 23	$7p\ {}^3P_1$— $7s''\ {}^3P_0^\circ$
5760. 72	1000*Z*	17354. 13	$6s'\ {}^3D_1^\circ$— $6p'\ {}^3D_2$	5946. 15	15*c*	16812. 95	$6p''\ {}^3D_2$— $6g\ {}^3G_3^\circ$
5763. 14	25	17346. 84	$4f\ {}^5F_4$— $6g\ {}^3G_5^\circ$	5947. 79	5	16808. 31	$4f\ {}^3F_3$— $6g\ {}^3G_3^\circ$
5765. 43	3*c*	17339. 95		5950. 25	5000*Z*	16801. 36	$6s\ {}^3S_1^\circ$— $6p\ {}^3P_1$
5765. 68	8	17339. 20	$4f\ {}^5F_4$— $6g\ {}^3G_4^\circ$ $4f\ {}^5F_4$— $6g\ {}^5G_3^\circ$	5952. 09	50	16796. 17	$4f\ {}^3F_3$— $6g\ {}^3G_4^\circ$ $4f\ {}^3F_3$— $6g\ {}^5G_3^\circ$
5767. 19	100	17334. 66	$4f\ {}^5F_4$— $6g\ {}^5G_5^\circ$				
5769. 01	8	17329. 19		5953. 66	20	16791. 74	$4f\ {}^3F_3$— $6g\ {}^5G_4^\circ$
5770. 46	3*h*	17324. 84	$7s'\ {}^3D_2^\circ$— $3_{2,3}$	5975. 83	25*w*	16729. 44	$5d'\ {}^3D_2^\circ$— $6p'\ {}^1P_1$
5771. 02	10	17323. 16	$4f\ {}^5F_3$— $6g\ {}^3G_3^\circ$	5983. 69	6*c*	16707. 47	$6p\ {}^3P_2$— $5d''\ {}^3D_2^\circ$
5774. 83	500*c*	17311. 73	$5p^5\ {}^3P_2^\circ$— $6p\ {}^5P_1$	5986. 27	3	16700. 27	
5776. 54	50	17306. 60	$4f\ {}^5F_3$— $6g\ {}^5G_4^\circ$	5988. 23	12	16694. 80	
5783. 34	100	17286. 25	$4f\ {}^5F_5$— $6g\ {}^5G_6^\circ$	5990. 17	20*c*	16689. 39	$5d'\ {}^1D_2^\circ$— $4f\ {}^3F_3$
5787. 02	500	17275. 26	$6p\ {}^3P_2$— $7s\ {}^3S_1^\circ$	5991. 86	30	16684. 69	$5d'\ {}^1D_2^\circ$— $6p''\ {}^3D_2$
5790. 26	10	17265. 59		6008. 19	15	16639. 34	
5794. 85	25	17251. 92	$4f\ {}^5F_2$— $6g\ {}^3G_3^\circ$	6013. 55	7*c*	16624. 51	$5d'\ {}^1D_2^\circ$— $6p''\ {}^3P_1$
5795. 30	10	17250. 58	$4f\ {}^5F_2$— $6g\ {}^5G_2^\circ$	6021. 88	50	16601. 51	$6s''\ {}^1P_1^\circ$— $6p''\ {}^3S_1$
5797. 02	50	17245. 46		6028. 43	10	16583. 47	$5d''\ {}^1F_3^\circ$— $7p'\ {}^1F_3$
5798. 95[b]	100	17239. 72	$4f\ {}^5F_2$— $6g\ {}^5G_3^\circ$	6031. 41	8*c*	16575. 28	$5f\ {}^3F_3$— $50_{3,4}^\circ$
5807. 29	15	17214. 96	$6p'\ {}^3P_1$— $6d'\ 1_2^\circ$	6032. 80	20*w*	16571. 46	
5808. 21	3	17212. 24	$6p'\ {}^3P_1$— $8s\ {}^3S_1^\circ$	6033. 44	10	16569. 70	$7p\ {}^5P_1$— $8d\ {}^3D_1^\circ$
5808. 38	5	17211. 73	$6p''\ {}^1D_2$— 37_2°	6035. 13	20	16565. 06	$5d''\ {}^3D_1^\circ$— $4f'\ {}^3P_2$

TABLE 10.1. *Observed lines of* I II—Continued

λ(air)	Intensity	Wave number	Classification
6036. 15	3*c*	16562. 27	
6039. 32	100	16553. 57	$4f\ {}^3F_4$— $6g\ {}^3G^\circ_5$
6041. 60	100	16547. 33	$5d'\ {}^1P^\circ_1$— $6p''\ {}^1D_2$
6043. 79	15	16541. 33	$4f\ {}^3F_4$— $6g\ {}^5G^\circ_5$
6048. 70	50	16527. 90	$5d''\ {}^1F^\circ_3$— $7p'\ {}^3F_4$
6051. 82	10*c*	16519. 38	$6p''\ {}^3P_2$— 21°_1
6055. 06[d]	50*d*	16510. 54	$4f\ {}^3F_2$— $6g\ {}^3G^\circ_3$
6059. 53	8*c*	16498. 36	$4f\ {}^3F_2$— $6g\ {}^5G^\circ_3$
6068. 93	500*Z*	16472. 81	$6s'\ {}^3D^\circ_1$— $6p'\ {}^3F_2$
6074. 98	2000*c*, *Z*	16456. 40	$6s'\ {}^1D^\circ_2$— $6p'\ {}^1F_3$
6077. 83	150	16448. 69	$5d\ {}^5D^\circ_2$— $6p\ {}^3P_2$
6084. 78	30	16429. 90	$6p\ {}^3P_1$— $5d'\ {}^3P^\circ_1$
6090. 90	12*c*	16413. 39	$5d'\ {}^1D^\circ_2$— $7p\ {}^5P_1$
6094. 08	20*c*	16404. 83	$5d''\ {}^1D^\circ_2$— $6p''\ {}^3P_2$ $5d''\ {}^3D^\circ_2$— $5f\ {}^3F_2$
6094. 33	15	16404. 15	
6103. 37	150	16379. 86	$5d'\ {}^1F^\circ_3$— $6p''\ {}^3P_2$
6103. 87	15	16378. 52	
6111. 35	6	16358. 47	$6p''\ {}^3P_1$— $8d\ {}^3D^\circ_1$
6127. 49	2000*c*, *Z*	16315. 38	$6s'\ {}^3D^\circ_2$— $6p'\ {}^3D_1$
6132. 86	20	16301. 09	$6p''\ {}^3P_1$— $8d\ {}^3D^\circ_2$
6137. 39	20	16289. 06	$5d'\ {}^3P^\circ_1$— $6p''\ {}^1S_0$
6148. 15	40*d*	16260. 56	
6148. 34	50*Z*	16260. 05	$5d\ {}^5D^\circ_0$— $6p\ {}^3P_1$
6155. 36	200	16241. 51	$6d\ {}^3D^\circ_3$— $6f\ {}^3F_4$
6155. 97	6	16239. 90	
6156. 77	12	16237. 79	
6157. 14	15	16236. 81	
6158. 18	20	16234. 07	
6160. 09	15*c*	16229. 04	$5d'\ {}^3S^\circ_1$— $4f\ {}^3F_2$
6162. 22	300*c*	16223. 43	$5p^5\ {}^1P^\circ_1$— $6p'\ {}^3D_2$ $6d\ {}^3D^\circ_2$— $6f\ {}^3F_2$
6164. 88	8*c*	16216. 43	
6166. 44	40*c*	16212. 33	
6172. 84	4	16195. 52	$6p''\ {}^1P_1$— 29°_1
6182. 28	60	16170. 79	
6184. 62	10	16164. 67	$5d''\ {}^3F^\circ_3$— $7p'\ {}^3D_3$
6186. 93	3	16158. 63	$4f\ {}^5F_3$— $8d\ {}^5D^\circ_2$
6189. 94	60	16150. 78	$6d\ {}^3D^\circ_2$— $6f\ {}^3F_3$ $7p\ {}^5P_3$— $8d\ {}^3D^\circ_3$
6197. 16	50*c*	16131. 96	$6d\ {}^3D^\circ_1$— $6f\ {}^3F_2$
6201. 69	2	16120. 18	
6203. 04	20*c*	16116. 67	$5d''\ {}^3D^\circ_3$— $6p''\ {}^3P_2$
6204. 86	1000*Z*	16111. 94	$6s'\ {}^1D^\circ_2$— $6p'\ {}^1P_1$
6205. 61	5	16109. 99	$6d\ {}^3D^\circ_3$— $6f\ {}^3F_3$
6222. 93	3	16065. 16	$6p''\ {}^3P_2$— $20^\circ_{1,2}$
6223. 15	2	16064. 59	$7p\ {}^2P_0$— $7s''\ {}^3P^\circ_1$
6223. 66	3	16063. 27	$5d''\ {}^1D^\circ_2$— $6p''\ {}^3D_3$
6225. 07	1	16059. 63	$5f\ {}^5F_5$—$12g\ {}^5G^\circ_6$
6238. 58	5*c*	16024. 86	
6239. 89	2*d*	16021. 49	$5d''\ {}^3D^\circ_2$— $5f\ {}^3F_3$
6250. 59	40	15994. 07	$6p\ {}^3P_2$— $7s\ {}^5S^\circ_2$
6255. 53	500*c*	15981. 44	$5d'\ {}^3D^\circ_3$— $6p'\ {}^1F_3$
6256. 33	40	15979. 39	$6p'\ {}^3P_0$— $7s'\ {}^3D^\circ_1$
6257. 49	900*c*	15976. 43	$5d'\ {}^3F^\circ_4$— $6p'\ {}^3F_4$
6269. 70	1*c*	15945. 32	$6s''\ {}^3P^\circ_2$— $7p\ {}^3P_2$
6272. 37	3*c*	15938. 53	$5d''\ {}^3D^\circ_1$— $4f'\ {}^3D_2$
6273. 16	15	15936. 52	$7p\ {}^5P_1$— $8d\ {}^5D^\circ_1$
6276. 65	40*c*	15927. 66	
6277. 05	30*c*	15926. 65	$5d'\ {}^3S^\circ_1$— $6p''\ {}^3D_2$
6279. 79	12	15919. 70	$7p\ {}^5P_1$— $8d\ {}^5D^\circ_2$
6280. 36	80*c*	15918. 25	$5d'\ {}^3P^\circ_0$— $6p'\ {}^1P_1$
6282. 61	20	15912. 55	$7p\ {}^5P_1$— $8d\ {}^5D^\circ_0$
6291. 39	500	15890. 34	$5d'\ {}^3F^\circ_4$— $6p'\ {}^3D_3$
6300. 47	3	15867. 44	
6300. 84	15	15866. 51	$5d'\ {}^3S^\circ_1$— $6p''\ {}^3P_1$
6320. 41	3*h*	15817. 38	$5d''\ {}^3D^\circ_2$— $5f\ {}^5F_3$
6326. 10	4	15803. 16	$7p\ {}^5P_2$— $8d\ {}^5D^\circ_1$
6326. 45	2*c*	15802. 28	
6329. 38	40	15794. 97	$7p\ {}^5P_2$— $8d\ {}^5D^\circ_3$
6331. 87	30*w*	15788. 76	$5d'\ {}^3S^\circ_1$— $7p\ {}^5P_2$
6332. 84	25	15786. 34	$7p\ {}^5P_2$— $8d\ {}^5D^\circ_2$
6336. 57	100*c*	15777. 05	$6s''\ {}^3P^\circ_2$— $7p\ {}^3P_1$
6339. 97	140*c*	15768. 59	$6s'\ {}^3D^\circ_3$— $6p'\ {}^3F_3$
6341. 24	100*c*	15765. 43	$5d'\ {}^3F^\circ_3$— $6p'\ {}^3P_2$
6347. 77	4	15749. 21	
6357. 37	6	15725. 43	$6p''\ {}^3P_1$— $8d\ {}^5D^\circ_1$
6363. 27	50	15710. 85	$6p'\ {}^3D_2$— $5d''\ {}^1P^\circ_1$ $5d'\ {}^3S^\circ_1$— $6p''\ {}^3P_0$
6364. 23	8	15708. 48	$6p''\ {}^3P_1$— $8d\ {}^5D^\circ_2$
6385. 14	5*c*	15657. 04	$6p''\ {}^3D_2$— $8d\ {}^5D^\circ_3$
6385. 46	8	15656. 25	$6p''\ {}^1P_1$— $24^\circ_{1,2}$
6385. 80	30	15655. 42	$5d'\ {}^3S^\circ_1$— $7p\ {}^5P_1$
6387. 38	5	15651. 55	
6388. 66	5*c*	15648. 41	$6p''\ {}^3D_2$— $8d\ {}^5D^\circ_2$
6389. 60	7	15646. 11	
6393. 58	3*h*	15636. 37	
6395. 33	15	15632. 09	
6420. 96	10	15569. 69	
6421. 12	20	15569. 30	
6430. 42	12	15546. 79	
6440. 46	400*c*	15522. 55	
6458. 41	30	15479. 41	$5d\ {}^5D^\circ_2$— $6p\ {}^3P_1$
6459. 46	2	15476. 89	$5f\ {}^5F_5$—$11g\ {}^5G^\circ_6$
6464. 79	30*w*	15464. 13	$6p'\ {}^1D_2$— $7d\ {}^5D^\circ_1$
6466. 42	4*h*	15460. 24	$6p''\ {}^3S_1$—$10s\ {}^5S^\circ_2$
6470. 25	8	15451. 08	$5d''\ {}^3D^\circ_1$— $4f'\ {}^3F_2$
6488. 97	50	15406. 51	$7p\ {}^5P_3$— $8d\ {}^5D^\circ_4$
6492. 86	6	15397. 28	$6d\ {}^5D^\circ_1$— $4f'\ {}^3P_2$
6493. 49	20	15395. 79	$7p\ {}^5P_3$— $8d\ {}^5D^\circ_3$
6497. 12	4	15387. 18	$7p\ {}^5P_3$— $8d\ {}^5D^\circ_2$
6509. 39	3*c*	15358. 18	
6512. 98	6*c*	15349. 71	$6p'\ {}^3D_3$— $7s'\ {}^3D^\circ_2$
6516. 18	250*c*, *Z*	15342. 18	$5p^5\ {}^1P^\circ_1$— $6p'\ {}^3F_2$
6518. 91	12*c*	15335. 75	
6520. 26	5	15332. 58	$5d''\ {}^3D^\circ_1$— $8p\ {}^3P_1$
6523. 60	20*c*	15324. 73	$5d'\ {}^3F^\circ_3$— $6p'\ {}^3D_3$
6525. 93	3	15319. 25	$7d\ {}^3D^\circ_2$— $12_{1,2}$
6526. 76	10	15317. 31	
6538. 32	20	15290. 23	$5d'\ {}^3P^\circ_2$— $6p''\ {}^3P_2$
6539. 96	2	15286. 39	
6540. 73	12	15284. 59	$5p\ {}^3P_1$— $8d\ {}^3D^\circ_1$
6544. 01	10*c*	15276. 93	
6545. 60	10	15273. 22	
6546. 97	20*c*	15270. 02	$5d\ {}^5D^\circ_1$— $6p\ {}^3P_0$
6555. 68	20	15249. 74	
6564. 14	40	15230. 08	$7p\ {}^3P_2$— $8d\ {}^3D^\circ_3$
6565. 37	15	15227. 23	$7p\ {}^3P_1$— $8d\ {}^3D^\circ_2$
6567. 76	2	15221. 69	$6d\ {}^3D^\circ_1$— $4f'\ {}^1P_1$

TABLE 10.1. *Observed lines of* I II—Continued

λ(air)	Intensity	Wave number	Classification
6567. 98	2	15221. 18	
6576. 04	3	15202. 52	
6578. 50	10	15196. 84	$5d'\ {}^1S^\circ_0$— $7p\ {}^3P_1$
6585. 21	400	15181. 35	$6s'\ {}^3D^\circ_1$— $6p'\ {}^3D_1$
6613. 82	4	15115. 68	$4f'\ {}^3H_4$— $50^\circ_{3,4}$
6618. 51	4	15104. 97	$5p^5\ {}^3P^\circ_1$— $6p\ {}^5P_2$
6621. 71	12	15097. 67	
6622. 35	120c	15096. 21	$5d'\ {}^3D^\circ_2$— $6p'\ {}^3D_2$
6633. 86	20	15070. 02	$6p\ {}^3P_0$— $5d'\ {}^3P^\circ_1$
6638. 72	15	15058. 99	$7p\ {}^3P_2$— $8d\ {}^3D^\circ_2$
6646. 73	3	15040. 84	
6659. 49	20	15012. 02	
6665. 96	600Z	14997. 45	$5p^5\ {}^3P^\circ_1$— $6p\ {}^5P_1$
6672. 27	100c	14983. 27	$5d'\ {}^1D^\circ_2$— $6p''\ {}^3D_1$
6679. 77	6c	14966. 44	
6685. 20	60c	14954. 29	$6p'\ {}^1D_2$— $7s'\ {}^1D^\circ_2$
6687. 71	40	14948. 67	$5d'\ {}^3P^\circ_2$— $6p''\ {}^3D_3$
6690. 84	6	14941. 68	$6d\ {}^3D^\circ_2$— $7p'\ {}^1D_2$
6705. 45	10c	14909. 13	$6p'\ {}^3P_2$— $7s'\ {}^3D^\circ_2$
6708. 73	5c	14901. 84	
6709. 12	3c	14900. 97	$6d\ {}^3D^\circ_3$— $7p'\ {}^1D_2$
6711. 79	1	14895. 04	
6712. 03	8	14894. 51	$5d''\ {}^3F^\circ_3$— $4f'\ {}^3G_4$
6717. 05	80	14883. 38	
6717. 74	10	14881. 85	$6d\ {}^5D^\circ_2$— $8p\ {}^3P_2$
6718. 83	300Z	14879. 44	$5d\ {}^5D^\circ_1$— $6p\ {}^3P_2$
6720. 66	100	14875. 30	$5d'\ {}^1P^\circ_1$— $6p''\ {}^3P_2$; $6d\ {}^3D^\circ_3$— $7p'\ {}^1F_3$
6721. 43	20	14873. 68	$7p\ {}^5P_2$— $9s\ {}^5S^\circ_2$
6725. 77	4c	14864. 08	
6739. 92	35	14832. 88	
6744. 30	5h	14823. 24	
6745. 90	6c	14819. 73	$6d\ {}^3D^\circ_3$— $7p'\ {}^3F_4$
6756. 74	6	14795. 95	$6p''\ {}^3P_1$— $9s\ {}^5S^\circ_2$
6764. 17	150c	14779. 70	$5d'\ {}^3F^\circ_4$— $6p'\ {}^1F_3$
6768. 30	4c	14770. 68	$6d\ {}^5D^\circ_1$— $4f'\ {}^3D_2$
6769. 53	3c	14768. 00	$6s''\ {}^3P^\circ_2$— $4f\ {}^3F_3$
6771. 69	12c	14763. 29	$6s''\ {}^3P^\circ_2$— $6p''\ {}^3D_2$
6776. 53	2	14752. 74	
6777. 46	3	14750. 72	
6779. 17	8c	14747. 00	
6787. 19	2	14729. 57	
6796. 21	4	14710. 02	$5f\ {}^5F_5$—$10g\ {}^5G^\circ_6$
6801. 80	2	14697. 93	$6d\ {}^3D^\circ_1$— $4f'\ {}^3D_1$
6812. 57	4000Z	14674. 70	$5d\ {}^5D^\circ_3$— $6p\ {}^5P_3$
6816. 46	4c	14666. 32	$7d\ {}^3D^\circ_3$— $11_{3,4}$
6820. 93	3	14656. 71	
6822. 98	2	14652. 31	$6d'\ 3^\circ_3$— $9f\ {}^3F_4$
6824. 09	2	14649. 93	$5d''\ {}^3D^\circ_1$— $5f\ {}^3F_2$
6825. 23	150c	14647. 48	$6s'\ {}^3D^\circ_3$— $6p'\ {}^3F_2$
6825. 79	3	14646. 28	
6826. 83	2	14644. 05	
6831. 15	3	14634. 79	$7p\ {}^3P_1$— $8d\ {}^5D^\circ_2$
6832. 89	10	14631. 06	
6838. 60	3	14618. 84	
6855. 90	3	14581. 95	$5d''\ {}^3F^\circ_2$— $7p'\ {}^3D_3$
6860. 47	1c	14572. 24	$6d\ {}^3D^\circ_1$— $7p'\ {}^3F_2$
6869. 78	1	14552. 49	
6879. 12	10	14532. 73	$6p'\ {}^3P_1$— $7s'\ {}^3D^\circ_2$
6880. 25	3	14530. 35	$6p'\ {}^3P_1$— $7s'\ {}^3D^\circ_1$
6888. 84	4	14512. 23	
6902. 13	200Z	14484. 29	$6s\ {}^3S^\circ_1$— $6p\ {}^5P_2$
6904. 77	10c	14478. 75	$6s'\ {}^1D^\circ_2$— $6p'\ {}^3D_2$
6906. 81	12	14474. 47	$7p\ {}^5P_3$— $9s\ {}^5S^\circ_2$
6909. 98	2	14467. 83	$6p'\ {}^1D_2$— $7s'\ {}^3D^\circ_2$
6956. 46	20	14371. 16	$6d\ {}^5D^\circ_4$— $8p\ {}^5P_3$?
6958. 78	1000Z	14366. 37	$5d\ {}^5D^\circ_4$— $6p\ {}^5P_3$
6970. 13	1	14342. 98	$6d\ {}^5D^\circ_4$— $4f'\ {}^3D_3$
6999. 29	1	14283. 22	$6d\ {}^5D^\circ_1$— $4f'\ {}^3F_2$
7018. 91	70c	14243. 30	$5d'\ {}^3D^\circ_3$— $6p'\ {}^3F_3$
7021. 60	20	14237. 84	$5d\ {}^5D^\circ_2$— $6p\ {}^5P_3$
7022. 54	2h	14235. 94	$5d''\ {}^3F^\circ_3$— $4f'\ {}^3D_2$
7027. 61	5	14225. 67	$6d\ {}^5D^\circ_2$— $8p\ {}^5P_2$?
7027. 88	3	14225. 12	$5d'\ {}^3S^\circ_1$— $6p''\ {}^3D_1$
7028. 04	1	14224. 80	
7032. 99	300c	14214. 78	$5d'\ {}^3D^\circ_2$— $6p'\ {}^3F_2$
7042. 26	100c	14196. 07	$5d'\ {}^3G^\circ_4$— $6p'\ {}^3F_4$
7057. 21	2h	14166. 00	$5d''\ {}^3D^\circ_1$— $5f\ {}^5F_1$
7057. 81	3h	14164. 80	$6d\ {}^5D^\circ_1$— $8p\ {}^3P_1$
7059. 07	1h	14162. 27	
7078. 72	20	14122. 95	$5d'\ {}^1S^\circ_0$— $6p''\ {}^3P_1$
7085. 21	200c	14110. 02	$5d'\ {}^3G^\circ_4$— $6p'\ {}^3D_3$
7100. 06	15	14080. 51	$5d'\ {}^3P^\circ_2$— $6p''\ {}^3S_1$
7101. 72	2	14077. 22	$6p'\ {}^1P_1$— $5d''\ {}^1P^\circ_1$
7115. 08	10c	14050. 78	$5p^5\ {}^1P^\circ_1$— $6p'\ {}^3D_1$
7133. 66	2	14014. 19	$7d\ {}^5D^\circ_4$— $9f\ {}^5F_5$?
7138. 97	100c	14003. 76	$5d'\ {}^3D^\circ_3$— $6p'\ {}^3D_2$
7161. 45	2	13959. 81	
7186. 15	20	13911. 82	$5d'\ {}^1S^\circ_0$— $7p\ {}^5P_1$
7221. 85	10c	13843. 05	
7225. 81	100Z	13835. 47	$5d\ {}^5D^\circ_0$— $6p\ {}^5P_1$
7248. 06	1c	13792. 99	$5d''\ {}^1F^\circ_3$— $7p'\ {}^3P_2$
7254. 78	3h	13780. 22	$5d''\ {}^1F^\circ_3$— $7p'\ {}^3D_3$
7282. 83	40c, Z	13727. 14	$5p^4\ {}^3P_2$— $5p^4\ {}^1D_2$
7289. 47	1	13714. 64	$5f\ {}^5F_3$— $9g\ {}^5G^\circ_4$?
7291. 34	1	13711. 12	$5f\ {}^5F_4$— $9g\ {}^5G^\circ_5$
7311. 57	2	13673. 19	$5f\ {}^5F_5$— $9g\ {}^5G^\circ_6$
7333. 13	1	13632. 99	$5f\ {}^5F_2$— $9g\ {}^5G^\circ_3$
7342. 10	1	13616. 33	$5f\ {}^5F_1$— $9g\ {}^5G^\circ_2$
7351. 35	500Z	13599. 20	$5d\ {}^5D^\circ_3$— $6p\ {}^5P_2$
7370. 31	3	13564. 21	$6d\ {}^5D^\circ_3$— $5f\ {}^3F_3$
7370. 83	4c	13563. 26	$6s''\ {}^1P^\circ_1$— $4f\ {}^3F_2$
7383. 49	15	13540. 00	$6d\ {}^5D^\circ_0$— $5f\ {}^5F_1$
7392. 26	10	13523. 94	$6d\ {}^5D^\circ_2$— $5f\ {}^3F_3$
7395. 57	5	13517. 89	$6d'\ 8^\circ_4$— $11_{3,4}$
7398. 91	4h	13511. 78	$5f\ {}^3F_3$— $9g\ {}^3G^\circ_4$; $5f\ {}^3F_3$— $9g\ {}^5G^\circ_3$
7400. 29	20c	13509. 26	$5d''\ {}^3P^\circ_2$— $6p''\ {}^1D_2$
7407. 75	5c	13495. 66	
7418. 52	6	13476. 07	$4f'\ {}^3F_2$— 42°_2
7423. 85	15	13466. 39	
7435. 26	2c	13445. 73	
7437. 64	2	13441. 42	
7437. 87	4	13441. 01	
7438. 90	12	13439. 15	
7444. 29	25	13429. 42	$6p''\ {}^1S_0$— 32°_1
7454. 79	3	13410. 50	
7454. 94	5	13410. 23	
7459. 00	20	13402. 93	$6d\ {}^5D^\circ_2$— $5f\ {}^5F_2$
7461. 52	2d	13398. 41	$7p\ {}^3P_1$— $6d'\ 14^\circ_2$
7477. 07	5c	13370. 54	$5d'\ {}^3P^\circ_1$— $6p''\ {}^1D_2$
7481. 52	25	13362. 59	$6d\ {}^5D^\circ_3$— $5f\ {}^5F_4$

TABLE 10.1. *Observed lines of* I II—Continued

λ(air)	Intensity	Wave number	Classification
7482.88	10	13360.16	$6d\ {}^5D^o_3$— $5f\ {}^5F_3$
7484.77	70	13356.79	$6d\ {}^5D^o_4$— $5f\ {}^5F_5$
7488.87	5	13349.47	
7505.54	30	13319.82	$6d\ {}^5D^o_2$— $5f\ {}^5F_3$
7506.31	6*h*	13318.46	$5d''\ {}^3F^o_2$— $4f'\ {}^3F_3$ $7p\ {}^3P^o_0$— $6d'\ 15^o_1$
7508.34	10	13314.86	$6d\ {}^5D^o_4$— $5f\ {}^5F_4$
7535.77	5	13266.39	
7544.05	3	13251.83	
7557.96	25	13227.44	
7563.20	25	13218.28	
7563.66	2*c*	13217.47	
7569.15	25	13207.89	
7573.40	7*d*	13200.48	$6s''\ {}^1P^o_1$— $6p''\ {}^3P_1$
7578.96	20	13190.79	
7579.95	4	13189.07	
7585.53	2*c*	13179.37	
7592.03	1	13168.08	$5f\ {}^3F_4$— $9g\ {}^5G^o_5$
7595.37	300Z	13162.29	$5d\ {}^5D^o_2$— $6p\ {}^5P_2$
7596.33	20	13160.63	$6d'\ 1^o_2$— $1_{2,3}$
7612.27	1	13133.07	$5f\ {}^3F_2$— $9g\ {}^3G^o_3$?
7617.95	3*h*	13123.28	$6d'\ 3^o_3$— $8f\ {}^3F_4$
7618.50	100*c*	13122.33	$5d'\ {}^3D^o_3$— $6p'\ {}^3F_2$
7623.23	20	13114.19	
7627.31	4*h*	13107.17	
7636.62	2	13091.20	$7d\ {}^3D^o_3$— $9f\ {}^3F_4$
7640.28	7*c*	13084.92	
7654.26	1*c*	13061.03	$7d\ {}^3D^o_3$— $4_{3,4}$
7657.94	150*c*, Z	13054.75	$5d\ {}^5D^o_2$— $6p\ {}^5P_1$
7665.69	200*c*	13041.55	$5d'\ {}^3F^o_4$— $6p'\ {}^3F_3$
7683.47	8*c*	13011.37	$5d'\ {}^1F^o_3$— $7p\ {}^3P_2$
7684.82	1*c*	13009.09	
7685.30	3*c*	13008.27	
7690.55	40*c*	12999.39	$5d'\ {}^3G^o_4$— $6p'\ {}^1F_3$
7691.29	3	12998.14	$6d\ {}^5D^o_1$— $5f\ {}^5F_1$
7703.21	5	12978.03	$6d\ {}^5D^o_1$— $5f\ {}^5F_2$
7707.95	3*c*	12970.05	
7713.17	4*h*	12961.27	
7724.21	3	12942.75	
7735.78	75*c*	12923.39	$5d'\ {}^3D^o_2$— $6p'\ {}^3D_1$
7756.05	15	12889.61	$5d''\ {}^2P^o_2$— $6p''\ {}^1P_1$
7757.58	5	12887.07	
7769.09	1*c*	12867.98	$5d''\ {}^1D^o_2$— $7p\ {}^3P_1$
7786.18	2	12839.74	
7787.04	3*c*	12838.32	$6p\ {}^3P_1$— $5d'\ {}^3P^o_2$
7798.98	500	12818.66	
7824.91	3	12776.18	
7840.37	2	12750.99	$5d'\ {}^3P^o_1$— $6p''\ {}^1P_1$
7840.46	2	12750.85	
7843.31	3*c*	12746.21	$6d'\ 9^o_3$— $11_{3,4}$
7862.79	3	12714.63	$6d'\ 9^o_3$— $10_{2,3}$
7876.51	1	12692.49	
7881.21	1	12684.92	$7d\ {}^5D^o_2$— $8f\ {}^3F_3$
7884.39	10*c*	12679.80	
7886.55	2*c*	12676.33	
7886.82	2	12675.89	
7887.70	3	12674.48	
7905.57	1	12645.83	
7925.58	2*c*	12613.90	
7956.47	1	12564.93	$7d\ {}^5D^o_2$— $8f\ {}^5F_3$
7956.89	3*c*	12564.27	$5d''\ {}^3F^o_2$— $5f\ {}^3F_3$
7968.61	5	12545.79	
7990.27	2	12511.78	
7991.36	10*c*	12510.07	$5d''\ {}^1F^o_3$— $4f'\ {}^3G_4$
7993.29	3	12507.05	
7994.65	2*c*	12504.93	$6d'\ 2^o_3$— $1_{2,3}$
8000.09	2	12496.42	$7d\ {}^5D^o_3$— $8f\ {}^5F_4$
8008.32	2	12483.58	
8009.28	3	12482.08	
8009.84	1	12481.21	
8014.03	1	12474.69	
8049.51	3	12419.70	$7d\ {}^5D^o_4$— $8f\ {}^5F_5$
8055.06	20	12411.14	
8056.54	2	12408.86	
8060.37	1	12402.97	$7d\ {}^5D^o_1$— $8f\ {}^5F_2$
8150.57	1	12265.71	$5f\ {}^5F_4$— $8g\ {}^3G^o_5$
8152.46	2	12262.87	$5f\ {}^5F_3$— $8g\ {}^5G^o_4$
8153.83	30*c*	12260.80	$6p''\ {}^3P^o_2$— $6g\ {}^5G^o_5$
8154.53	3	12259.75	$5f\ {}^5F_4$— $8g\ {}^5G^o_5$
8159.49	10	12252.30	$5d'\ {}^1G^o_4$— $6p'\ {}^3F_4$
8162.42	1	12247.90	$8p\ {}^3P_1$— 37^o_2
8166.29	1	12242.10	$6p''\ {}^1P_1$— $7s''\ {}^3P^o_0$
8170.07	100*c*	12236.43	$5d'\ {}^3F^o_3$— $6p'\ {}^3D_2$
8177.60	1*c*	12225.17	
8179.15	4	12222.85	$5f\ {}^5F_5$— $8g\ {}^5G^o_6$
8180.76	1*c*	12220.44	
8183.27	30	12216.70	
8185.11	8*c*	12213.95	
8194.84	40	12199.45	
8205.68	2	12183.33	
8206.08	4	12182.74	
8206.49	2	12182.13	$5f\ {}^5F_2$— $8g\ {}^5G^o_3$
8217.11[e]	8	12166.38	$5f\ {}^5F_1$— $8g\ {}^5G^o_2$
8217.27	30	12166.15	$5d'\ {}^1G^o_4$— $6p'\ {}^3D_3$
8235.20	15	12139.66	
8246.21	30	12123.45	$5d''\ {}^3D^o_2$— $6p''\ {}^1D_2$
8251.79	100*c*, Z	12115.25	$5d\ {}^3D^o_2$— $6p\ {}^3P_2$
8253.84	25	12112.24	$5d'\ {}^3P^o_0$— $6p'\ {}^3D_1$
8256.54	1*c*	12108.28	$7p'\ {}^3P^o_2$— 40^o_3
8272.90	1*c*	12084.34	$5d'\ {}^1F^o_3$— $4f\ {}^3F_4$
8286.65	2*c*	12064.29	
8288.55	2	12061.52	$5f\ {}^3F_3$— $8g\ {}^3G^o_4$
8296.73	2*c*	12049.63	$4f\ {}^5F_4$— $6d'\ 8^o_4$
8307.51	2	12033.99	$6d\ {}^3D^o_1$— $7p'\ {}^3P_2$
8316.16	15*c*	12021.48	$4f\ {}^5F_3$— $6d'\ 8^o_3$ $7p\ {}^5P_3$— $6d'\ 9^o_3$
8321.03	5*c*	12014.44	
8323.23	4	12011.27	
8330.75	1*h*	12000.42	$8p\ {}^3P_2$—$11d\ {}^3D^o_3$
8356.90	2*c*	11962.87	$6d'\ 10^o_2$— $12_{1,2}$
8366.51	3*c*	11949.13	
8372.94	35	11939.96	$4f\ {}^5F_4$— $5g\ {}^3G^o_5$
8380.68	1*c*	11928.93	$6p''\ {}^1S_0$— 21^o_1
8385.74	6*c*	11921.73	$5d'\ {}^3P^o_2$— $7p\ {}^3P_2$ $4f\ {}^5F_5$— $5g\ {}^3G^o_4$
8398.74	3*h*	11903.28	$6d'\ 10^o_2$— $10_{2,3}$
8400.03	15	11901.45	$4f\ {}^5F_5$— $5g\ {}^5G^o_5$
8403.62	12*c*	11896.36	$4f\ {}^5F_4$— $5g\ {}^5G^o_4$
8408.67	80	11889.22	$4f\ {}^5F_4$— $5g\ {}^5G^o_5$
8412.78	6	11883.41	$4f\ {}^5F_3$— $5g\ {}^3G^o_4$
8414.32[f]		11881.24	$4f\ {}^5F_5$— $5g\ {}^3G^o_5$

TABLE 10.1. *Observed lines of* I II—Continued

λ(air)	Intensity	Wave number	Classification
8414. 60	150*Z*	11880. 84	$4f\ {}^5F_5$— $5g\ {}^5G^0_6$
8417. 50	2	11876. 75	
8418. 93	7	11874. 73	
8421. 01	7	11871. 80	
8423. 60	60*w*, *Z*	11868. 15	$4f\ {}^5F_3$— $5g\ {}^5G^0_4$
8436. 08	20	11850. 59	$4f\ {}^5F_2$— $5g\ {}^3G^0_3$
8436. 92	5	11849. 41	$4f\ {}^5F_2$— $5g\ {}^5G^0_2$
8445. 31	6*c*	11837. 64	$5d''\ {}^3P^0_2$— $6p''\ {}^3P_2$ and $4f\ {}^5F_5$— $5g\ {}^5G^0_4$
8450. 62	30*Z*	11830. 20	$4f\ {}^5F_2$— $5g\ {}^5G^0_3$
8455. 66	8	11823. 15	
8474. 57	2*h*	11796. 77	
8475. 37	40	11795. 65	
8476. 46	10*c*	11794. 14	$5d''\ {}^1D^0_2$— $6p''\ {}^3P_1$
8478. 21	1*h*	11791. 70	
8478. 85	50	11790. 81	$4f\ {}^5F_1$— $5g\ {}^5G^0_2$
8479. 80	30	11789. 49	
8497. 89	2	11764. 40	
8505. 90	20	11753. 32	$5d'\ {}^3P^0_2$— $7p\ {}^3P_1$
8528. 14	1	11722. 67	$5f\ {}^3F_4$— $8g\ {}^3G^0_5$
8556. 54	1	11683. 76	$5f\ {}^3F_2$— $8g\ {}^3G^0_3$
8564. 35	3	11673. 10	
8605. 13	10	11617. 78	
8606. 54	2	11615. 88	
8623. 44	1*Z*	11593. 12	$5d\ {}^5D^0_1$— $6p\ {}^5P_2$
8638. 89	3	11572. 38	
8639. 88	3	11571. 06	$5d'\ {}^3F^0_2$— $6p'\ {}^1D_2$
8643. 72	3	11565. 92	$5d''\ {}^3D^0_3$— $6p''\ {}^3D_2$
8704. 22	10*Z*	11485. 53	$5d\ {}^5D^0_1$— $6p\ {}^5P_1$
8793. 87	10*Z*	11368. 44	$4f\ {}^3F_3$— $5g\ {}^3G^0_4$
8804. 23	10*c*	11355. 06	$5d'\ {}^3F^0_3$— $6p'\ {}^3F_2$
8877. 61	20	11261. 20	$5d'\ {}^3G^0_4$— $6p'\ {}^3F_3$
8968. 84[e]		11146. 66	$4f\ {}^3F_4$— $5g\ {}^5G^0_5$
8969. 42	30*Z*	11145. 93	$5d\ {}^3D^0_2$— $6p\ {}^3P_1$
8999. 07	7	11109. 21	$4f\ {}^3F_2$— $5g\ {}^3G^0_3$
9009. 86	10	11095. 91	$4f\ {}^3F_4$— $5g\ {}^5G^0_5$
9015. 63	2	11088. 80	$4f\ {}^3F_2$— $5g\ {}^5G^0_3$
9036. 92	2	11062. 68	
9042. 76	40	11055. 54	$5d'\ {}^1G^0_4$— $6p'\ {}^1F_3$
9063. 59	1	11030. 13	
9185. 41	3	10883. 84	$6s''\ {}^3P^0_0$— $6p'\ {}^3P_1$
9195. 87	30	10871. 46	$5d\ {}^3D^0_1$— $6p\ {}^3P_0$
9214. 67	2	10849. 28	$6d\ {}^3D^0_2$— $4f'\ {}^3F_3$
9236. 12	6	10824. 09	
9244. 02	1	10814. 84	
9255. 17	3	10801. 81	$6d\ {}^3D^0_3$— $4f'\ {}^3G_4$
9259. 42	1	10796. 85	$6d\ {}^3D^0_2$— $8p\ {}^5P_2$?
9260. 84	2	10795. 19	$4f'\ {}^3G_3$— $47^0_{1,2}$
9262. 73	3	10792. 99	
9265. 97	4	10789. 22	
9274. 68	1*h*	10779. 09	
9302. 41	1	10746. 95	
9304. 65	2*c*	10744. 37	$5d'\ {}^3P^0_2$— $4f\ {}^3F_3$
9361. 26	1	10679. 39	$5d'\ {}^3P^0_2$— $6p''\ {}^3P_1$
9394. 32	1*h*	10641. 81	
9405. 73	2	10628. 90	
9406. 75	1	10627. 75	$5d''\ {}^3P^0_2$— $6p''\ {}^3S_1$
9420. 09	1	10612. 70	
9480. 33	10*c*	10545. 26	$5d'\ {}^1D^0_2$— $6p'\ {}^1D_2$
9506. 70	1	10516. 01	
9538. 51	3	10480. 94	$5d\ {}^3D^0_1$— $6p\ {}^3P_2$
9541. 02	1	10478. 19	$6d\ {}^3D^0_2$— $5f\ {}^3F_2$
9616. 67	4	10395. 76	$6d\ {}^3D^0_3$— $5f\ {}^3F_4$
9625. 06	4	10386. 70	$6d\ {}^3D^0_1$— $5f\ {}^3F_2$
9766. 73	1	10236. 03	
9908. 38	1	10089. 70	$5d'\ {}^3D^0_1$— $6p'\ {}^3P_0$
10405. 49	6	9607. 68	$5d\ {}^3D^0_3$— $6p\ {}^3P_2$
10418. 15	1	9596. 00	$7p\ {}^5P_1$— $7d\ {}^5D^0_1$
10691. 12	1	9351. 00	
11084. 68	1	9018. 99	$7p\ {}^5P_3$— $7d\ {}^5D^0_4$

Meanings of the letters following the intensities in this table:

c Complex line, showing resolved or partially resolved structure. Most of the lines having large intensities not followed by this symbol actually have complex structures masked by line width.

d Double line. In the air region this is usually hyperfine structure.

h Hazy line.

w Wide line.

Z Zeeman pattern given in table 10.2.

NOTES:

[a] The wavelength of this line is calculated, since it is partly masked by the I I line at 4850.35 A.

[b] The line at this position belongs partly to I I.

[c] The relative intensities of this line in the high and low pressure discharges indicate that it belongs primarily to the I I spectrum; however, since both $7s''\ {}^3P_0$ and $7s''\ {}^3P_1$ of I II combine with $7p$ levels, it is likely that the transition given here occurs.

[d] Part of this double line is due to an I I transition.

[e] The intensity of this line is given as it appears on the plate. The line at 8217.27 A probably has a component overlapping the weaker line expected at 8217.11 A.

[f] The calculated wavelength of this line is coincident with an I I line of intensity 40.

[g] Line not resolved from the I I line of intensity 300 at 8969.04 A. The wavelength given for the expected I II line is a calculated value.

TABLE 10.2. *Zeeman effect data for* I II

λ	Zeeman patterns
4173. 810	(. . .) 0.659, 1.434
4225. 542	(0.00*w*) 1.187*w*
4235. 511	(. . .) **0.719,** 1.095
4342. 078	(0.841) 1.467, 2.304
4376. 139	(0.00*w*) 0.795 *A*
4403. 566	(0.00*w*) 1.238 *B*
4408. 954	(0.00*w*) 0.841 *A*
4412. 333	(. . .) 1.747
4423. 725	(**0.000,** 0.873) **0.602,** 1.440, 2.301
4428. 195	(0.00*w*) 1.33*w*
4442. 562	(0.000) 0.687
4444. 873	(0.272, **0.550**) 1.187, **1.452, 1.715,** 1.980
4446. 742	(0.000) 2.308
4452. 858	(**0.000,** 0.264, 0.548) **0.862,** 1.108, 1.432, 1.718
4456. 625	(. . .) 1.388, **1.821**
4460. 185	(1.512) 0.000
4464. 338	(0.00*w*) 1.127*w*
4473. 412	(0.00*w*) 1.252 *B*
4476. 037	(0.000) 0.674
4488. 552	(0.586) 0.908, 1.497
4540. 644	(. . .) **1.084,** 1.425
4560. 612	(0.00*w*) 1.136*w*
4574. 090	(0.841) 1.438, 2.298
4576. 550	(0.00*w*) 0.465*w*
4590. 930	(0.00*w*) 1.203 *B*
4599. 769	(0.00*w*) 0.561 *A*
4611. 224	(0.330) **0.671,** 1.083
4621. 854	(0.00*w*) 1.084*w*
4632. 446	(0.423, **0.814**) 1.160, **1.514, 1.899,** 2.314
4675. 530	(0.168*w*) 1.048*w*
4806. 402	(0.453*w*) 0.794, **1.105, 1.310***w*
4828. 252	(. . .) 1.478*w*
4884. 828	(0.00*w*) 1.104*w*
4986. 922	(**0.000,** 0.484) 0.686, 1.157, **1.629**
5046. 43	(0.000) 0.656
5065. 37	(0.00*w*) 1.565*w*
5156. 41	(**0.000,** 0.406) **1.507,** 1.891, 2.319
5161. 20	(**0.000,** 0.267, 0.589) **1.052,** 1.343, 1.720, 2.045
5214. 08	(0.00*w*) 1.590 *B*
5216. 27	(**0.000,** 0.218) 0.924, **1.143**
5245. 71	(0.00*w*) 1.353*w*
5265. 16	(0.351) 0.643, 1.016
5322. 80	(0.000) 1.536
5338. 22	(0.00*w*) 1.025*w*
5345. 15	(0.00*w*) 1.139*w*
5405. 42	(0.00*w*) 1.622*w*
5438. 00	(**0.000,** 0.380) **0.629,** 1.013, 1.397
5491. 50	(**0.000,** 0.262, 0.532) **1.084,** 1.353, 1.623, 1.882
5504. 72	(0.000) 1.773
5593. 12	(0.224) 0.680, 0.903
5625. 69	(**0.000,** 0.253) 1.232, 1.494, 1.743
5678. 08	(0.329, **0.659**) 0.567, 0.892, 1.242, 1.584
5690. 91	(**0.000,** 0.208, 0.415) 1.196, 1.454, **1.631**
5702. 05	(0.00*w*) 1.064*w*
5710. 53	(0.362, **0.529**) 1.275*w*
5738. 27	(0.000) 1.519
5760. 72	(**0.000,** 0.524) 0.649, 1.170, 1.681
5920. 59	(0.00*w*) 1.402*w*
5950. 25	(0.240) 1.514, 1.760
6068. 93	(**0.000,** 0.243) 0.911, **1.145**
6074. 98	(**0.000,** 0.139, 0.286) . . . 1.269, **1.393**
6127. 49	(**0.000,** 0.309) 0.932, 1.219, **1.548**
6148. 34	(0.000) 1.533
6204. 86	(0.00*w*) 1.026*w*
6516. 18	(0.00*w*) 0.847*w*
6665. 96	(0.785) 1.525, 2.316
6718. 83	(0.00*w*) 1.518*w*
6812. 57	(0.168, 0.341, **0.496**) 1.131, 1,303, **1.462, 1.623,** 1.791, 1.949
6902. 13	(0.00*w*) 1.715*w*
6958. 78	(**0.000,** 0.151, 0.300, 0.446) **1.028,** 1.173, 1,330, 1.491
7225. 81	(0.000) 2.310
7282. 83	(. . . 1.042*w*, 1.459, 1.860) 0.393, **0.808***W*
7351. 35	(**0.000,** 0.257, 0.527) **0.943,** 1.199, 1.472, 1.730, 1.968
7595. 37	(0.309, **0.570**) 1.136, **1.435, 1.737,** 2.047
7657. 94	(**0.000,** 0.874) **0.561,** 1.436, 2.316
8251. 79	(0.372, **0.759**) 0.751, **1.123, 1.502,** 1.886
8414. 60	(0.00*W*) 1.05*w*
8423. 60	(0.00*W*) 1.03*w*
8450. 62	(0.00*W*) 0.69*w*
8623. 44	(**0.000,** 0.304) 1.728, **1.995**
8704. 22	(0.823) **1.483,** 2.325
8793. 87	(0.00*w*) 0.97*w*
8969. 42	(**0.000,** 0.440) **0.713,** 1.134

The magnetic displacements, in Lorentz units, of the Zeeman components with polarization parallel to the field are given in parentheses. The displacements of the perpendicularly-polarized components follow, outside the parentheses. Bold type indicates strongest components.

The letters *A* and *B* in this table indicate the type of shading displayed by the unresolved patterns:

A indicates ,

B indicates ,

w Wide line, usually several unresolved components,

W Very wide line.

Unresolved or incomplete patterns were treated as "blend" or "strongest line only" patterns in the calculation of g_J values.

TABLE 10.3. *Even levels of* I II

Designation	Level	g_J	Designation	Level	g_J	Designation	Level	g_J
$5p^4\ ^3P_2$	0. 0	1. 457	$4f\ ^3F_4$	125477. 08		$7p'\ ^3P_0$	140327. 95	
$5p^4\ ^3P_1$	7087. 0	1. 51	$4f\ ^3F_3$	125226. 92		$7p'\ ^3F_3$	140383. 95	
$5p^4\ ^3P_0$	6447. 9		$4f\ ^3F_2$	125524. 56	0. 83 L	$7p'\ ^3D_2$	142039. 80	
$5p^4\ ^1D_2$	13727. 2	1. 046	$7p\ ^3P_2$	126404. 16		$8p\ ^3P_2$	136700. 57	
			$7p\ ^3P_1$	126235. 91		$8p\ ^3P_1$	136408. 45	
$5p^4\ ^1S_0$	29501. 3		$7p\ ^3P_0$	127181. 90				
						$6f\ ^5F_5$	141088. 90	
$6p\ ^5P_1$	99219. 61	2. 309	$5f\ ^5F_5$	135182. 87		$6f\ ^5F_4$	141073. 17	
$6p\ ^5P_2$	99327. 14	1. 714	$5f\ ^5F_4$	135140. 95		$6f\ ^5F_3$	141080. 89	
$6p\ ^5P_3$	100402. 68	1. 638	$5f\ ^5F_3$	135138. 51		$6f\ ^5F_2$	141094. 09 ?	
			$5f\ ^5F_2$	135221. 58				
$6p\ ^3P_2$	102613. 52	1. 501	$5f\ ^5F_1$	135241. 72		$6f\ ^3F_2$	141471. 00	
$6p\ ^3P_1$	101644. 21	1. 520				$6f\ ^3F_3$	141398. 31	
$6p\ ^3P_0$	103004. 04		$5f\ ^3F_4$	135684. 08		$6f\ ^3F_4$	141529. 89	
			$5f\ ^3F_3$	135342. 60				
$6p'\ ^3D_1$	110006. 71	0. 915	$5f\ ^3F_2$	135725. 82		$7f\ ^5F_5$	144629. 91	
$6p'\ ^3F_2$	111298. 09	0. 915				$7f\ ^5F_4$	144619. 97	
$6p'\ ^3D_2$	112179. 49	1. 158	$8p\ ^5P_2$?	136044. 28		$7f\ ^5F_3$	144630. 32	
$6p'\ ^3F_3$	112419. 04	1. 12	$8p\ ^5P_3$?	136197. 24				
$6p'\ ^1P_1$	113812. 79	0. 985				$7f\ ^3F_2$	144896. 23	
$6p'\ ^1F_3$	114157. 21	1. 13	$4f'\ ^3G_4$	136090. 15		$7f\ ^3F_3$	144810. 22	
$6p'\ ^3P_0$	114635. 82		$4f'\ ^3F_3$	136096. 79		$7f\ ^3F_4$	144919. 15	
$6p'\ ^3D_3$	115267. 82	1. 212	$4f'\ ^3D_3$	136169. 16				
$6p'\ ^3F_4$	115353. 94	1. 29	$4f'\ ^3F_2$	136526. 91		$5f'\ [1_{2,3}$	146460. 44	
$6p'\ ^3P_2$	115708. 45	1. 425	$4f'\ ^3H_5$	136752. 36		$\ 2_{2,3}$	146973. 00	
$6p'\ ^3P_1$	116084. 84	1. 39	$4f'\ ^3H_4$	136802. 13		$4f''\ 3_{2,3}$	147942. 43	
$6p'\ ^1D_2$	119082. 78	1. 11	$4f'\ ^3D_2$	137014. 34		$\ 4_{3,4}$	148646. 01	
			$4f'\ ^3P_1$	137393. 02		$7p''\ 5_{2,3}$	148830. 03	
$6p''\ ^3D_1$	123520. 74					$\ 6_{2,3,4}$	148972. 30	
$6p''\ ^3P_0$	125006. 38		$4f'\ ^3P_2$	137640. 93		$\ 7_{2,3}$	149204. 87	
$6p''\ ^3P_1$	125162. 00		$4f'\ ^3P_0$	138236. 41		$8p'\ 8_{1,2}$	149367. 05	
$6p''\ ^3D_2$	125222. 20	0. 83 L[a]	$4f'\ ^3G_5$	139449. 71		$\ 10_{2,3}$	150219. 69	
$6p''\ ^3S_1$	128563. 14	1. 73 L	$4f'\ ^3F_4$	139499. 57		$\ 11_{3,4}$	150251. 30	
$6p''\ ^3D_3$	129431. 27	1. 32 L	$4f'\ ^3G_3$	139691. 25		$\ 12_{1,2}$	150279. 40	
$6p''\ ^3P_2$	129772. 76		$4f'\ ^1G_4$	139719. 12		$\ 13_{2,3}$	150648. 09	
$6p''\ ^1P_1$	130824. 99		$4f'\ ^3D_1$	140036. 78				
$6p''\ ^1D_2$	131444. 69	1. 26 L	$4f'\ ^1F_3$	140387. 24		$8f\ ^5F_5$	146922. 08	
$6p''\ ^1S_0$	134363. 21		$4f'\ ^1D_2$	140492. 31		$8f\ ^5F_4$	146938. 07	
			$4f'\ ^1P_1$	140560. 53		$8f\ ^5F_3$	146934. 47	
$4f\ ^5F_5$	124742. 50					$8f\ ^5F_2$	146949. 97	
$4f\ ^5F_4$	124683. 79		$7p'\ ^3D_1$	136209. 25				
$4f\ ^5F_3$	124711. 93		$7p'\ ^5P_1$	136659. 84		$8f\ ^3F_3$	147054. 27	
$4f\ ^5F_2$	124783. 18		$7p'\ ^3D_3$	137360. 30		$8f\ ^3F_4$	147147. 10	
$4f\ ^5F_1$	124841. 77		$7p'\ ^3P_2$	137373. 06				
			$7p'\ ^3F_2$	139911. 38		$9f\ ^5F_5$	148516. 58 ?	
$7p\ ^5P_1$	124950. 92		$7p'\ ^3F_4$	140108. 06		$9f\ ^5F_4$	148513. 52 ?	
$7p\ ^5P_2$	125084. 32		$7p'\ ^1F_3$	140163. 63		$9f\ ^5F_3$	148519. 48 ?	
$7p\ ^5P_3$	125483. 51		$7p'\ ^1D_2$	140189. 27				
			$7p'\ ^1P_1$	140254. 97		$9f\ ^3F_4$	148676. 16	

[a] The letter "L" following a g_J value indicates that the value is taken from Lacroute [3].

TABLE 10.4. *Odd levels of* I II

Designation	Level	g_J	Designation	Level	g_J	Designation	Level	g_J
$6s\ ^5S_2^\circ$	81032. 70	1. 95	$5d\ ^5D_3^\circ$	85727. 98	1. 457	$6s'\ ^1D_2^\circ$	97700. 81	0. 996
			$5d\ ^5D_4^\circ$	86036. 32	1. 480			
$6s\ ^3S_1^\circ$	84842. 87	1. 753				$5d'\ ^3D_2^\circ$	97083. 30	1. 26 L[a]
			$5d\ ^3D_1^\circ$	92132. 61	0. 685	$5d'\ ^3P_0^\circ$	97894. 42	
$5p^5\ ^3P_2^\circ$	81907. 83	1. 54	$5d\ ^3D_2^\circ$	90498. 31	1. 138	$5d'\ ^3D_3^\circ$	98175. 75	
$5p^5\ ^3P_1^\circ$	84222. 19	1. 530	$5d\ ^3D_3^\circ$	93005. 95	1. 35	$5d'\ ^3F_4^\circ$	99377. 47	
$5p^5\ ^3P_0^\circ$	90404. 95					$5d'\ ^3F_3^\circ$	99943. 10	
			$6s'\ ^3D_1^\circ$	94825. 33	0. 653	$5d'\ ^3G_4^\circ$	101157. 79	
			$6s'\ ^3D_2^\circ$	93691. 35	1. 16	$5d'\ ^1G_4^\circ$	103101. 57	
$5d\ ^5D_0^\circ$	85384. 15		$6s'\ ^3D_3^\circ$	96650. 55	1. 36	$5d'\ ^3D_1^\circ$	104546. 19	
$5d\ ^5D_1^\circ$	87734. 06	1. 472				$5d'\ ^3F_2^\circ$	107511. 77	
$5d\ ^5D_2^\circ$	86164. 86	1. 434	$5p^5\ ^1P_1^\circ$	95955. 85	1. 05	$5d'\ ^3G_3^\circ$	107625. 89	

TABLE 10.4. *Odd levels of* I II—Continued

Designation	Level	g_J
$5d'\ ^1D^\circ_2$	108537. 50	1. 45 L
$5d'\ ^3S^\circ_1$	109295. 45	
$5d'\ ^1S^\circ_0$	111039. 06	
$5d'\ ^1F^\circ_3$	113392. 94	
$5d'\ ^3P^\circ_2$	114482. 59	
$5d'\ ^1P^\circ_1$	114897. 43	
$5d'\ ^3P^\circ_1$	118074. 09	
$6s''\ ^3P^\circ_0$	105200. 97	
$6s''\ ^3P^\circ_1$	106103. 28	
$6s''\ ^3P^\circ_2$	110458. 93	
$6s''\ ^1P^\circ_1$	111961. 58	
$5d''\ ^1D^\circ_2$	113367. 99	
$5d''\ ^3D^\circ_3$	113656. 16	
$5d''\ ^3P^\circ_2$	117935. 41	
$5d''\ ^3D^\circ_2$	119321. 09	
$5d''\ ^3D^\circ_1$	121075. 75	1. 443
$5d''\ ^3F^\circ_3$	121195. 57	1. 17 L
$5d''\ ^3F^\circ_2$	122778. 31	
$5d''\ ^1F^\circ_3$	123580. 02	
$5d''\ ^3P^\circ_0$	125040. ?	
$5d''\ ^1P^\circ_1$	127890. 23	0. 89 L
$5d''\ ^3P^\circ_1$	132734. 92	
$7s\ \ ^5S^\circ_2$	118607. 56	1. 894
$7s\ \ ^3S^\circ_1$	119888. 77	
$6d\ \ ^5D^\circ_0$	121701. 69	
$6d\ \ ^5D^\circ_1$	122243. 58	1. 466
$6d\ \ ^5D^\circ_2$	121818. 65	1. 453
$6d\ \ ^5D^\circ_3$	121778. 34	1. 424
$6d\ \ ^5D^\circ_4$	121826. 09	1. 476
$6d\ \ ^3D^\circ_3$	125288. 29	1. 28
$6d\ \ ^3D^\circ_2$	125247. 50	1. 095
$6d\ \ ^3D^\circ_1$	125339. 01	0. 674
$7s'\ ^3D^\circ_1$	130615. 21	
$7s'\ ^3D^\circ_2$	130617. 58	
$7s'\ ^3D^\circ_3$	133550. 54	1. 23 L
$8s\ \ ^5S^\circ_2$	132837. 24	
$8s\ \ ^3S^\circ_1$	133297. 08	
$6d'\ \ 1^\circ_2$	133299. 80	
$6d'\ \ 2^\circ_3$	133955. 51	1. 16
$6d'\ \ 3^\circ_3$	134023. 88	0. 81
$6d'\ \ 4^\circ_0$	134235. 94	
$6d'\ \ 5^\circ_1$	134913. 96	
$6d'\ \ 6^\circ_{1,2}$	136443. 37	
$6d'\ \ 7^\circ_{1,2}$	136561. 79	
$6d'\ \ 8^\circ_4$	136733. 42	1. 21
$6d'\ \ 9^\circ_3$	137505. 08	1. 24 L
$6d'\ \ 10^\circ_2$	138316. 49	1. 27 L
$6d'\ \ 11^\circ_0$	138364. 08	
$6d'\ \ 12^\circ_1$	138977. 84	
$6d'\ \ 13^\circ_{1,2}$	139551. 74	1. 09 L
$6d'\ \ 14^\circ_3$	139634. 07	1. 04 L
$6d'\ \ 15^\circ_1$	140500. 35	
$7s'\ ^1D^\circ_2$	134037. 06	1. 02 L
$7d\ \ ^5D^\circ_0$	134501. 34	
$7d\ \ ^5D^\circ_1$	134546. 93	
$7d\ \ ^5D^\circ_2$	134369. 52	
$7d\ \ ^5D^\circ_3$	134441. 71	
$7d\ \ ^5D^\circ_4$	134502. 39	
$7d\ \ ^3D^\circ_3$	135584. 94	
$7d\ \ ^3D^\circ_2$	134960. 14	
$7d\ \ ^3D^\circ_1$	136187. 03	
$5g\ \ ^5G^\circ_6$	136623. 34	
$5g\ \ ^5G^\circ_5$	136573. 00	
$5g\ \ ^5G^\circ_4$	136580. 12	
$5g\ \ ^5G^\circ_3$	136613. 38	
$5g\ \ ^5G^\circ_2$	136632. 59	
$5g\ \ ^3G^\circ_5$	136623. 74	
$5g\ \ ^3G^\circ_4$	136595. 35	
$5g\ \ ^3G^\circ_3$	136633. 77	
$9s\ \ ^5S^\circ_2$	139957. 94	
$9s\ \ ^3S^\circ_1$	140125. 66	
$8d\ \ ^5D^\circ_0$	140863. 42	
$8d\ \ ^5D^\circ_1$	140887. 40	
$8d\ \ ^5D^\circ_2$	140870. 64	
$8d\ \ ^5D^\circ_3$	140879. 23	
$8d\ \ ^5D^\circ_4$	140889. 98	
$8d\ \ ^3D^\circ_1$	141520. 48	
$8d\ \ ^3D^\circ_2$	141463. 16	
$8d\ \ ^3D^\circ_3$	141634. 22	
$6g\ \ ^5G^\circ_6$	142028. 75	
$6g\ \ ^5G^\circ_5$	142018. 43	
$6g\ \ ^5G^\circ_4$	142018. 60	
$6g\ \ ^5G^\circ_3$	142022. 92	
$6g\ \ ^5G^\circ_2$	142033. 75	
$6g\ \ ^3G^\circ_5$	142030. 64	
$6g\ \ ^3G^\circ_4$	142023. 04	
$6g\ \ ^3G^\circ_3$	142035. 14	
$7s''\ ^3P^\circ_0$	143067. 20	
$7s''\ ^3P^\circ_1$	143246. 49	
$10s\ \ ^5S^\circ_2$	144023. 57	
$10s\ \ ^3S^\circ_1$	144182. 29	
$9d\ \ ^5D^\circ_3$	144587. 78	
$9d\ \ ^5D^\circ_4$	144591. 35 ?	
$9d\ \ ^3D^\circ_2$	144832. 02	
$9d\ \ ^3D^\circ_3$	144964. 91	
$8s'\ ^3D^\circ_1$	144641. 34	
$8s'\ ^3D^\circ_2$	144677. 46	
$7g\ \ ^5G^\circ_6$	145289. 63	
$7g\ \ ^5G^\circ_5$	145282. 77	
$7g\ \ ^5G^\circ_4$	145283. 23	
$7g\ \ ^5G^\circ_3$	145285. 87	
$7g\ \ ^5G^\circ_2$	145292. 52	
$7g\ \ ^3G^\circ_5$	145291. 03	
$7g\ \ ^3G^\circ_4$	145285. 17	
$7g\ \ ^3G^\circ_3$	145293. 69	
$6d''\ ^5D^\circ_{1,2}$	145837. 74	
$6d''\ ^5D^\circ_1$	146291. 96	
$6d''\ ^5D^\circ_{1,2}$	146481. 11	
$7d'\ ^5D^\circ_{1,2}$	146784. 94	
$7d'\ ^5D^\circ_2$	146850. 17	
$7d'\ ^5D^\circ_1$	147020. 40	
$11s\ ^5S^\circ_2$	146577. 46	
$11s\ ^3S^\circ_1$	146589. 32	
$10d\ ^3D^\circ_2$?	147141. 92	
$10d\ ^3D^\circ_3$	147307. 25	
30°_2	147242. 50	
31°_0	147356. 42	
32°_1	147792. 67	
$6d''\ 33^\circ_3$	147824. 13	
$7d'\ 33.5^\circ_1$	147863. 97	
$7s''\ 34^\circ_2$	147987. 56	
$8s'\ 35^\circ_{2,3}$	148079. 42	
$5g'\ 36^\circ_2$	148307. 35	
37°_2	148656. 42	
38°_1	148898. 91	
39°_4	149266. 12	
40°_3	149481. 13	
$8g\ \ ^5G^\circ_6$	147405. 72	
$8g\ \ ^5G^\circ_5$	147400. 79	
$8g\ \ ^5G^\circ_4$	147401. 38	
$8g\ \ ^5G^\circ_3$	147403. 79	
$8g\ \ ^5G^\circ_2$	147408. 13	
$8g\ \ ^3G^\circ_5$	147406. 74	
$8g\ \ ^3G^\circ_4$	147404. 11	
$8g\ \ ^3G^\circ_3$	147409. 54	
$12s\ ^3S^\circ_1$	148354. ?	
$11d\ ^3D^\circ_3$	148700. 85	
$9g\ \ ^5G^\circ_6$	148856. 10	
$9g\ \ ^5G^\circ_5$	148852. 11	
$9g\ \ ^5G^\circ_4$	148853. 15 ?	
$9g\ \ ^5G^\circ_3$	148854. 55	
$9g\ \ ^5G^\circ_2$	148857. 98	
$9g\ \ ^3G^\circ_5$	148856. 65	
$9g\ \ ^3G^\circ_4$	148854. 34	
$9g\ \ ^3G^\circ_3$	148858. 89 ?	
$12d\ ^3D^\circ_3$	149644. 47	
$10g\ ^5G^\circ_6$	149892. 90	
$41^\circ_{1,2,3}$	149866. 64 ?	
42°_2	150002. 97	
$6d''\ 43^\circ_{1,2}$	150219. 03	
$44^\circ_{2,3}$	150324. 10	
$7d'\ 45^\circ_{1,2}$	150345. 98	
46°_2	150366. 61	
$5g'\ 47^\circ_{1,2}$	150486. 29	
$48^\circ_{1,2}$	150594.	
$49^\circ_{1,2}$	151744.	
$50^\circ_{3,4}$	151917. 75	
$51^\circ_{1,2,3}$	152199.	
$13d\ ^3D^\circ_3$	150608. ?	
$11g\ ^5G^\circ_6$	150659. 78	
$14d\ ^3D^\circ_3$	151192. ?	
$12g\ ^5G^\circ_6$	151242. 53	

(Paper 64A6–68)

[a] The letter "L" following a g_J value indicates that the value is taken from Lacroute [3].

JOURNAL OF RESEARCH of the National Bureau of Standards—A. Physics and Chemistry
Vol. 64A, No. 6, November–December 1960

The Third Spectrum of Gold (Au III)

Laura Iglesias [1]

(July 21, 1960)

The spark spectrum of gold has been photographed in a helium atmosphere from 500 A to 6600 A. About 500 lines have been assigned to the third spectrum, Au III, and separated from those belonging to different stages of ionization, by observation of the polarity of the lines. Sixty two levels have been found: 17 even levels, arising from the $5d^9$ and $5d^8$ $6s$ configurations; and 45 odd levels, belonging to the $5d^8$ $6p$ and $5d^7$ $6s$ $6p$ configurations. All of the expected levels from the configurations $5d^9$, $5d^8$ $6s$ and $5d^8$ $6p$ have been identified except for the very high terms based on the $5d^8(^1S)$ core of Au IV. With these levels it was possible to classify 256 lines.

1. Introduction

The first and second spectra of gold were studied some years ago, but apparently no attempt has been made to study the structure of the third spectrum, (Au III).

As in most spectra of the third long period, the Au III spectrum reveals a coupling intermediate between *LS*-coupling and *jj*-coupling since the spin-spin interaction and the spin-orbit interaction are both large. It approaches *jj*-coupling rather than *LS*, especially in the case of levels belonging to the $5d^8$ $6p$ configuration.

It is, therefore, very difficult to describe the observed levels rigorously in any one scheme. Accordingly, the even levels and the odd quartet levels based on $5d^8(^3F)$, which are perhaps closer to *LS*-coupling, have been given names in that system, and the other odd levels have been given numbers simply for identification.

2. Analysis and Results

The analysis is based mainly on plates taken on the 2-m vacuum spectrograph at Princeton, in the wavelength region 500 to 2200 A.

The light source was a condensed spark in helium at a pressure of approximately 1 atm.

In order to excite the third spectrum and to be able to differentiate it from the other stages of ionization, the same technique was used that A. G. Shenstone has described in his paper on Ni III.[2] Initially, the exposures were limited by the clogging of the slit by gold particles, sputtered from the spark source. Apparently gold has a pronounced tendency to sputter and the complete clogging of the slit took only one or two min, instead of the half hour or more which is commonly found with other metals. To avoid this limitation, it was necessary to fill the body of the spectrograph with helium to atmospheric pressure, so that there would be no flow through the slit. For the spectrograms taken above 1200 A, this was not necessary since the lithium fluoride window separated the spectrograph from the source.

The spectrograms were photographed on Ilford Q–2 plates and the exposures varied from 1 to 15 min. The impurity lines of nitrogen, oxygen, and carbon present on the plates were used as standards. The estimated probable error of the experimental wavelengths entered in table 1, column 1, is ± 0.01 A.

To complete the observations, other plates were taken on the 21-ft grating in a Wadsworth mounting by using Eastman 103aO plates, 103aD, and 103aF according to the region. About 500 lines in all were assigned to the third spectrum.

The lowest levels should be the $^2D_{2½}$ and $D_{1½}$ of the $5d^9$ cofinguration, and by comparison with the Au I and Au II spectra,[3] the interval between them should be about -13000 cm^{-1}. The equivalent interval in Au I and II is as follows:

Au I	$5d^9\,6s^2$	$^2D_{2½}$–$^2D_{1½}$	−12274
Au II	$5d^9(^2D)6s$	$^3D_3$ –$^3D_1$	−12725

In fact, we found it to be −12694.0 in Au III.

In order to have some idea about the position of the levels of the $5d^8$ $6s$ and $5d^8$ $6p$ configurations we plotted Ir I and Pt II and the analogous spectra of the second long period Rh I, Pd II and Ag III, using the values given in "Atomic Energy Levels".[3] To find the levels the usual method of searching for equal wave-number differences was used.

A remarkable similarity was found in the case of the terms arising from the $5d^8$ $6s$ configuration. This relationship is shown in figure 1 where the relative values of the levels of Ir I, Pt II and Au III are plotted against *J*-values.

Based on this similarity and the reason explained above, a tentative *LS*-term assignment has been made and is given in table 2, where all the known even levels are arranged in increasing numerical order.

In the case of the odd configuration $5d^8$ $6p$, the levels are so mixed in character that it is meaningless to group them into terms. A very tentative designation based on combinations and intensities appears

[1] Princeton University, Princeton, N.J.
[2] A. G. Shenstone, J. Opt. Soc. Am. **44**, 749 (1954).
[3] C. E. Moore, Atomic Energy Levels, NBS Circ. 467 (1958).

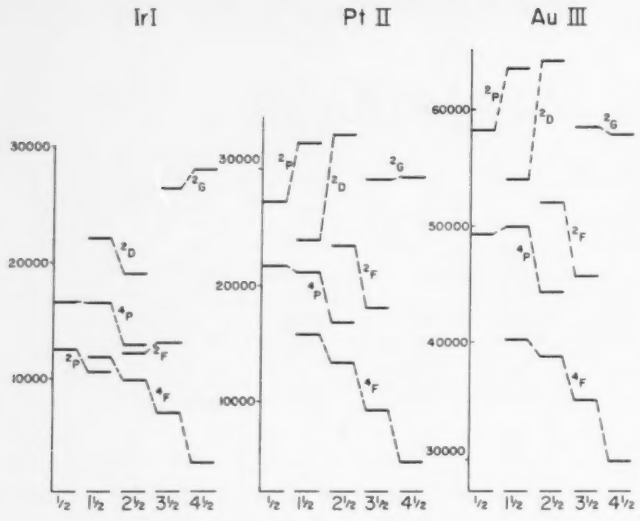

FIGURE 1. *Configuration* $5d^8\,6s$ *in* Ir I, Pt II, *and* Au III.

in table 3, but these names, except for the quartet levels based on $5d^8(^3F)$, are not used in the line list of table 1. Instead, the levels are assigned numbers for identification.

In table 3, 43 levels of the $5d^8\,6p$ configuration are listed, plus two more belonging to the $5d^7\,6s\,6p$ configuration.

The configurations $5d^9$, $5d^8\,6s$ and $5d^8\,6p$ are complete except for the usual failure to find the levels based on $5d^8(^1S)$ of Au IV.

With the 62 levels found, it was possible to classify 256 of the 500 observed lines attributable to Au III as they appear in table 1.

The author expresses gratitude to Professor A. G. Shenstone for his suggestion of this research and for his assistance during the course of the work. My thanks are also due to Princeton University which made my stay in Princeton possible through an appointment as a Research Assistant on the Eugene Higgins Fund.

TABLE 1. *Identified lines of* Au III

λ(vac.)	Intensity and character	Wave No.	Combination	λ(vac.)	Intensity and character	Wave No.	Combination
A		*cm*$^{-1}$		*A*		*cm*$^{-1}$	
751. 554	2	133057. 6	$a\ ^2D_{2\frac{1}{2}}$—$42^{\circ}_{2\frac{1}{2}}$	977. 318	40	102320. 8	$a\ ^2D_{2\frac{1}{2}}$— $z\ ^4G^{\circ}_{3\frac{1}{2}}$
763. 497	20	130976. 3	$a\ ^2D_{2\frac{1}{2}}$—$40^{\circ}_{3\frac{1}{2}}$	989. 408	25	101070. 5	$a\ ^2D_{1\frac{1}{2}}$—$19^{\circ}_{0\frac{1}{2}}$
779. 728	30	128249. 8	$a\ ^2D_{2\frac{1}{2}}$—$38^{\circ}_{1\frac{1}{2}}$	998. 156	20	100184. 7	$a\ ^2D_{1\frac{1}{2}}$— $z\ ^4F^{\circ}_{2\frac{1}{2}}$
788. 783	30	126777. 6	$a\ ^4F_{4\frac{1}{2}}$—$44^{\circ}_{3\frac{1}{2}}$	1034. 206	60	96692. 5	$a\ ^2D_{1\frac{1}{2}}$— $z\ ^4F^{\circ}_{1\frac{1}{2}}$
811. 394	25	123244. 7	$a\ ^4F_{3\frac{1}{2}}$—$45^{\circ}_{2\frac{1}{2}}$	1040. 650	100	96093. 8	$a\ ^2D_{2\frac{1}{2}}$— $z\ ^4G^{\circ}_{2\frac{1}{2}}$
811. 831	40	123178. 3	$a\ ^2D_{2\frac{1}{2}}$—$32^{\circ}_{1\frac{1}{2}}$	1044. 497	80	95739. 9	$a\ ^2D_{2\frac{1}{2}}$— $z\ ^4D^{\circ}_{1\frac{1}{2}}$
816. 129	3	122529. 6	$a\ ^2D_{2\frac{1}{2}}$—$31^{\circ}_{2\frac{1}{2}}$	1046. 825	80	95526. 9	$a\ ^2D_{1\frac{1}{2}}$—$14^{\circ}_{2\frac{1}{2}}$
817. 96	50	122256	$a\ ^2D_{1\frac{1}{2}}$—$43^{\circ}_{2\frac{1}{2}}$	1054. 192	40	94859. 4	$a\ ^2D_{1\frac{1}{2}}$—$13^{\circ}_{2\frac{1}{2}}$
820. 053	40	121943. 3	$a\ ^2D_{2\frac{1}{2}}$—$29^{\circ}_{1\frac{1}{2}}$	1086. 110	10	92072. 5	$a\ ^4F_{4\frac{1}{2}}$—$28^{\circ}_{3\frac{1}{2}}$
820. 846	5	121825. 5	$a\ ^2D_{2\frac{1}{2}}$—$28^{\circ}_{3\frac{1}{2}}$	1123. 172	5	89033. 5	$a\ ^2D_{1\frac{1}{2}}$— $z\ ^4D^{\circ}_{2\frac{1}{2}}$
823. 338	10	121456. 8	$a\ ^4F_{3\frac{1}{2}}$—$44^{\circ}_{3\frac{1}{2}}$	1199. 022	25	83401. 3	$a\ ^2D_{1\frac{1}{2}}$— $z\ ^4G^{\circ}_{2\frac{1}{2}}$
833. 149	80	120026. 5	$a\ ^2D_{2\frac{1}{2}}$—$27^{\circ}_{2\frac{1}{2}}$	1204. 155	30	83045. 8	$a\ ^2D_{1\frac{1}{2}}$— $z\ ^4D^{\circ}_{1\frac{1}{2}}$
836. 804	15	119502. 3	$a\ ^4F_{2\frac{1}{2}}$—$45^{\circ}_{2\frac{1}{2}}$	1229. 364	30	81342. 9	$a\ ^4P_{2\frac{1}{2}}$—$34^{\circ}_{1\frac{1}{2}}$
843. 454	100	118560. 1	$a\ ^2D_{2\frac{1}{2}}$—$26^{\circ}_{1\frac{1}{2}}$	1231. 060	20	81230. 8	$a\ ^4F_{4\frac{1}{2}}$—$16^{\circ}_{3\frac{1}{2}}$
845. 138	100	118323. 9	$a\ ^2D_{2\frac{1}{2}}$—$25^{\circ}_{3\frac{1}{2}}$	1231. 266	30	81217. 2	$a\ ^4F_{3\frac{1}{2}}$—$23^{\circ}_{3\frac{1}{2}}$
847. 619	5	117977. 5	$a\ ^4F_{1\frac{1}{2}}$—$45^{\circ}_{2\frac{1}{2}}$	1239. 961	100*w*	80647. 7	$a\ ^4F_{3\frac{1}{2}}$—$22^{\circ}_{4\frac{1}{2}}$
849. 546	5	117709. 9	$a\ ^4F_{2\frac{1}{2}}$—$44^{\circ}_{3\frac{1}{2}}$	1254. 996	30	79681. 5	$a\ ^4F_{1\frac{1}{2}}$—$27^{\circ}_{2\frac{1}{2}}$
855. 495	80	116891. 4	$a\ ^2D_{2\frac{1}{2}}$—$24^{\circ}_{1\frac{1}{2}}$	1277. 442	5	78281. 4	$a\ ^4P_{1\frac{1}{2}}$—$38^{\circ}_{1\frac{1}{2}}$
859. 891	80	116293. 8	$a\ ^2D_{2\frac{1}{2}}$—$23^{\circ}_{3\frac{1}{2}}$	1278. 514	100	78215. 8	$a\ ^4F_{1\frac{1}{2}}$—$26^{\circ}_{1\frac{1}{2}}$
863. 425	80	115817. 8	$a\ ^2D_{1\frac{1}{2}}$—$39^{\circ}_{2\frac{1}{2}}$	1280. 903	50	78069. 9	$a\ ^4F_{2\frac{1}{2}}$—$24^{\circ}_{1\frac{1}{2}}$
883. 782	50	113150. 1	$a\ ^2D_{1\frac{1}{2}}$—$35^{\circ}_{0\frac{1}{2}}$	1285. 302	50	77802. 7	$a\ ^4F_{3\frac{1}{2}}$— $z\ ^4F^{\circ}_{2\frac{1}{2}}$
885. 906	60	112878. 8	$a\ ^2D_{2\frac{1}{2}}$— $z\ ^4F^{\circ}_{2\frac{1}{2}}$	1290. 029	30	77517. 6	$a\ ^4P_{2\frac{1}{2}}$—$29^{\circ}_{1\frac{1}{2}}$
901. 025	80	110984. 6	$a\ ^2D_{2\frac{1}{2}}$—$16^{\circ}_{3\frac{1}{2}}$	1290. 358	40	77497. 9	$a\ ^4P_{1\frac{1}{2}}$—$37^{\circ}_{1\frac{1}{2}}$
905. 105	30	110484. 4	$a\ ^2D_{1\frac{1}{2}}$—$32^{\circ}_{1\frac{1}{2}}$	1290. 795	50	77471. 6	$a\ ^4F_{2\frac{1}{2}}$—$23^{\circ}_{3\frac{1}{2}}$
910. 446	80	109836. 3	$a\ ^2D_{1\frac{1}{2}}$—$31^{\circ}_{2\frac{1}{2}}$	1291. 979	60	77400. 6	$a\ ^4P_{2\frac{1}{2}}$—$28^{\circ}_{3\frac{1}{2}}$
911. 470	20	109712. 9	$a\ ^2D_{1\frac{1}{2}}$—$30^{\circ}_{0\frac{1}{2}}$	1306. 317	5	76551. 1	$a\ ^4F_{2\frac{1}{2}}$—$21^{\circ}_{2\frac{1}{2}}$
914. 175	5*h*	109388. 2	$a\ ^2D_{2\frac{1}{2}}$— $z\ ^4F^{\circ}_{1\frac{1}{2}}$	1306. 409	5	76545. 7	$a\ ^4F_{1\frac{1}{2}}$—$24^{\circ}_{1\frac{1}{2}}$
915. 338	8	109249. 3	$a\ ^2D_{1\frac{1}{2}}$—$29^{\circ}_{1\frac{1}{2}}$	1307. 988	20	76453. 3	$a\ ^2F_{2\frac{1}{2}}$—$39^{\circ}_{2\frac{1}{2}}$
924. 037	80	108220. 8	$a\ ^2D_{2\frac{1}{2}}$—$14^{\circ}_{2\frac{1}{2}}$	1308. 776	10	76407. 3	$a\ ^4P_{0\frac{1}{2}}$—$35^{\circ}_{0\frac{1}{2}}$
931. 675	10	107333. 6	$a\ ^2D_{1\frac{1}{2}}$—$27^{\circ}_{2\frac{1}{2}}$	1309. 440	40	76368. 5	$a\ ^2G_{3\frac{1}{2}}$—$43^{\circ}_{2\frac{1}{2}}$
941. 050	20	106264. 3	$a\ ^2D_{2\frac{1}{2}}$—$12^{\circ}_{1\frac{1}{2}}$	1314. 825	100	76055. 7	$a\ ^4F_{4\frac{1}{2}}$— $z\ ^4F^{\circ}_{3\frac{1}{2}}$
944. 581	50	105867. 0	$a\ ^2D_{1\frac{1}{2}}$—$26^{\circ}_{1\frac{1}{2}}$	1322. 728	30	75601. 3	$a\ ^4P_{2\frac{1}{2}}$—$27^{\circ}_{2\frac{1}{2}}$
945. 099	200	105809. 0	$a\ ^2D_{2\frac{1}{2}}$— $z\ ^4F^{\circ}_{3\frac{1}{2}}$	1326. 105	12	75408. 8	$a\ ^2F_{2\frac{1}{2}}$—$37^{\circ}_{1\frac{1}{2}}$
959. 720	15	104197. 0	$a\ ^2D_{1\frac{1}{2}}$—$24^{\circ}_{1\frac{1}{2}}$	1336. 700	200	74811. 1	$a\ ^4F_{4\frac{1}{2}}$— $z\ ^4F^{\circ}_{4\frac{1}{2}}$
973. 893	10	102680. 7	$a\ ^2D_{1\frac{1}{2}}$—$21^{\circ}_{2\frac{1}{2}}$	1341. 660	180	74534. 5	$a\ ^2G_{4\frac{1}{2}}$—$41^{\circ}_{3\frac{1}{2}}$

TABLE 1. *Identified lines of* Au III—Continued

λ(vac.)	Intensity and character	Wave No.	Combination	λ(vac.)	Intensity and character	Wave No.	Combination
A		cm^{-1}		*A*		cm^{-1}	
1346.129	12	74287.1	$a\ ^2F_{2\frac{1}{2}}$—$27^{\circ}_{2\frac{1}{2}}$	1502.441	200	66558.3	$a\ ^4P_{2\frac{1}{2}}$—$16^{\circ}_{3\frac{1}{2}}$
1348.873	100	74136.0	$a\ ^4P_{2\frac{1}{2}}$—$26^{\circ}_{1\frac{1}{2}}$	1503.716	200	66501.9	$a\ ^2F_{2\frac{1}{2}}$—$26^{\circ}_{1\frac{1}{2}}$
1349.200	30	74118.0	$b\ ^2D_{1\frac{1}{2}}$—$38^{\circ}_{1\frac{1}{2}}$	1517.049	10	65917.4	$a\ ^4F_{1\frac{1}{2}}$—$12^{\circ}_{1\frac{1}{2}}$
1350.302	150	74057.5	$a\ ^4F_{2\frac{1}{2}}$— $z\ ^4F^{\circ}_{2\frac{1}{2}}$	1528.941	40	65404.7	$a\ ^4P_{1\frac{1}{2}}$—$21^{\circ}_{2\frac{1}{2}}$
1353.200	50	73898.9	$a\ ^4P_{2\frac{1}{2}}$—$25^{\circ}_{3\frac{1}{2}}$	1540.258	80	64924.2	$a\ ^2G_{3\frac{1}{2}}$—$33^{\circ}_{4\frac{1}{2}}$?
1355.598	150	73768.2	$a\ ^2G_{3\frac{1}{2}}$—$41^{\circ}_{4\frac{1}{2}}$	1541.978	100	64851.8	$a\ ^2P_{0\frac{1}{2}}$—$32^{\circ}_{1\frac{1}{2}}$
1356.109	150	73740.4	$a\ ^4P_{0\frac{1}{2}}$—$32^{\circ}_{1\frac{1}{2}}$	1542.212	80	64841.9	$a\ ^2P_{1\frac{1}{2}}$—$39^{\circ}_{2\frac{1}{2}}$
1362.038	80	73419.4	$a\ ^4F_{1\frac{1}{2}}$—$19^{\circ}_{0\frac{1}{2}}$	1548.473	100	64579.7	$a\ ^2P_{1\frac{1}{2}}$—$38^{\circ}_{1\frac{1}{2}}$
1365.372	500	73240.1	$a\ ^4F_{4\frac{1}{2}}$— $z\ ^4G^{\circ}_{5\frac{1}{2}}$	1554.580	80	64326.0	$a\ ^4P_{0\frac{1}{2}}$—$19^{\circ}_{0\frac{1}{2}}$
1365.949	10	73209.2	$a\ ^4P_{1\frac{1}{2}}$—$32^{\circ}_{1\frac{1}{2}}$	1556.793	20	64234.6	$a\ ^2F_{2\frac{1}{2}}$—$23^{\circ}_{3\frac{1}{2}}$
1366.874	20	73159.6	$a\ ^2G_{4\frac{1}{2}}$—$40^{\circ}_{3\frac{1}{2}}$	1560.550	30	64080.0	$a\ ^2P_{0\frac{1}{2}}$—$30^{\circ}_{0\frac{1}{2}}$
1367.149	200	73144.9	$a\ ^4F_{3\frac{1}{2}}$—$14^{\circ}_{2\frac{1}{2}}$	1562.328	80	64007.0	$a\ ^2G_{4\frac{1}{2}}$—$28^{\circ}_{3\frac{1}{2}}$
1377.708	180	72584.3	$a\ ^2F_{3\frac{1}{2}}$—$25^{\circ}_{3\frac{1}{2}}$				$b\ ^2D_{2\frac{1}{2}}$—$38^{\circ}_{1\frac{1}{2}}$
1378.048	10	72566.4	$a\ ^4F_{4\frac{1}{2}}$— $z\ ^4G^{\circ}_{3\frac{1}{2}}$	1562.429	80	64002.9	$a\ ^4F_{1\frac{1}{2}}$— $9^{\circ}_{0\frac{1}{2}}$
1378.166	20	72560.2	$a\ ^4P_{1\frac{1}{2}}$—$31^{\circ}_{2\frac{1}{2}}$	1563.826	20	63945.7	$a\ ^2G_{3\frac{1}{2}}$—$31^{\circ}_{2\frac{1}{2}}$
1378.655	150	72534.5	$a\ ^4F_{1\frac{1}{2}}$— $z\ ^4F^{\circ}_{2\frac{1}{2}}$	1567.512	200	63795.4	$a\ ^4P_{1\frac{1}{2}}$—$19^{\circ}_{0\frac{1}{2}}$
1379.222	50	72504.6	$a\ ^4P_{0\frac{1}{2}}$—$29^{\circ}_{1\frac{1}{2}}$				$a\ ^4P_{2\frac{1}{2}}$—$14^{\circ}_{2\frac{1}{2}}$
1379.951	150	72466.3	$a\ ^4P_{2\frac{1}{2}}$—$24^{\circ}_{1\frac{1}{2}}$	1571.901	80	63617.2	$a\ ^2P_{0\frac{1}{2}}$—$29^{\circ}_{1\frac{1}{2}}$
1380.498	125	72437.6	$a\ ^4P_{1\frac{1}{2}}$—$30^{\circ}_{0\frac{1}{2}}$	1574.855	200	63497.9	$a\ ^4F_{2\frac{1}{2}}$— $z\ ^4G^{\circ}_{3\frac{1}{2}}$
1381.338	200	72393.6	$a\ ^2G_{3\frac{1}{2}}$—$40^{\circ}_{3\frac{1}{2}}$	1579.413	200	63314.7	$a\ ^2F_{2\frac{1}{2}}$—$21^{\circ}_{2\frac{1}{2}}$
1385.763	300	72162.4	$a\ ^4F_{2\frac{1}{2}}$—$16^{\circ}_{3\frac{1}{2}}$	1580.277	20	63280.0	$a\ ^2F_{2\frac{1}{2}}$—$20^{\circ}_{3\frac{1}{2}}$
1389.388	100	71974.1	$a\ ^4P_{1\frac{1}{2}}$—$29^{\circ}_{1\frac{1}{2}}$	1581.226	20	63242.0	$a\ ^2G_{3\frac{1}{2}}$—$28^{\circ}_{3\frac{1}{2}}$
1391.441	180	71867.9	$a\ ^4P_{2\frac{1}{2}}$—$23^{\circ}_{3\frac{1}{2}}$	1584.074	150	63128.4	$a\ ^4P_{2\frac{1}{2}}$—$13^{\circ}_{2\frac{1}{2}}$
1395.971	180	71634.7	$b\ ^2D_{1\frac{1}{2}}$—$34^{\circ}_{1\frac{1}{2}}$	1589.559	200	62910.5	$a\ ^4P_{1\frac{1}{2}}$— $z\ ^4F^{\circ}_{2\frac{1}{2}}$
1402.878	100	71282.0	$a\ ^2P_{1\frac{1}{2}}$—$43^{\circ}_{2\frac{1}{2}}$	1589.680	80	62905.7	$a\ ^4F_{2\frac{1}{2}}$— $z\ ^4D^{\circ}_{2\frac{1}{2}}$
1406.079	20	71119.7	$a\ ^2F_{2\frac{1}{2}}$—$32^{\circ}_{1\frac{1}{2}}$	1593.394	150	62759.1	$b\ ^2D_{1\frac{1}{2}}$—$24^{\circ}_{1\frac{1}{2}}$
1409.472	225	70948.5	$a\ ^4P_{2\frac{1}{2}}$—$21^{\circ}_{2\frac{1}{2}}$	1600.496	200	62480.6	$a\ ^2F_{3\frac{1}{2}}$—$14^{\circ}_{2\frac{1}{2}}$
1413.779	250	70732.4	$a\ ^4F_{3\frac{1}{2}}$— $z\ ^4F^{\circ}_{3\frac{1}{2}}$	1608.348	40	62175.6	$a\ ^2P_{1\frac{1}{2}}$—$35^{\circ}_{0\frac{1}{2}}$
1414.247	100	70709.0	$b\ ^2D_{2\frac{1}{2}}$—$43^{\circ}_{2\frac{1}{2}}$	1610.390	60	62096.7	$a\ ^2P_{1\frac{1}{2}}$—$34^{\circ}_{1\frac{1}{2}}$
1417.111	100	70566.1	$a\ ^4F_{2\frac{1}{2}}$— $z\ ^4F^{\circ}_{1\frac{1}{2}}$	1617.137	250	61837.7	$a\ ^4P_{2\frac{1}{2}}$—$12^{\circ}_{1\frac{1}{2}}$
1417.368	125	70553.3	$a\ ^2F_{3\frac{1}{2}}$—$23^{\circ}_{3\frac{1}{2}}$	1617.761	100	61813.8	$a\ ^2F_{3\frac{1}{2}}$—$13^{\circ}_{2\frac{1}{2}}$
1419.023	60	70471.0	$a\ ^2F_{2\frac{1}{2}}$—$31^{\circ}_{2\frac{1}{2}}$	1621.913	500	61655.6	$a\ ^4F_{4\frac{1}{2}}$— $z\ ^4G^{\circ}_{4\frac{1}{2}}$
1427.393	150	70057.8	$a\ ^4P_{1\frac{1}{2}}$—$27^{\circ}_{2\frac{1}{2}}$	1625.384	10	61523.9	$b\ ^2D_{2\frac{1}{2}}$—$34^{\circ}_{1\frac{1}{2}}$
1428.907	300	69983.6	$a\ ^2F_{3\frac{1}{2}}$—$22^{\circ}_{4\frac{1}{2}}$	1629.116	300*d*	61383.0	$a\ ^4P_{2\frac{1}{2}}$— $z\ ^4F^{\circ}_{3\frac{1}{2}}$
1430.037	250	69928.3	$a\ ^2G_{3\frac{1}{2}}$—$39^{\circ}_{2\frac{1}{2}}$				$a\ ^4F_{1\frac{1}{2}}$— $z\ ^4D^{\circ}_{2\frac{1}{2}}$
1433.344	275	69766.9	$a\ ^2F_{2\frac{1}{2}}$—$28^{\circ}_{3\frac{1}{2}}$	1632.891	60	61241.1	$b\ ^2D_{1\frac{1}{2}}$—$21^{\circ}_{2\frac{1}{2}}$
1435.784	250	69648.3	$a\ ^2G_{4\frac{1}{2}}$—$36^{\circ}_{5\frac{1}{2}}$?	1638.876	250	61017.6	$a\ ^4F_{3\frac{1}{2}}$— $z\ ^4G^{\circ}_{2\frac{1}{2}}$
1436.088	80	69633.6	$a\ ^2F_{3\frac{1}{2}}$—$21^{\circ}_{2\frac{1}{2}}$	1644.189	100	60820.3	$a\ ^2F_{2\frac{1}{2}}$— $z\ ^4F^{\circ}_{2\frac{1}{2}}$
1436.802	30	69599.0	$a\ ^2F_{3\frac{1}{2}}$—$20^{\circ}_{3\frac{1}{2}}$	1652.733	250	60505.8	$a\ ^2G_{4\frac{1}{2}}$—$25^{\circ}_{3\frac{1}{2}}$
1439.100	300	69487.9	$a\ ^4F_{3\frac{1}{2}}$— $z\ ^4F^{\circ}_{4\frac{1}{2}}$	1664.778	250	60068.1	$a\ ^2F_{3\frac{1}{2}}$— $z\ ^4F^{\circ}_{3\frac{1}{2}}$
1441.173	200	69387.9	$a\ ^2P_{1\frac{1}{2}}$—$42^{\circ}_{2\frac{1}{2}}$	1668.098	100	59948.5	$a\ ^4P_{0\frac{1}{2}}$— $z\ ^4F^{\circ}_{1\frac{1}{2}}$
1446.334	150	69140.3	$a\ ^2P_{0\frac{1}{2}}$—$37^{\circ}_{1\frac{1}{2}}$	1673.919	125	59740.0	$a\ ^2G_{3\frac{1}{2}}$—$25^{\circ}_{3\frac{1}{2}}$
1446.701	80	69122.8	$a\ ^4P_{0\frac{1}{2}}$—$26^{\circ}_{1\frac{1}{2}}$	1676.957	40	59631.8	$b\ ^2D_{1\frac{1}{2}}$—$19^{\circ}_{0\frac{1}{2}}$
1448.393	250	69042.0	$a\ ^4F_{1\frac{1}{2}}$— $z\ ^4F^{\circ}_{1\frac{1}{2}}$	1693.917	1000	59034.8	$a\ ^4F_{4\frac{1}{2}}$— $z\ ^4D^{\circ}_{3\frac{1}{2}}$
1453.173	50	68814.9	$b\ ^2D_{2\frac{1}{2}}$—$42^{\circ}_{2\frac{1}{2}}$	1697.081	150	58924.7	$a\ ^2F_{2\frac{1}{2}}$—$16^{\circ}_{3\frac{1}{2}}$
1454.927	250	68732.0	$a\ ^4F_{2\frac{1}{2}}$—$13^{\circ}_{2\frac{1}{2}}$	1698.970	200	58859.2	$a\ ^2P_{1\frac{1}{2}}$—$31^{\circ}_{2\frac{1}{2}}$
1462.048	40	68397.2	$b\ ^2D_{1\frac{1}{2}}$—$31^{\circ}_{2\frac{1}{2}}$	1699.990	200	58823.9	$a\ ^2F_{3\frac{1}{2}}$— $z\ ^4F^{\circ}_{4\frac{1}{2}}$
1464.692	100	68273.7	$b\ ^2D_{1\frac{1}{2}}$—$30^{\circ}_{0\frac{1}{2}}$	1702.235	200	58746.3	$b\ ^2D_{1\frac{1}{2}}$— $z\ ^4F^{\circ}_{2\frac{1}{2}}$
1471.281	150	67968.0	$a\ ^2F_{2\frac{1}{2}}$—$27^{\circ}_{2\frac{1}{2}}$	1707.508	100	58564.9	$a\ ^2P_{0\frac{1}{2}}$—$24^{\circ}_{1\frac{1}{2}}$
1473.279	80	67875.8	$a\ ^4F_{1\frac{1}{2}}$—$14^{\circ}_{2\frac{1}{2}}$	1710.125	250	58475.2	$a\ ^2G_{4\frac{1}{2}}$—$23^{\circ}_{3\frac{1}{2}}$
1474.707	100	67810.0	$b\ ^2D_{1\frac{1}{2}}$—$29^{\circ}_{1\frac{1}{2}}$	1715.670	200	58286.3	$b\ ^2D_{2\frac{1}{2}}$—$31^{\circ}_{2\frac{1}{2}}$
1481.066	150	67518.9	$a\ ^2P_{0\frac{1}{2}}$—$35^{\circ}_{0\frac{1}{2}}$	1716.697	100	58251.4	$a\ ^4P_{1\frac{1}{2}}$—$14^{\circ}_{2\frac{1}{2}}$
1482.510	30	67453.2	$a\ ^4P_{0\frac{1}{2}}$—$24^{\circ}_{1\frac{1}{2}}$	1717.820	300	58213.3	$a\ ^4F_{1\frac{1}{2}}$— $z\ ^4D^{\circ}_{0\frac{1}{2}}$
1482.775	30	67441.1	$a\ ^4F_{2\frac{1}{2}}$—$12^{\circ}_{1\frac{1}{2}}$	1726.952	5	57905.5	$a\ ^2G_{4\frac{1}{2}}$—$22^{\circ}_{4\frac{1}{2}}$
1487.133	300	67243.5	$a\ ^4F_{3\frac{1}{2}}$— $z\ ^4G^{\circ}_{3\frac{1}{2}}$	1727.281	500	57894.5	$a\ ^4P_{2\frac{1}{2}}$— $z\ ^4G^{\circ}_{3\frac{1}{2}}$
1487.906	250	67208.5	$a\ ^4F_{1\frac{1}{2}}$—$13^{\circ}_{2\frac{1}{2}}$	1733.140	100*d*	57698.9	$b\ ^2D_{2\frac{1}{2}}$—$29^{\circ}_{1\frac{1}{2}}$
1489.446	200	67139.0	$a\ ^2F_{3\frac{1}{2}}$— $z\ ^4F^{\circ}_{2\frac{1}{2}}$	1736.590	60	57584.1	$a\ ^4P_{1\frac{1}{2}}$—$13^{\circ}_{2\frac{1}{2}}$
1492.829	( )	66986.9	$a\ ^4F_{2\frac{1}{2}}$— $z\ ^4F^{\circ}_{3\frac{1}{2}}$	1738.484	300	57521.4	$a\ ^2G_{4\frac{1}{2}}$—$20^{\circ}_{3\frac{1}{2}}$
1494.266	20	66922.5	$a\ ^4P_{1\frac{1}{2}}$—$24^{\circ}_{1\frac{1}{2}}$	1744.346	150	57328.1	$a\ ^2F_{2\frac{1}{2}}$— $z\ ^4F^{\circ}_{1\frac{1}{2}}$
1500.334	250	66651.8	$a\ ^4F_{3\frac{1}{2}}$— $z\ ^4D^{\circ}_{2\frac{1}{2}}$	1745.098	40	57303.4	$a\ ^4P_{2\frac{1}{2}}$— $z\ ^4D^{\circ}_{2\frac{1}{2}}$

TABLE 1. *Identified lines of* Au III—Continued

λ(vac.)	Intensity and character	Wave No.	Combination	λ(vac.)	Intensity and character	Wave No.	Combination
A		cm^{-1}		*A*		cm^{-1}	
1746.037	500	57272.5	$a\ ^4F_{2\frac{1}{2}}$— $z\ ^4G^\circ_{2\frac{1}{2}}$	1989.631	400	50260.6	$a\ ^2F_{2\frac{1}{2}}$— $z\ ^4G^\circ_{3\frac{1}{2}}$
1750.095	30	57139.9	$a\ ^2G_{3\frac{1}{2}}$—$22^\circ_{4\frac{1}{2}}$	1996.853	150	50078.8	$a\ ^2P_{1\frac{1}{2}}$—$18^\circ_{0\frac{1}{2}}$
1756.917	500	56917.9	$a\ ^4F_{2\frac{1}{2}}$— $z\ ^4D^\circ_{1\frac{1}{2}}$	2041.435	60	48969.4	$a\ ^2G_{3\frac{1}{2}}$—$13^\circ_{2\frac{1}{2}}$
1759.800	20	56824.6	$a\ ^4P_{0\frac{1}{2}}$—$12^\circ_{1\frac{1}{2}}$	2055.459	60	48635.4	$b\ ^2D_{2\frac{1}{2}}$— $z\ ^4F^\circ_{2\frac{1}{2}}$
1760.881	60	56789.7	$a\ ^2G_{3\frac{1}{2}}$—$21^\circ_{2\frac{1}{2}}$	2083.092	300	47990.3	$a\ ^2G_{4\frac{1}{2}}$— $z\ ^4F^\circ_{3\frac{1}{2}}$
1761.947	500	56755.4	$a\ ^2G_{3\frac{1}{2}}$—$20^\circ_{3\frac{1}{2}}$	2085.452	80	47936.0	$a\ ^2P_{0\frac{1}{2}}$—$12^\circ_{1\frac{1}{2}}$
1767.415	300	56579.8	$a\ ^2F_{3\frac{1}{2}}$— $z\ ^4G^\circ_{3\frac{1}{2}}$	2100.392	20	47595.0	$b\ ^2D_{1\frac{1}{2}}$— $z\ ^4D^\circ_{2\frac{1}{2}}$
1774.419	100	56356.5	$a\ ^2P_{1\frac{1}{2}}$—$27^\circ_{2\frac{1}{2}}$	2116.879	2	47224.4	$a\ ^2G_{3\frac{1}{2}}$— $z\ ^4F^\circ_{3\frac{1}{2}}$
1775.166	800	56332.8	$a\ ^4F_{3\frac{1}{2}}$— $z\ ^4G^\circ_{4\frac{1}{2}}$	2159.085	100	46301.2	$a\ ^4P_{0\frac{1}{2}}$— $z\ ^4D^\circ_{1\frac{1}{2}}$
1776.396	200	56293.8	$a\ ^4P_{1\frac{1}{2}}$—$12^\circ_{1\frac{1}{2}}$	2167.332	80	46125.2	$a\ ^4P_{1\frac{1}{2}}$— $z\ ^4G^\circ_{2\frac{1}{2}}$
1780.571	100	56161.8	$a\ ^2F_{2\frac{1}{2}}$—$14^\circ_{2\frac{1}{2}}$	2172.200	200	46021.8	$a\ ^2P_{0\frac{1}{2}}$— $9^\circ_{0\frac{1}{2}}$
1786.106	300	55987.7	$a\ ^2F_{3\frac{1}{2}}$— $z\ ^4D^\circ_{2\frac{1}{2}}$	2184.108	100	45770.9	$a\ ^4P_{1\frac{1}{2}}$— $z\ ^4D^\circ_{1\frac{1}{2}}$
1792.653	150	55783.2	$b\ ^2D_{2\frac{1}{2}}$—$27^\circ_{2\frac{1}{2}}$	2186.673	50	45717.3	$a\ ^2P_{1\frac{1}{2}}$— $z\ ^4F^\circ_{1\frac{1}{2}}$
1793.762	500	55748.8	$a\ ^4F_{1\frac{1}{2}}$— $z\ ^4G^\circ_{2\frac{1}{2}}$	2188.966	500	45669.4	$a\ ^2F_{3\frac{1}{2}}$— $z\ ^4G^\circ_{4\frac{1}{2}}$
1801.982	200	55494.4	$a\ ^2F_{2\frac{1}{2}}$—$13^\circ_{2\frac{1}{2}}$	2253.448	40	44362.7	$a\ ^4P_{2\frac{1}{2}}$— $z\ ^4D^\circ_{3\frac{1}{2}}$
1805.235	400	55394.4	$a\ ^4F_{1\frac{1}{2}}$— $z\ ^4D^\circ_{1\frac{1}{2}}$	2270.217	10	44035.2	$a\ ^2F_{2\frac{1}{2}}$— $z\ ^4G^\circ_{2\frac{1}{2}}$
1809.811	100	55254.4	$b\ ^2D_{1\frac{1}{2}}$— $z\ ^4F^\circ_{1\frac{1}{2}}$	2278.045	5	43883.7	$a\ ^2P_{1\frac{1}{2}}$—$13^\circ_{2\frac{1}{2}}$
1821.169	400	54909.8	$a\ ^4P_{0\frac{1}{2}}$— $9^\circ_{0\frac{1}{2}}$	2288.626	40	43680.8	$a\ ^2F_{2\frac{1}{2}}$— $z\ ^4D^\circ_{1\frac{1}{2}}$
1821.801	20	54890.7	$a\ ^2P_{1\frac{1}{2}}$—$26^\circ_{1\frac{1}{2}}$	2308.200	10	43310.5	$b\ ^2D_{2\frac{1}{2}}$—$13^\circ_{2\frac{1}{2}}$
1841.019	20	54317.7	$b\ ^2D_{2\frac{1}{2}}$—$26^\circ_{1\frac{1}{2}}$	2322.267	300	43048.1	$a\ ^2F_{3\frac{1}{2}}$— $z\ ^4D^\circ_{3\frac{1}{2}}$
1844.889	400	54203.8	$a\ ^2F_{2\frac{1}{2}}$—$12^\circ_{1\frac{1}{2}}$	2347.105	20	42592.6	$a\ ^2P_{1\frac{1}{2}}$—$12^\circ_{1\frac{1}{2}}$
1848.833	150	54088.2	$b\ ^2D_{1\frac{1}{2}}$—$14^\circ_{2\frac{1}{2}}$	2379.106	10	42019.8	$b\ ^2D_{2\frac{1}{2}}$—$12^\circ_{1\frac{1}{2}}$
1849.088	50	54080.7	$b\ ^2D_{2\frac{1}{2}}$—$25^\circ_{3\frac{1}{2}}$	2382.403	100	41961.6	$b\ ^2D_{1\frac{1}{2}}$— $z\ ^4G^\circ_{2\frac{1}{2}}$
1860.484	40	53749.5	$a\ ^2F_{2\frac{1}{2}}$— $z\ ^4F^\circ_{3\frac{1}{2}}$	2402.706	150	41607.1	$b\ ^2D_{1\frac{1}{2}}$— $z\ ^4D^\circ_{1\frac{1}{2}}$
1861.799	500	53711.5	$a\ ^4F_{3\frac{1}{2}}$— $z\ ^4D^\circ_{3\frac{1}{2}}$	2405.118	150	41565.3	$b\ ^2D_{2\frac{1}{2}}$— $z\ ^4F^\circ_{3\frac{1}{2}}$
1871.922	150	53421.0	$b\ ^2D_{1\frac{1}{2}}$—$13^\circ_{2\frac{1}{2}}$	2625.522	10*d*	38076.3	$b\ ^2D_{2\frac{1}{2}}$— $z\ ^4G^\circ_{3\frac{1}{2}}$
1880.911	30	53165.7	$a\ ^2G_{4\frac{1}{2}}$—$16^\circ_{3\frac{1}{2}}$	2665.159	10	37510.1	$a\ ^2G_{3\frac{1}{2}}$— $z\ ^4G^\circ_{2\frac{1}{2}}$
1899.405	60	52648.1	$b\ ^2D_{2\frac{1}{2}}$—$24^\circ_{1\frac{1}{2}}$	2666.994	10	37484.3	$b\ ^2D_{2\frac{1}{2}}$— $z\ ^4D^\circ_{2\frac{1}{2}}$
1918.278	150	52130.1	$b\ ^2D_{1\frac{1}{2}}$—$12^\circ_{1\frac{1}{2}}$	2721.835	50	36729.0	$a\ ^2F_{2\frac{1}{2}}$— $z\ ^4D^\circ_{3\frac{1}{2}}$
1932.038	100	51758.8	$a\ ^4P_{1\frac{1}{2}}$— $z\ ^4D^\circ_{2\frac{1}{2}}$	3117.339	10	32069.3	$a\ ^2P_{1\frac{1}{2}}$— $z\ ^4D^\circ_{1\frac{1}{2}}$
1934.114	60	51703.3	$a\ ^2P_{1\frac{1}{2}}$—$21^\circ_{2\frac{1}{2}}$	3138.730	10	31850.8	$b\ ^2D_{2\frac{1}{2}}$— $z\ ^4G^\circ_{2\frac{1}{2}}$
1935.416	100	51668.2	$a\ ^4P_{2\frac{1}{2}}$— $z\ ^4G^\circ_{2\frac{1}{2}}$	3174.057	20	31496.3	$b\ ^2D_{2\frac{1}{2}}$— $z\ ^4D^\circ_{1\frac{1}{2}}$
1948.792	200	51313.8	$a\ ^4P_{2\frac{1}{2}}$— $z\ ^4D^\circ_{1\frac{1}{2}}$	3227.991	100	30970.0	$a\ ^2G_{4\frac{1}{2}}$— $z\ ^4D^\circ_{3\frac{1}{2}}$
1958.472	100	51060.2	$a\ ^2P_{0\frac{1}{2}}$— $z\ ^4F^\circ_{1\frac{1}{2}}$	3309.856	100	30204.1	$a\ ^2G_{3\frac{1}{2}}$— $z\ ^4D^\circ_{3\frac{1}{2}}$
1985.951	20*d*	50353.7	$a\ ^2F_{3\frac{1}{2}}$— $z\ ^4G^\circ_{2\frac{1}{2}}$				

NOTE.—*h*=hazy; *w*=wide; ( )=masked by another line; *d*=double.

TABLE 2. *Even levels of* Au III

Electron structure	Possible designation	*J*	Level	Interval	Electron structure	Possible designation	*J*	Level	Interval
$5d^9$	$a\ ^2D$	$2\frac{1}{2}$	0.0	−12694.0	$5d^8(^3P_1)6s$	$a\ ^4P$	$0\frac{1}{2}$	49438.9	
$5d^9$	$a\ ^2D$	$1\frac{1}{2}$	12694.0		$5d^8(^3P_2)6s$	$a\ ^4P$	$1\frac{1}{2}$	49969.4	
					$5d^8(^3F_2)6s$	$a\ ^2F$	$2\frac{1}{2}$	52059.6	
$5d^8(^3F_4)6s$	$a\ ^4F$	$4\frac{1}{2}$	29753.6	−5323.1	$5d^8(^1D_2)6s$	$b\ ^2D$	$1\frac{1}{2}$	54133.2	
$5d^8(^3F_4)6s$	$a\ ^4F$	$3\frac{1}{2}$	35076.7	−3745.5	$5d^8(^1G_4)6s$	$a\ ^2G$	$4\frac{1}{2}$	57818.6	
$5d^8(^3F_3)6s$	$a\ ^4F$	$2\frac{1}{2}$	38822.2	−1523.4	$5d^8(^3P_0)6s$	$a\ ^2P$	$0\frac{1}{2}$	58327.1	
$5d^8(^3F_2)6s$	$a\ ^4F$	$1\frac{1}{2}$	40345.6		$5d^8(^1G_4)6s$	$a\ ^2G$	$3\frac{1}{2}$	58584.6	
					$5d^8(^3P_1)6s$	$a\ ^2P$	$1\frac{1}{2}$	63670.9	
$5d^8(^3P_2)6s$	$a\ ^4P$	$2\frac{1}{2}$	44425.9		$5d^8(^1D_2)6s$	$b\ ^2D$	$2\frac{1}{2}$	64244.0	
$5d^8(^3F_3)6s$	$a\ ^2F$	$3\frac{1}{2}$	45740.5						

TABLE 3. *Odd levels of* Au III

Electron structure	Possible designation	Number	J	Level	Electron structure	Possible designation	Number	J	Level
$5d^8(^3F)6p$	$z\ ^4D°$	1°	3½	*88788. 5*	$5d^8(^3P)6p$	$^4S°$	24°	1½	*116892. 1*
$5d^8(^3F)6p$	$z\ ^4G°$	2°	4½	*91409. 4*	$5d^8(^1D)6p$	$^2F°$	25°	3½	*118324. 6*
$5d^8(^3F)6p$	$z\ ^4D°$	3°	1½	*95740. 0*	$5d^8(^3F)6p$	$^2D°$	26°	1½	*118561. 7*
$5d^8(^3F)6p$	$z\ ^4G°$	4°	2½	*96094. 5*	$5d^8(^3P)6p$	$^4D°$	27°	2½	*120027. 3*
$5d^8(^3F)6p$	$z\ ^4D°$	5°	0½	*98559. 1*	$5d^8(^3F)6p$	$^2G°$	28°	3½	*121826. 4*
$5d^8(^3F)6p$	$z\ ^4D°$	6°	2½	*101728. 2*	$5d^8(^1D)6p$	$^2P°$	29°	1½	*121943. 5*
$5d^8(^3F)6p$	$z\ ^4G°$	7°	3½	*102320. 2*	$5d^8(^3P)6p$	$^4D°$	30°	0½	*122407. 0*
$5d^8(^3F)6p$	$z\ ^4G°$	8°	5½	*102993. 7*	$5d^8(^1D)6p$	$^2F°$	31°	2½	*122530. 3*
$5d^8(^3P)6p$	$^4P°$	9°	0½	*104348. 3*	$5d^8(^3P)6p$	$^4D°$	32°	1½	*123179. 0*
$5d^8(^3F)6p$	$z\ ^4F°$	10°	4½	*104564. 6*	$5d^8(^1G)6p$	$^2H°$	33°	4½	*123508. 8?*
$5d^8(^3F)6p$	$z\ ^4F°$	11°	3½	*105809. 1*	$5d^8(^1D)6p$	$^2D°$	34°	1½	*125767. 9*
$5d^8(^3P)6p$	$^4P°$	12°	1½	*106263. 1*	$5d^8(^3P)6p$	$^2P°$	35°	0½	*125846. 2*
$5d^8(^3P)6p$	$^4P°$	13°	2½	*107554. 2*	$5d^8(^1G)6p$	$^2H°$	36°	5½	*127467. 0?*
$5d^8(^3F)6p$	$^2D°$	14°	2½	*108221. 2*	$5d^8(^3P)6p$	$^2D°$	37°	1½	*127467. 6*
$5d^8(^3F)6p$	$z\ ^4F°$	15°	1½	*109387. 6*	$5d^8(^3P)6p$	$^2P°$	38°	1½	*128250. 9*
$5d^8(^3P)6p$	$^4D°$	16°	3½	*110984. 1*	$5d^8(^1G)6p$	$^2F°$	39°	2½	*128512. 7*
$3d^8(^3F)6p$	$z\ ^4F°$	17°	2½	*112879. 6*	$5d^8(^1G)6p$	$^2G°$	40°	3½	*130978. 2*
$5d^8(^3P)6p$	$^2S°$	18°	0½	*113749. 9*	$5d^8(^1G)6p$	$^2G°$	41°	4½	*132353. 0*
$5d^8(^1D)6p$	$^2P°$	19°	0½	*113764. 9*	$5d^8(^3P)6p$	$^2D°$	42°	2½	*133058. 9*
$5d^8(^1G)6p$	$^2F°$	20°	3½	*115339. 9*	$5d^8(^1D)6p$	$^2D°$	43°	2½	*134953. 0*
$5d^8(^3F)6p$	$^2F°$	21°	2½	*115374. 2*	$5d^7\ 6s\ 6p$		44°	3½	*156532. 0*
$5d^8(^3F)6p$	$^2G°$	22°	4½	*115724. 2*	$5d^7\ 6s\ 6p$		45°	2½	*158323. 1*
$5d^8(^3F)6p$	$^2F°$	23°	3½	*116293. 8*					

(Paper 64A6–69)

JOURNAL OF RESEARCH of the National Bureau of Standards—A. Physics and Chemistry
Vol. 64A, No. 6, November–December 1960

Tolerances For Layer Thicknesses in Dielectric Multilayer Coatings and Interference Filters

Klaus D. Mielenz*

(July 26, 1960)

A theory is developed for dielectric multilayer coatings in which the layers depart from calculated thickness. The theory is applied to alternating systems of quarter wave layers of ZnS and MgF_2. The effects of thickness errors are: (1) A shift of the wavelength at which maximum reflectance occurs; and (2) a change in phase shift upon reflection. The magnitude of these effects, and also their dependence on various parameters, are determined. Statistical tolerances for layer thicknesses are computed for given tolerances on the multilayer performance. The accuracy required for producing dielectric interference filters is up to about 40 times higher than the accuracy sufficient for the production of dielectric mirrors and beam splitters. Various techniques of experimentally controlling film thicknesses, and their accuracies, are discussed. The production of mirrors and beam splitters deviating from theoretical maximum reflectance by only 1 percent seems to be possible with Dufour's simple single photocell method of monitoring film thicknesses. With more precise methods, such as those developed by Giacomo and Jacquinot, or Traub, the production of interference filters appears to be possible to within plus or minus one half their half widths.

1. Introduction

In the production of dielectric multilayer coatings, such as mirrors, beam splitters, or interference filters, it is important to control the thickness of the layers with an accuracy sufficient to attain experimentally the high performance of which these coatings are capable.

Heavens [1] [1] has calculated, in some few examples, the effect of errors in layer thicknesses on the energy reflected from high-reflecting multilayer coatings, and Giacomo [2] has done similar work on the effect of these errors on the phase change upon reflection from such coatings. Neither author, however, has derived the tolerances on individual layer thicknesses that may be allowed if the coating is to meet a given performance within certain explicitly specified limits.

Such tolerances are computed in this paper, and various techniques of monitoring layer thicknesses are compared from the point of view of these tolerances.

2. Basic Formulas

2.1. General Case

The electromagnetic field at the plane of incidence on a stack of N dielectric layers is, according to Koehler [3],

$$\begin{pmatrix} E \\ H \end{pmatrix} = \mathfrak{A}_1 \mathfrak{A}_2 \ldots \mathfrak{A}_N \begin{pmatrix} 1 \\ n_s \end{pmatrix} \tag{1}$$

(n_s=substrate index), with

$$\mathfrak{A}_\nu = \cos \beta_\nu \, \mathfrak{U} + i \sin \beta_\nu \, \mathfrak{N}_\nu, \tag{2}$$

$$\mathfrak{U} = \begin{pmatrix} 1 & 0 \\ 0 & 1 \end{pmatrix}, \quad \mathfrak{N}_\nu = \begin{pmatrix} 0 & 1/n_\nu \\ n_\nu & 0 \end{pmatrix}. \tag{3}$$

Here,

$$\beta_\nu = (2\pi/\lambda) n_\nu d_\nu, \quad \nu = 1,2, \ldots N \tag{4}$$

(n_ν=refractive index, d_ν=geometrical thickness, λ=vacuum wavelength) represents the optical thickness of the νth layer.

The amplitudes transmitted and reflected by the multilayer are

$$T = (2\sqrt{n_0 n_s})/C^+ = \sqrt{\tau}\, e^{i\theta}, \tag{5}$$

$$R = C^-/C^+ = \sqrt{\rho}\, e^{i\Phi}, \tag{6}$$

where τ and ρ denote energy transmittance and reflectance, and with

$$C^\pm = n_0 E \pm H \tag{7}$$

(n_0=index of medium of incidence). Hence

$$\tau = \frac{4 n_0 n_s}{(\mathcal{R}C^+)^2 + (\mathcal{I}C^+)^2} \tag{8}$$

and, for truly dielectric layers,

$$\rho = 1 - \tau. \tag{9}$$

Furthermore,

$$\Phi = \theta + \alpha, \quad \tan\theta = -\mathcal{I}C^+/\mathcal{R}C^+, \quad \tan\alpha = \mathcal{I}C^-/\mathcal{R}C^-. \tag{10}$$

Here, $\mathcal{R}$ and $\mathcal{I}$ denote real and imaginary part, respectively.

Of the two phase angles θ and Φ, only Φ, the phase change upon reflection, is of practical significance in most cases, as, for instance, for the energy transmit-

*Present address: Ceciliengaerten 45, Berlin-Friedenau, Germany.

[1] Figures in brackets indicate the literature references at the end of this paper.

ted by a Fabry-Perot interferometer (see eq (60)). Throughout this paper, therefore, θ is an auxiliary quantity only that is needed for the computation of Φ.

2.2. Alternating Multilayers

Consider an odd number, $N=2m+1$, of layers of nominally equal optical thickness, alternately of high index n_H and low index n_L, with a high index on the outside. If all layers are a quarter wave thick at a wavelength λ_0,

$$\beta_1=\beta_2= \ . \ . \ . \ =\beta=(\pi/2)(\lambda_0/\lambda), \tag{11}$$

eq (2) may be written as

$$\begin{pmatrix}E\\H\end{pmatrix}=[S_m(x)\mathfrak{A}_H-S_{m-1}(x)\mathfrak{A}_L^{-1}]\begin{pmatrix}1\\n_s\end{pmatrix}, \tag{12}$$

with

$$\mathfrak{A}_H=\cos\beta\ \mathfrak{U}+i\sin\beta\ \mathfrak{N}_H, \tag{13}$$

$$\mathfrak{A}_L^{-1}=\cos\beta\ \mathfrak{U}-i\sin\beta\ \mathfrak{N}_L. \tag{14}$$

S_m and S_{m-1} are Chebychev polynomials of the argument

$$x=2-\frac{(n_H+n_L)^2}{n_H n_L}\sin^2\beta, \tag{15}$$

defined by

$$S_{m-1}(x)=\sin m\gamma/\sin\gamma, \quad x=2\cos\gamma, \tag{16}$$

etc., see [4]. From eqs (12) to (14), and (7),

$$C^{\pm}=A^{\pm}\cos\beta+iB^{\pm}\sin\beta, \tag{17}$$

with

$$A^{\pm}=K^{\pm}\ (S_m-S_{m-1}), \quad K^{\pm}=n_0\pm n_s, \tag{18}$$

$$\left.\begin{aligned}B^{\pm}=P^{\pm}\ S_m+Q^{\pm}\ S_{m-1}, \quad P^{\pm}=n_0n_s/n_H\pm n_H,\\ Q^{\pm}=n_0n_s/n_L\pm n_L.\end{aligned}\right\} \tag{19}$$

Hence, eqs (8), (9), (10), and (17) yield

$$\tau=1-\rho=\frac{4n_0n_s}{(A^+\cos\beta)^2+(B^+\sin\beta)^2} \tag{20}$$

$$\left.\begin{aligned}\tan\theta=-(B^+/A^+)\tan\beta,\\ \tan\alpha=(B^-/A^-)\tan\beta,\\ \Phi=\theta+\alpha.\end{aligned}\right\} \tag{21}$$

3. Multilayers With Layer Thickness Errors

3.1. General Case

If, in the multilayer, the optical thicknesses $n_\nu d_\nu$ of the films differ from their calculated values by slight amounts $\Delta_\nu=\Delta(n_\nu d_\nu)$, the $(\beta_\nu)'$s of section 2.1 must be replaced by

$$\beta'_\nu=\beta_\nu+\Delta\beta_\nu, \text{ with } \Delta\beta_\nu=(2\pi/\lambda)\Delta_\nu. \tag{22}$$

Let $\Delta\beta_\nu$ be sufficiently small, so that

$$\cos\beta'_\nu=\cos\beta_\nu-\Delta\beta_\nu\sin\beta_\nu, \tag{23}$$

$$\sin\beta'_\nu=\sin\beta_\nu+\Delta\beta_\nu\cos\beta_\nu. \tag{24}$$

Then, the matrices $\mathfrak{A}_\nu$ will be changed to

$$\mathfrak{A}'_\nu=\mathfrak{A}_\nu+\Delta\beta_\nu\mathfrak{B}_\nu, \tag{25}$$

with $\mathfrak{A}_\nu$ from eq (3), and

$$\mathfrak{B}_\nu=-\sin\beta_\nu\ \mathfrak{U}+i\cos\beta_\nu\ \mathfrak{N}_\nu. \tag{26}$$

Therefore, eq (2) is transformed into

$$\begin{pmatrix}E'\\H'\end{pmatrix}=\mathfrak{A}'_1\,\mathfrak{A}'_2\ \ldots\ \mathfrak{A}'_N\begin{pmatrix}1\\n_s\end{pmatrix}=\begin{pmatrix}E\\H\end{pmatrix}+\sum_{\nu=1}^{N}\begin{pmatrix}\Delta E_\nu\\\Delta H_\nu\end{pmatrix}, \tag{27}$$

with $\begin{pmatrix}E\\H\end{pmatrix}$ from eq. (2), and

$$\left.\begin{aligned}\begin{pmatrix}\Delta E_\nu\\\Delta H_\nu\end{pmatrix}=\Delta\beta_\nu\mathfrak{D}_\nu\begin{pmatrix}1\\n_s\end{pmatrix},\\ \mathfrak{D}_\nu=\mathfrak{A}_1\mathfrak{A}_2\ \ldots\ \mathfrak{A}_{\nu-1}\mathfrak{B}_\nu\mathfrak{A}_{\nu+1}\ \ldots\ \mathfrak{A}_N.\end{aligned}\right\} \tag{28}$$

In this first-order approximation, accordingly, each $\Delta\beta_\nu$ causes separate additive terms in E and H, so that

$$\left.\begin{aligned}(C^{\pm})'&=n_0E'\pm H'\\ &=(n_0E\pm H)+\sum_{\nu=1}^{N}(n_0\Delta E_\nu\pm\Delta H_\nu)\\ &=C^{\pm}+\sum_{\nu=1}^{N}\Delta C^{\pm}_\nu.\end{aligned}\right\} \tag{29}$$

Thus, the individual errors $\Delta\beta_\nu$ may be considered separately.

3.2. Alternating Multilayers

a. Incorrect High-Index Layer

Consider an error in thickness in one of the high-index layers, $\nu=2k+1$. Then, eq (28) yields

$$\mathfrak{D}_{2k+1}=(\mathfrak{A}_H\mathfrak{A}_L)^k\mathfrak{B}_H(\mathfrak{A}_L\mathfrak{A}_H)^{m-k}. \tag{30}$$

According to [4],

$$(\mathfrak{A}_H\mathfrak{A}_L)^n=S_{n-1}\mathfrak{A}_H\mathfrak{A}_L-S_{n-2}\mathfrak{U},$$

and therefore,

$$\left.\begin{aligned}\mathfrak{D}_{2k+1}=S_{k-1}S_{m-k-1}\mathfrak{A}_H\mathfrak{A}_L\mathfrak{B}_H\mathfrak{A}_L\mathfrak{A}_H\\ -S_{k-2}S_{m-k-1}\mathfrak{B}_H\mathfrak{A}_L\mathfrak{A}_H\\ -S_{k-1}S_{m-k-2}\mathfrak{A}_H\mathfrak{A}_L\mathfrak{B}_H\\ +S_{k-2}S_{m-k-2}\mathfrak{B}_H.\end{aligned}\right\} \tag{31}$$

From (13), (14), (15), and (26), the following identities can be derived:

$$\mathfrak{A}_H\mathfrak{A}_L\mathfrak{B}_H\mathfrak{A}_L\mathfrak{A}_H=-[(x^2-x+1)\mathfrak{U}+(x-1)$$
$$(\mathfrak{N}_H\mathfrak{N}_L+\mathfrak{N}_L\mathfrak{N}_H)]\sin\beta+i[(x-1)^2\mathfrak{N}_H+(x-2)\mathfrak{N}_L]\cos\beta,$$
$$\mathfrak{B}_H\mathfrak{A}_L\mathfrak{A}_H=-(x\mathfrak{U}+\mathfrak{N}_H\mathfrak{N}_L)\sin\beta+i(x-1)\mathfrak{N}_H\cos\beta,$$
$$\mathfrak{A}_H\mathfrak{A}_L\mathfrak{B}_H=-(x\mathfrak{U}+\mathfrak{N}_L\mathfrak{N}_H)\sin\beta+i(x-1)\mathfrak{N}_H\cos\beta,$$

with

$$\mathfrak{N}_H\mathfrak{N}_L=\begin{pmatrix} n_L/n_H & 0 \\ 0 & n_H/n_L \end{pmatrix}, \tag{32}$$

$$\mathfrak{N}_L\mathfrak{N}_H=\begin{pmatrix} n_H/n_L & 0 \\ 0 & n_L/n_H \end{pmatrix}. \tag{33}$$

These together with the following recurrence relation between Chebychev polynomials:

$$S_n=xS_{n-1}-S_{n-2},$$

provide

$$\left.\begin{aligned}\mathfrak{D}_{2k-1}=&-[(S_kS_{m-k}-[x-1]S_{k-1}S_{m-k-1})\mathfrak{U}\\&+S_{m-k-1}(S_k-S_{k-1})\mathfrak{N}_H\mathfrak{N}_L\\&+S_{k-1}(S_{m-k}-S_{m-k-1})\mathfrak{N}_L\mathfrak{N}_H]\sin\beta\\&+i[(S_k-S_{k-1})(S_{m-k}-S_{m-k-1})\mathfrak{N}_H\\&+(x-2)S_{k-1}S_{m-k-1}\mathfrak{N}_L]\cos\beta.\end{aligned}\right\} \tag{34}$$

Thus, it follows from (28), (29), and (34),

$$\Delta C^{\pm}_{2k+1}=\Delta\beta_{2k+1}(A^{\pm}_{2k+1}\sin\beta+iB^{\pm}_{2k+1}\cos\beta), \tag{35}$$

with

$$\left.\begin{aligned}A^{\pm}_{2k+1}=&-K^{\pm}[S_kS_{m-k}-(x-1)S_{k-1}S_{m-k-1}]\\&-L^{\pm}S_{m-k-1}(S_k-S_{k-1})\\&-M^{\pm}S_{k-1}(S_{m-k}-S_{m-k-1}),\end{aligned}\right\} \tag{36}$$

$$\left.\begin{aligned}B^{\pm}_{2k+1}=&P^{\pm}(S_k-S_{k-1})(S_{m-k}-S_{m-k-1})\\&+Q^{\pm}(x-2)S_{k-1}S_{m-k-1},\end{aligned}\right\} \tag{37}$$

$K^{\pm}$, $P^{\pm}$, and $Q^{\pm}$, from eqs (18) and (19), and

$$\left.\begin{aligned}L^{\pm}&=n_0n_L/n_H\pm n_sn_H/n_L,\\M^{\pm}&=n_0n_H/n_L\pm n_sn_L/n_H.\end{aligned}\right\} \tag{38}$$

b. Incorrect Low-Index Layer

Next, consider a thickness error in one of the low-index layers, $v=2k$, so that

$$\mathfrak{D}_{2k}=(\mathfrak{A}_H\mathfrak{A}_L)^{k-1}\mathfrak{A}_H\mathfrak{B}_L(\mathfrak{A}_H\mathfrak{A}_L)^{m-k}\mathfrak{A}_H. \tag{39}$$

Because of [4]

$$(\mathfrak{A}_H\mathfrak{A}_L)^n\mathfrak{A}_H=S_n\mathfrak{A}_H-S_{n-1}\mathfrak{A}_L^{-1},$$

this is equal to

$$\left.\begin{aligned}\mathfrak{D}_{2k}=&S_{k-1}S_{m-k}\mathfrak{A}_H\mathfrak{B}_L\mathfrak{A}_H-S_{k-2}S_{m-k}\mathfrak{A}_L^{-1}\mathfrak{B}_L\mathfrak{A}_H\\&-S_{k-1}S_{m-k-1}\mathfrak{A}_H\mathfrak{B}_L\mathfrak{A}_L^{-1}\\&+S_{k-2}S_{m-k-1}\mathfrak{A}_L^{-1}\mathfrak{B}_L\mathfrak{A}_L{}^{-1}.\end{aligned}\right\} \tag{40}$$

From (13), (14), (15), and (26), it can be shown that

$$\mathfrak{A}_H\mathfrak{B}_L\mathfrak{A}_H=-[(x-1)\mathfrak{U}+\mathfrak{N}_H\mathfrak{N}_L+\mathfrak{N}_L\mathfrak{N}_H]\sin\beta$$
$$+i[(x-2)\mathfrak{N}_H+\mathfrak{N}_L]\cos\beta,$$
$$\mathfrak{A}_L^{-1}\mathfrak{B}_L\mathfrak{A}_H=-\mathfrak{N}_L\mathfrak{N}_H\sin\beta+i\mathfrak{N}_L\cos\beta,$$
$$\mathfrak{A}_H\mathfrak{B}_L\mathfrak{A}_L^{-1}=-\mathfrak{N}_H\mathfrak{N}_L\sin\beta+i\mathfrak{N}_L\cos\beta,$$
$$\mathfrak{A}_L^{-1}\mathfrak{B}_L\mathfrak{A}_L^{-1}=\sin\beta\,\mathfrak{U}+i\mathfrak{N}_L\cos\beta,$$

so that

$$\left.\begin{aligned}\mathfrak{D}_{2k}=&-[([x-1]S_{k-1}S_{m-k}-S_{k-2}S_{m-k-1})\mathfrak{U}\\&+S_{k-1}(S_{m-k}-S_{m-k-1})\mathfrak{N}_H\mathfrak{N}_L\\&+S_{m-k}(S_{k-1}-S_{k-2})\mathfrak{N}_L\mathfrak{N}_H]\sin\beta\\&+i[(x-2)S_{k-1}S_{m-k}\mathfrak{N}_H\\&+(S_{k-1}-S_{k-2})(S_{m-k}-S_{m-k-1})\mathfrak{N}_L]\cos\beta.\end{aligned}\right\} \tag{41}$$

Eventually, (28), (29), and (41) provide the result

$$\Delta C^{\pm}_{2k}=\Delta\beta_{2k}(A^{\pm}_{2k}\sin\beta+iB^{\pm}_{2k}\cos\beta), \tag{42}$$

with

$$\left.\begin{aligned}A^{\pm}_{2k}=&-K^{\pm}[(x-1)S_{k-1}S_{m-k}-S_{k-2}S_{m-k-1}]\\&-L^{\pm}S_{k-1}(S_{m-k}-S_{m-k-1})\\&-M^{\pm}S_{m-k}(S_{k-1}-S_{k-2}),\end{aligned}\right\} \tag{43}$$

$$\left.\begin{aligned}B^{\pm}_{2k}=&P^{\pm}(x-2)S_{k-1}S_{m-k}\\&+Q^{\pm}(S_{k-1}-S_{k-2})(S_{m-k}-S_{m-k-1}),\end{aligned}\right\} \tag{44}$$

and coefficients $K^{\pm}$, $L^{\pm}$, etc., already known.

c. Validity of Approximation

Introducing into (29) and (6) the ΔC's of eqs (35) and (42), one may calculate the desired amplitudes,

$$R'=\sqrt{\rho'}\,e^{i\Phi'}, \tag{45}$$

reflected from multilayers in which one, or several,

film thicknesses differ from their calculated values β by given amounts $\Delta\beta$. The mathematics developed is based upon the assumption of small $\Delta\beta$'s, made by eqs (23) and (24). In order to establish the validity of this approximation, the ρ' and Φ'-values of three different zinc sulphide-magnesium fluoride multilayers with in each case one film deviating by $\Delta\beta=$ 10 percent were calculated both from the formulas derived here and also by exact computation. A comparison of results is given in figures 1a, b, and c. Agreement of exact and approximate ρ'-values, while poor for the single film (where an approximation is hardly needed), is good for higher numbers of layers (within 0.005 for the 5-layer, 0.001 for the 9-layer). The Φ'-values are in almost perfect agreement (within 0.1°) in all cases, including the monolayer.

4. Effects of Errors in Layer Thicknesses

Besides showing ρ' and Φ' for various nonideal coatings, figures 1a, b, and c also show ρ and Φ for the respective ideal coatings, thus making apparent the results of thickness errors:

Contrary to what might be expected, such errors do not result in a noticeable decrease in reflectance at the central wavelength λ_0, see [1]. This is illustrated once more by table 1; in the examples chosen, a 10 percent error causes a decrease ranging from only 0.004 for a single film to 0.001 for a 9-layer.[2]

TABLE 1. *Effect of 10 percent thickness errors Δ on reflectance, at central wavelength λ_0, of alternating quarter wave layers of ZnS and MgF_2 between air and a glass substrate* ($n_0=1$, $n_H=2.3$, $n_L=1.38$, $n_s=1.52$); *ZnS bottom layer*

Type of Coating	Reflectance at λ_0	
	$\Delta=0$	$\Delta=\lambda_0/40$
Single ZnS film	0.306	0.302
Five-layer, error in top layer	.861	.859
Nine-layer, error in central layer	.981	.980

The noticeable results of incorrect layer thicknesses are a parallel shift of the ρ and Φ-curves.

Maximum reflectance ρ_0' occurs at $\beta=90°+\delta\beta_\nu$, or at a wavelength $\lambda=\lambda_0+\delta\lambda_\nu$, instead of at $\beta=90°$, or $\lambda=\lambda_0$. All other ρ's are shifted correspondingly. To find $\delta\beta_\nu$, plot ρ' as a function of β, and read the displacement $\delta\beta_\nu$ of the maximum. Then, eq (11) provides

$$\left.\begin{aligned} 90°+\delta\beta_\nu&=90°\lambda_0/(\lambda_0+\delta\lambda_\nu),\\ \text{or } \delta\lambda_\nu&=-\lambda_0\delta\beta_\nu/(90°+\delta\beta_\nu).\end{aligned}\right\} \quad (46)$$

The phase angles Φ' differ from their nominal values Φ by amounts $\delta\Phi_\nu$ that practically are constants over a wide wavelength range,

$$\Phi'=\Phi+\delta\Phi_\nu. \quad (47)$$

[2] Table 1 was obtained by exact computation. Because of the smallness of the effect, the approximation is not accurate enough here.

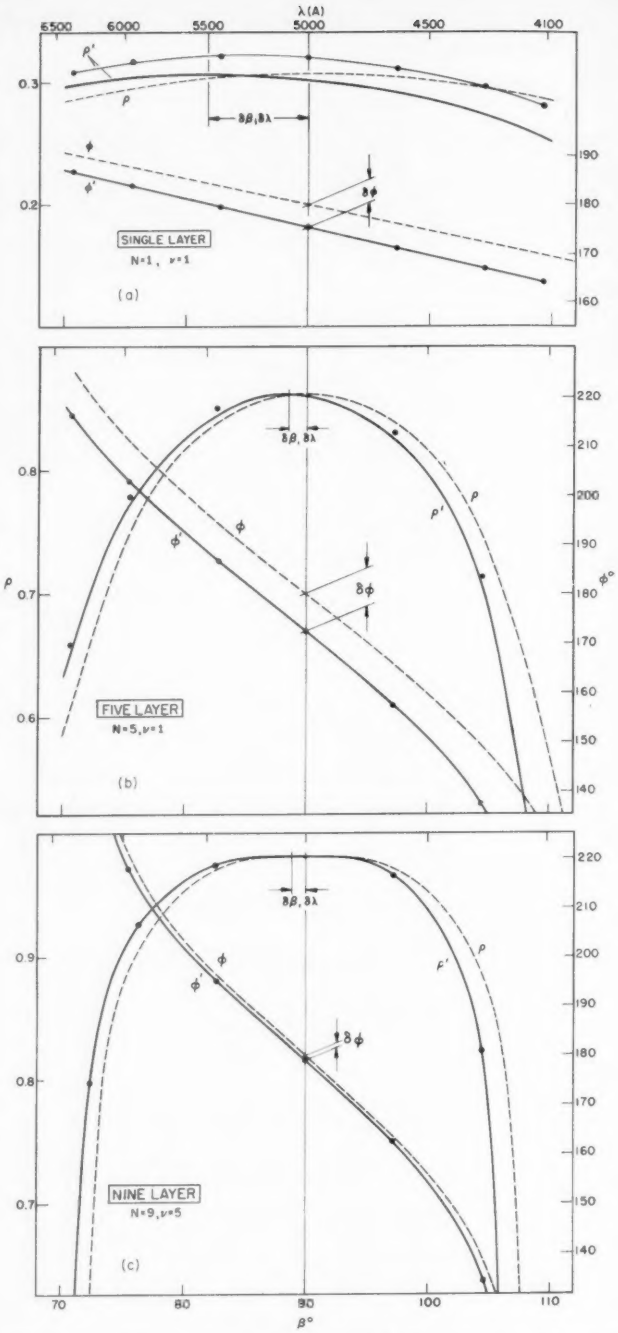

FIGURE 1. *Effects of errors in layer thickness on reflectance ρ and phase shift upon reflection Φ of alternating quarter wave layers of* ZnS *and* MgF_2 *between air and a glass substrate* ($n_0=1$, $n_H=2.3$, $n_L=1.38$, $n_s=1.52$), ZnS *bottom layer.*

(a) Single film of ZnS, off by 10 percent,
(b) five-layer with top layer ($\nu=1$) off by 10 percent, and
(c) nine-layer with central layer ($\nu=5$) off by 10 percent.
Solid lines: exact values. Dots: approximate values. Wavelength scale for $\lambda_0=5000$ A. For comparison broken lines show ρ and Φ for the respective correct multilayers. Effects of errors are wavelength shift $\delta\beta$, or $\delta\lambda$, of maximum reflectance, and change $\delta\Phi$ in phase shift upon reflection.

Since the nominal values are $\Phi=180°$ for $\beta=90°$, $\delta\Phi_\nu$ is found by computing Φ' at $\beta=90°$, only, and taking the difference to 180°. This is readily done

because of the simplified expressions of $C^{\pm}$ and $\Delta C^{\pm}$ at that particular β.

Note that, for the multilayers with thickness errors the values of β at which maximum reflectance occurs are distinct from those at which the phase change upon reflection is 180°. The five layer of figure 1b, for instance, exhibits maximum reflectance at $\beta=88.5°$, and 180° phase change at $\beta=86.0°$, the two being as much as 2.5° or, for $\lambda_0=5000$ A, 135 A apart. Therefore, $\Phi=180°$ is no criterion for maximum reflectance.

Figures 2 a and b show how, in two typical examples, $\delta\beta_\nu$ and $\delta\Phi_\nu$ depend upon the magnitude of the thickness error Δ $(n_\nu d_\nu)$. The relationship is a straight proportionality

$$\delta_\nu = a_\nu \Delta_\nu, \tag{48}$$

where δ_ν stands for either $\delta\beta_\nu$ or $\delta\Phi_\nu$, a_ν for coefficients $a_\nu(\beta)$ and $a_\nu(\Phi)$, and Δ_ν for Δ $(n_\nu d_\nu)$.

As, in general, the thickness of more than one layer will be in error, it is important to know the total errors $\delta\beta$ and $\delta\Phi$ produced by simultaneously occurring Δ_ν's.

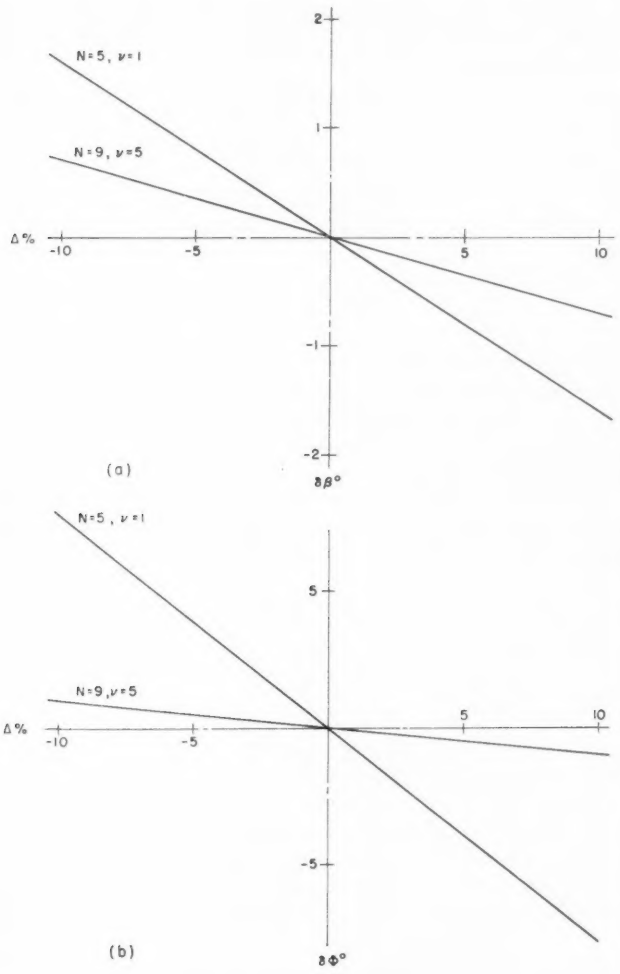

FIGURE 2. *Dependence of (a) $\delta\beta$ and (b) $\delta\Phi$ upon $\delta\Delta$.*

$N=5$, $\nu=1$: 5-layer with wrong top layer; $N=9$, $\nu=5$: 9-layer with wrong central layer. ZnS-MgF_2-films.

For three examples chosen at random, both the individual δ_ν's as well as the total δ's were computed, using eq (29) for the latter. These computations, of which the result is given in table 2, provide with good accuracy

$$\delta = \sum_{\nu=1}^{N} \delta_\nu \tag{49}$$

or, with (48),

$$\delta = \sum_{\nu=1}^{N} a_\nu \Delta_\nu, \tag{50}$$

δ standing for either $\delta\beta$ or $\delta\Phi$. For $\delta=\delta\Phi$, (48) is in accordance with Giacomo [2].

TABLE 2. *Individual and total errors*

Δ_ν=thickness error of νth layer in percent of $\lambda_0/4$; $\delta\beta_\nu$, $\delta\phi_\nu$=results of Δ_ν if occurring alone; $\delta\beta$, $\delta\phi$=results of all Δ_ν's occurring simultaneously. ZnS-MgF_2-films.

Type of Coating	$\Sigma\delta\beta_\nu$	$\delta\beta$	$\Sigma\delta\phi_\nu$	$\delta\phi$
Five-layer, $\Delta_1=10\%$, $\Delta_2=5\%$, $\Delta_4=-5\%$, $\Delta_5=-10\%$	−0.7°	−0.6°	−8.8°	−8.7°
Seven-layer, $\Delta_1=\Delta_7=5\%$, $\Delta_4=10\%$	−1.7°	−2.0°	−5.6°	−5.6°
Nine-layer, all Δ_ν's=10%	−8.0°	−8.2°	−19.2°	−19.0°

For a number of stacks of alternating zinc sulphide and magnesium fluoride layers between air and a glass substrate with, in each case, an error of +10 percent in one of the layers, $\delta\beta_\nu$ and $\delta\Phi_\nu$, as well as $a_\nu(\beta)$ and $a_\nu(\Phi)$, were computed. In figures 3 a and b, the a_ν's are plotted versus the number, $N=2m+1$, of films in the stack. For either a_ν, the three curves show the effect of thickness errors occurring in the top, central, or bottom layer ($\nu=1$, $m+1$, or N, respectively). With the exception of $a_1(\Phi)$, all a_ν's tend to decrease as N increases.

According to figures 3a, b, and furthermore to figure 4, the a_ν's also show a pronounced dependence upon ν; i.e., upon where in the stack of layers the incorrect one is located:

The wavelength shift of the reflection maximum, or $a_\nu(\beta)$, is greatest if caused by the central layer, smallest for the bottom layer, and intermediate for the top layer. This result is not in agreement with Heavens' statement [1] that the effect is greatest for the top layer, apparently because Heavens did not include in his treatment others than top or bottom layers.

The dependence of $a_\nu(\Phi)$ upon ν is different. Here, the effect increases steadily from the bottom towards the top layer, which is in agreement with Giacomo's result [2].

5. Statistical Tolerances

5.1. Propagation of Errors

The observed general trend of $\delta\beta_\nu$ and $\delta\Phi_\nu$ to decrease with increasing N does not imply that monitoring film thicknesses becomes easier as the number

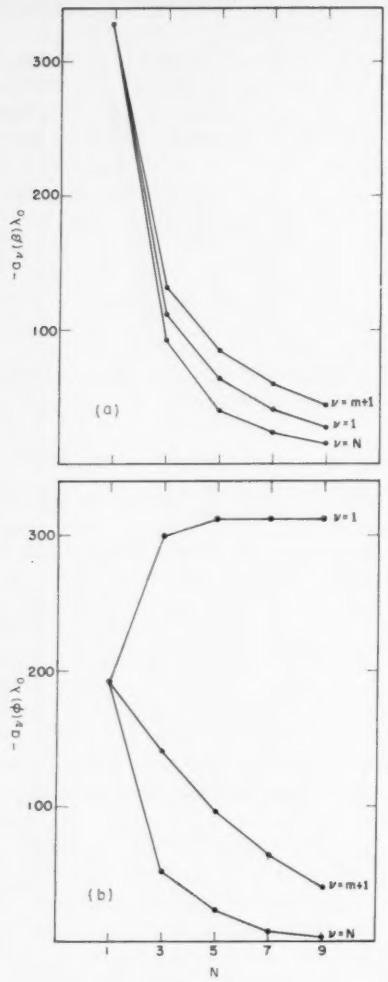

FIGURE 3a, b. $a_\nu(\beta)$ *and* $a_\nu(\Phi)$ *as functions of* N *and* ν *for* $ZnS\text{-}MgF_2$*-multilayers.*

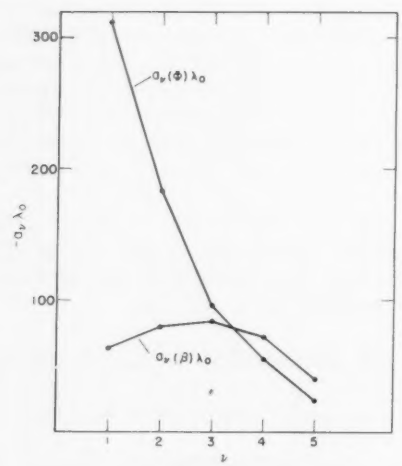

FIGURE 4. *Dependence of* $a_\nu(\beta)$ *and* $a_\nu(\Phi)$ *upon* ν *for a* $ZnS\text{-}MgF_2$*-5-layer.*

of films increases. It must also be taken into account that at high N's the production of the multilayer requires control of a larger number of layers, so that there is an increased number of sources of error.

Let $\pm s(\Delta_\nu)$ be the random thickness error (standard deviation) of the νth film, determined by sampling Z multilayers,

$$s^2(\Delta_\nu)=(\sum_i \Delta_{\nu i}^2)/(Z-1) \tag{51}$$

($i=1, 2, \ldots Z$), and $\pm s(\delta)$ the standard deviation from the multilayer performance,

$$s^2(\delta)=(\sum_i \delta_i^2)/(Z-1), \tag{52}$$

with δ standing for either $\delta\beta$ or $\delta\Phi$. Equation (50) and the law of propagation of errors then provide

$$s^2(\delta)=\sum_{\nu=1}^{N} a_\nu^2\, s^2(\Delta_\nu). \tag{53}$$

Assume that monitoring the film thickness is equally difficult for each layer; i.e., that $s(\Delta_\nu)$ is independent of ν,

$$s(\Delta_\nu)=s(\Delta). \tag{54}$$

Hence,

$$s^2(\delta)=A^2 s^2(\Delta),$$

or

$$s(\Delta)=s(\delta)/A, \tag{55}$$

with

$$A^2=\sum_{\nu=1}^{N} a_\nu^2. \tag{56}$$

By means of (55) it is now possible to determine within what limits $\pm s(\Delta)$ each film thickness has to be controlled so that, on the basis of standard deviations, the finished multilayer will stay within a given tolerance $\pm s(\delta)$.

For the accuracy required, $A(\beta)$ and $A(\Phi)$, not a (β_ν) and $a(\Phi_\nu)$, are the determining factors. $A(\beta)$ and $A(\Phi)$ are plotted versus N in figure 5 showing

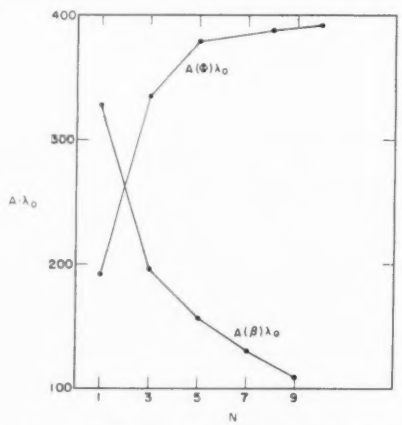

FIGURE 5. $A(\beta)$ *and* $A(\Phi)$ *as functions of* N *for* $ZnS\text{-}MgF_2$*-multilayers.*

that, besides being quite different in magnitude, $A(\beta)$ is a rapidly decreasing and $A(\Phi)$ a rapidly increasing function of N.

These important differences between the effects of thickness errors upon the intensities of reflected waves and upon their phases lead to a separate consideration of the two cases; i.e., the "intensity" and the "phase" case.

5.2. Intensity Case: Mirrors and Beam Splitters

Consider a multilayer designed to render a certain maximum reflectance ρ_0 at a wavelength λ_0. Let

$$\pm\Delta\rho=(1-f)\rho_0 \tag{57}$$

be the permissible deviation from ρ_0, with $f<1$. If, then, $2\ \beta_f$ is the "f—width" of the ideal multilayer; i.e., the width of the range of β's for which $f\rho_0\leq\rho\leq\rho_0$; it follows immediately from figure 6 that the permissible wavelength shift of the reflection maximum is

$$\delta\beta=\pm\Delta\beta_f. \tag{58}$$

With this value substituted for $s(\delta\beta)$, eq (55) then provides, for the thickness tolerance,

$$s(\Delta)=\pm\Delta\beta_f/A(\beta). \tag{59}$$

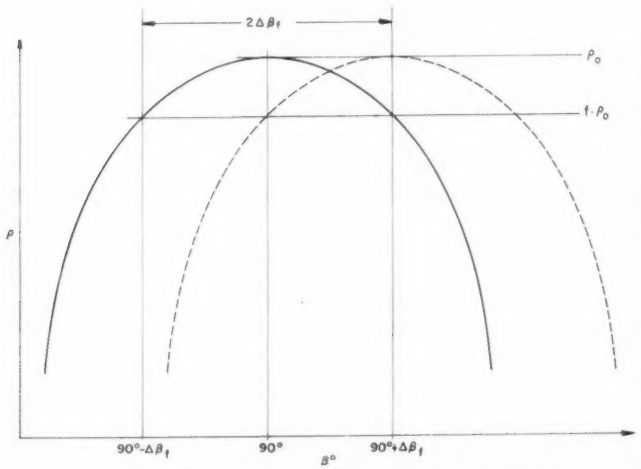

FIGURE 6. *f-width $2\Delta\beta_f$ of multilayers and permissible wavelength shift of the reflection maximum.*

Assume $f=0.99$, corresponding to the rather strict requirement that theoretical reflectance has to be reproduced within 1 percent. The 0.99-widths of zinc sulphide-magnesium fluoride multilayers, taken from reflection curves as in figures 1a, b, c, are given in figure 7. Figure 8 shows the corresponding $s(\Delta)$'s computed from (59) with the $A(\beta)$ values of figure 5.

The obvious conclusion from figure 8 is that, even if very narrow tolerances are to be met, the production of a multilayer mirrow or beam splitter hardly presents any experimental difficulties. The permissible thickness error rises sharply as N increases so that, the more complicated the multilayer gets, the easier it becomes to produce its individual layers. In the example chosen, the permissible thickness error varies from 0.023 λ_0 for the single film to 0.069

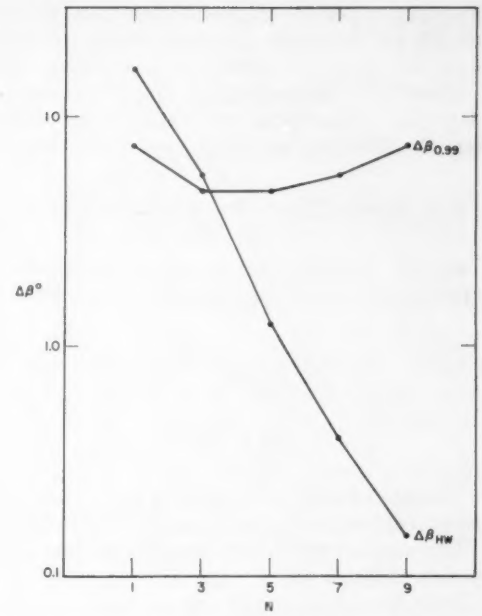

FIGURE 7. *0.99-widths of $ZnS\text{-}MgF_2$-multilayers versus number of layers N. Half widths of first-order interference filters having N alternating $ZnS\text{-}MgF_2$-layers on each side of the (air) spacer.*

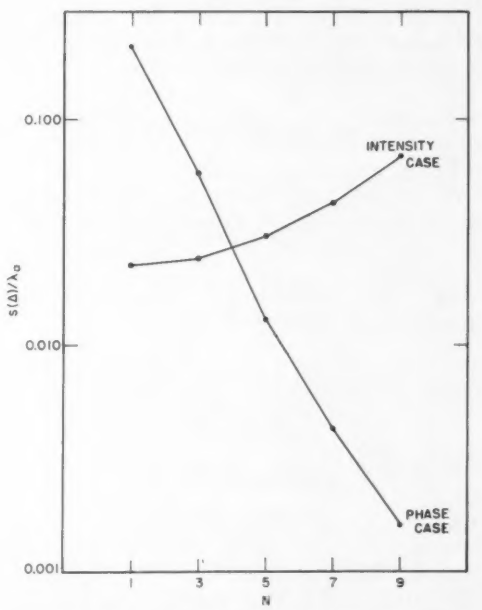

FIGURE 8. *Thickness tolerances s(Δ) for mirrors or beam splitters to yield specified reflectance at λ_0 within 1 percent (intensity case) and for interference filters to yield maximum transmission plus or minus one half their halfwidth (phase case).*

$ZnS\text{-}MgF_2$-films.

λ_0 for the nine-layer stack, corresponding to as much as about 10, or 28 percent, respectively, of the nominal thickness of $\lambda_0/4$. Simple monitoring systems should, therefore, be sufficient for obtaining experimentally the theoretical reflectances of which alternating multilayer coatings are capable.

5.3. Phase Case: Interference Filters

The energy transmittance of a Fabry-Perot interferometer is given by the familiar Airy formula [5],

$$T=\frac{\tau^2/(1-\rho)^2}{1+4\rho\sin^2\gamma/(1-\rho)^2}, \tag{60}$$

with

$$\gamma=(\pi/\lambda)\,OPD. \tag{61}$$

ρ and τ denote energy reflectance and transmittance of either interferometer plate, and OPD is the optical path difference between two successive beams, which at normal incidence is

$$OPD=2n(t+\Delta t),$$

where n is the refractive index of the spacing medium, t its geometrical thickness, and Δt the change in path due to phase change upon reflection from one of the interferometer plates. By convention [6], the calculated value for the phase change represents an increase in optical path of

$$nt=(\lambda/2\pi)\,(\mu 2\pi-\Phi),$$

μ being an integer. Thus,

$$\gamma=\mu 2\pi+2\pi nt/\lambda-\Phi.$$

Consider an all-dielectric (nonabsorbing) first-order interference filter. Then

$$\rho=1-\tau,$$

$$nt=\lambda_0/2,$$

and because of (11),

$$\gamma=\mu 2\pi+2\beta-\Phi.$$

Therefore,

$$T=\left[1+\frac{4\rho}{(1-\rho)^2}\sin^2(2\beta-\Phi)\right]^{-1}. \tag{62}$$

For the ideal interference filter, having ideal quarter wave multilayer coatings on either side of the spacer layer, one has $\Phi=180°$ and therefore maximum transmission, $T=1$, at $\beta=90°$ where

$$2\beta-\Phi=0. \tag{63}$$

The half width of the pass band,

$$2\Delta\beta_{HW}=2\,|90^0-\beta_{HW}|, \tag{64}$$

follows from $T=\frac{1}{2}$, or

$$\sin(2\beta_{HW}-\Phi)=(1-\rho)/2\sqrt{\rho}. \tag{65}$$

Using the values of Φ and ρ calculated previously in this paper (and thereby assuming the somewhat simplified case of an air spacer), the half widths shown in figure 7 were obtained for interference filters with $N=1$, 3, 5, 7, and 9 alternating zinc sulphide-magnesium fluoride layers on each side of the spacer.

Incorrect layer thicknesses will cause a phase change of $\Phi+\delta\Phi$, rather than of Φ. As a result, the center of the pass band will be shifted from $\beta=90°$ to $\beta=90°+\nabla\beta$, the maximum being again $T=1$. One may obtain $\nabla\beta$ from (63), or

$$2\,(90°+\nabla\beta)=\Phi+\delta\Phi.$$

According to sec. 4, $\delta\Phi$ is independent of β. In the neighborhood of $\beta=90°$, Φ is a linear function of β,

$$\Phi=-m\beta+p$$

(see figs. 1a, b, c), with

$$p=(m+2)\;90°$$

because of $\Phi=180°$ for $\beta=90°$. Therefore,

$$2\,(90°+\nabla\beta)=-m(90°+\nabla\beta)+(m+2)\;90°+\delta\Phi,$$

or

$$\nabla\beta=\delta\Phi/(m+2). \tag{66}$$

Allow a tolerance of one half the width of the pass band,

$$\nabla\beta=\pm\Delta\beta_{HW}, \tag{67}$$

which, according to (66), corresponds to a tolerance on the phase shift upon reflection of

$$\delta\Phi=\pm(m+2)\Delta\beta_{HW}. \tag{68}$$

Transmittance at λ_0, then, may depart from the desired value $T=1$ by 50 percent.

With $\delta\Phi$ from eq (68) substituted for $s(\delta\Phi)$, eq (55) then provides the thickness tolerance

$$s(\Delta)=\pm(m+2)\Delta\beta_{HW}/A(\Phi). \tag{69}$$

Using the values of $A(\Phi)$ and $\Delta\beta_{HW}$ from figures 5 and 7, and with m's taken from Φ–versus–β–curves as in figures 1a, b, c, the $s(\Delta)$'s of figure 8 were obtained.

It is obvious from figure 8 that, in the phase case, monitoring film thicknesses is by far more demanding than in the intensity case. The permissible thickness errors decrease very rapidly as N increases so that production of the filter becomes increasingly difficult with increasing filter performance. For the

widely used seven layer coatings on each side of the spacer, a tolerance of as little as $s(\Delta)=\pm 0.0043$ λ_0, or 1.7 percent of the nominal thickness of $\lambda_0/4$, is required in the example chosen. For 9-layer coatings, the tolerance is even further reduced to $s(\Delta)=\pm 0.0016$ λ_0, or 0.65 percent of $\lambda_0/4$. Compared hereto, the permissible $s(\Delta)$'s for 7- and 9-layer reflectors are about 10 and 42 times greater in the example chosen for the intensity case; see figure 8.

The production of all-dielectric interference filters, therefore, requires monitoring equipment much more efficient than that sufficient for producing dielectric mirrors and beam splitters.

6. Comparison of Monitoring Techniques

A simple and widely used method of controlling layer thicknesses, first described by Dufour [7], is measuring with a photo cell and a galvanometer the intensity of a fairly monochromatic light beam reflected from the growing dielectric film, and ceasing evaporation whenever a maximum or minimum galvanometer deflection is reached. In this author's experience, an accuracy of about ± 6 percent of the desired thickness of a quarter wavelength of visible light can be obtained with this "single photo cell" technique, using as light source an incandescent lamp plus a gelatine filter of about 300 A half width. Somewhat better accuracies may be obtained by employing, instead of the simple gelatine filter, a narrow pass band interference filter or a monochromator. According to the results of sec. 5.2, therefore, this technique of controlling film thicknesses should be fully sufficient for the production of multilayer mirrors and beam splitters.

Provision has to be made, however, to fulfill eq (54), according to which each layer in the stack can be prepared with equal facility, and upon which the conclusions of sec. 5 were based. Towards the completion of a high reflection multilayer, the difference in reflectance caused by each additional layer is rapidly decreasing; see table 3. Direct monitoring of more than five or seven layers is, therefore, impossible with the described method. To overcome this difficulty, one may either use the technique of monitoring on separate glass plates only a few layers at a time [7], or employ a differential photometer such as described by Linberg and Irland [8].

TABLE. 3. *Reflectance ρ of N alternating layers of ZnS and MgF_2 between air and a glass substrate.*

ZnS bottom layer.

N	ρ	Change in ρ caused by Nth layer	N	ρ	Change in ρ caused by Nth layer
	%	%		%	%
0	4.3		6	75.3	−10.8
1	30.6	+26.3	7	94.8	+19.5
2	8.6	−22.0	8	90.3	−4.5
3	66.0	+57.4	9	98.1	+7.8
4	45.0	−21.0	10	96.9	−1.2
5	86.1	+41.1	11	99.3	+2.4

If eq (54) is not fulfilled, appropriate weight factors w_ν must be applied so that

$$s(\Delta_\nu)=w_\nu\, s(\Delta),$$

instead of (54), and with $s(\Delta)$ being a suitable starting value. Equation (56) would then be changed to

$$A^2=\sum_{\nu=1}^{N} w_\nu^2 a_\nu^2,$$

and the results that follow would have to be altered accordingly. In view of the vast range of possible weight factors, however, their consideration is beyond the scope of this paper.

The accuracy of the single photo cell method is limited by the fact that it measures the change in reflectance with thickness and that, at the desired quarter wave thickness, this change is zero [7]. The method, therefore, is not likely to provide the high accurancies required for the production of dielectric interference filters.

Giaccmo and Jacquinot [9] have developed a more precise monitoring technique in which, rather than reflectance, its differential quotient with respect to wavelength is observed. At a quarter wave layer thickness, this differential quotient goes through zero, its change with thickness being a maximum. A similar but in practice simpler method was described by Traub [10]. The accuracy of these methods is better than 1 percent of the layer thickness [10]. According to sec. 5.3, the production of dielectric interference filters to within plus or minus one-half the width of their pass bands, therefore, appears to be possible with Giacomo and Jacquinot's or Traub's techniques. Equation (52) may be satisfied by using separate monitor glasses.

The author is indebted to Theodore R. Young for valuable discussions and suggestions concerning this paper.

7. References

[1] O. S. Heavens, J. Opt. Soc. Am. **44,** 371 (1954).
[2] P. Giacomo, Rev. optique **35,** 317 (1956).
[3] W. F. Koehler, J. Opt. Soc. Am. **45,** 934 (1955).
[4] K. D. Mielenz, J. Research NBS **63A,** 297 (1959).
[5] A. Steudel, Naturwissenschaften **44,** 249 (1957).
[6] C. J. Koester, J. Research NBS **64A,** 191 (1960).
[7] C. Dufour, Le Vide **3,** 480 (1948).
[8] V. L. Linberg and M. J. Irland, J. Opt. Soc. Am. **45,** 328 (1955).
[9] P. Giacomo and P. Jacquinot, J. phys. radium **13,** 59A (1952).
[10] A. C. Traub, J. Opt. Soc. Am. **46,** 999 (1956).

(Paper 64A6–70)

JOURNAL OF RESEARCH of the National Bureau of Standards—A. Physics and Chemistry
Vol. 64A, No. 6, November–December 1960

Note on Particle Velocity in Collisions Between Liquid Drops and Solids

Olive G. Engel

(June 29, 1960)

Equations are developed for plane-wave particle velocity produced in solid-against-liquid collisions. An explicit expression for the dimensionless coefficient α that appears in these equations is deduced.

Collisions between liquid drops and the planar surfaces of solids have become important in the present era of high-speed flight. Except for the pressure that results when a drop of incompressible liquid collides with the planar surface of an unyielding solid [1],[1] exact hydrodynamic treatments of the various aspects of this type of collision have not been developed. Plane-wave theory has been used in several approximate treatments [2, 3, 4]. One of the unknowns encountered in the use of plane-wave theory for solid-against-liquid collisions was the particle velocity in the compressed zones.

During collision between a solid rod A having flat ends and moving with velocity V in the $(+z)$-direction of a stationary coordinate system (fig. 1) and a similar liquid rod B that is at rest, there is a radial flow of liquid at the impacted end of rod B. In order that the rods remain in contact while the compressional waves initiated by the collision move through them, the interface velocity (I) must obey the inequality $V-v'>v$ where v', v are the particle velocities in the compressed zones.

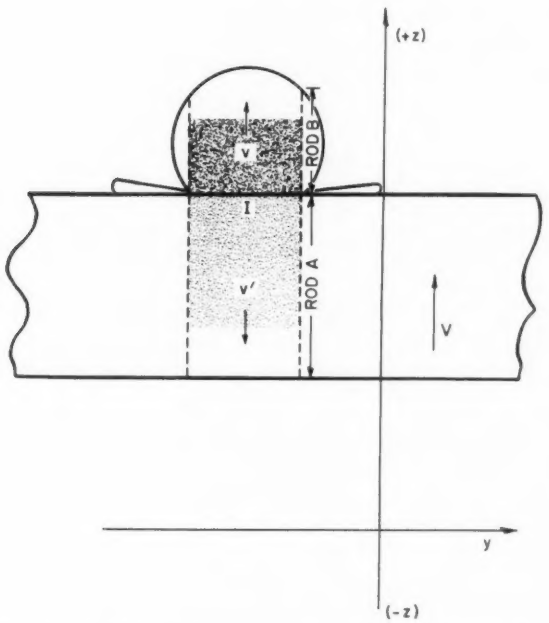

FIGURE 1. *Collision between a plate moving at velocity* V *and a liquid drop at rest idealized as collision between a solid rod A and a liquid rod B.*

We can then write $\alpha(V-v')=v$ where α is a dimensionless coefficient having a value less than one, and

$$v+\alpha v'=\alpha V. \tag{1}$$

Using the relation that exists between stress and particle velocity for plane waves, the equality of stresses at the surfaces of contact is given by

$$zv=z'v', \tag{2}$$

where z is the acoustic impedance (product of sound speed and density). From eq (1) and (2), the particle velocities v, v' are found to be

$$v=\alpha z'V/(z'+\alpha z) \tag{3}$$

$$v'=\alpha zV/(z'+\alpha z), \tag{4}$$

and the plane-wave stress σ is given by

$$\sigma=\sigma'=\alpha zz'V/(z'+\alpha z). \tag{5}$$

The quantity that must be determined to make these equations useful is the coefficient α.

One of the approximate treatments in which plane-wave theory was used for solid-against-liquid collisions [3] provides a means of deducing an explicit expression for the coefficient α. In this treatment the complicated situation of collision between a moving target plate and a relatively stationary liquid drop was idealized as the simple case of the collision of two rods with flat ends. If a plate is fired against a drop (fig. 1), a core of material extending through the plate under the contact area is slowed down with respect to the remainder of the plate and a similar core of material through the drop is set in motion. The cores were regarded as true cylinders free to

[1] Figures in brackets indicate the literature references at the end of this paper.

move in the z-directions (fig. 1) but restrained laterally. The compressional waves that move through the cylinders were regarded as plane waves.

With use of this simple model, an equation was developed that gives pit depth δ' as a function of impingement velocity V for collisions of metal target plates with liquid drops [3]. For impingement velocities for which elastic recovery of the plate is complete, the pit depth was taken to be the product of a numerical constant, the particle velocity given to the cylindrical core of material under the collision area, and the time that the particle velocity exists. The particle velocity was taken to be $zV/(z+z')$, which is the plane-wave particle velocity for solid-against-solid collisions. The time during which the particle velocity exists was taken to be $2d/c$ where d is the diameter of the drop and c is the sound speed of the liquid of which it is composed. Therefore, $\delta' = (\text{constant})(d/c)[zV/(z+z')]$.

The pit-depth equation that was developed was applied first to collisions of mercury drops and waterdrops with target plates of copper, 1100–O aluminum, 2024–O aluminum, steel, and lead. The constant was found empirically to be 7.2. The equation was then found to apply without change of the constant to collisions between metal target plates and soft ductile metal spheres that flowed during and as a result of the collision.

The same equation was later applied [4] to collision of steel spheres against target plates of 1100–O aluminum, 2024–O aluminum, and copper. It was found empirically that if the target plate was struck by a rigid hardened steel sphere that did not flow as a result of the collision the constant was 17.5.

The constants found for the pit-depth equation for the case that a target plate collides with a liquid drop or soft ductile metal sphere and for the case that it collides with a rigid hardened steel sphere provide a means of obtaining an explicit expression for the coefficient α. The two cases differ only in the particle velocity given to the core of material through the target plate. The particle velocity v' for solid-against-solid collisions was used in each case. The particle velocity v' for solid-against-liquid collisions should have been used for the case that the target plate collided with a liquid drop or with a soft deforming metal sphere that would flow as a result of the collision.

Because it is the particle velocity given to the core of target material under the collision area that is different, and because the constant 7.2 is 0.41 of the constant 17.5, it follows that $\alpha zV/(z'+\alpha z) = 0.41zV/(z'+z)$ from which

$$\alpha = 0.41/[1+(0.59\ z/z')]. \qquad (6)$$

Values of α calculated with use of eq (6) for collisions of waterdrops and mercury drops with target plates of aluminum, copper, lead, and glass are given in table 1. It can be seen that the value of α for waterdrop collisions with the solid materials cited is very close to 0.4. This is in exact agreement with an independent determination of α made earlier [2]. It was found experimentally [2] that 0.00118 sec were required for a glass plate to move through a 0.57-cm-diam waterdrop when the relative impingement velocity was 820 cm/sec (26.9 ft/sec). The velocity at which the plate moved through the drop was 484 cm/sec. It was assumed that no particle velocity was given to the cylinder of glass through the plate under the collision area. Then the velocity at which the plate moved through the drop was $(1-\alpha)V$. To this degree of approximation $(1-\alpha)820=484$ and $\alpha=0.4$.

In consideration of this independent evaluation of the coefficient α for waterdrop collisions, it appears, in retrospect, that had the proper particle velocity been used in [3], the numerical constant found empirically for the equation to calculate the depth of pits produced by collision of a metal plate with liquid drops would have been the same as that with rigid steel spheres, namely, 17.5 [4].

TABLE 1. *Some values of the coefficient* α

Drop \ Target	Aluminum	Copper	Lead	Glass
Water	0.39	0.40	0.40	0.38
Mercury	.24	.32	.28	.22

References

[1] P. Savic and G. T. Boult, The fluid flow associated with the impact of liquid drops with solid surfaces, Report No. MT–26, National Research Council of Canada, Ottawa, 1955.

[2] Olive G. Engel, Waterdrop collisions with solid surfaces, J. Research NBS **54,** 281 (1955) RP2591.

[3] Olive G. Engel, Pits in metals caused by collision with liquid drops and soft metal spheres, J. Research NBS **62,** 229 (1959) RP2958.

[4] Olive G. Engel, Pits in metals caused by collision with liquid drops and rigid steel spheres, J. Research NBS **64A,** 61 (1960). (Paper 64A1–29).

(Paper 64A6–71)

JOURNAL OF RESEARCH of the National Bureau of Standards—A. Physics and Chemistry
Vol. 64A, No. 6, November–December 1960

Resistance of White Sapphire and Hot-Pressed Alumina to Collision With Liquid Drops

Olive G. Engel

(June 22, 1960)

Fused alumina has been reported to be one of the most promising materials for resistance to erosion due to high-speed collision with liquid drops. In this paper, data are presented that show the resistance of 0.318-cm (0.125-in.)-thick plates of white sapphire and hot-pressed alumina to impingement damage by 0.2-cm-diam waterdrops and mercury drops. The type of damage done to these high-strength ceramics as a result of collision with a mercury drop at high velocity was found to be qualitatively the same as that produced on low-strength plastics as a result of collision with a waterdrop at relatively low velocity.

In collision with mercury drops, the velocity at which damage was first observed was 3.514×10^4 cm/sec (1,153 ft/sec) for white sapphire and 4.276×10^4 cm/sec (1,403 ft/sec) for hot-pressed alumina; the difference in the velocities found for the two ceramics is not considered to be significant.

The velocity required to damage these ceramic materials on collision with a waterdrop was not reached experimentally. A theoretical extrapolation suggests that plates of these ceramics of the indicated thickness can be expected to survive collision with a 0.2-cm waterdrop without damage up to a velocity of 33.7×10^4 cm/sec (11,100 ft/sec). For air at 0 °C, this is equivalent to a Mach Number of 10.

1. Introduction

The leading surfaces of objects that fly at high speed through rain are eroded as a result of collision with raindrops. The erosion damage increases in severity as the relative impingement velocity is increased. It has become a major problem in the present era of high-speed flight.

A search for materials that will resist this type of damage has been made for the past 10 years. Experimental testing of materials has been carried out at many laboratories of the aircraft industry. An effort to determine the cause of the damage and the mechanism by which it is produced has been in progress at the National Bureau of Standards; this research has been conducted under the sponsorship of the Nonmetallic Materials Laboratory, Materials Central, Wright Air Development Division.

One of the questions asked at the time that the research program on the mechanism of high-speed rain erosion was initiated was whether a soft rubbery material or a hard rigid material should be sought as the solution to the problem. The answer to this question is now at hand. In practical terms, the answer is that there are rubbery coating materials that can withstand collision with waterdrops up to impingement velocities of roughly 3×10^4 cm/sec (1,000 ft/sec) but that at higher velocities the solution to the problem must be sought among the hard rigid materials of high strength.

Fused alumina is one of the most promising materials of the latter type for resistance to erosion due to high-speed collision with liquid drops. In this paper results of an investigation of the overall resistance and particular mode of failure of white sapphire and hot-pressed alumina, under high-speed liquid-drop impingement, are presented.

2. Materials and Test Method

2.1. White Sapphire

White sapphire is a pure, single crystal alpha alumina made by dropping finely powdered alumina through a postmixed oxyhydrogen flame onto the molten cap of a seed crystal supported in an insulating furnace. Crystallization occurs at the interface between the body of the crystal and the molten cap. Under proper operating conditions, the material that crystallizes has the same orientation as the seed crystal. The as-grown crystals are annealed at 1,900 °C (3,452 °F) to remove strains.

Five disk-shaped target plates of white sapphire 1.59 cm (0.625 in.) in diameter and 0.318 cm (0.125 in.) thick were obtained from the Linde Air Products Company. They were crystal clear and had the appearance of high-quality glass. The face of the target plate that would strike the liquid drop was given a high polish by the manufacturer.

The physical properties of white sapphire, taken from data supplied by the manufacturer, are listed in table 1.

2.2. Hot-Pressed Alumina

Hot-pressed alumina (gray) differs from polycrystalline alumina (cream white) in that it is heated and pressed in one operation rather than in two. The heating and pressing is done in graphite dies and hot-pressed alumina is gray in color because it picks up a carbon impurity from the dies. The amount of carbon that diffuses into the alumina depends on the pressure, temperature, and time involved in the hot-pressing operation. Hot pressing

TABLE 1. *Physical properties of white sapphire and hot-pressed alumina*

Material	Hot-pressed alumina[a]	White sapphire [b]	
Density g/cm³	3.95	3.98	depending on position of crystal C-axis.
Modulus of elasticity d/cm²	3.4×10¹²	(3.4 to 3.8)×10¹²	
Modulus of elasticity psi	50×10⁶	(50 to 55)×10⁶	
Modulus of rupture [c] d/cm²	2.4×10⁹	(2.8 to 9.0)×10⁹	at 30 °C.
Modulus of rupture [c] psi	35×10³	(40 to 130)×10³	
Compressive strength d/cm²	2.8×10¹⁰	2.1×10¹⁰	at 25 °C.
Compressive strength psi	400×10³	300×10³	
Knoop hardness (K 100)	2,000	1,525 to 2,000	
Mohs hardness	9 to 9.5	9	
Melting point °C	2,000	2,040	

[a] Tabulated data supplied by Norton Co. for H. P. Alundum. H. P. Alundum is hot-pressed alumina of uniform density and hardness manufactured by sintering the pure aluminum oxide crystals; no bonding matrix is used.

[b] Data supplied by Linde Air Products Co.

[c] The modulus of rupture (flexural strength) is probably 20- to 30-percent higher than the tensile strength of these ceramic materials; measurement of their true tensile strength is complicated by factors related to their brittleness and the difficulty in alining the specimens.

produces an alumina having a density close to that of white sapphire; there is, however, a considerable amount of variability in the product from lot to lot.

Five plates of this alumina of the same size and shape as the white sapphire plates were obtained from the Norton Company. They were opaque and light gray. The impact face of each plate was given a high polish by the manufacturer by means of diamond grinding and lapping.

Properties of hot-pressed alumina also are listed in table 1.

2.3. Liquid-Drop Collision Test

The collision experiments were carried out by Convair, Division of General Dynamics Corporation. The ceramic target plates were fastened with adhesive to metal disks of the same size and were fired against mercury drops and waterdrops at velocities ranging from 2.89×10^4 cm/sec (948 ft/sec) to 11.88×10^4 cm/sec (3,898 ft/sec). The metal backing disks kept the ceramic target plates that were shattered by the liquid-drop collisions from falling into pieces.

The drop size specified for the collisions was 0.2-cm diam. The mercury drops were weighed on an analytical balance and the diameter of each drop was calculated from its weight. The mercury drops that struck the target plates ranged from 5 percent above to 1 percent below the specified size. It was estimated by the experimenters that the waterdrops were within ±10 percent of the nominal size.

An attempt was made to distribute the velocities at which the target plates were fired. Closely similar velocities were sometimes unavoidably obtained, however, because the velocity produced by a given weight of powder is affected by temperature variation, amount of casing crimp, and the density of powder pack. The velocities at which the target plates were fired are listed in table 2.

3. Observations

The target plates of white sapphire and hot-pressed alumina that had collided with mercury drops and waterdrops were examined with a stereo-

TABLE 2. *Data for collisions of target plates of white sapphire and hot-pressed alumina with 0.2-cm-diam drops*

Specimen	Firing	Drop liquid	Collision velocity [a] 10^4 cm/sec	Collision velocity [a] ft/sec	Effect on target plate
Target plates of white sapphire					
I	a	water	4.779	1,568	No damage.
	b	water	6.620	2,172	No damage.
	c	water	7.529	2,470	Missed waterdrop; target plate cracked due to firing shock.
II	a	mercury	2.890	948	No damage.
	b	mercury	3.197	1,049	No damage.
	c	mercury	3.216	1,055	No damage.
	d	mercury	3.514	1,153	Damaged; see fig. 1.
III		mercury	3.581	1,175	Damaged; see figs 2 and 3.
IV		mercury	4.420	1,450	Damaged; see fig. 4.
V		mercury	4.584	1,504	Damaged; see fig. 5.
Target plates of hot-pressed alumina					
I		water	7.346	2,410	No conclusive evidence of damage.
II		water	9.144	3,000	Target plate shattered due to to firing shock.
III		water	11.88	3,898	No conclusive evidence of damage.
IV		mercury	4.276	1,403	Damaged; see fig. 6.
V	a	mercury	4.996	1,639	Damaged by edge collision; see figs. 7A and 7C.
	b	mercury	4.100	1,345	Damaged; see figs. 7A and 7B.

[a] The velocity data were supplied by Donald E. Hurd, Convair, Division of General Dynamics Corp., San Diego, Calif.

microscope. The following observations were made.

No damage was done to either ceramic by collision with a 0.2-cm-diam waterdrop at the highest collision velocities that were used, namely, 6.620×10^4 cm/sec (2,172 ft/sec) for white sapphire and 11.88×10^4 cm/sec (3,898 ft/sec) for hot-pressed alumina. In collision with 0.2-cm-diam mercury drops, the velocity at which damage was first observed was 3.514×10^4 cm/sec (1,153 ft/sec) for white sapphire and 4.276×10^4 cm/sec (1 403 ft/sec) for hot-pressed alumina; the difference in the velocities found for the two ceramics is not significant because the velocity given for hot-pressed alumina is the lowest velocity at which collision between a mercury drop and this ceramic occurred.

The first evidence of failure of these high-strength ceramics under high-speed mercury-drop impingement was the formation of cracks that bound a more or less circular undamaged area around the central point or eye of the collision. In white sapphire these cracks were polygonal; in hot-pressed alumina they were circular. These cracks ran deep into the ceramic material. The cracks nearest to the central point of the collision were nearly perpendicular to the surface of the target plate but the outer-lying cracks were inclined at an angle to the surface.

The material of the target plate was broken out of the surface along these cracks and on the side of the cracks away from the central point of the collision, that is, in the direction of the radial flow of the liquid of the drop that impinged. The erosion

damage was more severe the higher the velocity at which the collision occurred.

At high-impingement velocities radial cracks formed. They ran out from the center of the collision and extended completely across and through the target plate.

Curved cracks that appear to reflect the curved edge of the target plates also formed when the impingement velocity was high. Cracks of this kind observed in white sapphire were below the surface of the target plate; the curved crack observed in hot-pressed alumina extended to the surface.

The observations of damage caused by collision with mercury drops are detailed in the following sections.

3.1. White Sapphire

The highest velocity at which plate No. II collided is the lowest at which any damage was produced (see table 2). Figure 1A shows that the damage on plate II is restricted to the immediate site of the collision at the edge of the plate. Machining marks in the metal backing plate can be seen through the clear sapphire.

Figure 1B shows that *the eye of the collision consists of an undamaged central area surrounded by an imperfectly developed polygon of short straight cracks that are almost parallel to one another;* possible explanations are given in sections 4.2(a) and 4.2(b). Evidence that these cracks extend down into the target plate in a conchoidal type of fracture is presented below. *Sapphire has been broken out of the surface along the polygonal cracks and on the side of the cracks away from the center of the collision, that is, in the direction of the radial flow of the liquid of the drop that impinged;* a possible cause is discussed in section 4.2(c).

Plate No. III collided at a slightly higher velocity (see table 2). Figure 2A shows that the damage is still restricted to the immediate site of the collision close to the edge of the plate; a piece of sapphire was chipped away. Machining marks in the metal backing plate and bubbles in the adhesive can be seen through the sapphire. Figure 2B shows that the eye of the collision is again an imperfectly developed polygon of cracks around an undamaged

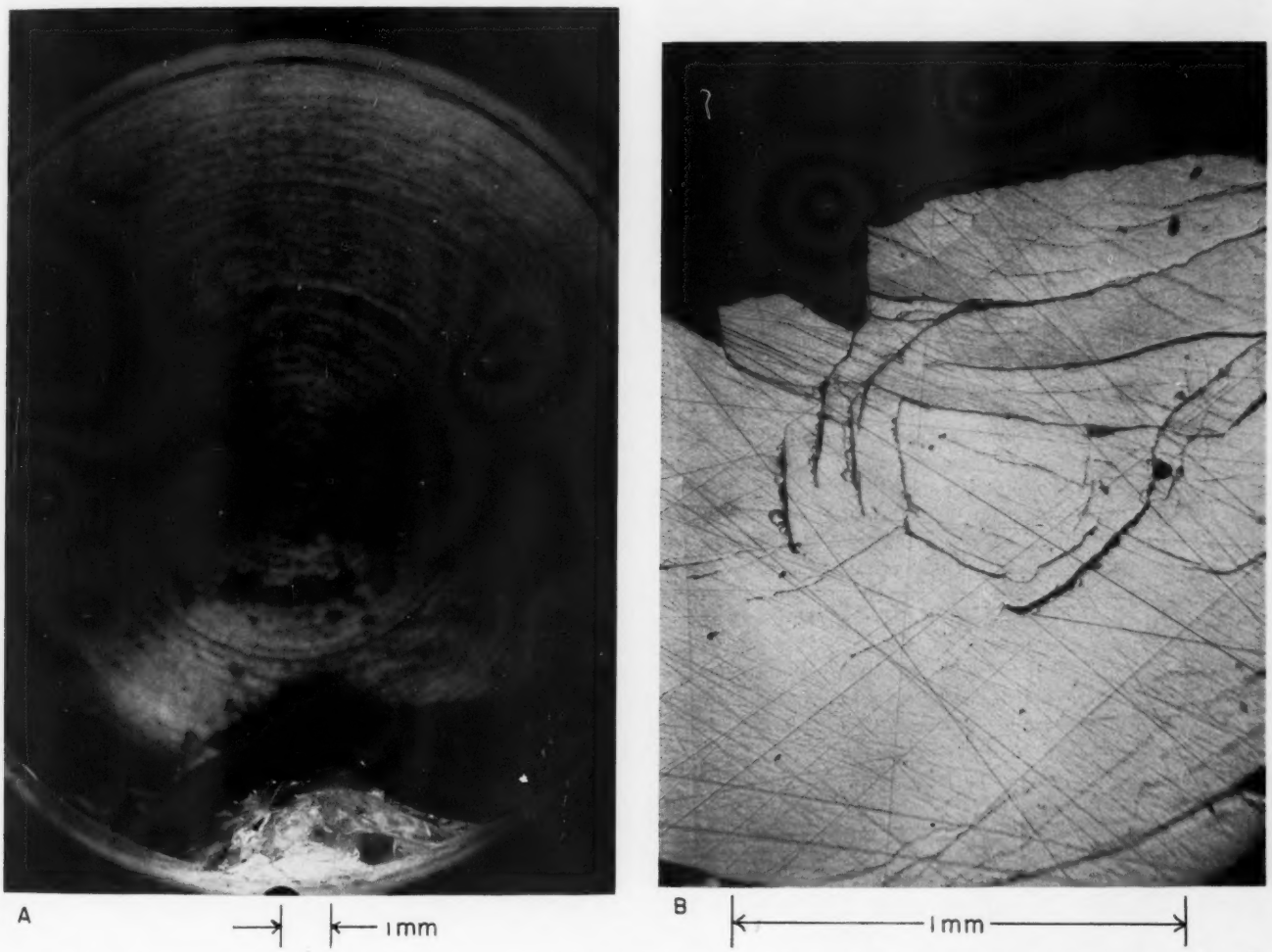

FIGURE 1. *White sapphire target plate No. II that collided with a 0.2-cm mercury drop at a velocity of 3.514 × 10⁴ cm/sec (1,153 ft/sec).*

A, View showing extent of damage to the target plate. B, View of the central point of the collision.

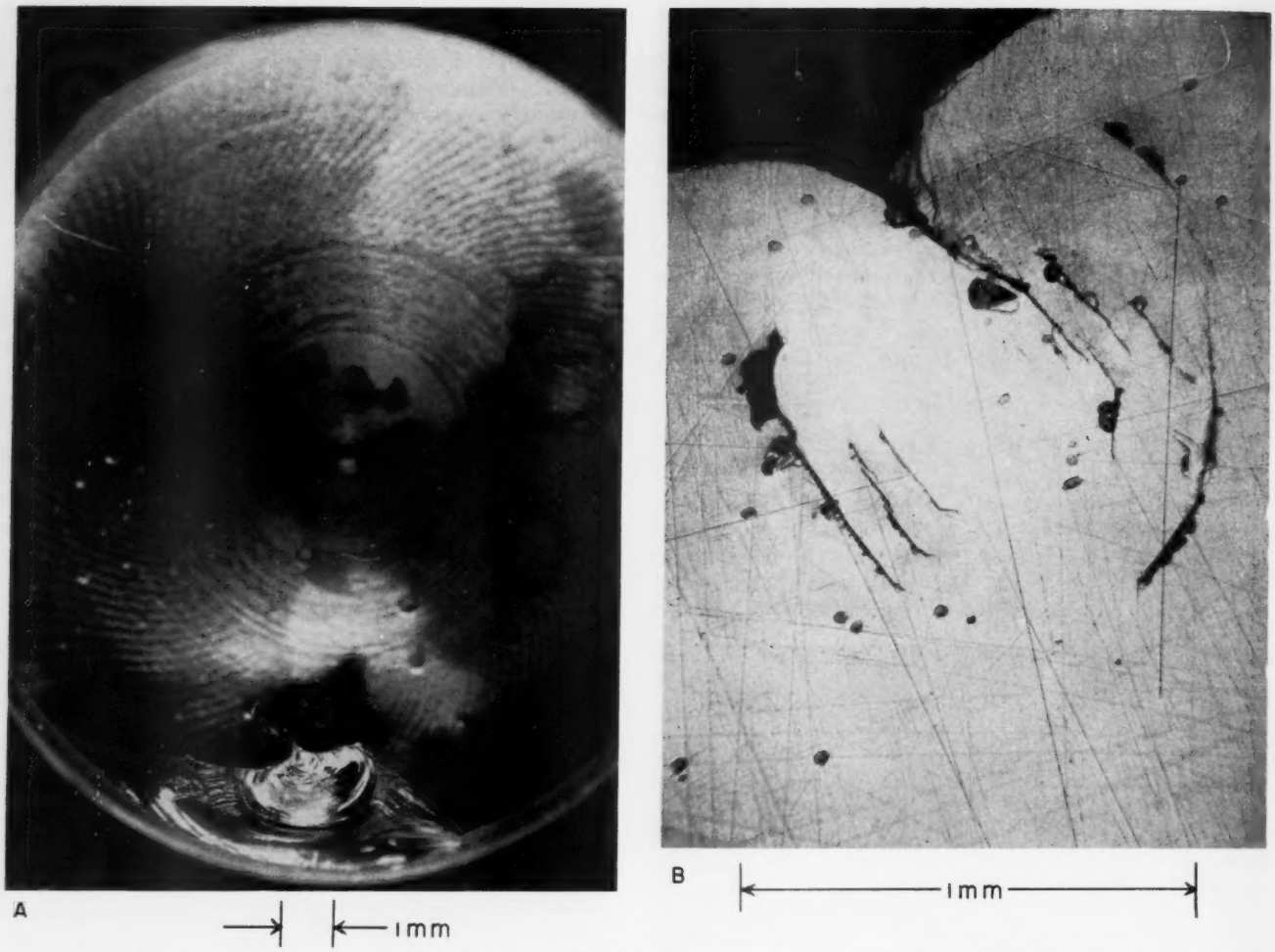

FIGURE 2. *White sapphire target plate No. III that collided with a 0.2-cm mercury drop at a velocity of 3.581×10⁴ cm/sec (1,175 ft/sec).*

A, View showing extent of damage to the target plate. B, View of the central point of the collision.

center. Sapphire is broken out in much the same way as on plate No. II (see above).

The polygonal cracks extend below the surface in a conchoidal fracture, as can be seen in the views of the eye of this collision shown in figure 3. These pictures were taken with a different mode of lighting, at lower magnification, and with greater depth of focus. In figure 3A the structure of the subsurface fractures can be seen best but the polygonal cracks on the surface are dim. In figure 3B it can be seen that the subsurface fractures extend from the surface cracks and that, *with increasing depth, they diverge from a line taken through the central point of the collision.*

The high velocity at which collision between plate No. IV *and a mercury drop occurred* (see table 2) *resulted in radial cracks that extend completely across and through the thickness of the plate.* They are shown in figure 4A and discussed in section 4.2(d).

Figure 4B shows the eye of this collision. Sapphire has been broken out in much the same way as on plate No. II (see above). The large dark regions are areas where sapphire appears to have been chipped from the surface between intersecting cracks.

Figure 5A shows damage done to plate No. V at the highest velocity at which a white sapphire plate collided with a mercury drop (see table 2). Extensive radial cracks run out from the center of the collision where a considerable amount of sapphire has been chipped out of the surface, apparently between intersecting cracks. *Two semicircular cracks, which appear to reflect the curved side of the plate, formed as a result of this highest-velocity collision.* They are indicated with arrows in figure 5A and are discussed in section 4.2(e).

Figure 5B shows the eye of this collision.

3.2. Hot-Pressed Alumina

Views of damaged hot-pressed alumina target plate No. IV, which collided with a mercury drop (see table 2), are shown in figures 6A and 6B. The experimenters at Convair drew a circle around the damage mark, which they reported was 0.0005 cm (0.0002 in.) deep and 0.071 cm (0.028 in.) in diameter.

FIGURE 3. *View of the subsurface fractures extending from the surface cracks shown in figure 2B.*

The eye of the collision (see fig. 6B) *consists of an undamaged central area surrounded by circles of short cracks.* Because the hot-pressed alumina is opaque, damage below the surface cannot be assessed.

Hot-pressed alumina target plant No. V was fired twice. It was chipped by an edge collision at 4.996×10^4 cm/sec (1,639 ft/sec) and then shattered by collision at 4.100×10^4 cm/sec (1,345 ft/sec). See figures 7A, 7B, and 7C.

Figure 7A shows that a crack runs across the target plate between the two points of collision. If this crack existed even partially before the second (lower-velocity) collision occurred, the extent of damage caused by this collision at 4.100×10^4 cm/sec (1,345 ft/sec) may not be representative. In this connection, it should be pointed out that the degree of damage seen in figure 7A was not produced in the collision of hot-pressed alumina target plate No. IV with a mercury drop at 4.276×10^4 cm/sec (1,403 ft/sec). See figure 6A.

Figures 7B and 7C show that the eye of the collision is again bounded by a circle of short cracks. Less than half of the eye of the collision that occurred at 4.996×10^4 cm/sec (1,639 ft/sec) can be seen in figure 7C; the remaining part of this area was apparently lost when a chip from the edge of the specimen broke away. Because the eye was broken in half, the crack structure below the surface of the opaque hot-pressed alumina can be observed. Microscopic inspection with the target plate turned at an angle revealed that *the short and more or less parallel cracks that bound the eye run deep into the ceramic;* they may extend through the target plate. *The innermost cracks of the ring may have formed nearly perpendicular to the surface, but the outermost cracks formed at an angle estimated roughly to be close to* 45° *to the surface.*

Figure 7A shows that seven radial cracks formed around the eye of the lower-velocity collision; the longer cracks are characterized by dichotomous branching. Comparison of the damage on hot-pressed alumina target plate No. V with that on plate No. IV suggests that the circular cracks that bound the eye of the collision form either with or without the formation of the long radial cracks (see fig. 6). On the other hand, the damage resulting from collision with the drop at 4.100×10^4 cm/sec (1,345 ft/sec) may be misleading, as was pointed out above. Almost invisible cracks may have been produced in this plate as a result of the edge collision with a mercury drop it had already suffered.

An interesting crack, which appears to reflect the contour of the edge of the target plate, is indicated with an arrow in figure 7A. This crack intersects five of the seven radial cracks that run out from the eye of the lower-velocity collision. The possible origin of this crack is discussed in section 4.2 (e).

4. Failure

In order to understand how the observed damage was produced, it is necessary to review the stresses imposed by an impinging liquid drop.

4.1. Stresses Produced in Liquid Drop Collisions

When a liquid drop collides with the planar surface of a solid, (a) it exerts a localized pressure and (b) it flows out radially around the central point of impingement.

a. Localized Pressure

During the early stages of the collision between a liquid drop and the planar surface of a solid, maxi-

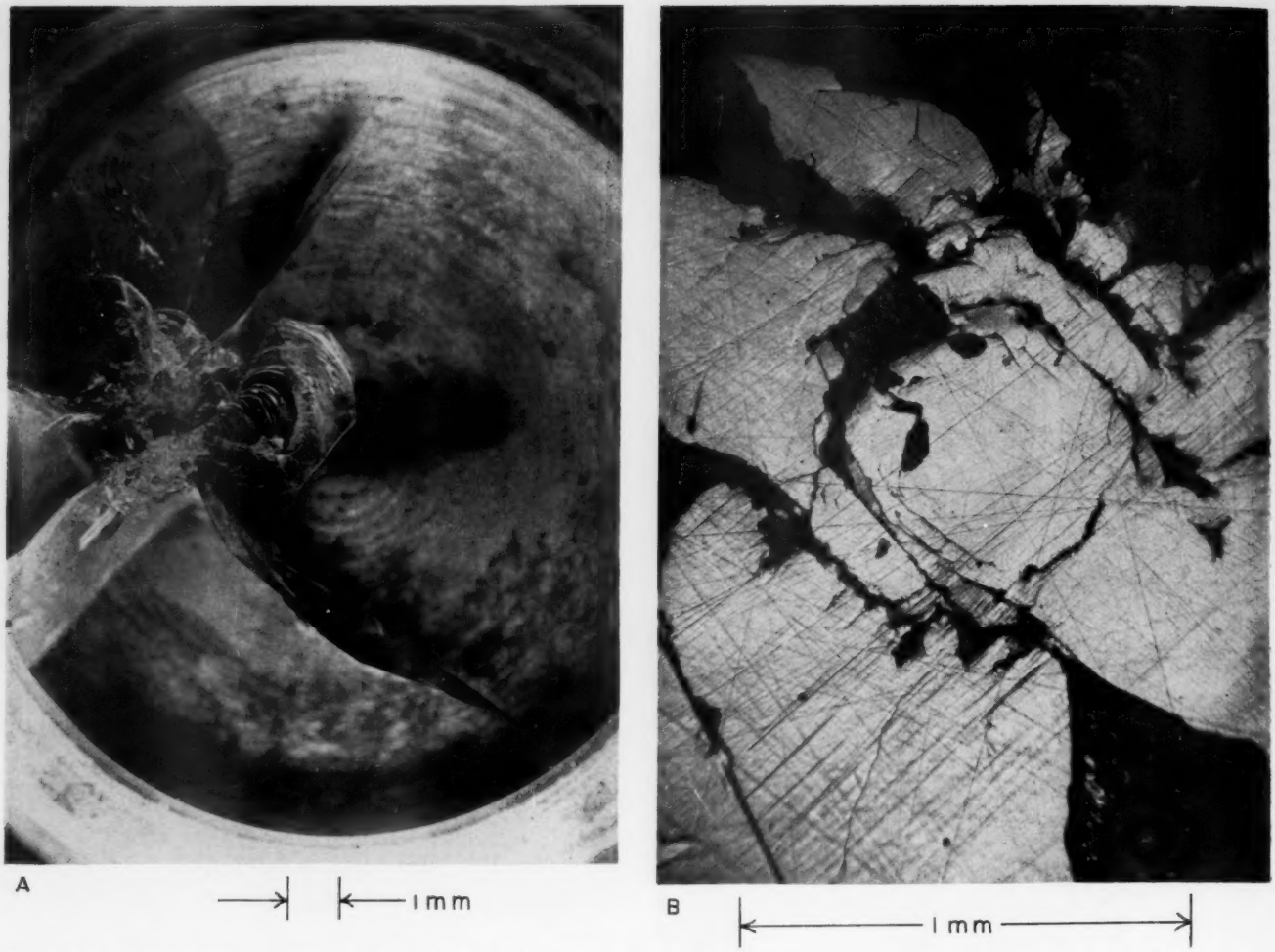

FIGURE 4. *White sapphire target plate No. IV that collided with a 0.2-cm mercury drop at a velocity of 4.420×10⁴ cm/sec (1,450 ft/sec).*

A, View showing extent of damage to the target plate. B, View of the central point of the collision.

mum pressure exists in a ring around the central point of the collision. At the first instant of the collision, when the maximum pressure is higher than at any later time, this ring may be regarded as a point circle. The radius of the ring of maximum pressure increases and the value of the maximum pressure in the ring decreases with time until the radius of the circle of contact between the drop and the solid is about 0.6 of the original radius of the drop. When this stage of the collision is reached, the ring of maximum pressure vanishes.

Savic and Boult [1][1] have given a hydrodynamic treatment of the collision of a drop of incompressible liquid with a completely unyielding solid. They found that the pressure is infinite at the first instant of the collision when the ring of maximum pressure may be regarded as a point circle. They state that this infinity is prevented physically by the fact that the high-initial pressure is absorbed in the bulk compressibility of the liquid, giving rise to an emitted compression wave.

According to the treatment of Savic and Boult [1], very high pressure maxima are developed during the early stages of the collision when the pressure maximum exists in a ring around the central point of the collision. Approximate values of the pressure maxima found by them for various values of the radius of the circle of contact between the drop and solid surface are given in table 3. They found that when the radius of the circle of contact is about 0.6 of the original radius of the drop, the ring of maximum pressure vanishes, maximum pressure then exists at the center of the drop, and the pressure profile across the contact area decreases from the center to the periphery of the circle of contact.

TABLE 3. *Maximum pressure in an impinging liquid drop*[a]

Radius of circle of contact	Approximate value of maximum pressure
0.1 R	3 ρU^2
.2 R	3½ ρU^2
.3 R	ρU^2
~0.6 R	½ ρU^2

[a] R is the original radius of the drop, ρ is the density of the liquid of which the drop is composed, and U is the impingement velocity.

[1] Figures in brackets indicate the literature references at the end of this paper.

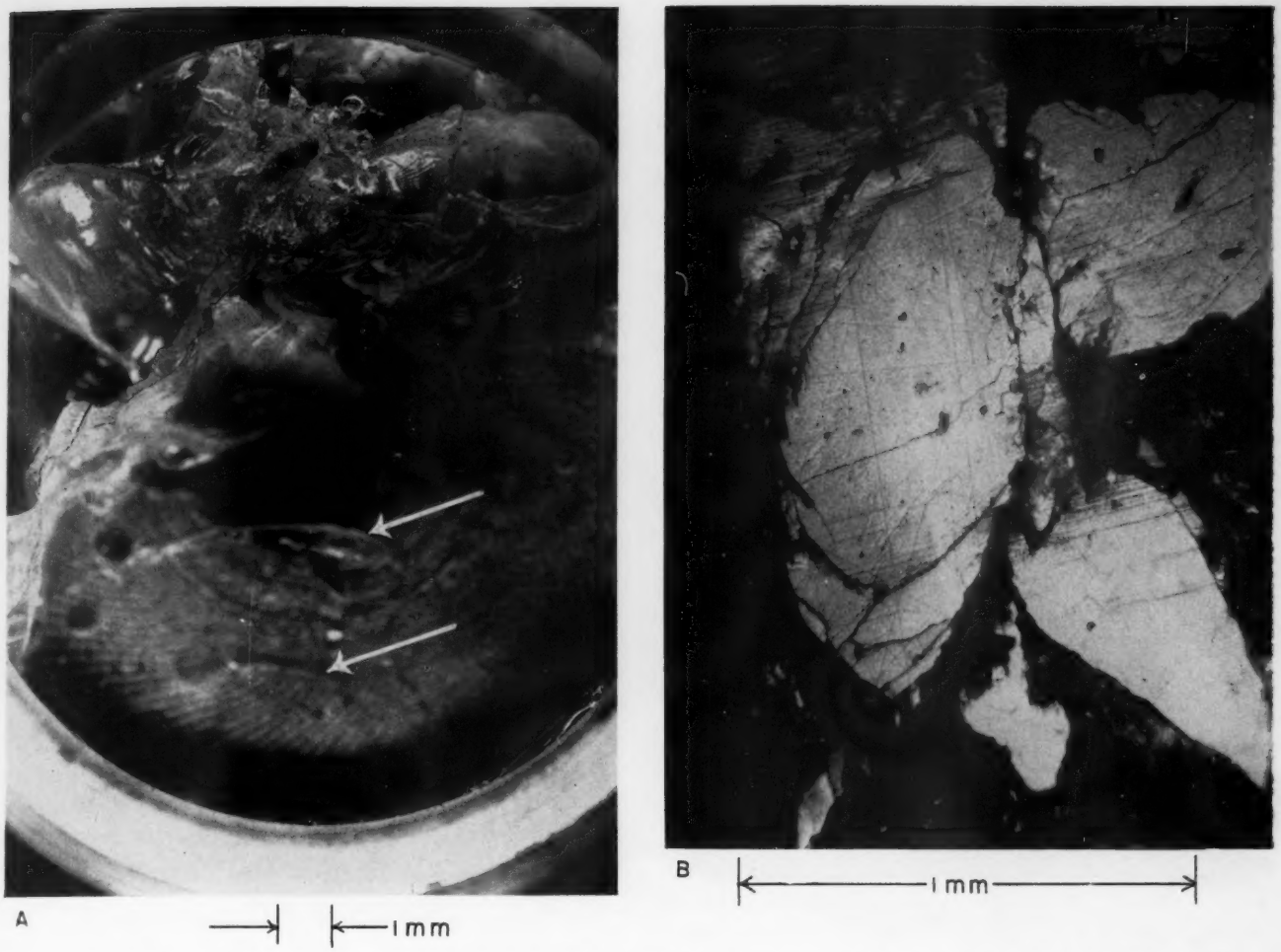

FIGURE 5. *White sapphire target plate No. V that collided with a 0.2-cm mercury drop at a velocity of 4.584×10^4 cm/sec (1,504 ft/sec).*

A, View showing extent of damage to the target plate. B, View of the central point of the collision.

In its ability to exert a localized pressure on the surface of a solid with which it collides, an impinging drop acts like a spherical indenter. The stresses that are introduced into an elastic plate by a spherical indenter were studied with the use of small foam rubber pads and spherical indenters of glass and steel. The kinds of stresses that act and the directions in which they act were deduced from the behavior of blemishes (holes and scratches) in the rubber as observed under low-power magnification.

The principal stresses at the periphery of the area compressed by an indenter are tensile and compressive (see fig. 8). This was shown by pressing a steel sphere into a rubber pad. Near the center of the compressed area below an indenter the principal stresses are all compressive (see fig. 8). This was shown by use of a spherical glass indenter flattened on one side; the behavior of the rubber under the indenter as it was pressed into the pad was observed through the flat area on the sphere. The principal stresses at the convexity on the reverse side of a plate into which an indenter is pressed are all tensile (see fig. 8). This was shown by pressing a rubber pad over a steel sphere.

Although an impinging liquid drop acts like a spherical indenter or like an impinging solid sphere in exerting a localized pressure, the pressure it exerts is never as great as that exerted by an impinging solid sphere for any given impingement velocity. This is because part of the collision energy of an impinging drop is transformed into radial flow of the liquid of which it is composed. An impinging solid sphere can inflict damage only by exerting a localized pressure; an impinging liquid drop can inflict damage both by the localized pressure it exerts and by its radial flow.

b. Radial Flow

The impact pressure produced by the collision of a liquid drop with the planar surface of a solid drives the liquid that is close to the solid surface radially outward around a central stagnation point. The flow velocity can become very high. In the case of a waterdrop colliding with a glass plate at free-fall velocity, it has been found to approach ten times the value of the impingement velocity for

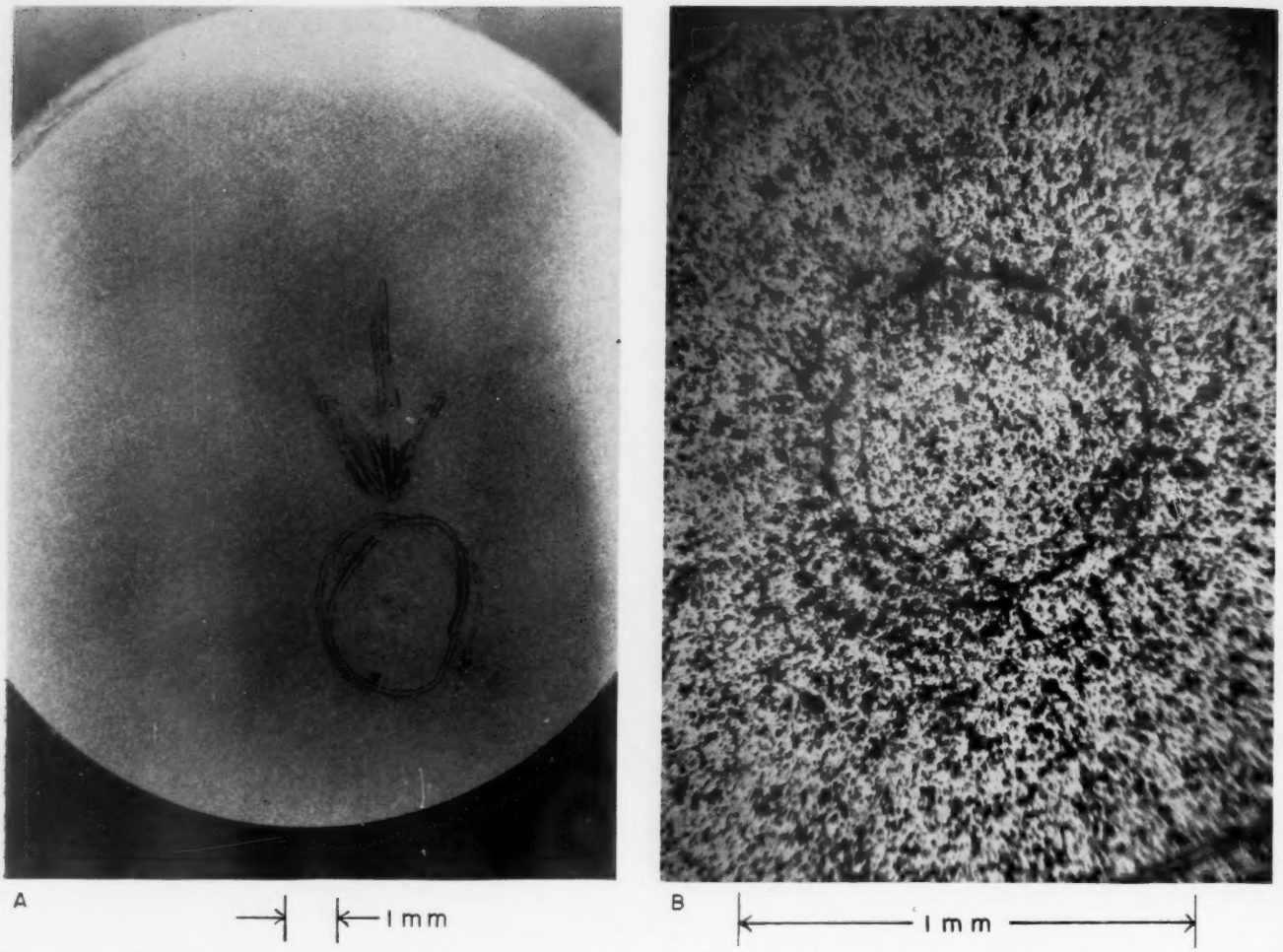

FIGURE 6. *Hot-pressed alumina target plate No. IV that collided with a 0.2-cm mercury drop at a velocity of 4.276×10^4 cm/sec (1,403 ft/sec).*

A, View showing extent of damage to the target plate. B, View of the central point of the collision.

short times after the collision incident [2].

The radially flowing liquid of an impinging drop exerts a shear stress on the surface of the solid over which it is running. The shear stress τ between layers of liquid in laminar flow is given by $\mu(\partial v/\partial z)$ where μ is the viscosity of the liquid, v is the velocity at which the liquid is moving, and z is the direction through the thickness of the liquid sheet. The layer of liquid molecules in direct contact with the surface of the solid has zero velocity, but the velocity gradient is not zero and the shear stress is applied to the solid.

If the radial flow of an impinging liquid drop runs over a surface protrusion, it exerts forces against the protrusion that tend to separate the protrusion from the underlying layers of material. Pressure exerted against the protrusion by the flowing liquid tends to move the protrusion along the planar surface of the solid and results in a shear stress at the base of the protrusion. The pressure exerted by the liquid also results in a turning moment that tends to bend the protrusion over. If the forces exerted by the rapid flow of liquid are large enough, failure may occur. The protrusion may be bent over, it may be broken off, or part of the solid material below the surface may be torn out with it.

4.2 Correlation of Observed Failures With Stresses

a. Undamaged Center

The damage marks consisted of an undamaged center surrounded by a polygon of cracks on sapphire and by a circle of cracks on hot-pressed alumina. The undamaged center is the part of the damage mark that was under high pressure during the collision. If a cavity formed during the collision, the undamaged center was the highly compressed material at the bottom of the cavity where the principal stresses are all compressive (see fig. 8). Brittle materials, such as glass, fail in tension [3], and it can be surmised that white sapphire and hot-pressed alumina will fail in tension. Because no tensile stresses form in the compressed solid material near the center of the collision, failure would not be expected here.

b. Polygonal or Circular Cracks

The polygonal and circular cracks formed in the region of tensile stress around the central compressed area (see fig. 8). It seems reasonable to suppose that these cracks are the result of a tensile failure.

In the case of a hemispherical distribution of pressure on the surface of a semi-infinite medium, the maximum tensile stress is radial, exists at the periphery of the compressed area, and is given by [3],

$$\sigma_r = (1-2\nu)/3q_0$$

where ν is Poisson's ratio and q_0 is the maximum pressure at the center of the compressed area. The type of pressure distribution for which this equation applies exists under an impinging liquid drop only after the circular pressure peaks that develop during the earliest stages of the collision have vanished. This occurs when the radius of the circle of contact is about 0.6 of the original radius of the drop (see sec. 4.1). The maximum pressure at this time according to the hydrodynamic treatment of Savic and Boult [1] for a drop of incompressible liquid impinging against the planar surface of an unyielding solid, is 9.3×10^9 d/cm^2 (135,000 psi) for a mercury drop colliding at 3.581×10^4 cm/sec (1,175 ft/sec). The damage mark made on a white sapphire target plate on collision with a 0.2-cm mercury drop at this velocity is shown in figure 2B. Using this value for the maximum pressure, g_0, and 0.26 for an average value [2] of Poisson's ratio, ν, a value of 1.5×10^9 d/cm^2 (22,000 psi) is obtained for the radial tensile stress, σ_r. This is only about half of the tensile strength of white sapphire. See modulus of rupture in table 1. From figure 2B it can be seen that the radius of the area enclosed by the outermost polygonal cracks is about 0.05 cm or half the original radius of the 0.2-cm-diam mercury drop, whereas the calculated value of σ_r is for a radius of about 0.06 cm.

Furthermore, polygonal cracks have formed at distances from the central point of the collision that range from about 0.025 to about 0.05 cm. From the treatment of Savic and Boult [1], the maximum pressure would be increased by a factor of 2 for the case that the radius of the circle of contact is 0.03 cm, 0.3 of the radius of the original drop, and would be increased by very close to a factor of 3 for the case that the radius of the circle of contact is 0.02 cm, 0.2 of the radius of the original drop. See table 3. Hence it can be surmised that the radial tensile stresses are from 2 to 3 times higher than 1.5×10^9 d/cm^2 (22,000 psi) at the distances from the central point of the collision where polygonal cracks are observed to have formed, and are in excess of the tensile strength of white sapphire. However, because the equation given for the radial tensile stress, σ_r, is based on a different pressure distribution from that which exists in a liquid drop when the radius of the circle of contact is less than about 0.6 of the original radius of the drop, this equation cannot validly be used to compute them.

The difference in the type of cracks (polygonal or circular) appears to result from the degree of anisotropy of the two ceramics. The single-crystal white sapphire is characterized by cleavage planes on which failure occurs first whereas polycrystalline hot-pressed alumina is isotropic.

c. Breaking Out of Material

White sapphire is eroded away along the polygonal cracks that formed in it. This damage appears to be the result of the radial flow of the mercury drops that impinged. If the broken edges of the cracks were raised above the planar surface of the target plate by plastic flow, they may have provided protrusions against which the radially flowing mercury exerted pressure. The pressure would result in a shear stress below the protrusion and a turning moment exerted against it, which may have caused the loss of material.

The reasoning just given is supported by the observation that the loss of sapphire material occurred on the side of the crack away from the central point of the collision. If the raised broken edge of the crack provided a protrusion against which the radial flow of the mercury of the drop could exert a pressure, this is the side of the crack against which the pressure would be exerted.

There are two other observations that support the reasoning given. One of these is that the outermost polygonal cracks are more eroded than the innermost. This may be explained in terms of the magnitude of the radial flow velocity at different distances from the stagnation point (zero flow velocity) at the center of the collision. On the other hand, there may have been an increase in the magnitude of the radial tensile stress with increase in distance from the center of the collision and the outermost cracks may, therefore, have developed higher raised edges due to plastic flow. The other observation is that the erosion damage increased in severity as the impingement velocity was increased. This could be in agreement with the fact that the velocity of the radial flow is increased as the impingement velocity is increased. However, the magnitude of the radial tensile stresses introduced is also increased as the impingement velocity is increased and this could explain the observation in terms of higher raised edges along the cracks.

d. Radial Cracks

Radial cracks formed at the highest impingement velocities at which mercury drops struck the target plates of both white sapphire and hot-pressed alumina. They ran out from the center of the collision and extended completely across and through the target plates.

[2] This average value of Poisson's ratio for white sapphire and polycrystalline alumina was kindly supplied by J. B. Wachtman, Jr., of NBS Engineering Ceramics Section.

These cracks are probably also the result of a tensile failure. Tensile stresses perpendicular to the radial principal planes of stress are required to account for them. The stresses perpendicular to the radial principal planes of stress around the periphery of the area of the target plate compressed by the colliding drop are compressive (see sec. 4.1 and fig. 8).

It is possible that these cracks may originate on the reverse face of the target plate if the compressional wave initiated by the collision reflects appreciably as a tension wave.[3] The principal stresses that exist on the reverse face of the plate if this reflection occurs are all tensile stresses (see fig. 8). Hence radial cracks could form on the reverse face of the plate as a result of a tensile failure. It is possible that the radial cracks originate on the reverse face of the target plate and progress through it to the collision surface.

e. Curved Cracks

Cracks that reflect the curvature of the bounding edge of the target plates formed in both white sapphire and hot-pressed alumina. A wave of compression is initiated in the target plate as a result of the collision. When this wave reaches the curved edges of the target plate, it reflects both as a tension wave and as a transverse wave. It seems very likely that the curved cracks formed when the level of stress in the reflected tension wave exceeded the tensile strength of the ceramic material.

From figures 5A and 7A it can be seen that the distance from the edge of the hot-pressed alumina target plate to the curved crack is about the same as the distance from the edge of the white sapphire target plate to the curved crack that formed furthest from the edge of it. On the basis of the observation that no second crack formed in hot-pressed alumina, and of the information that the tensile strengths of the ceramics and the sizes and velocities of the impinging drops were closely similar, it can be deduced that the crack furthest from the edge of the white sapphire target plate formed first. This deduction is in agreement with the observation that the curvature of the two cracks is in the same direction. If the crack nearest the edge of the sapphire target plate had formed first, the compressional wave initiated by the collision would have begun to reflect from the curved surface of this crack, and it would be expected that, if the level of tensile stress in the tension wave reflected from this crack again exceeded the tensile strength of the ceramic, the second crack to form would curve in the opposite direction.

The curved edges of the target plates focus the reflected tension waves in the same way that a curved mirror focuses reflected light waves. This is in agreement with the observation that the curved cracks are isolated; they do not extend from edge to edge of the target plate. The curved cracks formed

[3] The extent to which reflection and transmission of the compressional wave may have occurred at the adhesive bond between the ceramic target plate and the aluminum backing plate is not known.

FIGURE 7. *Hot-pressed alumina target plate No. V that collided with 0.2-cm mercury drops at velocities of 4.100×10^4 cm/sec (1,345 ft/sec) and 4.996×10^4 cm/sec (1,639 ft/sec).*

A, View showing extent of damage to the target plate.

in white sapphire are below the surface. This may be ascribed to the effect of the bevelled edge of the target plate on the reflected wave. In hot-pressed alumina, however, the curved crack extends to the surface.

If the curved crack furthest from the edge of the white sapphire target plate formed first, as seems to be the case from the evidence at hand, the mechanism by means of which the crack nearest the edge of the target plate then formed needs to be explained.

At the time that the curved crack furthest from the edge of the target plate forms, a tension wave superposed on a pressure wave is trapped between this curved crack and the curved edge of the target plate. The curvature of both bounding surfaces between which the trapped wave must travel is such as to focus the wave further. This is in agreement with the observation that the crack that eventually forms closest to the edge of the target plate is shorter than the crack that appeared first and that formed furthest from the edge of the target plate. If the

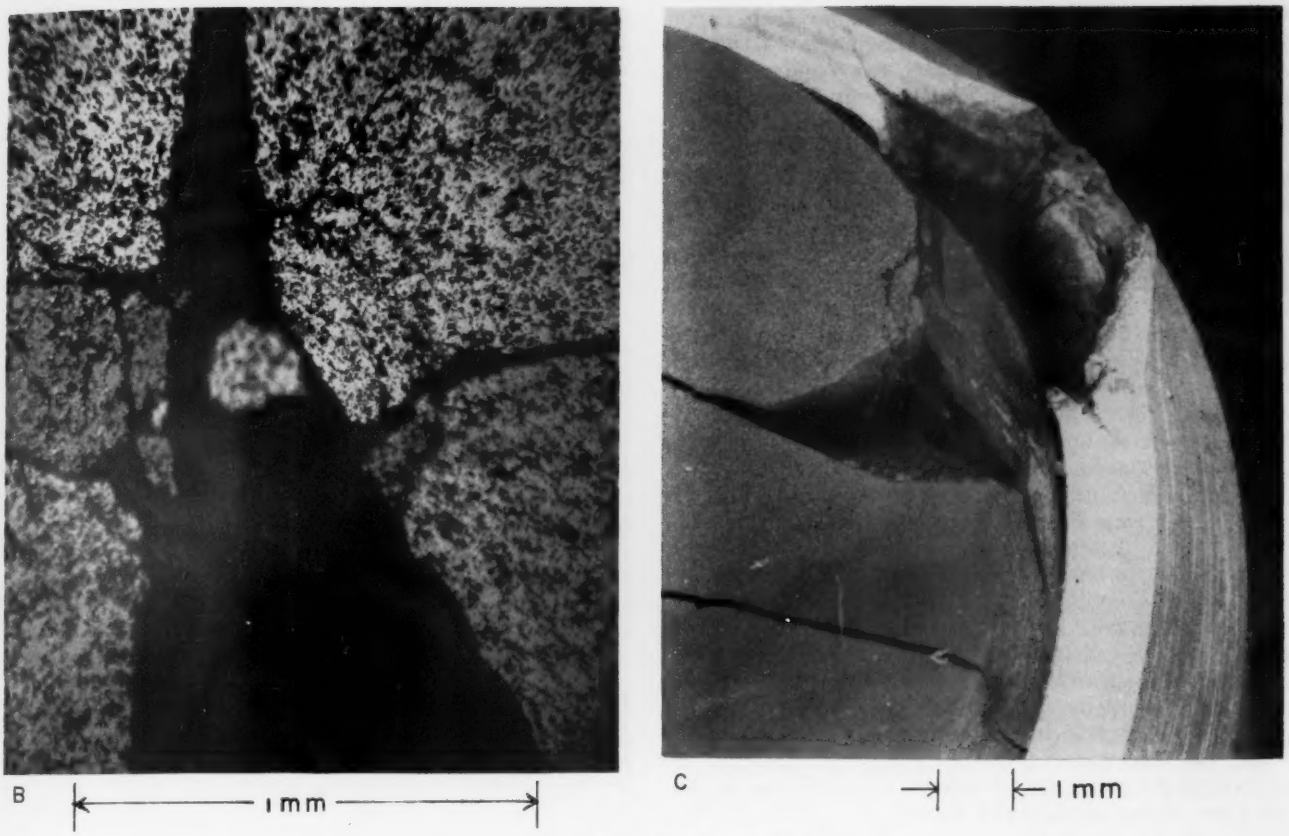

FIGURE 7.—*Continued*

B, View of the central point of the lower-velocity collision. C, View of the higher-velocity collision site (edge of plate).

boundaries between which the trapped wave must reflect were straight, the level of tensile stress in the tension wave would never again exceed the tensile strength of the ceramic. In the case of reflection between curved boundaries, the focusing effect of the boundaries may make the formation of the second fracture possible.

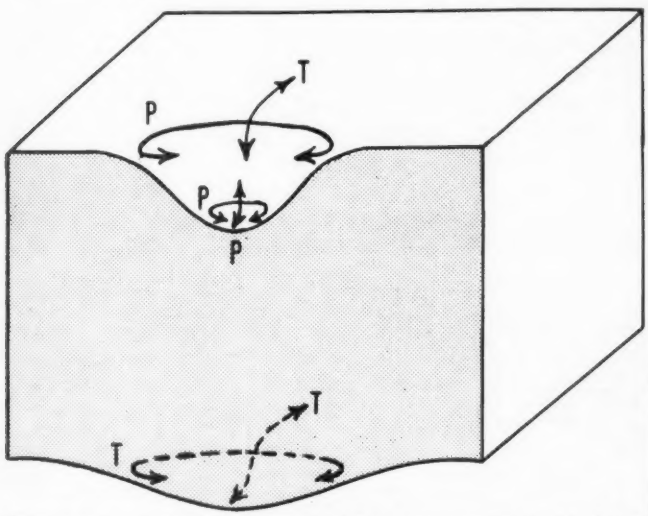

FIGURE 8. *Principal stresses (P, pressure; T, tension) at the concavity and convexity produced by a spherical indenter pressing against an elastic solid plate.*

5. Resistance to Waterdrop Impingement

The information of greatest interest from a practical standpoint is the resistance of white sapphire and of hot-pressed alumina to waterdrop impingement. This information was not obtained in the tests because impingement velocities high enough to fracture these ceramics on colliding with a waterdrop were not reached. In this section an equation is developed from which an estimate of the resistance of these ceramics to waterdrop impingement can be obtained by extrapolation of their resistance to mercury drop impingement.

To develop this equation the following assumptions are made: (1) A concavity (no matter how small) forms in a thin ceramic plate, whose reverse face is a free surface, as a result of high-speed liquid-drop impingement; (2) elastic recovery without fracture occurs when the impingement velocities are low and the depth of the concavity is small; and (3) corresponding velocities to produce equal depth of concavity in a given edge-supported ceramic plate by impingement with drops of a liquid A and drops of a liquid B are corresponding velocities for fracture when the concavity reaches the depth at which the tensile stresses that develop around it (either by themselves or when they are reinforced by the tension wave reflected from the reverse face of the plate) are sufficient to produce fracture.

Assumptions (1) and (2) are reasonable because, although microscopic plastic deformation at stress concentrations has been found to take place in white sapphire and ruby [4], in macroscopic terms these ceramics may be said to yield elastically until fracture occurs. The validity of assumption (3) is open to question. It depends on similarity considerations and, therefore, on the implication that concavities of equal depth produced by impingement of drops of different liquids are of similar shape. However, it may be sufficiently reliable for a rough estimate if the diameters of the drops and the viscosity and surface tension of the liquids used are not too widely different. Within the validity of the assumptions made, an equation from which extrapolated corresponding velocities for equal fracture of thin edge-supported ceramic plates by liquid-drop impingement can be calculated, has been developed as follows.

When a fast-moving target plate collides with a stationary liquid drop, a core of material through the target plate under the collision area is slowed down with respect to the remainder of the target plate as a result of the collision. As in a previous treatment [5], the situation is idealized in two ways. First, the core is regarded as a true cylinder that is free to move in the direction of the collision blow but is restrained laterally. A similar cylinder exists in the liquid of which the drop is composed. Secondly, the compressional waves that move through the cylinder in the target plate and through the cylinder in the drop are regarded as plane waves.

The depth, δ', of the concavity that forms elastically in a ceramic target plate as a result of high-speed collision with a liquid drop is proportional both to the particle velocity, v', produced in the core of target material under the contact area as a result of the collision, and to the time, t, that this particle velocity exists. Then,

$$\delta'=kv't \tag{1}$$

where k is a constant. It has been shown [6] that, for the case that the target plate collides with a liquid drop rather than with a solid sphere,

$$v'=\frac{\alpha zV}{z'+\alpha z} \tag{2}$$

where α is a coefficient having a value less than one, V is the impingement velocity, and $z=c\rho$ where ρ is the density and c is the speed of irrotational waves in infinite medium. Primed quantities refer to the material of the solid target plate; unprimed quantities refer to the liquid of which the drop is composed. All quantities are in cgs units. It has also been shown [6] that

$$\alpha=0.41/[1+(0.59\ z/z')]. \tag{3}$$

As before [5], the time t is the time required for the compressional wave initiated in the liquid of the drop to move through the drop, reflect as a tension wave from the free liquid-to-air interface, and return to the contact area between the drop and the target plate. Then,

$$t=2d/c \tag{4}$$

where d is the diameter of the drop.

By substituting eq (2) and (4) into (1), the depth of concavity produced by collision of the target plate with a drop of liquid A is

$$\delta'_A=k\left(\frac{\alpha_A z_A V_A}{z'+\alpha_A z_A}\right)\left(\frac{2d_A}{c_A}\right). \tag{5}$$

Similarly, for a drop of a liquid B,

$$\delta'_B=k\left(\frac{\alpha_B z_B V_B}{z'+\alpha_B z_B}\right)\left(\frac{2d_B}{c_B}\right). \tag{6}$$

By equating eq (5) and (6), it is found that

$$V_A=\left(\frac{\alpha_B z_B}{\alpha_A z_A}\right)\left(\frac{z'+\alpha_A z_A}{z'+\alpha_B z_B}\right)\left(\frac{c_A}{c_B}\right)\left(\frac{d_B}{d_A}\right)V_B. \tag{7}$$

If fracture of the ceramic occurs when the concavity that forms reaches a certain depth, then, by substituting into eq (7) the velocity known to produce fracture on a brittle elastic solid by impingement of drops of a liquid B, the velocity required to produce fracture of the same solid by impingement of drops of a liquid A can be calculated.

Let liquid A be water, liquid B be mercury, and the target plate be of white sapphire. From eq (3), and the data of table 4, the coefficient α for waterdrops impinging against white sapphire is 0.40, and the coefficient α for mercury drops impinging against white sapphire is 0.32. Then, from eq (7) and the data of table 4,

$$V_W=9.6\left(\frac{d_M}{d_W}\right)V_M, \tag{8}$$

where sub-W indicates water and sub-M indicates mercury. For the condition that the waterdrop and mercury drop have the same diameter, $V_W=9.6\ V_M$. It required an impingement velocity of 3.514×10^4

TABLE 4. *Acoustic impedance*

Material	Density	Sound speed	Acoustic impedance
	g/cm^3	cm/sec	$g/(cm^2\cdot sec)$
Water	[a] 0.99707	[b] 1.497×10^5	0.1493×10^6
Mercury	[a] 13.546	[b] 1.451×10^5	1.966×10^6
Polyethylene	[a] 0.92	[c] 1.95×10^5	0.1794×10^6
White sapphire	[d] 3.98	[f] 11.00×10^5	4.378×10^6
Hot-pressed alumina	[e] 3.95	[f] 11.90×10^5	4.345×10^6

[a] Data from Handbook of Chemistry and Physics.
[b] Data from L. Bergmann, Der Ultraschall, S. Hirzel, Stuttgart, 1954.
[c] Data from American Institute of Physics Handbook, 1958.
[d] Data supplied by Linde Air Products Company.
[e] Data supplied for H. P. Alundum by Norton Company.
[f] Approximate average value supplied by John B. Wachtman, Jr., of NBS Engineering Ceramics Section.

cm/sec (1,153 ft/sec) to produce fracture of a white sapphire target plate 0.318 cm (0.125 in.) thick in collision with a 0.2-cm mercury drop (see fig. 1). From eq (8), a 0.2-cm waterdrop would have to collide with the same target plate at a velocity of 33.7×10^4 cm/sec (11,100 ft/sec) in order to produce fracture. Taking the speed of sound in air at 0° C to be 3.317×10^4 cm/sec (1,088 ft/sec), the Mach Number equivalent is 10.

Experimental verification of eq (7) is needed before corresponding velocities calculated by use of it can be relied upon. The only experimental data available to check eq (7) are those being obtained in a study currently in progress on the fracture of an unidentified polycrystalline alumina by impingement of polyethylene pellets [7]. In this study, 12.7-cm (5-in.) square plates of 99+ percent pure polycrystalline alumina 0.635 cm (0.25 in.) thick are being used as targets for impingement of 0.5-cm polyethylene pellets fired at a constant velocity of 23.5×10^4 cm/sec (7,700 ft/sec). The ceramic plates are maintained at a temperature of 1,371 °C (2,500 °F) during the firings. The angle at which the polyethylene pellets strike the target plates is increased until erosion, and finally breakage failure, occurs. The data available at present are for two plates tested to complete failure. Significant erosion was not noted until the impact angle was in each case 40°. One of the plates failed to the point of breakage at an impact angle of 40° and the other plate failed to the same extent at an impact angle of 60°. These impact angles were reported to correspond to normal velocities of 14.9×10^4 cm/sec (4,900 ft/sec) and 20.4×10^4 cm/sec (6,700 ft/sec), respectively [7].

Because the resistance of white sapphire and of hot-pressed alumina to mercury-drop impingement was found to be nearly the same, and because the more common, cream-white polycrystalline alumina is a ceramic of comparable strength properties, the reliability of eq (7) can be tested roughly by calculating the velocity required to damage white sapphire to the point of radial crack formation by impingement of a 0.5-cm polyethylene pellet.

By use of eq (3) and the data of table 4, it is found that the coefficient α for collision of a polyethylene pellet with a white sapphire plate is 0.40. By use of eq (7) and the data of table 4, it is found that

$$V_P=10.5\left(\frac{d_M}{d_P}\right)V_M \qquad (9)$$

where the sub-P notation indicates polyethylene. From figure 4 it can be seen that radial fracture of a white sapphire target plate occurred as a result of impingement of a 0.2-cm mercury drop at a velocity of 4.420×10^4 cm/sec (1,450 ft/sec). Using this velocity for V_M, 0.2 cm for d_M, and 0.5 cm for d_P, eq (9) predicts that an impingement velocity of 18.6×10^4 cm/sec (6,090 ft/sec) would be required to produce the extent of fracture seen in figure 4 with use of a 0.5-cm polyethylene pellet.

The velocity calculated by use of eq (9) is between the two values that have been found experimentally. However, the fact that the ceramic target plates were held at a temperature of 1,371 °C (2,500 °F) during the test firings, which may have affected their resistance, the fact that the polyethylene pellets impinged at an angle, which should result in an unsymmetrical distribution of stress, and the fact that the drop size was considerably different raise questions that reduce the significance of this good agreement.

Jackman and Roberts [8] have found that the strength of polycrystalline alumina is not changed by an increase in temperature until the temperature reaches 700 °C (1,292 °F). If the temperature is increased further, there is a gradual decrease of strength with increase of temperature [8]. At 1,300 °C (2,372 °F) the strength is roughly one-third of its room-temperature value [8]. The strength of white sapphire has a very different temperature dependence [5, 8]. It decreases with increase of temperature to a minimum in the range of 300 to 600 °C (572 to 1,112 °F) and then increases with further increase in temperature until, at about 1,000 to 1,200 °C (1,832 to 2,192 °F), it is very close to its room-temperature value.

It is possible that, at the high rates of loading involved in the impingement tests, the temperature of the ceramic plates may not have an important effect on the velocity that an impinging pellet must have to break them.[4] But this effect, the effect of drop size, and the effect of the angle at which the collision occurs need to be determined.

Until eq (7) is verified more conclusively with experimental evidence, *corresponding velocities calculated by use of it should not be regarded as more than estimates.*

6. Ultimate Failure

In order to extrapolate from the observed liquid-drop-impingement failure of white sapphire and hot-pressed alumina to what may be expected at higher collision velocities, it is useful to consider the failure of low-strength brittle solids, such as poly(methyl methacrylate) and polystyrene, under imposed stresses of the same kind.

Polygonal cracks have been observed in poly (methyl methacrylate) as a result of waterdrop impingement at a velocity of 2.234×10^4 cm/sec (733 ft/sec) [9]. The cracks were widened by breaking out of the surface material along them in a direction away from the central point of impact as a result of the radial flow of the water. With respect to these features, the damage marks produced on low-strength poly(methyl methacrylate) by waterdrops impinging at a velocity of 2.234×10^4 cm/sec

[4] I am indebted to J. B. Wachtman, Jr. of NBS Engineering Ceramics Section for this suggestion.

(733 ft/sec) are similar to the damage marks produced on high-strength white sapphire by mercury drops impinging at a velocity of 3.514×10^4 cm/sec (1,153 ft/sec).

The ultimate kind of failure that white sapphire will undergo may be predicted from the observed damage done to a plate of polystyrene 0.318-cm (0.125-in.) thick that collided with a waterdrop at a velocity of 7.666×10^4 cm/sec (2,515 ft/sec). A circular plug of polystyrene was cut out of the plate as a result of the collision (see fig. 9). It can be expected that similar damage will be done to white sapphire and to hot-pressed alumina as a result of collision with a waterdrop. The only difference will be that the collision velocity required to produce this degree of damage will be much higher for the high-strength ceramics than for the relatively weak polystyrene. Indeed, it has already been reported informally [7] that a plug has been cut out of a plate of polycrystalline alumina as a result of collision with a polyethylene pellet.

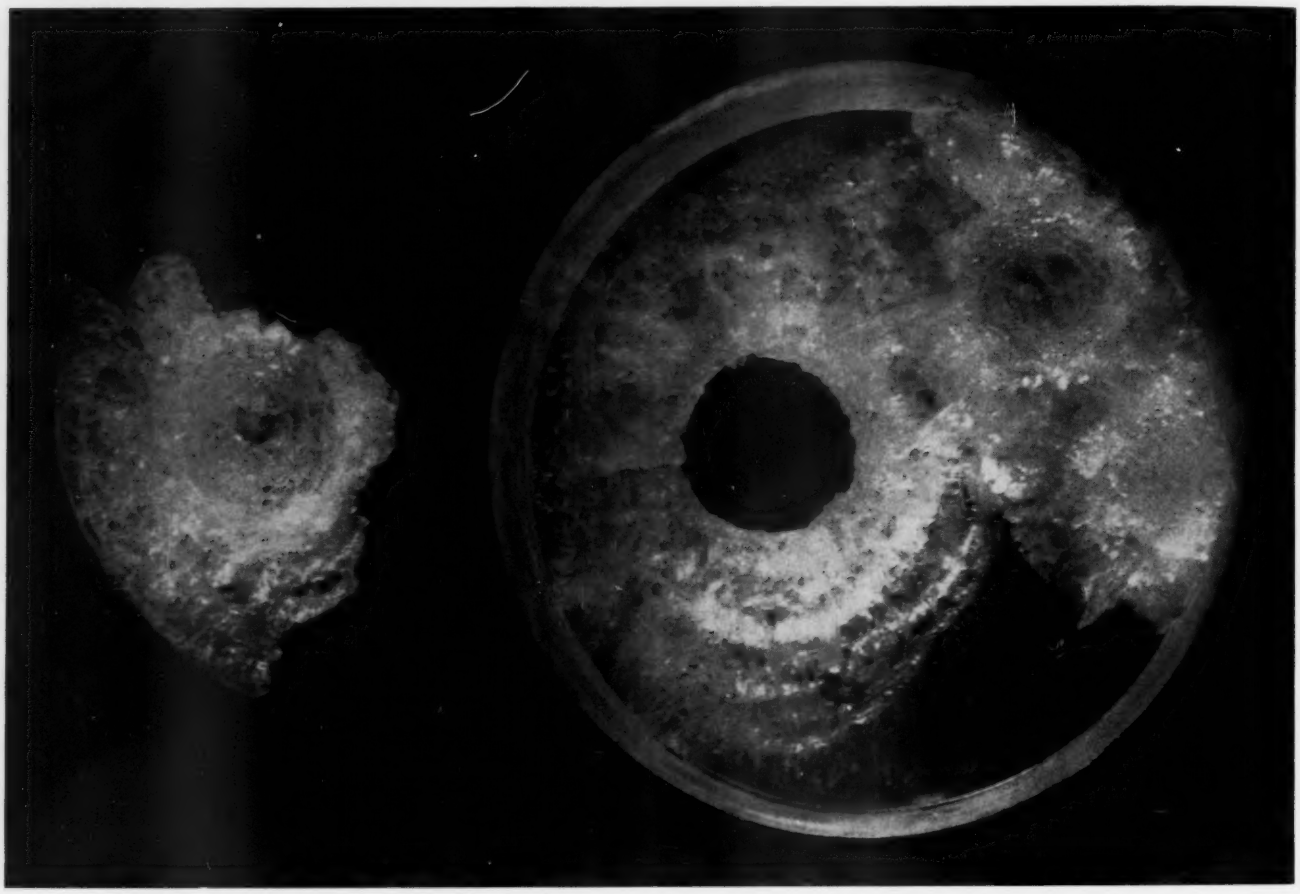

FIGURE 9. *Polystyrene target plate that collided with waterdrops at a velocity of 7.666×10^4 cm/sec (2,515 ft/sec).*

The plug of polystyrene cut out of the target plate is also shown.

(Magnification × 6.1)

7. References

[1] P. Savic and G. T. Boult, The fluid flow associated with the impact of liquid drops with solid surfaces, Report No. MT–26, National Research Council of Canada, Ottawa (May 1955).

[2] Olive Engel, Waterdrop collisions with solid surfaces, J. Research NBS **54,** 281 (1955) RP2591.

[3] S. Timoshenko and J. N. Goodier, Theory of elasticity (McGraw-Hill Book Co., Inc., New York, N.Y., 1951).

[4] J. B. Wachtman, Jr. and L. H. Maxwell, Strength of synthetic single crystal sapphire and ruby as a function of temperature and orientation, J. Am. Ceram. Soc. **42,** 432 (1959).

[5] Olive Engel, Pits in metals caused by collision with liquid drops and soft metal spheres, J. Research NBS **62,** 229 (1959) RP2958.

[6] Olive Engel, Particle velocity in solid-against-liquid collisions, J. Research NBS 64A6–71 (1960).

[7] L. D. Ryan, Aero-Space Division of Boeing Airplane Company, letter and informal conversation.

[8] Elizabeth A. Jackman and J. P. Roberts, On the strength of polycrystalline and single crystal corundum, Trans. Brit. Ceram. Soc. **54,** 389 (1955).

[9] Olive Engel, Mechanism of high-speed-waterdrop erosion of methyl methacrylate plastic, J. Research NBS **54,** 51 (1955) RP2565.

(Paper 64A6–72)

JOURNAL OF RESEARCH of the National Bureau of Standards—A. Physics and Chemistry
Vol. 64A, No. 6, November–December 1960

Note on the Thermal Degradation of Polytetrafluoroethylene as a First-Order Reaction

S. L. Madorsky and S. Straus

(June 23, 1960)

Additional experiments on the rates of thermal degradation of polytetrafluoroethylene in a vacuum confirm an earlier conclusion that a first-order rate law is involved in the degradation reaction.

In a study made by Madorsky, Hart, Straus, and Sedlak [1] on the rates and activation energy of thermal degradation of polytetrafluoroethylene in a vacuum, two methods were employed: a gravimetric method, using a very sensitive tungsten spring balance in a vacuum system to measure the rate of loss of weight of the degrading sample, and a pressure method, using a multiplying manometer to measure the pressure of the C_2F_4 formed in the reaction. The material that was used was in the form of a tape 0.07 mm thick. Weight of the sample was about 7 mg in the gravimetric experiments and 5 to 306 mg in the pressure experiments.

The rates obtained by the gravimetric method are reproduced in figure 1, plotted as a function of percentage loss of weight of the sample for 480, 490, 500, and 510 °C. The initial rates were obtained by extrapolating the rate curves to the ordinate. The rate curves beyond the initial 5 to 18 percent loss of weight of the sample are straight lines, and when extended to the right they approach near the zero rate at 100 percent volatilization. The rates obtained by the pressure method were studied at 10 different temperatures ranging from 423.5 to 513.0 °C. Logarithms of the initial rates obtained by both methods are shown in figure 2 plotted against the inverse of absolute temperature.[2] From the Arrhenius equation the slope of the resulting straight line indicates an activation energy of 80.5 kcal/mole. From the appearance of the curves in figure 1 it seemed logical to conclude that the reaction involved in the thermal degradation of polytetrafluoroethylene in a vacuum follows a first-order law.

At a later date Wall and Michaelson [3] studied the rate of thermal degradation of polytetrafluoroethylene at 460 °C in a stream of nitrogen. They used a gravimetric method by heating 1-g samples of a powdered material and weighing the residues at

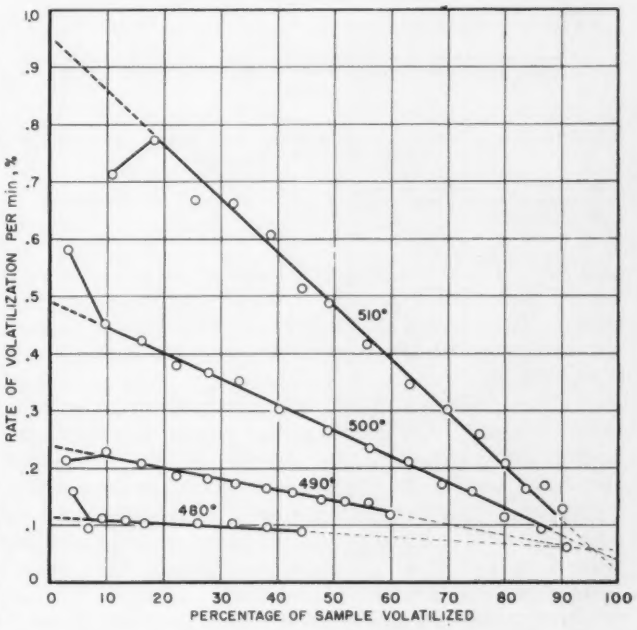

FIGURE 1. *Rate of thermal degradation of polytetrafluoroethylene by the weight method as a function of percentage volatilization.*

intervals. They state that below about 480 °C the reaction is zero order, whereas above 510 °C they concede it is first order.

In view of this result by Wall and Michaelson, it was deemed advisable to check further on the rate order involved in the thermal degradation of this material in a vacuum. Although experiments by the pressure method were carried out in our earlier work at temperatures below 480 °C, the extent of volatilization was at most only 6.4 percent. Degradation had not been carried far enough to determine accurately whether the percentage loss versus time plots were straight or curved lines, i.e., whether the indicated reaction is of zero or first order. Rate experiments were therefore carried out by the weight method at lower temperatures, namely at 460, 475,

[1] S. L. Madorsky, V. E. Hart, S. Straus, and V. A. Sedlak, J. Research NBS **51**, 327 (1953) RP2461.
[2] In the earlier paper (see footnote 1), the abscissa of a similar graph (fig. 5) was incorrectly labelled log $(1/T)\times10^3$, whereas it should have been $(1/T)\times10^3$.
[3] L. A. Wall and J. D. Michaelson, J. Research, NBS **56**, 27 (1956) RP2644.

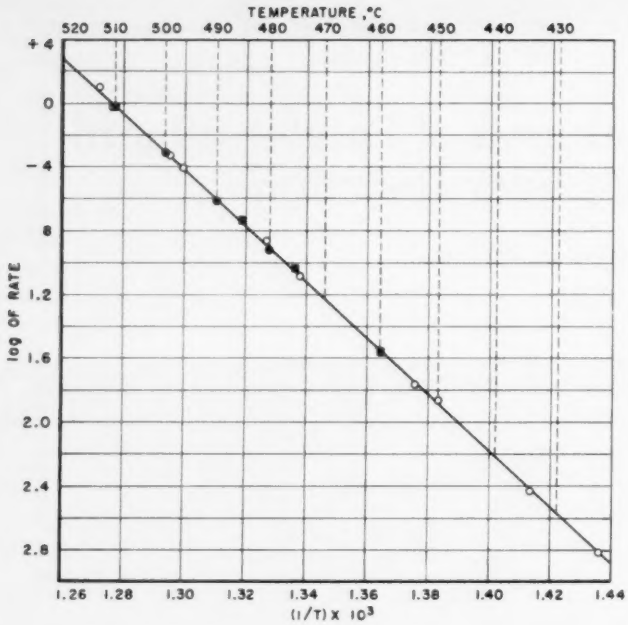

FIGURE 2. *Activation energy slope for thermal degradation of polytetrafluoroethylene.*

●—weight method (see footnote 1)
○—pressure method (see footnote 1)
■—present work.

and 485 °C, and the results are shown in figure 3, where percentage loss of weight is plotted against time. The curves are definitely not straight lines, as would have been the case if the reaction had followed a zero order.

In our previous work (see footnote 1) the rates were obtained by plotting the slopes between two neighboring experimental points in the volatilization-time plots. In the present work the slopes were calculated from the curves shown in figure 3, and the resulting rate curves based on these calculations are shown in figure 4. The same type of rate curves were obtained as in the earlier work. Values obtained for the initial rates at these three temperatures fit nicely into the Arrhenius plot, as shown by the squares in figure 2.

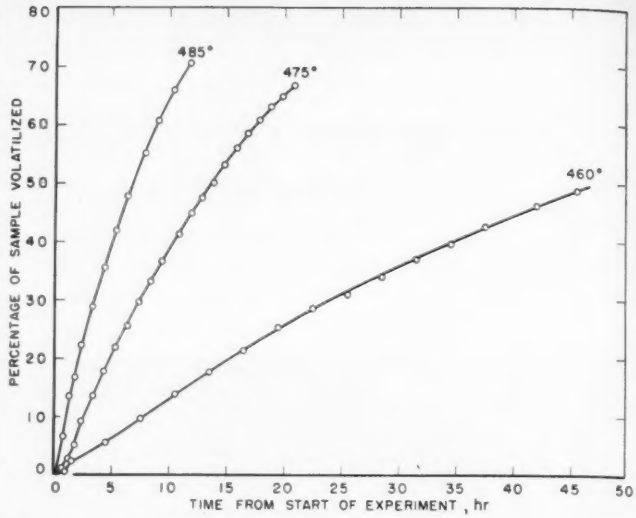

FIGURE 3. *Pyrolysis of polytetrafluoroethylene at low temperatures.*

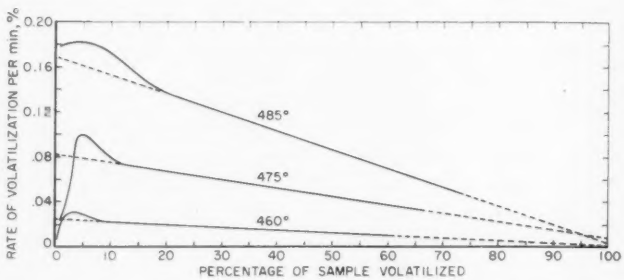

FIGURE 4. *Rates of thermal degradation of polytetrafluoroethylene at low temperatures.*

The present work therefore confirms our earlier conclusion that the degradation of polytetrafluoroethylene in a vacuum follows a first-order rate law, where the rate of volatilization, based on the sample, is directly proportional to the amount of residue.

(Paper 64A6–73)

JOURNAL OF RESEARCH of the National Bureau of Standards—A. Physics and Chemistry
Vol. 64A, No. 6, November–December 1960

Heat of Formation of Titanium Trichloride

Walter H. Johnson, Alexis A. Gilliland, and Edward J. Prosen

(August 2, 1960)

A calorimetric comparison of the heat of hydrolysis of $TiCl_4$(liq) with the heat of oxidation and hydrolysis of $TiCl_3$(c) has been made. The following value is reported for the combination of these data according to the process:

$$TiCl_3(c) + \tfrac{1}{2}I_2(c) + HCl(g) \rightarrow TiCl_4(liq) + HI(g),$$

$$\Delta H°(25\ °C) = 8.37 \pm 0.30\ \text{kcal/mole}.$$

A combination of this value with -192.3 ± 0.7 kcal/mole for the heat of formation of $TiCl_4$(liq) and with the standard heats of formation of HCl(g) and HI(g) gives for $TiCl_3$(c), $\Delta Hf°(25\ °C) = -172.4 \pm 0.8$ kcal/mole.

1. Introduction

Several independent determinations of the heat of formation of titanium trichloride have been reported during the past few years [1, 2, 3, 4, 5, 6].[1] The only values previously available were those estimated by Brewer, Bromley, Gilles, and Lofgren [7] and by Kubaschewski and Evans [8], which are now generally known to be low. The difficulties encountered in the purification of titanium trichloride and its reactivity toward oxygen and moisture have no doubt contributed to the scarcity of experimental data.

We conducted a number of experiments on the reaction between crystalline $TiCl_3$ and gaseous chlorine in a calorimetric vessel originally designed for measurement of the heat of formation of boron trichloride [9]. Although $TiCl_3$(c) is readily converted to $TiCl_4$(g) by the action of chlorine at about 300 °C, a portion of the finely divided sample was carried away by the gas stream. The insertion of a glass wool plug tended to reduce the transfer of $TiCl_3$, but the presence of adsorbed moisture introduced significant errors in the determination of the quantity of reaction.

We therefore decided to use a solution calorimeter to make a comparison between the heats of formation of $TiCl_3$(c) and $TiCl_4$(liq). When $TiCl_3$(c) is added to aqueous acid containing an oxidizing agent, the titanium is converted to the tetravalent state; the resulting solution may be reproduced by adding $TiCl_4$ to an acid solution which contains the reduced form of the oxidizing agent. The difference between the heats of formation of $TiCl_4$ and $TiCl_3$ may be determined from a combination of the heat of oxidation and hydrolysis of $TiCl_3$ with the heat of hydrolysis of $TiCl_4$ and with certain auxiliary data. This method is similar to that employed by Clifton and MacWood [1], except that the experiments were performed at 30 °C instead of 0 °C and iodine was used as the oxidizing agent instead of $FeCl_3$.

[1] Figures in brackets indicate the literature references at the end of this paper.

2. Source and Purity of Materials

The $TiCl_4$ and $TiCl_3$ were prepared by the Inorganic Chemistry Section of the Chemistry Division. The purity of the $TiCl_4$ was determined to be 99.99 mole percent by freezing point determinations made in the Pure Substances Section of the Chemistry Division. This material was the same as that used previously for the determination of the heat of formation of TiI_4 [9].

The purity of the $TiCl_3$ was determined by the Inorganic Chemistry Section to be greater than 99.8 percent. Analyses of the solutions obtained after hydrolysis indicated the purity to be 100 ± 0.2 percent.

The iodine, potassium iodide, and hydrochloric acid were reagent-grade materials used with no further purification. The hydriodic acid was redistilled and the constant-boiling fraction collected under a nitrogen atmosphere.

3. Apparatus and Procedure

The apparatus was the same as that used for the determination of the heat of formation of TiI_4 [9], except for minor changes. Capillary inlet and exit tubes were inserted through the calorimeter head to permit removal of oxygen by flushing with nitrogen. Calorimeter temperatures were measured by means of a platinum resistance thermometer. The thermometric system, the apparatus for measurement of electrical energy, and the calorimetric procedure have been described in previous reports [11, 12].

3.1. Hydrolysis of $TiCl_4$ (liq)

Samples, approximately 0.01 mole each, of the $TiCl_4$ were transferred into thin-walled, spherical Pyrex bulbs and sealed in vacuum. The calorimetric solution consisted of 0.01 mole KI, 0.02 mole I_2, 0.40 mole HCl, 0.01 mole HI, and 25.33 moles water. The iodine and KI were dissolved in a small quantity of water before adding the other

materials; the HI was taken from a constant-boiling solution and the HCl from a prepared 4N solution. The remainder of the water was added to bring the total weight up to the previously calculated value. The calorimeter was then assembled, placed in the constant-temperature calorimeter jacket, the stirrer connected, and oxygen removed by flushing with nitrogen. The inlet and exit tubes were then closed, leaving a slight positive pressure of about 1 mm above atmospheric pressure in the calorimeter.

Calorimeter temperatures were noted at 2-minute intervals during the initial rating-period, after which the sample bulb was crushed and temperatures measured at 1-minute intervals until thermal equilibrium was reestablished. Temperatures were then noted at 2-minute intervals during a final rating-period.

The rate of hydrolysis was quite rapid, the hydrolysis being essentially complete within one minute. In a few cases some of the calorimetric solution was splashed upon the upper walls of the vessel; in such cases the experiment was discarded. The reaction produced no noticeable difference in the color of the solution.

The calorimeter was calibrated in the same manner, except that an empty bulb was used and the temperature rise was derived from a carefully measured quantity of electrical energy introduced into the system.

3.2. Hydrolysis of $TiCl_3$(s)

Samples, approximately 0.01 mole each, of the finely divided $TiCl_3$ were transferred into glass bulbs in a dry-box under an atmosphere of nitrogen. The bulbs were capped while in the box, then removed and sealed.

The calorimetric solution was the same as that used for the experiments with $TiCl_4$, except that the HI was omitted and the quantities of iodine and HCl were increased to 0.025 and 0.41 mole respectively. The calorimetric procedure was the same as that described for the $TiCl_4$ experiments.

The rate of hydrolysis was quite rapid at first, but quickly slowed down; the hydrolysis was not complete after 1½ hrs at 25 °C. We found it necessary to raise the calorimeter temperature to 30 °C in order to obtain complete hydrolysis within one hour. The resulting solutions developed some turbidity after standing in air for a few hours. In a few cases the solutions were stored in completely filled and stoppered amber bottles; in these cases no turbidity appeared even after several days.

The system was calibrated with electrical energy, at 25 and at 30 °C, using both the initial and final solutions in order to obtain ΔCp for the actual calorimetric process. The effective heat capacity of the empty calorimeter was determined by substituting a known weight of distilled water for the calorimetric solution.

3.3. Heat of Solution of Iodine

The iodine samples, approximately 0.005 mole each, were sealed into glass bulbs. The calorimetric solution was the same as used for $TiCl_3$ experiments, except that only 0.02 mole of iodine was used. Because the solution of iodine resulted in a relatively small drop in the calorimeter temperature, it was possible to calibrate the actual system immediately prior to the measurement of the heat of solution and it was not necessary to duplicate the system exactly for replicate experiments.

3.4. Heat of Dilution of Hydrochloric Acid

A solution of hydrochloric acid containing 13.5 moles of water per mole of HCl was prepared. Samples of this solution, each containing approximately 0.01 mole of HCl, were sealed into glass bulbs. The calorimetric solution consisted of 0.10 mole KI, 0.02 mole I_2, 0.40 mole HCl, and 25.195 moles of water. Since the increase in the calorimeter temperature was small, it was possible to calibrate the actual system before each experiment as described above.

4. Data and Calculations

Values from the 1955 table of International Atomic Weights [13] were used in all calculations. Except where specified to the contrary, the final temperature and pressure were 25 °C and 1 atmosphere. One thermochemical calorie is taken as equivalent to 4.1840 joules.

The results of the calibration experiments on the $TiCl_4$ system are given in table 1. E is the electrical energy introduced into the system as measured by a method described previously [11, 12]. ΔRc is the temperature rise of the calorimetric system as measured with a particular platinum resistance thermometer and bridge, corrected by a method described previously [14]. The energy equivalent of the system E_s, is the ratio of the quantity of electrical energy to the resulting rise in temperature:

$$E_s = \frac{E}{\Delta Rc}.$$

TABLE 1. *Results of the calibration experiments on the* $TiCl_4$ *system*

Experiment	E	ΔRc	E_s
	j	*ohm*	*j/ohm*
1	1939.62	0.090254	21491
2	1937.46	.090022	21522
3	1936.64	.090053	21506
4	1934.99	.090001	21500
5	1936.37	.090235	21459
6	1931.84	.090000	21465
Mean			21490
Standard deviation of the mean			±10

The results of the experiments on the hydrolysis of $TiCl_4$ are given in table 2, where Δe is the deviation in the energy equivalent of the actual system from that of the calibrated system, ΔRc is the temperature

TABLE 2. *Results of the experiments on the hydrolysis of* $TiCl_4$

Experiment	Δe	ΔRc	q	$TiCl_4$ mole	$-\Delta H(25\ ^\circ C)$
	j/ohm	*ohm*	*j*		*kj/mole*
1	7.9	0.069850	1501.7	0.0062711	239.46
2	9.7	.082721	1778.3	.0074704	238.04
3	11.0	.091447	1966.2	.0082202	239.20
4	10.2	.085143	1830.6	.0076219	240.18
5	12.2	.099699	2143.8	.0089877	238.53
Mean					239.08
Standard deviation of the mean					±0.37

rise of the system, and q is the total energy evolved in the actual process. The following relationship was used:

$$q=(E_s+\Delta e)(\Delta Rc).$$

The data given in table 2 for the hydrolysis of $TiCl_4$ correspond to the process:

$$TiCl_4(liq)+[10KI+2I_2+Hf+40HCl+2533H_2O] \text{ (soln)} \rightarrow$$

$$[Ti^{4+}+4Cl^-+10KI+2I_2+HI+40HCl+2533H_2O] \text{ (soln)}; \quad (1)$$

$$\Delta H(25\ ^\circ C)=-57.14\pm0.18 \text{ kcal/mole.}$$

The results of the calibration experiments on the $TiCl_3$ system and of the oxidation and hydrolysis experiments on $TiCl_3$ are given in tables 3 and 4 respectively. These experiments were conducted at 30 °C in order to increase the rate of hydrolysis. Because of the relatively long period of time required for the establishment of thermal equilibrium, we failed to adjust the system precisely to a final temperature of 30 °C. A correction (q_t) for the thermal coefficient of the process was made to correct all data to this temperature. The data given in table 4 correspond to the process:

$$TiCl_3(c)+[10KI+2.5I_2+41HCl+2533H_2O] \text{ (soln)} \rightarrow$$

$$[Ti^{4+}+4Cl^-+10KI+2I_2+HI+40HCl+2533H_2O] \text{ (soln)}, \quad (2)$$

$$\Delta H(30\ ^\circ C)=-51.87\pm0.21 \text{ kcal/mole.}$$

The value of ΔCp for the process corresponding to eq (2) was determined to be −82 cal/°C mole; this gives for eq (2),

$$\Delta H(25\ ^\circ C)=-51.46\pm0.21 \text{ kcal/mole.}$$

The results of the experiments on the heat of solution of iodine, given in table 5, correspond to the process:

$$\tfrac{1}{2}\ I_2(c)+[10KI+2I_2+41HCl+2533H_2O] \text{ (soln)} \rightarrow$$

$$[10KI+2.5I_2+41HCl+2533H_2O] \text{ (soln)}; \quad (3)$$

$$\Delta H(25\ ^\circ C)=1.101\pm0.035 \text{ kcal/mole } I_2.$$

The results of the experiments on the dilution of hydrochloric acid are given in table 6 and correspond to the process:

$$[HCl+13.5H_2O] \text{ (soln)}+[10KI+2I_2+40HCl+2519.5H_2O] \text{ (soln)} \rightarrow$$

$$[10KI+2I_2+41HCl+2533H_2O] \text{ (soln)}; \quad (4)$$

$$\Delta H(25\ ^\circ C)=-0.603\pm0.004 \text{ kcal/mole HCl.}$$

TABLE 3. *Results of the calibration experiments on the* $TiCl_3$ *system*

Experiment	E	ΔRc	$E_s(30\ ^\circ C)$
	j	*ohm*	*j/ohm*
1	2282.25	0.105484	21636.0
2	2420.74	.111916	21630.0
3	2447.40	.113123	21634.9
4	2407.39	.111278	21634.0
5	2406.49	.111193	21642.5
Mean			21635.5
Standard deviation of the mean			±2.0

TABLE 4. *Results of the* $TiCl_3$ *oxidation and hydrolysis experiments*

Experiment	Δe	ΔRc	q	q_t	$TiCl_3$ mole	$-\Delta H(30\ ^\circ C)$
	j/ohm	*ohm*	*j*	*j*		*kj/mole*
1	11.5	0.126488	2738.09	5.59	0.0127267	215.58
2	7.8	.089936	1946.51	−0.13	.0089266	218.04
3	8.4	.095814	2073.79	−0.26	.0095228	217.74
4	8.2	.095842	2074.38	−0.31	.0095531	217.11
5	10.1	.109841	2377.57	−0.15	.0109743	216.64
Mean						217.02
Standard deviation of the mean						±0.44

TABLE 5. *Results of the experiments on the solution of iodine*

Experiment	E_s	$-\Delta Rc$	q	I_2 mole	$\Delta H(25\ ^\circ C)$
	j/ohm	*ohm*	*j*		*kj/mole*
1	21231	0.001051	22.31	0.0050000	4.462
2	21463	.000850	18.24	.0041636	4.381
3	21438	.000912	19.55	.0044386	4.405
4	21605	.001088	23.51	.0050785	4.629
5	21454	.001149	24.65	.0050579	4.874
6	21468	.001013	21.75	.0048742	4.462
7	21574	.001086	23.43	.0049308	4.752
8	21535	.001136	24.46	.0049956	4.896
Mean					4.608
Standard deviation of the mean					±0.074

TABLE 6. *Results of the experiments on the dilution of hydrochloric acid*

Experiment	E_s	ΔRc	q	HCl mole	$-\Delta H(25\ ^\circ C)$
	j/ohm	*ohm*	*j*		*kj/mole*
1	21622	0.001109	23.98	0.0094364	2.541
2	21588	.000972	20.98	.0083074	2.525
3	21441	.001158	24.83	.0099317	2.500
4	21425	.001236	26.48	.0104966	2.523
Mean					2.522
Standard deviation of the mean					±0.008

The heats of solution of HCl(gas) and of HI(gas) have been calculated from available data [15] for the following processes:

$$HCl(gas)+13.5H_2O(liq)\rightarrow [HCl+13.5H_2O]\ (soln);\quad (5)$$

$$\Delta H(25\ °C)=-16.77\pm0.01\ \text{kcal/mole},$$

$$HI(gas)+[10KI+2I_2+40HCl+2533H_2O]\ (soln)\rightarrow [10KI+2I_2+HI+40HCl+2533H_2O]\ (soln);\quad (6)$$

$$\Delta H(25\ °C)=-19.51\pm0.10\ \text{kcal/mole}.$$

The heat involved in diluting the KI–I_2–HCl solution by approximately 0.5 percent has been calculated to be negligible within the precision of these experiments. For simplification of calculations, however, the following process has been included:

$$13.5H_2O(liq)+[10KI+2I_2+40HCl+2519.5H_2O]\ (soln)\rightarrow [10KI+2I_2+40HCl+2533H_2O]\ (soln);\quad (7)$$

$$\Delta H(25\ °C)=0.00\pm0.01\ \text{kcal/mole}.$$

We may subtract eqs (1), (6), and (7) from the sum of eqs (2), (3), (4), and (5) to obtain the following theoretical process:

$$TiCl_3(c)+\tfrac{1}{2}I_2(c)+HCl(gas)\rightarrow TiCl_4(liq)+HI(gas);\quad (8)$$

$$\Delta H°(25\ °C)=8.37\pm0.30\ \text{kcal/mole}.$$

The change in enthalpy for eq (8) may be combined with -22.063 ± 0.002 and 6.20 ± 0.10 kcal/mole, the standard heats of formation of HCl(gas) and HI(gas) [15] respectively, to give:

$$TiCl_3(c)+\tfrac{1}{2}Cl_2(gas)\rightarrow TiCl_4(liq);\quad (9)$$

$$\Delta H°(25\ °C)=-19.89\pm0.32\ \text{kcal/mole}.$$

By taking -192.3 ± 0.7 kcal/mole for the heat of formation of $TiCl_4$(liq) [16],[2] we obtain:

$$TiCl_3(c),\ \Delta Hf°(25\ °C)=-172.4\pm0.8\ \text{kcal/mole}.$$

The results obtained from the experiments on the direct chlorination gave -19.9 ± 1.3 kcal/mole for the process corresponding to eq (9).

The uncertainties assigned to the values given in this paper are over-all uncertainties obtained by combining twice the standard deviation of the mean for the calibration and reaction experiments with reasonable estimates of all other known sources of error.

[2] The heat of vaporization of $TiCl_4$(liq) has been taken as 9.9 ±0.2 kcal/mole from the calorimetric data of Schaffer, Breil, and Pfeffer [2].

5. Discussion

The value obtained in this investigation is essentially the same as that obtained by Clifton and MacWood [1] from measurements of the energies evolved when $TiCl_3$(c) and $TiCl_4$(liq) were dissolved in an aqueous solution of HCl and $FeCl_3$.

Schaffer, Breil, and Pfeffer [2] measured the heat of chlorination of $TiCl_3$ at 57 °C and obtained −20.3 kcal/mole for the process corresponding to eq (9). They also measured the heat of reduction of $TiCl_4$ at 153 °C, with mercury as the reducing agent, and obtained −19.8 kcal/mole for eq (9). The values which they reported for the heat of formation of $TiCl_3$, however, were based upon the value calculated by Bichowsky and Rossini [17] for the heat of formation of $TiCl_4$(liq), which has since been shown to be low. If we combine the data obtained by Schaffer, Breil, and Pfeffer with -192.3 ± 0.7 kcal/mole for the heat of formation of $TiCl_4$(liq), we obtain −172.0 and −172.5 kcal/mole for the heats of formation of $TiCl_3$(c) obtained by the chlorination and reduction processes, respectively.

Krieve and Mason [3] studied the equilibrium:

$$TiCl_3(c)+HCl(gas)=TiCl_4(gas)+\tfrac{1}{2}H_2(gas),$$

and obtained $\Delta H_{690}=10.4$ kcal/mole. They estimated the ΔCp of the process to be −6 cal/deg mole, used Kelley's value of 9.6 kcal/mole [18] for the heat of vaporization of $TiCl_4$(liq) [2], and obtained −19.0 kcal/mole for eq (9). We have corrected their data by the use of 9.9 kcal/mole for the heat of vaporization of liquid $TiCl_4$ [2] and have obtained −19.3 kcal/mole for the process corresponding to eq (9). Combination of this value with −192.3 kcal/mole for the heat of formation of $TiCl_4$(liq), gives −173.0 kcal/mole for the heat of formation of $TiCl_3$(c).

Krieve, Vango, and Mason [4] reacted Ti(c), $TiCl_2$(c), and $TiCl_3$(c) with chlorine under pressure in a nickel-bomb calorimeter to form $TiCl_4$(liq). They obtained −190.0 and −20.9 kcal/mole for the heats of chlorination of Ti(c) and $TiCl_3$(c), respectively, and reported −169.1 kcal/mole for the heat of formation of $TiCl_3$(c). If we take their value for the heat of chlorination of $TiCl_3$(c) and use our value for the heat of formation of $TiCl_4$(liq), we obtain −171.4 kcal/mole for the heat of formation of $TiCl_3$(c).

Skinner and Ruehrwein [5] measured the heats of solution of Ti(c) and $TiCl_3$(c) in aqueous hydrofluroic acid. They obtained −170.0 kcal/mole for the heat of formation of $TiCl_3$(c).

Altman, Farber, and Mason [6] have reported values of −169.4 and −171.0 kcal/mole for the heat of formation of $TiCl_3$(c), based upon disproportionation and sublimation studies by Farber and Darnell [19, 20].

A summary of the results obtained by the various investigators is given in table 7. An examination of the results in this table indicates substantial

agreement on the difference between the heats of formation of $TiCl_3$(c) and $TiCl_4$(liq).

TABLE 7. *Heat of formation of* $TiCl_3$ *reported by the various investigators, kcal/mole at 25 °C*

$\Delta Hf_{TiCl_3(s)} - \Delta Hf_{TiCl_4(liq)}$	$-\Delta Hf_{TiCl_3(s)}$	Reference
19.9	172.4	1
20.3	172.0	2
19.8	172.5	2
19.3	173.0	3
20.9	169.1	4
	171.4	4
	170.0	5
	169.4	6
	171.0	6
19.9±0.3	172.4±0.8	This investigation.

6. References

[1] D. G. Clifton and G. E. MacWood, J. Phys. Chem. **60,** 309 (1956).

[2] H. Schaffer, G. Breil, and G. Pfeffer, Z. anorg. u. allgem. Chem. **276,** 325 (1954).

[3] W. F. Krieve and D. M. Mason, J. Chem. Phys. **25,** 524 (1956).

[4] W. F. Krieve, S. P. Vango, and D. M. Mason, J. Chem. Phys. **25,** 519 (1956).

[5] G. B. Skinner and R. A. Ruehrwein, J. Phys. Chem. **59,** 113 (1955).

[6] D. Altman, M. Farber, and D. M. Mason, J. Chem. Phys. **25,** 531 (1956).

[7] L. Brewer, L. A. Bromley, P. W. Gilles, and N. L. Lofgren, Paper No. 6 in L. L. Quill, Chemistry and metallurgy of miscellaneous materials, thermodynamics, National Nuclear Energy Series IV–19B, (McGraw-Hill Book Company, Inc., New York, N.Y., 1950).

[8] O. Kubaschewski and E. LL. Evans, Metallurgical thermochemistry, Vol. I (Academic Press Inc., New York 10, N. Y., 1951).

[9] W. H. Johnson, R. G. Miller, and E. J. Prosen, J. Research NBS **62,** 213 (1959) RP2956.

[10] W. H. Johnson, A. A. Gilliland, and E. J. Prosen, J. Research NBS **63A,** 161, (1959).

[11] E. J. Prosen, F. W. Maron, and F. D. Rossini, J. Research NBS **46,** 106 (1951) RP2181.

[12] J. R. Eckman and F. D. Rossini, BS J. Research **3,** 597 (1929) RP111.

[13] E. Wichers, J. Am. Chem. Soc. **78,** 3238 (1956).

[14] E. J. Prosen, Chapter 6 in Experimental thermochemistry, F. D. Rossini, ed. (Interscience Publishers, Inc., New York, N.Y., 1956).

[15] F. D. Rossini, D. D. Wagman, W. H. Evans, S. Levine, and I. Jaffe, Selected values of chemical thermodynamic properties, NBS Circ. 500 (U.S. Government Printing Office, Washington 25, D.C., 1952).

[16] W. H. Johnson, R. A. Nelson, and E. J. Prosen, J. Research NBS **62,** 1 (1959), RP2928.

[17] F. R. Bichowsky and F. D. Rossini, Thermochemistry of the chemical substances (Reinhold Publishing Corp., New York, N.Y., 1936).

[18] K. K. Kelley, Contributions to the data on theoretical metallurgy, III. The free energies of vaporization and vapor pressures of inorganic substances, U.S. Bureau of Mines, Bull. 383, (U.S. Government Printing Office, Washington 25, D.C., 1935).

[19] M. Farber and A. J. Darnell, J. Chem. Phys. **25,** 526 (1956).

[20] M. Farber and A. J. Darnell, J. Phys. Chem. **59,** 156 (1955).

(Paper 64A6–74)

JOURNAL OF RESEARCH of the National Bureau of Standards—A. Physics and Chemistry
Vol. 64A. No. 6, November–December 1960

Heat of Formation of Decaborane

Walter H. Johnson, Marthada V. Kilday, and Edward J. Prosen

(August 8, 1960)

The heat of formation of crystalline decaborane has been determined by calorimetric measurement of the heat of decomposition:

$$B_{10}H_{14}(c) \rightarrow 10B(am) + 7H_2(g),$$

$$\Delta H(25\ °C) = 82.8 \pm 5.9\ \text{kj/mole},\ (19.8 \pm 1.4\ \text{kcal/mole}).$$

With the heat of transition of crystalline to amorphous boron taken as 0.40 kcal/mole, we obtain for the heat of formation of decaborane:

$$\Delta Hf^{\circ}_{298.15} = -66.1\ \text{kj/mole},\ (-15.8\ \text{kcal/mole}).$$

1. Introduction

Combustion methods afford a convenient and precise method for determination of the heats of formation of a large number of compounds. In the case of decaborane, however, preliminary measurements of the heat of combustion of decaborane have been found to be very unreliable. Combustion experiments in an oxygen bomb failed to yield results of the required precision; the sample detonated in practically all cases and the combustion products included varying amounts of elemental boron and higher boron hydrides. There was also some uncertainty in the amount of dissolved boric acid and the possibility of the presence of boron oxides. In general, the experiments were performed with the decaborane sample in the form of a pellet. In some cases, in which the sample was burned in the form of loose crystals or of crystals intermixed with quartz fibers, the combustion residue also included decaborane. In other experiments a solution of decaborane in toluene was burned; the resulting quantity of carbon dioxide, however, indicated the formation either of elemental carbon or of boron carbide.

The quantity of boric acid found in the water-soluble portion of the combustion products varied from 75 to 95 percent of the theoretical amount calculated from the mass of sample. The resulting heat of combustion of decaborane (to crystalline boric oxide and liquid water) was −2004 kcal/mole. A reasonable estimate of the probable error in the heat of combustion of decaborane, as determined by the oxygen bomb process, is about 1 percent. In view of this information, it is obvious that the heat of formation calculated from the heat of combustion is subject to a relatively large uncertainty.

Liebhafsky [1][1] also determined the heat of combustion of decaborane. The heat of formation of decaborane [2] was taken as 8 kcal/mole, calculated from his results.

The decomposition of crystalline decaborane into amorphous boron and gaseous hydrogen proved to be the best method for calorimetric determination of the heat of formation. The results of this investigation are presented here.

2. Source and Purity of Materials

The decaborane was obtained from the General Electric Research Laboratory through the courtesy of A. E. Newkirk and A. L. Marshall. It was prepared by the pyrolysis of diborane and purified by several vacuum sublimations, the last two of which produced materials with no measurable difference in melting point. Prior to this investigation it was further purified by two successive vacuum sublimations and stored in a desiccator over magnesium perchlorate.

A mass spectrometric analysis of the helium[2] used showed it to contain less than 0.01 volume percent of air; the helium was further treated as described in the next section of this paper.

3. Apparatus

The isothermal jacket calorimeter has been described previously [3]. The calorimetric system consisted of the nickel-plated copper calorimeter can and cover into which was placed a weighed quantity of water, the calorimetric reaction vessel, and the platinum resistance thermometer. The apparatus for measuring calorimeter temperatures and electrical energy have been described previously [3, 4, 5].

[1] Figures in brackets indicate the literature references at the end of this paper.

[2] This analysis was performed by V. H. Dibeler of the Mass Spectrometry Section of the Atomic and Radiation Physics Division.

A diagram of the calorimetric decomposition vessel is given in figure 1. The vessel consisted of a quartz tube, wound with a 183-ohm nichrome heating coil, surrounded with a silver radiation shield, and a vacuum jacket. The decaborane sample was placed in the Vycor crucible at the lower end of the quartz tube. Helium entered at the top through a coarse capillary immediately above the vessel, flowed around the crucible and out through the glass helix. A nichrome wire attached to the crucible was led out of the vessel through the inlet tube and fastened to a circularly ground stopcock in the helium line. By turning the stopcock, the crucible could be raised without interrupting the flow of helium or permitting air to enter the vessel. An aluminum cover (not shown in the diagram) which fitted over the top of the vessel served to prevent loss of energy by radiation through the opening in the calorimeter can cover.

A diagram of the gas train is shown in figure 2. The helium was purified by passing it successively over titanium, copper, and copper oxide in a Vycor tube which was heated to 600 °C and through absorbers containing Ascarite, anhydrous magnesium perchlorate, and phosphorus pentoxide. The exit gases were passed successively through a capillary flowmeter, a trap cooled with liquid nitrogen, a Vycor tube containing copper oxide at 600 °C, two water-absorption tubes, each containing magnesium

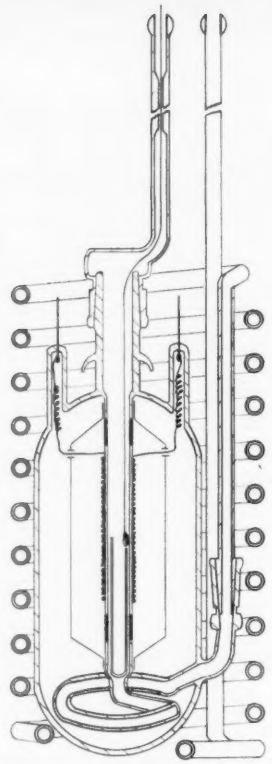

FIGURE 1. *Decomposition vessel.*

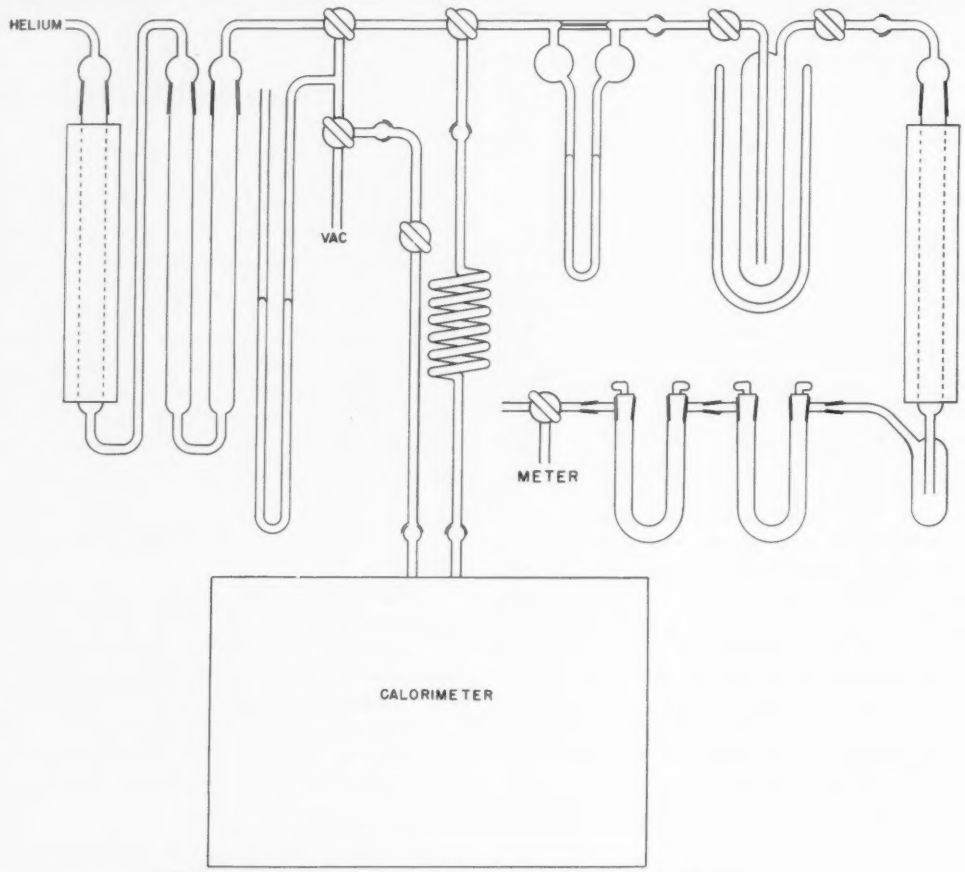

FIGURE 2. *Gas train used in decomposition of decaborane.*

perchlorate and phosphorus pentoxide, and a recording gas-volume meter.

The capillary flowmeter served for the approximate adjustment of the rate of flow of helium and also to indicate the rate of the decomposition process. The cold trap was included to collect any traces of volatile boron hydrides. The hydrogen evolved in the decomposition was burned to water in the copper-oxide heater and carried, as vapor, into the weighed absorption tube by the stream of dry helium. The portion of the water which collected as liquid in the bulb below the heater was evaporated by warming the bulb slightly. The second absorption tube served only to protect the first from moisture in the atmosphere. The total quantity of helium was measured by means of the recording gas-volume meter at the exit end of the gas train. The approximate temperature of the helium which entered the system during the experiment was measured by means of a thermometer placed in contact with the inlet tube of the decomposition vessel.

4. Procedure

The decaborane sample was placed in the weighed Vycor crucible and melted by heating with care in a helium atmosphere. When cool, the crucible plus sample was weighed, transferred to the decomposition vessel, and the vessel assembled. The vessel was placed in the calorimeter can, which contained 5,653 g water at 25.0 °C. The calorimeter assembly was lowered into the water bath, the temperature of which was adjusted to 27.0 °C and maintained constant to ± 0.001 °C.

Air was removed from the vessel by evacuation and by flushing with helium. Thermal equilibrium was established after about 20 minutes; the helium was then directed to by-pass the decomposition vessel and temperatures were observed at 2-minute intervals during a 20-minute initial rating period. Helium was then directed through the vessel and recording gas-volume meter, and an electric current was passed through the heating coil. About 6 minutes were required for the quartz tube to attain the decomposition temperature of about 650 °C. The crucible was then raised very slowly by turning the circularly ground stopcock until hydrogen began to be evolved as indicated by the increase in the reading on the capillary flowmeter. When the evolution subsided the crucible was again raised slightly; this process was continued until the crucible was located completely within the heated zone of the decomposition vessel. A period of about 6 minutes was required for elevation of the crucible and an additional period of 6 to 8 minutes was allowed for completion of the decomposition process. The heating current was then interrupted and the flow of helium through the vessel was continued for an additional 40 minutes to re-establish thermal equilibrium.

Measurements of the current through the heating coil and the potential drop across the coil were made alternately at 1-minute intervals during the heating period. Calorimeter temperatures were observed at 1-minute intervals during the entire 1-hour "reaction" period. The helium flow was then directed to by-pass the decomposition vessel and the recording gas-volume meter, and calorimeter temperatures were observed at 2-minute intervals during a final 20-minute rating period.

After the experiment the decomposition vessel was removed from the calorimeter and disassembled. Although most of the boron remained in the crucible, a significant amount was transported to the walls of the vessel. It was necessary to place a plug of glass wool in the helix in order to prevent some of the boron from being carried out of the calorimeter by the helium and hydrogen. Some small crystals of decaborane, apparently formed by sublimation, were found in the upper part of the vessel. These usually became dislodged and fell into the crucible during removal of the crucible from the vessel. It was therefore not possible to collect, quantitatively, all of the boron produced in the decomposition.

The quantity of decaborane decomposed was calculated from the weight of hydrogen, as water, produced by the process. The accuracy of this determination was checked by dissolving a weighed quantity of zinc in dilute sulfuric acid while a slow stream of helium was bubbled through the solution and directed through the gas train. The water vaporized from the solution was retained in the cold trap; the mass of water produced by burning the hydrogen agreed within 0.2 percent with the theoretical quantity calculated from the mass of zinc.

There was usually a small quantity of nonvolatile brownish material remaining at the top of the crucible which was assumed to consist of higher boron hydrides. The analysis of this material was complicated by contamination with decaborane as described above. An attempt was made to remove the decaborane by placing the residue in a tantalum boat and heating slowly to 300 °C in a stream of helium. The material which remained was weighed and then heated to 800 °C for 1 hour in vacuum. The loss in weight resulting from this treatment may be assumed to be due to removal of hydrogen from the residue. The amount of hydrogen remaining in the residue was indicated by this procedure to be approximately 0.2 percent by weight which corresponds to slightly less than 2 percent of the total hydrogen in the original material.

The energy equivalent of the calorimeter was determined in a separate series of experiments which were performed in the same manner as the decomposition experiments. In each case the calorimeter system was made to be nearly identical with that used in the decomposition experiments except that the decaborane sample was not present.

5. Results and Calculations

The molecular weights of boron, hydrogen, and water have been taken as 10.82, 2.016, and 18.016 g/mole, respectively. The following mean heat

capacities in j/° C mole for the range of 25 to 27 °C were used:

He(gas)	20.8	[2]
H_2(gas)	28.8	[2]
$B_{10}H_{14}$(c)	219.7	[6]
B(amorph)	11.1	[7].

The results of the electrical calibration experiments are given in table 1, where ΔRc is the corrected temperature rise [4, 8, 9], E is the quantity of electrical energy introduced, q_{He} is a correction applied to convert the temperatures of the inlet and exit helium to 25 °C, and E_s is the heat capacity of the standard calorimetric system obtained by the relationship:

$$\frac{E+q_{He}}{\Delta Rc}=E_s.$$

TABLE 1. *Results of the electrical calibration experiments*

Experiment	ΔRc	E	q_{He}	E_s
	ohm	*j*	*j*	*j/ohm*
1	0.183984	37350.3	1.0	203014
2	.161826	32848.2	2.8	203002
3	.169807	34488.3	2.0	203115
4	.188565	38301.9	2.6	203137
5	.235845	47888.1	3.5	203064
6	.256337	52016.6	3.1	202923
Mean				203042
Standard deviation of the mean				±32.4

The results of the decaborane decomposition experiments are given in table 2. The quantities q_{He}, q_{H_2}, q_B, and $q_{B_{10}H_{14}}$ are the corrections required to convert the actual decomposition process to the isothermal process at 25 °C. The change in enthalpy corresponding to the decomposition process was determined for each experiment by the relationship:

$$\Delta H(25\,°C)=\frac{E+q_{He}+q_{H_2}+q_B+q_{B_{10}H_{14}}-\Delta Rc(E_s)}{\text{mole } B_{10}H_{14}}.$$

Table 2. Results of the $B_{10}H_{14}$ decomposition experiments

Experiment	ΔRc	E	q_{He}	q_{H_2}	q_B	$q_{B_{10}H_{14}}$	Moles $B_{10}H_{14}$	ΔH(25 °C)
	ohm	*j*	*j*	*j*	*j*	*j*		*kj/mole*
1	0.178111	36330.0	2.9	−0.1	−0.4	−0.5	0.0018321	91.64
2	.180650	36806.8	1.8	.0	−.4	−.5	.0016701	76.76
3	.178745	36422.6	2.2	.0	−.3	−.5	.0016462	79.76
4	.176884	36023.9	2.2	−.1	−.3	−.4	.0016111	68.52
5	.215651	43948.5	3.6	−.2	−.4	−.4	.0017796	92.66
6	.236409	48154.4	2.8	−.3	−.3	−.4	.0016620	93.38
7	.213561	43512.3	1.6	−.2	−.4	−.5	.0017852	84.53
8	.238218	48496.6	2.7	−.3	−.4	−.4	.0017660	73.56
9	.221232 [a]	45046.1	3.5	−.2	−.3	−.4	.0016111	84.79
Mean								82.84
Standard Deviation of the mean								±2.96

[a] There is a correction of −33.0 j/ohm in the energy equivalent of the calorimeter system used for this experiment.

For conversion to the conventional thermochemical calorie, 1 calorie has been taken as equivalent to 4.1840 joules. The mean of the values given for ΔH in table 2 corresponds to the process:

$$B_{10}H_{14}(c)\rightarrow 10B(\text{amorph})+7H_2(g)$$

$$\Delta H(25\,°C)=82.8\pm5.9 \text{ kj/mole},$$

$$=19.8\pm1.4 \text{ kcal/mole}.$$

With the value 0.40 kcal/mole taken for the heat of transition of crystalline to amorphous boron [2], there is obtained for the heat of formation of decaborane:

$$\Delta Hf\,°(25\,°C)=-66.1 \text{ kj/mole},$$

$$=-15.8 \text{ kcal/mole}.$$

The heat of the transition from amorphous boron to the stable crystalline form has not been determined. Some preliminary measurements in this laboratory have indicated that it is small. The enthalpy change for the process:

$$B(c)\rightarrow B(\text{amorph}),$$

has been estimated to be 0.40 kcal/mole [1]. No uncertainty has been assigned to this arbitrary value.

There is also some ambiguity in regard to the thermodynamic state of the amorphous boron obtained from the decomposition of the hydride. Several types of amorphous boron may exist. In addition, the effect of the particle size is not known. The decomposition of the hydride, however, is believed to be a step-wise process and the nature of the resulting amorphous product, obtained at a given temperature, is expected to be independent of the boron-hydrogen ratio of the initial hydride.

The heat of formation of decaborane may be combined with the heats of formation of boric oxide [3] and water [2] to obtain the heat of combustion:

$$B_{10}H_{14}(c)+11\,O_2(g)\rightarrow 5B_2O_3(c)+7H_2O(liq),$$

$$\Delta Hc°(25\,°C)=-1989.1\pm4.0 \text{ kcal/mole}.$$

The uncertainties assigned to the values given in this paper have been taken as twice the standard deviation of the means of the calibration and decomposition experiments, combined with reasonable estimates of all other known sources of error.

6. Discussion

The heats of formation of diborane and pentaborane were determined in a similar manner by measurement of the heats of decomposition of the vapors [10]. In each of these cases the decomposition process was accompanied by the evolution of energy; in the case of decaborane, however, the process involves the absorption of energy. In every case the quantity of material decomposed was deter-

mined by measurement of the amount of hydrogen evolved. This method has the advantage of limiting the error introduced by incomplete decomposition to the difference between the mean energies of the broken and unbroken boron-hydrogen bonds multiplied by the fraction of unbroken bonds.

There is a possibility that some of the hydrogen may remain adsorbed on the amorphous boron at the decomposition temperature, but this quantity is believed to be small. Samples of amorphous boron produced by pyrolysis of diborane at 600 °C were heated to 850 °C in vacuum with no significant loss of weight.

Simons, Balis, and Liebhafsky [11] made an elemental analysis by heating decaborane in sealed palladium tubes to 900 °C in vacuum and were able to remove 99.99 percent of the available hydrogen. In view of these data it appears that any error introduced by incomplete decomposition or by adsorption of hydrogen on the amorphous boron residue is small in comparison with the uncertainty assigned to the experimental values.

7. References

[1] H. A. Liebhafsky, unpublished data.
[2] F. D. Rossini, D. D. Wagman, W. H. Evans, S. Levine, and I. Jaffe, Selected values of chemical thermodynamic properties, NBS Circ. 500 (U.S. Government Printing Office, Washington 25, D.C., 1952).
[3] E. J. Prosen, W. H. Johnson, and F. Y. Pergiel, J. Research NBS **62,** 43 (1959) RP2927.
[4] E. J. Prosen, F. W. Maron, and F. D. Rossini, J. Research NBS **46,** 106 (1951) RP2181.
[5] E. J. Prosen and F. D. Rossini, J. Research NBS **33,** 255 (1944) RP1607.
[6] G. T. Furukawa and R. P. Park, J. Research NBS **55,** 255 (1955) RP2627.
[7] H. L. Johnston, H. N. Hersh, and E. C. Kerr, J. Am. Chem. Soc. **73,** 1112 (1951).
[8] J. R. Eckman and F. D. Rossini, BS J. Research **3,** 597 (1929) RP111.
[9] E. J. Prosen, Chapter 6 in Experimental thermochemistry, F. D. Rossini, ed. (Interscience Publishers, Inc., New York, N.Y., 1956).
[10] E. J. Prosen, W. H. Johnson, and F. Y. Pergiel, J. Research NBS **61,** 247 (1958) RP 2901.
[11] E. L. Simons, E. W. Balis, and H. A. Liebhafsky, Anal. Chem. **25,** 635 (1953).

(Paper 64A6–75)

JOURNAL OF RESEARCH of the National Bureau of Standards—A. Physics and Chemistry
Vol. 64A, No. 6, November–December 1960

Ultra Low-Conductivity Water by Electrophoretic Ion Exclusion

Wolfgang Haller and H. C. Duecker

(July 11, 1960)

Ultra low-conductivity water has been prepared by recirculating it through an electric field of 1,000 volts/centimeter maintained between two ion selective membranes. It was possible to obtain consistently water with an electrical conductivity below the lowest values reported in the literature. The lowest conductivity value which could be reached was 0.039×10^{-6} ohm^{-1} cm^{-1} at 18 °C, indicating an ionic impurity content of only one third of the minimum previously reported. This corresponds to the conductivity of a sodium chloride solution at a concentration of 0.0010 parts per million.

1. Introduction

In the course of a kinetic diffusion study the authors were faced with the problem of preparing and maintaining ultra low-conductivity water which was to be circulated across the surface of a solid from which very small amounts of an ionic substance were released. It was considered important to remove continuously the incoming ions and to record simultaneously their flux. The method developed for this purpose was found to maintain the water at an extremely low conductivity level. In view of the fundamental importance of the properties of purest water to the physical sciences and because the method exceeds certain previous practical limits in the purification of water, this account of the method applied and the results obtained is given.

Ultra low-conductivity water has been prepared by distillation, ion exchange, and electrodialysis. The lowest conductivity water reported in the literature was obtained by Kohlrausch and Heydweiller [1] [1] after 36 consecutive vacuum distillations. The present authors chose a modified electrophoretic procedure as such a method served best the dual functions of ion removal and ion detection as required for the diffusion study. This paper, however, deals strictly with the purification function so that the detection function enters the discussion only to the extent that it appears necessary in describing the performance of the apparatus.

Electrophoretic water purification methods have in the past been used largely for processing of brine to obtain water of potable quality [2 through 6], an application where its use is rather a matter of cost than of ultimate purity. The general method of electrophoretically purifying an ion-containing liquid consists of subjecting it to an electrical field in which the cations and anions move toward their respective electrodes and recovering a portion of the liquid which has been depleted of ionic impurities. The isolation of the ion-depleted liquid is very difficult so that it has become the practice to introduce flow-channeling diaphragms. Such diaphragms can be simple porous separators [7], natural organic membranes [8], or synthetic membranes of preferred anionic or cationic permeability [9, 10, 11]. Because of the use of such membranes, electrophoretic purification procedures have been generally called electrodialysis, even in cases where the ion discriminating function of the membranes is not necessarily a fundamental feature of the purification mechanism.

[1] Figures in brackets indicate the literature references at the end of this paper.

2. Method and Materials

The basic features of the purification apparatus used in this study are illustrated in figure 1. A platinum impeller pump (A) circulates water through a closed loop consisting of a heat exchanger (B), the center compartment of the purification cell (C), the conductivity cell (D), and thermometer well (E). The impeller pump produces a head, or level difference, in the loop which is indicated by (Z) in the drawing. The center compartment of the purification cell is separated from the side cells by a cation permeable membrane (F) and an anion-permeable membrane (G). Electrodes (H, I) supply a d-c voltage to the electrolyte solutions contained in the side compartment of the purification cell. The cathode compartment (J) is filled with 0.05 N ammonium hydroxide and the anode compartment (K) is filled with 0.02 N sulfuric acid. The anodal and cathodal electrolytes are circulated through separate closed loops by means of a peristaltic action pump (L). The most important purpose of circulating the electrodal liquids is homogenization of the electrolyte concentration in the side compartments of the purification cell. Under the influence of the electric field anionic and cationic impurities migrate from the water in the center cell through the respective membranes, thus depleting the water in the center cell of ionic impurities. The regions of the electrolyte solutions next to the membranes tend to become reduced in their concentration of sulfate and ammonium ions. This tendency, if not counteracted by rapid circulation, would lead to regional

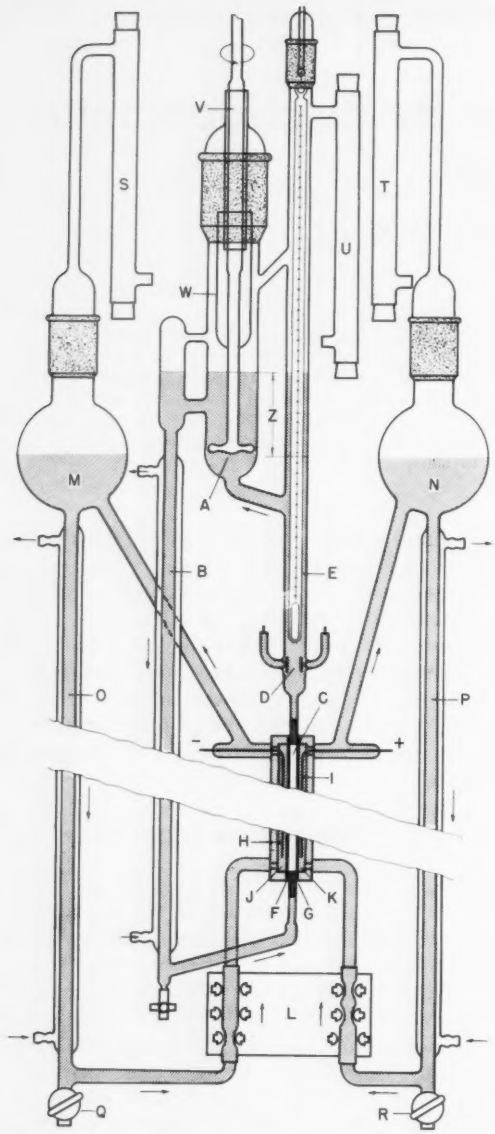

FIGURE 1. *Schematic of water purification apparatus.*

A, Impeller pump; B, heat exchanger; C, center compartment; D, conductivity cell; E, thermometer well; F, cation permeable membrane; G, anion permeable membrane; H, cathode; I, anode; J, cathode compartment; K, anode compartment; L, peristaltic pump; M, cathodal reservoir; N, anodal reservoir; O, heat exchanger; P, heat exchanger; Q,R, drainage stopcocks; S,T,U, breathing tubes; V, glass bearing; W, cup; Z, head produced by pump.

increases in the electrical resistance within the side cells, reducing the effective voltage gradient across the center cell. The rapid flow of the electrolyte past the platinum electrodes reduces gas polarization of the electrodes by carrying the gas bubbles into the reservoirs (M, N) where they are allowed to escape. The temperature of the electrodal liquids can be controlled by means of the heat exchangers (O, P).

The main body of the apparatus in contact with the liquids is constructed of borosilicate glass (Pyrex 7740) except the Teflon stopcocks of the drainage valves (Q, R). Tubing connections in the electrodal circuits and the flexible tubing sections through the peristaltic pump are made from plasticized polyvinyl resin (Tygon R–3603). Breathing tubes filled with silica gel and Ascarite (S, T, U) protect the system from the carbon dioxide of the atmosphere.

The water is circulated through the purification cell by means of a motor driven platinum impeller pump. The shaft of the impeller pump enters the system through a precision-bore ground glass bearing (V) which is lubricated with a medium-viscosity petroleum grease. A glass cup (W) sealed to the pump shaft prevents excess lubricant from being splattered into the circulating water.

An exploded view of the electrophoretic cell is given in figure 2. In operation, the two side cells (A, B) are pressed against the center cell (C), thus holding the two strips of ion selective membrane (D, E) in place. The side cells and the center cell are machined from high-density polyethylene sheet. The ion selective membranes are Nalfilm-1 and Nalfilm-2 (manufactured by National Aluminate Corp.). By application of sufficient pressure by means of a clamping device (not shown in the figure), the system is maintained leak-free without gaskets or sealant. The water enters and leaves the center cell through the nipples F and G respectively. The anodal liquid enters the side cell B through nipple H and leaves through I. Similarly the cathodal liquid enters and leaves the side cell A through nipples not visible in the drawing. The center compartment of the electrophoretic cell measures 0.3 cm from membrane to membrane, has a width of 0.6 cm and a length of 30.0 cm.

The electrophoretic cell is operated from a voltage stabilized d-c power supply capable of delivering up

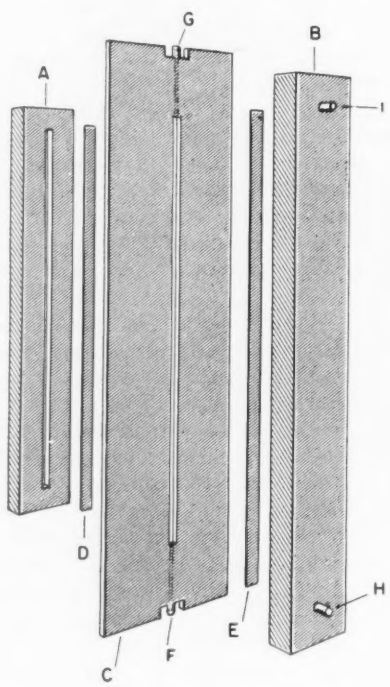

FIGURE 2. *Exploded view of electrophoretic cell.*

A, Cathodal side cell; B, anodal side cell; C, center cell; D, cation permeable membrane; E, anion permeable membrane; F,G, connections to center cell; H,I, connections to side cell.

to 200 ma between 0 and 1500 v. The cell current and voltage are measured with conventional instruments. Inasmuch as the resistance through the side cells is very much lower than that through the water in the center cell, the voltage drop across the center cell is almost identical to that across the electrodes. With the cell geometry and power supply described above, a voltage gradient of up to 5,000 v/cm can be produced.

3. Procedure and Performance

The cell constant of the conductivity cell was determined with 0.01 N potassium chloride solution at 18 and 25 °C using the method described by Daniels [12] and the conductivity values of Jones and Bradshaw [13]. The resistance measurements for the cell calibration were made with a calibrated a-c resistance bridge (General Radio type 650–A) capable of being read to within 0.3 percent. The cell constant was found to be 0.368 cm^{-1} with an error of ± 0.5 percent.

The resistance of the water in the conductivity cell was measured with a calibrated d-c megohm resistance bridge (General Radio type 544-BS8) since the polarization effects were found to be negligible. The thermometer above the conductivity cell was calibrated by comparison with a certified standard thermometer. The deviation of the temperature of the water between the electrodes of the conductivity cell and the temperature indicated on the thermometer was investigated by circulating water of constant and high purity through the system while lowering and raising the temperature of the water. Temperature readings were taken at the moment of bridge balance at unaltered bridge settings by approaching the resistance from both above and below. The maximum temperature deviation observed for identical conductivities at the rates of temperature change employed in the experiments was always smaller than 0.15 °C, and at room temperature was only 0.05 °C. The maximum conductivity error introduced by the temperature measurement was calculated to be ± 0.5 percent.

A number of precautions were taken to prevent the contamination of the water with organic substances and to reduce the influx of ions from the surface of the glass. Among these precautions were: (1) Before operating the purification apparatus, the glass parts were steamed for over 200 hr in such a way that the steam condensed on the inner surface of the equipment and washed away ions extracted from the glass; (2) the ion-permeable membranes were converted into the acid and hydroxyl forms, respectively, and soaked in successive portions of distilled water over a period of days to remove water-soluble residues; (3) the apparatus was operated several days in advance of an experiment with successive portions of organic-free distilled water to remove further traces of impurities in the apparatus.

During the purification of distilled water, the electrical conductivity, k, of the water in the conductivity cell was found to decrease with time, t, according to a power function, $k=at^b+c$, in which the value of the constant b depends on the operational parameters, such as the temperature, the type of contamination in the water, the voltage drop across the membranes, and the flow rates of the water and of the electrolyte. A plot of conductivity versus time in a typical experiment is shown in figure 3, the value of b in this case being —0.75. The values of b in other experiments were between —0.5 and —0.8. Upon approaching the terminal conductivity, the curve deviates from the power function and approaches a limiting, finite value.

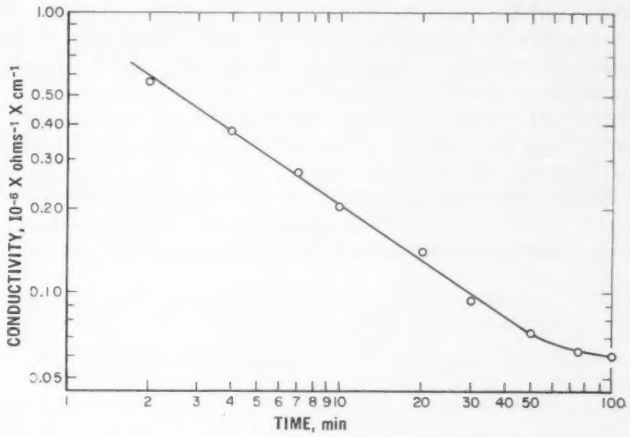

FIGURE 3. *Progress of water purification.*

The current consumption of the purification cell depends on the conductivity of the circulated water. Upon introduction of water with a conductivity of about 6×10^{-6} ohm^{-1} cm^{-1}, the current through the purification cell assumes within a few seconds a value of about 20 ma at 1,000 v. When the terminal conductivity is reached, the current consumption at 18° is approximately 2.2 ma at 1,000 v and obeys Ohm's law within 1 percent over the voltage range available. From the dimensions of the purification cell, and the electrical resistance of the cell at the terminal conductivity, a specific conductance of the water in the purification cell can be calculated. The average of the conductivities calculated in this manner from 20 experiments is tabulated in column (a) of table 1. Although the cell constant of the purification cell cannot be very accurately determined, it appears that the water leaving the purification cell is purer than in the conductivity cell.

TABLE 1. *Terminal experimental conductivities*

Temperatures	Specific conductivity in 10^{-6} ohm^{-1} cm^{-1}		
	(a) Purification cell		(b) Conductivity cell
°C	*avg*	*std dev*	*min values observed*
15.0±0.1	----	----	0.0330
18.0± .1	0.038	0.0006	.0390
20.0± .1	----	----	.0440
25.0± .05	.057	.0010	.0589
30.0± .1	----	----	.0775

4. Results and Discussion

Using the precautions outlined earlier it takes approximately 1 hr to approach a terminal conductivity after filling the apparatus with a good grade of distilled water. The terminal conductivity of the most successful of 20 experiments is tabulated in column (b) of table 1. Each value is subject to an estimated error of ± 1 percent. Prolonged operation of the apparatus over extended periods will not yield a water of higher purity than obtained after about 2 hrs.

The conductivities of ultra low-conductivity water reported by various researchers are given in table 2. For a better comparison the concentration of a solution of sodium chloride is calculated which would possess a specific conductivity corresponding to the reported values. These equivalent concentrations are given in table 2. The values are calculated using a theoretical conductivity of pure water equal to 0.0371×10^{-6} ohm^{-1} cm^{-1} at 18° and 0.0549×10^{-6} ohm^{-1} cm^{-1} at 25°. These values are calculated using the recent tabulations of the ionization constant and equivalent conductivities of the H^+ and OH^- ions given by Robinson and Stokes [23].

Kohlrausch and Heydweiller [1] obtained their water after 36 consecutive distillations in a vacuum and measured its conductivity in a fused silica cell which had been exposed to water for 10 yr. (Attempts by Nernst to reproduce this value were unsuccessful [24]). Kunin and McGarvey [20] report on water from a monobed ion exchange column although the temperature is not given. Those workers who used distillation methods incorporated one or more of the following modifications: (1) Distillation from an alkaline permanganate solution, (2) purging the solution and/or the distillate in the column with an inert gas to remove carbon dioxide, (3) use of materials of construction such as tin or organic substances to reduce mineral content.

The apparatus described by the present authors affords a method to produce water of lower ionic content than any previously reported in the literature. It is expected to be particularly applicable where it is desired to conduct experiments with small quantities (10 to 50 ml) of extremely ion-free water.

TABLE 2. *Data on ultra low-conductivity water, obtained by various workers*

Worker	Conductivity in 10^{-6} ohm^{-1} cm^{-1}	Temperature	Concentr. of a sodium chloride solution in ppm with same conductivity	Method of purification
		°C		
This work	0. 0390	18	0. 0010	Electrophoresis.
	. 0589	25	. 0018	
Kohlrausch and Heydweiller [1]	. 0429	18	. 0031	Distillation.
	. 062	25	. 0032	
Bengough, Stuart, and Lee [14]	. 045	18	. 0043	Do.
Kraus and Dexter [15]	. 048	18	. 0059	Do.
Weiland [16]	0. 053 to 0. 066	18	0. 0086 to 0. 0156	Do.
Bencowitz and Hotchkiss [17]	. 06 to . 07	Not given		Do.
Thiessen and Herrmann [18]	. 065 to . 080	25	. 0046 to . 0118	Do.
Kunin and McGarvey [19]	0. 07	Not given		Ion exchange.
Gostkowski [20]	. 07	0	0. 0280	Distillation.
Hulett [21]	. 081	Not given		Do.
Bourdillon [22]	. 086	18	. 0260	Do.
Pure water (theoretical)	. 0371	18	. 0000	
	. 0549	25	. 0000	
	. 0111	0	. 0000	

5. References

[1] F. Kohlrausch and A. Heydweiller, Wied. Ann. **53,** 209–235 (1894); Z. physik. Chem. **14,** 317–330 (1894).
[2] F. Bergsma, Chem. Weekblad **48,** 361–364 (1952).
[3] W. F. Langelier, J. Am. Water Works Assoc. **44,** 845–848 (1952).
[4] S. G. Wiechers and C. Van Hoek, Research **6,** 192–194 (1953).
[5] R. E. Eliassen, Civil Eng. **24,** (no. 6) 44–47 (1954).
[6] A. G. Winger et al., Ind. Eng. Chem. **47,** 50–60 (1955).
[7] P. H. Prausnitz, Glas und Keramische Filter, Akad. Verlagsgesellschaft MBH, Leipzig, p. 151 (1933).
[8] H. W. Morse and G. W. Pierce, Z. physik. Chem. **45,** 589–607 (1903).
[9] K. H. Meyer and W. Straus, Helv. Chim. Acta **23,** 795–800 (1940).
[10] T. R. E. Kressman, Nature **165,** 568 (1950).
[11] W. Juda and E. A. Mason, Chem. Eng. Progr. **55,** 155–162 (1959).
[12] F. Daniels et al., Experimental Physical Chemistry, pp. 163, 459 (McGraw-Hill Book Co., Inc. New York, N.Y., 1949).
[13] G. Jones and B. C. Bradshaw, J. Am. Chem. Soc. **55,** 1780–1800 (1933).
[14] G. D. Bengough, J. M. Stuart and A. R. Lee, J. Chem. Soc. **1927,** 2156–2161.
[15] C. A. Kraus and W. B. Dexter, J. Am. Chem. Soc. **44,** 2468–2471 (1922).
[16] H. J. Weiland, J. Am. Chem. Soc. **40,** 131–150 (1918).
[17] I. Bencowitz and H. T. Hotchkiss, Jr., J. Phys. Chem. **29,** 705–712 (1925).
[18] P. A. Thiessen and K. Herrmann, Chem. Fabrik **10,** 18 (1937).
[19] R. Kunin and F. McGarvey, Ind. Eng. Chem. **43,** 734–740 (1951).
[20] K. Gostkowski, Z. physik. Chem. **170,** 149–152 (1934).
[21] G. A. Hulett, Z. physik. Chem. **21,** 297–301 (1896).
[22] R. Bourdillon, J. Chem. Soc. **103,** 791–795 (1913).
[23] R. A. Robinson and R. H. Stokes, Electrolyte Solutions, 2d ed. (Academic Press Inc., New York, N.Y., 1959).
[24] H. S. Taylor, A Treatise on Physical Chemistry **1,** (D. Van Nostrand Co., New York, N.Y. 1925) (see footnote p. 521).

(Paper 64A6–76)

JOURNAL OF RESEARCH of the National Bureau of Standards—A. Physics and Chemistry
Vol. 64A, No. 6, November–December 1960

Spectrophotometric Determination of the Ionization Constant of Dimethylpicric Acid (2,4,6-Trinitro-3,5-xylenol) in Water at 25 °C

Marion Maclean Davis, Maya Paabo, and Robert A. Robinson[1]

(August 8, 1960)

The ionization constant of dimethylpicric acid (2,4,6-trinitro-3,5-xylenol) in water at 25 °C has been determined by a spectrophotometric method. The pK value 1.38 (K ≈ 0.042) was obtained. Potentiometric titrations, although less precise, yielded a pK value of the same magnitude.

1. Introduction

Moore and Peck [1][2] determined the pK of dimethylpicric acid by potentiometric titration, and reported the value 3.3. On the assumption that the effects of substituents on the ionization constant of phenol are additive, data on the ionization constants of phenol and its monosubstituted derivatives [2, 3] can be used to calculate 1.76 as an approximate pK value for dimethylpicric acid. Alternatively, data for 2,6-dinitrophenol [4], p-nitrophenol, and 3,5-xylenol [5] can be combined to give another estimate, 1.05. Combining data for 2,6-dinitrophenol and 4-nitro-3,5-xylenol [6] yields the estimate 1.96, whereas utilizing data for 2,4-dinitrophenol [7], o-nitrophenol, and 3,5-xylenol leads to the value 1.50. These four estimates, even though not in close agreement, suggest that dimethylpicric acid may be too strong for a reliable application of the method previously used for estimating pK [1]. Redetermination of its pK by a different method is therefore desirable.

This paper describes the determination of pK for dimethylpicric acid by a spectrophotometric procedure.

2. Experimental Procedure

2.1. Dimethylpicric Acid

Dimethylpicric acid (2,4,6-trinitro-3,5-xylenol) was prepared by nitrating 3,5-xylenol [1]. After isolation by conventional procedures, the product was finally recrystallized from cyclohexane and dried at 90 °C; mp 106.4 to 106.8 °C.[3] Potentiometric weight-titrations indicated a purity of not less than 99.9 percent.

2.2. Determination of pK Value by Spectrophotometry

The pK value was calculated from the equation

$$p\mathrm{K} = -\log[\mathrm{H}^+] - 2\log\gamma_{\pm} - \log[(D-D_1)/(D_2-D)], \quad (1)$$

in which $[\mathrm{H}^+]$ signifies the total hydrogen ion concentration in moles per liter, $\gamma_{\pm}$ is taken as the mean activity coefficient of aqueous hydrochloric acid of equivalent molarity,[4] and the symbols D_1, D_2, and D denote the spectral absorbances (optical densities) of solutions containing the same total molar concentration of dimethylpicric acid present as nonionized molecules, ionized molecules, or mixtures of the two, respectively. Dimethylpicric acid is so nearly completely ionized in water at the concentration used (5.004×10^{-5} M) in determining D_2 and D_1 values that addition of sodium hydroxide (pH ≈ 12) did not measurably alter the absorption curve. In determining D_1 values, the dimethylpicric acid was dissolved in ~2.2-M hydrochloric acid. The measurements of D values were made with solutions containing 1.250×10^{-4} M dimethylpicric acid together with hydrochloric acid in concentrations varying from ~0.01-M to ~0.1-M. The absorbances were obtained with a Beckman Model DU quartz spectrophotometer.

3. Results and Discussion

3.1. Spectrophotometric Determination of pK

Absorption curves for dimethylpicric acid in alkaline and acidic solutions are presented in figure 1. In measuring the absorption of dimethylpicric acid in hydrochloric acid solutions which varied from 1-M to 6-M in concentration, it was observed that with increasing concentrations of hydrochloric acid the absorption in the region from about 380 mμ to about 420 mμ gradually decreased to constant values. At

[1] Consultant to the Chemistry Division. Present address: University of New England, Armidale, New South Wales, Australia.
[2] Figures in brackets indicate the literature references at the end of this paper.
[3] The mp reported in [1] was 106.5 °C (uncor.).
[4] Values of $\gamma_{\pm}$ were interpolated from a graph of the mean activity coefficient of hydrochloric acid at 25 ° versus its molality (see [8], table 11-4-1A, p. 547). Harned and Ehler's function derived for 1:1 electrolytes in water was used to convert molarities of acid to the corresponding molalities (see table 12-1-1A of [8]).

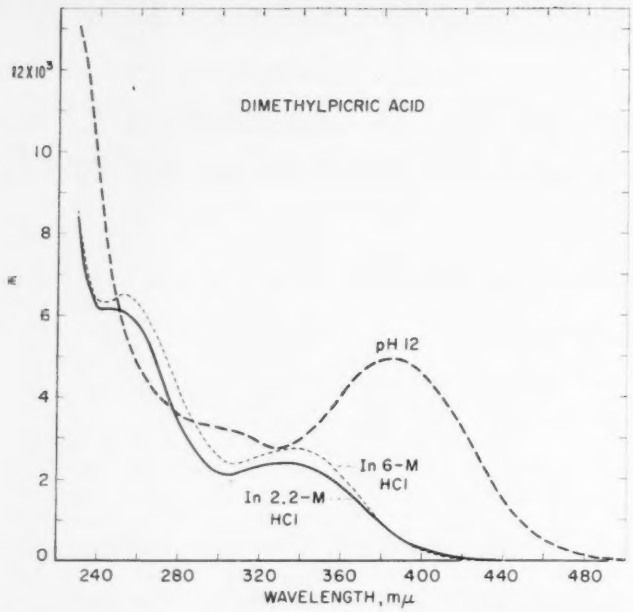

FIGURE 1. *Spectral absorption curves of dimethylpicric acid (2,4,6-trinitro-3,5-xylenol) in aqueous acid (approx. 2.2–*M HCl *and approx. 6–*M HCl*) and in aqueous alkali* (NaOH, pH ≈ *12*).

The curve for the solution containing 2.2-*M* HCl is believed to approximate closely the spectral absorption of nonionized dimethylpicric acid.

wavelengths shorter than 380 mμ, however, the absorption at first decreased and then progessively increased. It seems unlikely that this secondary change can be attributed to an impurity in the solutions; possibly, it involves nitro groups. The curves obtained for solutions of dimethylpicric acid in 2.2-*M* and 6-*M* hydrochloric acid illustrate the secondary change. The curve for 2.2-*M* hydrochloric acid solution is believed to approximate closely the spectral absorption of nonionized dimethylpicric acid.

In determining *p*K, absorbance values at 390, 400, and 410 mμ were used. Since the values of D_1 at these wavelengths are low and do not vary measurably with concentrations of hydrochloric acid greater than 3-*M*, the secondary change in absorption is believed not to have caused errors in determining *p*K.

The tabulated data and results are presented in table 1. The average *p*K value obtained was 1.376, or approximately 1.38 (corresponding to an ionization constant of about 0.042). This *p*K value falls within the range of the various estimated constants (see sec. 1).

3.2. Attempted Potentiometric Determination of *p*K

Attempts were made to determine *p*K by titrating 0.005-M dimethylpicric acid with alkali about 10 times as concentrated, using glass and saturated calomel electrodes [9].[5] This concentration of dimethylpicric acid is close to the limit of its solubility in water at 25 °C. Values of *p*K were calculated from the equation

$$pK = pH - \log\{([B^-]+[H^+])/([HB]-[H^+])\} + 0.5115\sqrt{I}/(1+1.5\sqrt{I}). \quad (2)$$

The *p*K values obtained from eight titrations varied from 1.26 to 1.66, yielding the average value 1.49. Considering the limited solubility and relatively high acidity of dimethylpicric acid, high precision and accuracy by potentiometric titration do not appear feasible for this compound. However, the average *p*K value obtained in this work agrees in general magnitude with the value determined spectrophotometrically.

TABLE 1. *Ionization constant of dimethylpicric acid (2,4,6-trinitro-3,5-xylenol) in water at 25 °C*[a,b]

Concentration of HCl[b]	D	$\log[(D-D_1)/(D_2-D)]$	$-\log[H^+]$[b]	$-2\log\gamma_\pm$	pK
		$\lambda=390$ mμ $D_1=0.064$, $D_2=0.612$			
0.0102	0.521	0.701	1.989	0.087	1.375
.0203	.462	.424	1.691	.115	1.382
.0332	.413	.244	1.478	.140	1.374
.0519	.359	.067	1.284	.164	1.381
.0623	.340	.006	1.205	.174	1.373
.104	.277	−.197	0.984	.200	1.381
		$\lambda=400$ mμ $D_1=0.029$, $D_2=0.568$			
0.0102	0.477	0.692	1.989	0.087	1.384
.0203	.422	.430	1.691	.115	1.376
.0332	.373	.246	1.478	.140	1.372
.0519	.321	.073	1.284	.164	1.375
.0623	.302	.011	1.205	.174	1.368
.104	.244	−.178	0.984	.200	1.362
		$\lambda=410$ mμ $D_1=0.011$, $D_2=0.495$			
0.0102	0.411	0.678	1.989	0.087	1.398
.0203	.366	.440	1.691	.115	1.366
.0332	.318	.239	1.478	.140	1.379
.0519	.271	.065	1.284	.164	1.383
.0623	.254	.003	1.205	.174	1.376
.104	.203	−.182	0.984	.200	1.366
Average					1.376
					K=0.042

[a] Concentration of dimethylpicric acid, 1.250×10^{-4} *M*. Optical absorption cells were 1 cm in length.
[b] All concentrations are in moles per liter.

4. References

[1] C. E. Moore and R. Peck, J. Org. Chem. **20,** 673 (1955).
[2] R. A. Robinson and A. I. Biggs, Trans. Faraday Soc. **51,** 901 (1955).
[3] A. I. Biggs, Trans. Faraday Soc. **52,** 35 (1956).
[4] G. Kortüm and H. Wilski, Z. physik. Chem. Frankfurt **2,** 256 (1954); J. F. J. Dippy, S. R. C. Hughes, and J. W. Laxton, J. Chem. Soc. (London) **1956,** 2995.
[5] E. F. G. Herington and W. Kynaston, Trans. Faraday Soc. **53,** 138 (1957).
[6] G. W. Wheland, R. M. Brownell, and E. C. Mayo, J. Am. Chem. Soc. **70,** 2492 (1948).
[7] R. G. Bates and G. Schwarzenbach, Helv. chim. acta **37,** 1069 (1954). See also H. von Halban and G. Kortüm, Z. physik. Chem. **A170,** 351 (1934); W. D. Bale and C. B. Monk, Trans. Faraday Soc. **53,** 450 (1957).
[8] H. S. Harned and B. B. Owen, The physical chemistry of electrolytic solutions (Reinhold Publishing Corp., New York, N.Y., 2d ed., 1950).
[9] M. M. Davis and H. B. Hetzer, J. Phys. Chem. **61,** 123 (1957).

(Paper 64A6–77)

[5] In part of the titrations a Precision-Shell titrometer was used; in others, a Beckman *p*H meter, model G.

JOURNAL OF RESEARCH of the National Bureau of Standards—A. Physics and Chemistry
Vol. 64A, No. 6, November–December 1960

Spectrophotometric Determination of the Ionization Constant of 2,4,6-Trinitro-*m*-cresol in Water at 25 °C

Marion Maclean Davis and Maya Paabo

(August 10, 1960)

The ionization constant of 2,4,6-trinitro-*m*-cresol in water at 25 °C was determined by a spectrophotometric procedure. The *p*K value 0.81 (K ≈0.16) was obtained.

1. Introduction

J. Kendall [1] [1] determined the conductivity of 2,4,6-trinitro-*m*-cresol (methylpicric acid) and its sodium salt in water, and concluded that a saturated solution (0.01–*M*) at 25 °C is about 92-percent dissociated. Applying the method of calculation described in [2] to these data gives a *p*K value of about 1 for trinitro-*m*-cresol. Values of *p*K for trinitro-*m*-cresol can be estimated by assuming that effects of substituents on the ionization constants of phenols are additive [2]. For example, by applying data for phenol and its monosubstituted derivatives the estimated *p*K value 1.66 is obtained. Data for 2,4-dinitrophenol, *o*-nitrophenol, and *m*-cresol lead to the *p*K value 1.41. A lower *p*K value, 0.95, is obtained by using *p*K values for 2,6-dinitrophenol, *p*-nitrophenol, and *m*-cresol. However, a substantially higher *p*K value (2.8) was obtained by a potentiometric procedure [3].

This paper describes the determination of *p*K for trinitro-*m*-cresol by a spectrophotometric procedure.

2. Method and Results

Commercial 2,4,6-trinitro-*m*-cresol of high purity was recrystallized successively from water, aqueous ethanol, and benzene-cyclohexane, and then dried at 80 °C for 2 hr; mp, 107.0 to 107.5 °C. Potentiometric weight-titrations indicated the purity was greater than 99.8 percent.

The spectrophotometric procedure used for determining *p*K was closely analogous to that described in [2]. In figure 1 molar absorption curves for ionized and nonionized trinitro-*m*-cresol are shown. Additional absorption curves were obtained in which the hydrochloric acid content varied from about 0.05–*M* to 6–*M*. The two isosbestic points shown in figure 1 remained fixed throughout.

Values of *p*K were calculated from absorbance measurements at 350 mμ, 380 mμ, and 410 mμ. The data and the calculated values of *p*K are summarized in table 1. These yield the average *p*K value 0.806, or approximately 0.81. The corresponding ionization constant is 0.156.

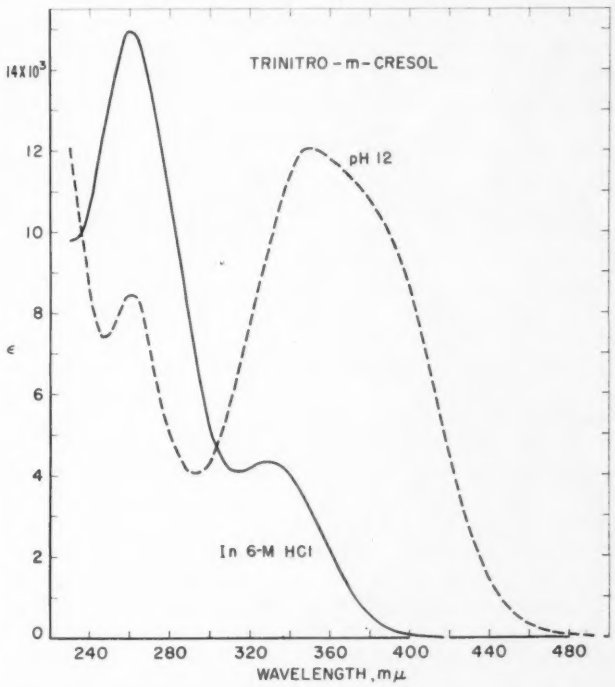

FIGURE 1. *Spectral absorption curves of 2,4,6-trinitro-m-cresol in aqueous acid (approx. 6–M HCl) and in aqueous alkali* (NaOH, *p*H ≈12).

The curve for a solution containing 4.5–*M* HCl was almost identical with that shown for 6–*M* hydrochloric acid solution.

3. References

[1] J. Kendall, Proc. Roy. Soc. (London) **A85,** 200 (1911).
[2] M. M. Davis, M. Paabo, and R. A. Robinson, J. Research NBS **64A,** 531 (1960).
[3] C. E. Moore and R. Peck, J. Org. Chem. **20,** 673 (1955).

[1] Figures in brackets indicate the literature references at the end of this paper.

TABLE 1. *Ionization constant of 2,4,6-trinitro-m-cresol in water at 25 °C* [a,b]

Concentration of HCl[b]	D	$\log[(D-D_1)/(D_2-D)]$	$-\log[H^+]$[b]	$-2\log\gamma_\pm$	pK[c]
		$\lambda=350$ mμ $D_1=0.156$, $D_2=0.604$			
0.0483	0.523	0.656	1.316	0.160	0.820
.0676	.503	.536	1.170	.177	.811
.0966	.477	.403	1.015	.196	.808
.171	.424	.173	0.766	.225	.818
.214	.405	.097	.669	.234	.806
.257	.380	.000	.590	.240	.830
.343	.357	−.089	.465	.244	.798
.483	.315	−.259	.316	.242	.817
		$\lambda=380$ mμ $D_1=0.027$, $D_2=0.538$			
0.0483	0.447	0.664	1.316	0.160	0.812
.0676	.423	.537	1.170	.177	.810
.0966	.395	.410	1.015	.196	.801
.171	.337	.188	0.766	.225	.803
.214	.312	.101	.669	.234	.802
.257	.286	.012	.590	.240	.818
.343	.259	−.080	.465	.244	.789
.483	.212	−.246	.316	.242	.804
		$\lambda=410$ mμ $D_1=0$, $D_2=0.329$			
0.0483	0.270	0.661	1.316	0.160	0.815
.0676	.257	.553	1.170	.177	.794
.0966	.237	.411	1.015	.196	.800
.171	.199	.185	0.766	.225	.806
.214	.184	.104	.669	.234	.799
.257	.165	.002	.590	.240	.828
.343	.155	−.050	.465	.244	[d] .759
.483	.120	−.241	.316	.242	.799
Average pK					0.808
K					.156

[a] The concentration of trinitro-*m*-cresol was 5.001×10^{-5} *M*. The optical absorption cells were 1 cm in length.
[b] All concentrations are in moles per liter.
[c] $pK=-\log[H^+]-2\log\gamma_\pm-\log[(D-D_1)/(D_2-D)]$. See [2].
[d] Discarded.

(Paper 64A6-78)

JOURNAL OF RESEARCH of the National Bureau of Standards—A. Physics and Chemistry
Vol. 64A, No. 6, November–December 1960

Method for the Separation of Titanium, Zirconium, Iron, and Aluminum from One Another and for their Subsequent Determination[1]

Thomas J. Murphy, W. Stanley Clabaugh, and Raleigh Gilchrist

(August 5, 1960)

A method is described for the separation of titanium, zirconium, iron, and aluminum from one another and for their subsequent determination. Iron is first precipitated with 1-nitroso-2-naphthol after complexing the titanium and zirconium with citrate to prevent their precipitation. Titanium and zirconium are then collectively precipitated with cupferron and subsequently separated from each other by precipitating the titanium with 8-hydroxyquinoline after complexing the zirconium with ethylenediaminetetraacetic acid. Aluminum and zirconium are recovered from their respective solutions by precipitation with cupferron.

The accuracy of the method was proved by analyzing synthetic solutions containing known amounts of the four elements.

1. Introduction

This paper describes the separation and determination of titanium, zirconium, iron, and aluminum in barium titanate ceramic dielectrics. These ceramic dielectrics may be dissolved by digestion on the steam bath overnight in a solution containing equal volumes of hydrochloric acid and water. Any undissolved residue may be brought into solution by fusing it with sodium carbonate and treating the resulting fusion with diluted hydrochloric acid. Titanium, zirconium, iron, and aluminum can then be sharply separated from the alkaline earths, the alkalies, and silicon by a double precipitation with 8-hydroxyquinoline.

The procedure described here starts with the collective precipitation of the four elements by 8-hydroxyquinoline. Much of the analytical chemistry involved is new and should have application to analytical problems other than those of ceramic dielectrics.

2. Reagents

Standard Titanium Solution: Fifty milliliters of titanium tetrachloride, purified according to the directions of Clabaugh, Leslie, and Gilchrist [1],[2] was slowly added to 100 ml of ice cold water. The resulting solution was diluted to 2.5 liters with diluted hydrochloric acid (1+1).[3] Three 50-g portions of this diluted solution, measured with a weight buret, were each diluted to 250 ml and the titanium content determined by precipitating with cupferron and igniting the precipitate to TiO_2.

Standard Iron Solution: About 20 g of ferric chloride hexahydrate, American Chemical Society Reagent grade, was dissolved in 200 ml of diluted hydrochloric acid (1+1). The resulting solution was diluted to 2 liters with water. The titer was determined in a manner similar to that for titanium.

Standard Zirconium Solution: About 65 g of zirconium sulfate tetrahydrate, purified according to the procedure described by Clabaugh and Gilchrist [2], was dissolved in 1 liter of diluted hydrochloric acid (1+3) and the resulting solution then diluted to 2 liters with diluted hydrochloric acid (1+3). The titer was determined in a manner similar to that for titanium. This titer also includes any hafnium present in the zirconium.

Standard Aluminum Solution: About 4 g of pure metallic aluminum was dissolved in 400 ml of diluted hydrochloric acid (1+2) and the resulting solution then diluted to 2 liters with water. Three 50-g portions of this diluted solution, measured with a weight buret, were each diluted to 250 ml. To each of these solutions 10 ml of acetic acid was added. The acidity was then reduced to value of *p*H 5.0 with diluted ammonium hydroxide (1+1). The aluminum content was determined by precipitating with 8-hydroxyquinoline and igniting the precipitate to Al_2O_3.

1-Nitroso-2-Naphthol Reagent Solution: Commercially available samples of 1-nitroso-2-naphthol were found to contain significant amounts of residue on ignition. For three different samples the residues amounted to 0.07 percent, 0.14 percent, and 0.19 percent. Spectrochemical examination of one of the residues showed that it was primarily Fe_2O_3, and also contained about 10 percent each of MgO and SiO_2.

Five grams of 1-nitroso-2-naphthol was placed in a 25-ml porous porcelain filtering crucible and

[1] Financial support of this work was furnished by the Diamond Ordnance Fuze Laboratories, Department of the Army, Washington 25, D.C.

[2] Figures in brackets indicate the literature references at the end of this paper.

[3] When the use of an acid is prescribed with no indication of strength or dilution, the acid to be used is the concentrated acid. Dilutions are indicated by the volumes of acid and water mixed to prepare a diluted reagent. Diluted hydrochloric acid (1+x) means a diluted acid prepared by mixing 1 volume of the concentrated acid with x volumes of distilled water. Similar designations are used for ammonium hydroxide.

leached with 800 ml of water heated to 60 °C. This treatment dissolved about 0.5 g of the reagent. Five hundread ml of diluted ethanol (1+1), heated to about 60 °C, was then passed through the filter and this dissolved most of the water-washed material. The porcelain filter and residue were air-dried and weighed. The concentration of the reagent in the alcoholic solution was determined by difference. This treatment reduced the residue on ignition from 0.07 to 0.01 percent. *This reagent solution must be freshly prepared since it decomposes on standing.*

Cupferron Reagent Solution: Five grams of cupferron, the ammonium salt of nitrosophenylhydroxylamine, was dissolved in 100 ml of water. *This solution must be freshly prepared since it decomposes on standing.*

Ammonium Acetate Reagent Solution: Five hundred milliliters of acetic acid was cooled in an ice bath and ammonium hydroxide was slowly added to the cold solution until the *p*H of the resulting solution was 7.[4]

Ethylenediaminetetraacetic Acid: To prepare ethylenediaminetetraacetic acid suitable for use, the practical grade was dissolved in a solution of ammonium hydroxide. This solution was filtered and then neutralized to *p*H 1 with hydrochloric acid to reprecipitate the ethylenediaminetetraacetic acid. The precipitate was caught on a filter, washed well with distilled water, and dried at 100 °C.

Other Reagents: All the other reagents used conformed to the specifications of the American Chemical Society for reagent chemicals.

3. Development of the Procedure

3.1. Separation of Iron From Titanium, Zirconium, and Aluminum

Ferric iron is reported to be quantitatively precipitated by 1-nitroso-2-naphthol, ($C_{10}H_7O_2N$), in the *p*H range 0.95 to 2.00 [3]. The iron is precipitated as ferric nitrosonaphtholate [4], $Fe(C_{10}H_6O_2N)_3$, which can be ignited to ferric oxide [5], Fe_2O_3. Titanium and zirconium are also reported to precipitate with 1-nitroso-2-naphthol from weak acid solutions [6]. Aluminum does not form an insoluble precipitate with 1-nitroso-2-naphthol.

Citrate ion was found to prevent the precipitation of titanium and zirconium nitrosonaphtholates from weakly acid solution, at about *p*H 1.5. Ferric iron was found to precipitate quantitatively from a citrate solution in the *p*H range 1.0 to 2.0. Since aluminum is not precipitated by 1-nitroso-2-naphthol, and since citrate ion prevents the precipitation of titanium and zirconium, the possibility of separating iron from these elements by the precipitation of ferric nitrosonaphtholate from a citrate solution was investigated.

It was found that when precipitations of iron were attempted from solutions having a volume of about 350 ml and containing 500 mg of TiO_2 and 50 mg of Fe_2O_3, or 500 mg of ZrO_2 and 50 mg of Fe_2O_3, or 500 mg of Al_2O_3 and 50 mg of Fe_2O_3, the results were always high. This was thought to be due to the fact that 1-nitroso-2-naphthol is not very soluble under these conditions and that the ferric nitrosonaphtholate forms so slowly that most of the 1-nitroso-2-naphthol precipitates from solution and adsorbs some of the metallic ions. Ethanol increased the solubility of 1-nitroso-2-naphthol and improved the separation, provided that the ethanol content did not exceed 75 ml of 95-percent ethanol in 350 ml of solution and provided that at least a 0.2-g excess of 1-nitroso-2-naphthol was present. If more ethanol or less 1-nitroso-2-naphthol were present, the precipitation of iron was not complete.

a. Separation of Iron From Titanium

Eight synthetic mixtures of iron and titanium were prepared from the respective standard solutions. Each solution contained an amount of titanium equivalent to 500 mg of TiO_2 and an amount of iron equivalent to from 0.2 mg to 50 mg of Fe_2O_3. Ten grams of citric acid and 1.8 g of 8-hydroxyquinoline were added to each solution. The citric acid was added to complex the titanium. The 8-hydroxyquinoline was added to approximate the amount of this reagent that would be present if the mixture was first precipitated with 8-hydroxyquinoline to separate this group of elements from the alkalies and alkaline earths and then taken into solution as described in section 4.1.

The acidity of each solution was adjusted to *p*H 1.5 with diluted ammonium hydroxide (1+1), and then the iron was precipitated with 1-nitroso-2-naphthol reagent solution as described in section 4.2.

The results of these separations are given in table 1.

TABLE 1. *Results obtained in the separation of iron from titanium by 1-nitroso-2-naphthol*

Experiment	Titanium dioxide	Ferric oxide		
	Added	Added	Found	Error
	mg	*mg*	*mg*	*mg*
1	500	0.2	0.2	0.0
2	500	.5	.5	.0
3	500	2.5	2.6	+.1
4	500	4.1	4.3	+.2
5	500	5.1	5.2	+.1
6	500	11.2	11.3	+.1
7	500	23.4	23.6	+.2
8	500	48.8	48.9	+.1

Chemical analysis of 50 mg of Fe_2O_3, separated from 500 mg of TiO_2, showed that the Fe_2O_3 contained slightly more than 0.1 mg, but less than 0.2 mg of TiO_2.

b. Separation of Iron From Zirconium

Five synthetic mixtures of iron and zirconium were prepared from the respective standard solutions. Each solution contained an amount of zir-

[4] All *p*H measurements were made with a glass-electrode *p*H meter.

conium equivalent to 500 mg of ZrO_2 and an amount of iron equivalent to from 0.5 mg to 50 mg of Fe_2O_3.

The synthetic mixtures were treated exactly as the iron-titanium mixtures in section a, and the iron in each solution was separated and determined by the method described in section 4.2.

The results of these separations are given in table 2.

TABLE 2. *Results obtained in the separation of iron from zirconium by 1-nitroso-2-naphthol*

Experiment	Zirconium dioxide	Ferric oxide		
	Added	Added	Found	Error
	mg	*mg*	*mg*	*mg*
1	500	0.5	0.5	0.0
2	500	2.6	2.6	.0
3	500	11.1	11.0	−.1
4	500	24.0	24.1	+.1
5	500	51.4	51.6	+.2

Chemical analysis of 50 mg of Fe_2O_3, separated from 500 mg of ZrO_2, showed that the ferric oxide contained about 0.1 mg of ZrO_2.

c. Separation of Iron From Aluminum

Five synthetic mixtures of iron and aluminum were prepared from the respective standard solutions. Each solution contained an amount of aluminum equivalent to 500 mg of Al_2O_3 and an amount of iron equivalent to from 0.5 mg to 50 mg of Fe_2O_3.

The synthetic mixtures were treated exactly as the iron-titanium mixtures in section a, and the iron in each solution was separated and determined by the method described in section 4.2.

The results of these separations are given in table 3.

TABLE 3. *Results obtained in the separation of iron from aluminum by 1-nitroso-2-naphthol*

Experiment	Aluminum oxide	Ferric oxide		
	Added	Added	Found	Error
	mg	*mg*	*mg*	*mg*
1	500	0.5	0.6	+0.1
2	500	2.5	2.6	+.1
3	500	10.2	10.3	+.1
4	500	24.6	24.5	−.1
5	500	50.5	50.4	−.1

Chemical analysis of 50 mg of Fe_2O_3, separated from 500 mg of Al_2O_3, showed that the ferric oxide contained about 0.1 mg of Al_2O_3.

3.2. Separation of Titanium and Zirconium From Aluminum

Titanium and zirconium are reported to be quantitatively separated from aluminum by precipitation with cupferron from strongly acidic solution [7]. Titanium is precipitated as titanium cupferrate [8], $Ti(C_6H_5N_2O_2)_4$, which can be ignited to TiO_2. The literature does not report the formula of the zirconium cupferrate, but, by analogy, it is probably $Zr(C_6H_5N_2O_2)_4$, which can be ignited to zirconium dioxide [9], ZrO_2.

Synthetic mixtures containing 50 mg of Al_2O_3 and 500 mg of TiO_2, and synthetic mixtures containing 50 mg of Al_2O_3 and 500 mg of ZrO_2 were prepared from their respective standard solutions and the volumes adjusted to approximately 400 ml. Ten grams of citric acid was added to each solution, the solutions were neutralized to *p*H 1.5 with diluted ammonium hydroxide (1+1), and 50 ml of hydrochloric acid added to each. A sufficient quantity of cupferron reagent solution was added to each solution to precipitate the titanium or zirconium and provide about 10 ml, 0.5 gram of cupferron, in excess. The solutions were allowed to stand in a refrigerator for about 4 hr and were filtered through 12.5-cm papers.[5] The filters and precipitates were washed with a 0.1-percent solution of cupferron in diluted hydrochloric acid (1+9), then transferred to 150-ml beakers and decomposed by heating with an infrared lamp. The beakers were then placed in an electric furnace at 450° C and maintained at this temperature overnight or until there was no visible evidence of carbon. The beakers were gradually cooled to room temperature, and 30 ml of diluted sulfuric acid (1+1) was added to each. The beakers were covered and heated gently on an electric hot plate until the oxides were dissolved. The solutions were cooled, transferred to 600-ml beakers, and diluted to 400 ml with water.

The titanium or zirconium in each solution was reprecipitated, filtered, and washed as described above. To determine the amount of aluminum that contaminated the first precipitate, the filtrates from the second precipitation of titanium or zirconium were cooled in an ice bath and their acidities adjusted to *p*H 4.0 with ammonium hydroxide. The solutions, after standing overnight in a refrigerator, were filtered through 9-cm papers, and the precipitates were washed with a 0.5-percent aqueous solution of cupferron, ignited in porcelain crucibles, and weighed as Al_2O_3. The results, given in table 4, show that a considerable amount of aluminum had precipitated with the first titanium or zirconium cupferrates.

TABLE 4. *Comparison of results obtained by varying the conditions of precipitation in the separation of titanium and zirconium from aluminum by cupferron*

Experiment	Conditions of precipitation	TiO_2	ZrO_2	Al_2O_3	Al_2O_3 found in cupferron precipitate
		Added	Added	Added	
		mg	*mg*	*mg*	*mg*
1	Normal	500		50	1.0
2	Revised	500		50	0.1
3	Normal		500	50	.3
4	Revised		500	50	.0

[5] All filter paper used was quantitative, ashless filter paper of close, dense texture suitable for retaining the finest precipitates.

It was found, however, that if slightly less cupferron than the amount necessary to precipitate completely the titanium or zirconium was added, and the solution heated to about 60° C and stirred continually, the precipitated cupferrates changed from a bulky, flocculent form to a dense and compact form. The precipitation of titanium or zirconium was then completed by the slow addition of cupferron reagent solution until a permanent precipitate no longer formed. Finally, the solutions were cooled and an additional 10 ml of the cupferron reagent solution was added to each.

Figure 1 shows a comparison of the volumes of equal amounts of titanium precipitated with cupferron by the normal method and by the revised method. Figure 2 shows a similar comparison in the case of zirconium. The amounts of titanium and of zirconium involved were equivalent to 500 mg of their respective dioxides.

FIGURE 1. *Comparison of the volumes of equal amounts of titanium precipitated with cupferron by the normal method, A, and the revised method, B.*

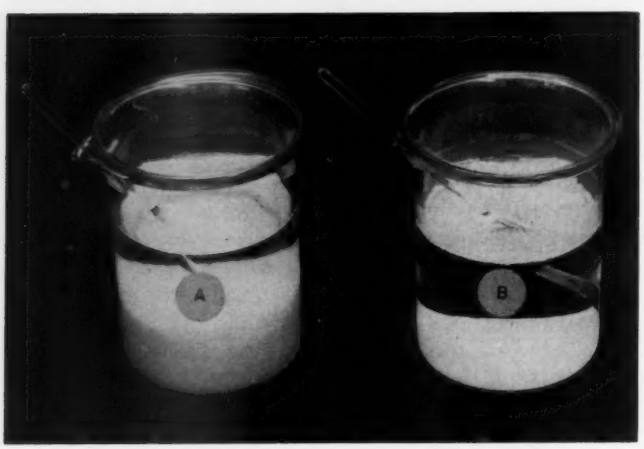

FIGURE 2. *Comparison of the volumes of equal amounts of zirconium precipitated with cupferron by the normal method, A, and the revised method, B.*

It was reasoned that since the volumes of the precipitates were much smaller by the revised method of precipitation, a better separation of titanium and zirconium from aluminum might be effected. Synthetic mixtures containing 50 mg of Al_2O_3 and 500 mg of TiO_2, and also mixtures containing 50 mg of Al_2O_3 and 500 mg of ZrO_2, were prepared from the standard solutions. The separations were effected by the revised procedure described above. The results, also reported in table 4, show that the amount of aluminum that was precipitated with the titanium and zirconium was significantly reduced.

3.3. Recovery and Determination of Aluminum

Aluminum is reported to be quantitatively precipitated by cupferron from weakly acid solution, probably as $Al(C_6H_5N_2O_2)_3$. This compound can be ignited to [10] Al_2O_3.

The completeness of precipitation of aluminum by cupferron from a solution containing large amounts of ammonium chloride and ammonium citrate was determined by the analyses of four synthetic solutions of aluminum containing from 0.5 mg to 50 mg of Al_2O_3 which were prepared from the standard solutions. Ten grams of citric acid and 50 ml of hydrochloric acid were added to each solution and the solutions were then diluted to 400 ml. The acidity of each solution was adjusted to *p*H 4.0 with ammonium hydroxide. Enough cupferron reagent solution was added to furnish a 1-g excess of cupferron. The solutions were allowed to stand overnight in a cold box. The precipitates were caught on 12.5-cm papers, washed with a 1-percent solution of cupferron, and ignited to Al_2O_3 in porcelain crucibles at 1,100 °C.

The results of these determinations are given in table 5. In each instance the recovery of the added aluminum was complete.

TABLE 5. *Recovery of aluminum by precipitation with cupferron*

Experiment	Aluminum Oxide		
	Added	Found	Error
	mg	*mg*	*mg*
1	0.5	0.5	0.0
2	4.8	4.7	−.1
3	23.4	23.3	−.1
4	51.5	51.7	+.2

3.4. Separation of Titanium From Zirconium

In weakly acid solution, ethylenediaminetetraacetic acid forms a strong mole-to-mole complex with zirconium [11] and a weaker one with titanium [12]. Sen Sarma and Mallik [13] state that the zirconium complex is strong enough to prevent the precipitation of zirconium by 8-hydroxyquinoline in weakly acid solution. Experiments in our laboratory showed that titanium could be almost completely precipitated as titanyl quinolate, TiO-

$(C_9H_6NO)_2 \cdot 2H_2O$, at *p*H 4.5 in the presence of ethylenediaminetetraacetic acid, under certain conditions. A 1-g excess of 8-hydroxyquinoline over the amount necessary to precipitate the titanyl quinolate must be present. The excess of ethylenediaminetetraacetic acid should not be greater than 0.5 g over the amount needed to complex the zirconium. The solution should be cooled in an ice bath before filtering. When these conditions are observed, the amount of titanium remaining in solution was found to be about 0.05 mg as TiO_2. This solubility of titanium was low enough to regard the precipitation as complete.

The titanyl quinolate precipitate can be decomposed by heat from an infrared lamp and converted to TiO_2 by ignition in an electric furnace. Berg and Teitelbaum [14] reported that this decomposition should be done under a layer of oxalic acid, because of the volatility of titanyl quinolate. Arend and Schnellenbach [15] used a direct decomposition and ignition of titanyl quinolate without the addition of oxalic acid. Experiments in our laboratory showed that when the decomposition was performed with heat from an infrared lamp, no titanyl quinolate was volatilized. Known amounts of titanium were precipitated by 8-hydroxyquinoline, decomposed by heat from an infrared lamp, and ignited to TiO_2 without any loss of titanium. No trace of titanium was found when the decomposition products from heating titanyl quinolate with an infrared lamp were passed through a solution of sulfuric acid.

Synthetic solutions containing from 475 mg of TiO_2 and 25 mg of ZrO_2 to 100 mg of TiO_2 and 400 mg of ZrO_2 were prepared from the standard solutions. These mixtures were converted to sulfates by the addition of 15 ml of sulfuric acid and subsequent evaporation to fumes of sulfuric acid. Each solution was then treated as described in section 4.5. Each precipitate of titanyl quinolate was dissolved in 100 ml of diluted sulfuric acid (15+85) and the titanium reprecipitated. To determine the contamination of the first precipitate by zirconium, the filtrates from the second precipitation were made acid with hydrochloric acid and the zirconium recovered by precipitation with cupferron. The solutions were allowed to stand for about 4 hr and filtered through 9-cm papers. The filters and precipitates were washed with a solution of cupferron, transferred to porcelain crucibles, decomposed by an infrared lamp, and ignited to ZrO_2 at 1000 °C.

The degree of contamination of the titanyl quinolate by zirconium, over the range studied, is given in table 6.

The separation was satisfactory up to the concentration range of about 200 mg of TiO_2 and 300 mg of ZrO_2. For amounts of zirconium in excess of this amount a double precipitation should be made, but this increases the amount of soluble titanium weighed with the ZrO_2 to 0.1 mg of TiO_2.

Eight synthetic mixtures of titanium and zirconium were prepared from the standard solutions. Fifteen milliliters of sulfuric acid was added to each and the solutions were evaporated to fumes of sulfuric acid. The titanium was then separated and determined by the procedure described in section 4.5. The filtrates were reserved for the determination of zirconium according to the directions in section 3.5. The results of these separations and determinations are given in table 7.

TABLE 6. *Experiments which show the degree of contamination of titanium quinolate by zirconium*

Experiment	TiO_2	ZrO_2	ZrO_2 found in Ti precipitate
	Added	Added	
	mg	*mg*	*mg*
1	475	25	0.0
2	450	50	.0
3	425	75	.0
4	400	100	.1
5	300	200	.2
6	200	300	.1
7	100	400	.4

TABLE 7. *Results obtained in the separation of titanium from zirconium by precipitation with 8-hydroxyquinoline in a solution containing ethylenediaminetetraacetic acid*

Experiment No.	Titanium dioxide			Zirconium dioxide		
	Added	Found	Error	Added	Found	Error
	g	*g*	*mg*	*g*	*g*	*mg*
1	0.5037	0.5037	0.0	0.0005	0.0006	+0.1
2	.4981	.4984	+.3	.0009	.0009	.0
3	.4831	.4830	−.1	.0067	.0066	−.1
4	.4808	.4809	+.1	.0093	.0092	−.1
5	.4605	.4608	+.3	.0268	.0268	.0
6	.4468	.4471	+.3	.0606	.0604	−.2
7	.3941	.3944	+.3	.1035	.1035	.0
8	.2905	.2907	+.2	.2185	.2185	.0

3.5. Recovery and Determination of Zirconium

Majumdar and Chowdhury [16] reported that, in the presence of ethylenediaminetetraacetic acid, zirconium can be quantitatively precipitated by cupferron from hydrochloric acid solution.

To confirm this observation, five solutions containing known amounts of zirconium in the range of 0.5 mg to 55 mg of ZrO_2 were prepared. Fifteen milliliters of sulfuric acid was added to each solution and enough ethylenediaminetetraacetic acid to furnish a 0.5-g excess over the amount necessary to complex the zirconium. The acidity of each solution was adjusted to *p*H 1.5 with ammonium hydroxide, and then to *p*H 4.5 with the ammonium acetate reagent solution. Fifty milliliters of hydrochloric acid was added to each solution and enough cupferron to furnish an excess of 1 g. The solutions were allowed to stand overnight in a cold box, then filtered through 12.5-cm papers. The filters and precipitates were decomposed in porcelain crucibles, and ignited to ZrO_2.

The results are given in table 8.

TABLE 8. *Recovery of zirconium by precipitation with cupferron in a solution containing ethylenediaminetetraacetic acid*

Experiment	Zirconium dioxide		
	Added	Found	Error
	mg	*mg*	*mg*
1	0.6	0.6	0.0
2	10.3	10.3	.0
3	25.2	25.1	−.1
4	55.1	55.2	+.1

The filtrates obtained according to the procedure in section 3.4 were acidified with 50 ml of hydrochloric acid and the zirconium recovered and determined by the above procedure. These results are given in table 7.

4. Procedure for Separating Titanium, Zirconium, Iron, and Aluminum From One Another

The following procedure is designed for a total quantity of about 0.5 g of mixed oxides. The maximum amount of each oxide that can be present is: 0.5 g of TiO_2; 0.25 g of ZrO_2; 0.05 g of Fe_2O_3; and 0.05 g of Al_2O_3. The minimum amount of ZrO_2, Fe_2O_3, and Al_2O_3 that can be determined is about 0.0005 g each. A very accurate determination of these elements requires a knowledge of the approximate composition of the sample.

4.1. Preparation of the Solution for Analysis

Synthetic solutions were prepared by mixing weighed portions of each of the four standard solutions so that the above maxima and minima were observed. Each of the synthetic solutions was treated as follows:

Dilute the synthetic solution to about 250 ml. To precipitate the metals as their respective quinolates, add 20 ml of acetic acid containing sufficient 8-hydroxyquinoline to provide approximately 1 g in excess of the amount required to precipitate all four metals. The nominal compositions of the metal quinolates are: $TiO(C_9H_6NO)_2$; $Zr(C_9H_6NO)_4$; $Fe(C_9H_6NO)_3$; and $Al(C_9H_6NO)_3$.

Neutralize the solution to an acidity of *p*H 5 by adding diluted ammonium hydroxide (1+1). Wash the electrodes of the *p*H meter with water and wipe them with bits of filter paper. Reserve these bits of paper and later add them to the mixed quinolate precipitate.

Digest the solution containing the mixed quinolate precipitate for a few hours on the steam bath and then cool it to room temperature. Filter the solution through a 12.5-cm paper and wash the precipitate and filter with a solution of water that has been saturated with 8-hydroxyquinoline.

Dissolve the mixed quinolates of titanium zirconium, iron, and aluminum in the following manner. Place the filter and precipitate in the beaker in which the precipitation was made and add 100 ml of a 10-percent solution of citric acid in diluted hydrochloric acid (5+95) and digest on the steam bath until solution of the precipitate is effected. Break up the filter paper by stirring the solution. Filter the solution through an 11-cm paper and wash the filter with a hot (70 °C) 2-percent solution of citric acid in diluted hydrochloric acid (1+99). Next, wash it with a hot (70 °C) solution of ammonium citrate, prepared by dissolving 10 g of citric acid in 400 ml of water, adjusting the alkalinity to between *p*H 8.5 and 9.0 with ammonium hydroxide, and finally diluting to a volume of 500 ml.[6]

4.2. Separation of Iron From Titanium, Zirconium, and Aluminum and its Subsequent Determination

Evaporate the solution obtained as described above to about 150 ml. Add 10 ml of hydrochloric acid and adjust the acidity of the solution to *p*H 1.5 with diluted ammonium hydroxide (1+3). Digest the solution on a steam bath for one-half hour. Add enough ethanol so that the final solution will contain 75 ml of ethanol after the addition of the 1-nitroso-2-naphthol reagent solution which contains 50 percent of ethanol by volume. Slowly add the 1-nitroso-2-naphthol reagent solution to the warm solution until the approximate amount necessary to precipitate the iron as $Fe(C_{10}H_6O_2N)_3$ has been added and/allow the solution to stand at room temperature for one-half hour. Determine the *p*H of the solution and adjust, if necessary, to *p*H 1.5 with diluted hydrochloric acid (1+9). Add enough 1-nitroso-2-naphthol solution to produce a 0.2-g excess of the reagent and allow the solution to stand overnight. Filter the solution through a 9-cm paper and thoroughly wash the precipitate and filter with a warm (60 °C) solution of ammonium citrate. The wash solution is prepared by dissolving 10 g of citric acid in 400 ml of water, adjusting the acidity to *p*H 4.5 with ammonium hydroxide, and diluting to 500 ml.

Decompose the precipitate and filter in a porcelain crucible by heat from an infrared lamp. Complete the ignition at 900 °C in an electric furnace, and weigh the residue as Fe_2O_3.

4.3. Separation of Titanium and Zirconium From Aluminum

Add 50 ml of hydrochloric acid to the filtrate obtained in the separation of iron by 1-nitroso-2-naphthol. Evaporate the solution to about 200 ml on a steam bath to free it of ethanol. Cool the resulting solution to about 60 °C and slowly add enough cupferron reagent solution to precipitate only about 90 percent of the titanium and zirconium. Digest the solution at this temperature and stir the solution until the precipitate changes from a bulky, flocculent form to one of dense compact nature. Then, slowly add cupferron reagent solution until a permanent precipitate no longer forms. Cool

[6] When filters were ignited after the above treatment, no residue was found.

the solution to room temperature and add 10 ml more of the cupferron reagent solution. Allow the solution to stand about 4 hr in a refrigerator. Catch the precipitate on a 12.5-cm paper, and wash it with a 0.1-percent solution of cupferron in diluted hydrochloric acid (1+9).

Reserve the filtrate for the determination of aluminum as described in section 4.4. Reserve the precipitate for the separation of titanium from zirconium as described in section 4.5.

4.4. Recovery and Determination of Aluminum

Cool the filtrate obtained in the separation of titanium and zirconium from aluminum (section 4.3) in an ice-bath and neutralize it to *p*H 4.0 with diluted ammonium hydroxide (1+1). Add 20 ml of the cupferron reagent solution and allow the solution to stand overnight in a refrigerator. Catch the precipitate on a 12.5-cm paper and wash it with a 1-percent aqueous solution of cupferron. Place the filter and precipitate in a porcelain crucible and decompose them by heating with an infrared lamp. Complete the ignition in an electric furnace at 1,100°C. and weigh the residue as Al_2O_3.

4.5. Separation of Titanium From Zirconium and its Subsequent Determination

Place the precipitate of titanium and zirconium cupferrates obtained in section 4.3 in a 150-ml beaker and decompose it and the filter with heat from an infrared lamp. Then place the beaker and its contents in an electric furnace and raise the temperature to 450 °C. Heat them at this temperature overnight or until carbon is no longer visible. Do not heat above 450 °C because the oxides so formed are difficultly soluble in sulfuric acid. Allow the beaker and its contents to cool to room temperature.

To the beaker containing the mixed titanium and zirconium oxides, add 30 ml of diluted sulfuric acid (1+1). Place the covered beaker on an electric hot plate and dissolve the oxides by heating at a medium heat. Cool the solution, dilute it to 100 ml with water, and filter it through a 9-cm paper, to free the solution of dehydrated silica and to retain any undissolved oxides. To determine the amount of undissolved oxides, wash the paper with diluted sulfuric acid (1+9) and ignite it in a platinum crucible. Treat the ash with 2 ml of hydrofluoric acid and 2 drops of sulfuric acid and heat to volatilize any silica present as silicon tetrafluoride. Ignite the crucible again and weigh any residue as TiO_2.[7] If significant, this amount should be added to that determined later.

Add enough solid ethylenediaminetetraacetic acid to the solution to give an excess of 0.5 g over the approximate amount required to complex the zirconium. Then add enough solid 8-hydroxyquinoline to the solution to give an excess of 1 g over the amount required to precipitate the titanium. Zirconium forms a one-to-one molar complex with ethylenediaminetetraacetic acid, and one mole of titanyl ion is precipitated by two moles of 8-hydroxyquinoline. Heat the solution on the steam bath until the solid ethylenediaminetetraacetic acid and solid 8-hydroxyquinoline are dissolved. Neutralize the clear solution to *p*H 1.0 with diluted ammonium hydroxide (1+1) and allow it to stand for 30 min. Dilute it to about 450 ml and add 1-ml portions of the ammonium acetate reagent solution until a permanent precipitate forms or an acidity of *p*H 2.0 is obtained, whichever occurs first. Heat the solution on the steam bath until the precipitate settles. Add four 5-ml portions of the ammonium acetate reagent solution at 10-minute intervals. Next heat the solution for about 1 hour longer and then cool it to room temperature. Adjust the acidity of the solution to *p*H 4.5 with the ammonium acetate reagent solution. Heat the solution on the steam bath overnight, cool it in an ice bath for 4 hr, and filter it through a 12.5-cm paper. Wash the precipitate and filter with a solution prepared by dissolving 1 g of 8-hydroxyquinoline in 15 ml of acetic acid, diluting it to 400 ml, adding 0.5 g of ethylenediaminetetraacetic acid, neutralizing the solution to *p*H 4.5 with diluted ammonium hydroxide (1+1), and finally diluting to a volume of 500 ml.

Place the precipitate and filter in a porcelain crucible. Decompose the precipitate and filter by heating with an infrared lamp. Ignite the residue in an electric furnace at 1,000 °C, and weigh it as TiO_2.

4.6. Recovery and Determination of Zirconium

To the filtrate reserved from section 4.5, add 50 ml of hydrochloric acid. Add a sufficient quantity of cupferron reagent solution to precipitate the zirconium and to provide an excess of about 1 g of cupferron. It requires 4 moles of cupferron to precipitate 1 mole of zirconium. Allow the solution and precipitate to stand in a refrigerator overnight. Catch the precipitate on a 12.5-cm paper and wash it with a 0.2-percent solution of cupferron in diluted hydrochloric acid (1+19). Decompose the precipitate and filter in a porcelain crucible by heat from an infrared lamp. Complete the ignition in an electric furnace at 1,000 °C and weigh the residue as ZrO_2.

5. Results

The results obtained when the foregoing procedure was applied to the analysis of synthetic mixtures of titanium, zirconium, iron, and aluminum are given in table 9.

[7] The residue in most cases was found to be less than 0.1 mg. In those cases in which it exceeded 0.1 mg, it was found to be TiO_2.

TABLE 9.—*Results obtained in the separation of titanium, zirconium, iron, and aluminum from one another*

Experiment	Titanium dioxide			Zirconium dioxide			Ferric oxide			Aluminum oxide		
	Added	Found	Error	Added	Found	Error	Added	Found	Error	Added	Found	Error
	g	*g*	*mg*	*g*	*g*	*mg*	*g*	*g*	*mg*	*g*	*g*	*mg*
1	0.4964	0.4962	−0.2	0.0006	0.0007	+0.1	0.0005	0.0006	+0.1	0.0005	0.0007	+0.2
2	.4980	.4979	−.1	.0102	.0102	.0	.0051	.0051	.0	.0047	.0048	+.1
3	.4269	.4269	.0	.0244	.0245	+.1	.0209	.0210	+.1	.0226	.0228	+.2
4	.3476	.3477	+.1	.0544	.0543	−.1	.0479	.0480	+.1	.0522	.0520	−.2
5	.3422	.3424	+.2	.1028	.1027	−.1	.0124	.0122	−.2	.0050	.0051	+.1
6	.3210	.3208	−.2	.1530	.1528	−.2	.0055	.0054	−.1	.0097	.0100	+.3
7	.2829	.2832	+.3	.2064	.2062	−.2	.0105	.0105	.0	.0048	.0049	+.1
8	.2323	.2326	+.3	.2511	.2510	−.1	.0054	.0055	+.1	.0092	.0090	−.2

6. References

[1] W. S. Clabaugh, R. T. Leslie, and R. Gilchrist, J. Research NBS **55,** 261 (1955) RP2628.
[2] W. S. Clabaugh and R. Gilchrist, J. Am. Chem. Soc. **74,** 2104 (1952).
[3] K. Tanii, H. Hosimiya, T. Ikeda, J. Chem. Soc., Japan **61,** 269 (1940).
[4] A. Jolles, Z. anal. Chem. **36,** 149 (1897).
[5] Gantois, Lejeune, Noel, and Scohy, Bull. soc. chim., Belg. **43,** 545 (1934).
[6] J. F. Flagg, Organic Reagents, p. 207 (Interscience Publishers, New York, N.Y., 1948).
[7] J. Brown, J. Am. Chem. Soc. **39,** 2358 (1917).
[8] I. Bellucci and L. Grassi, Gazz. chim. ital. **43,** I, 570 (1913).
[9] K. Schroeder, Z. anorg. Chem. **72,** 89 (1911).
[10] A. Pinkus and E. Belche, Bull. soc. chim. Belg. **36,** 277 (1927).
[11] J. S. Fritz and M. O. Fulda, Anal. Chem. **26,** 1206. (1954).
[12] R. L. Pecsok and E. F. Maverick, J. Am. Chem. Soc. **76,** 358 (1954).
[13] R. M. Sen Sarma and A. K. Mallik, Anal. chim. Acta **12,** 329 (1955).
[14] R. Berg and M. Teitelbaum, Z. anal. Chem. **81,** 1 (1930).
[15] J. Arend and H. Schnellenbach, Arch. Eisenhüttenw. **4,** 265 (1930).
[16] A. K. Majumdar and J. B. R. Chowdhury, Anal. chim. Acta **15,** 105 (1956).

(Paper 64A6–79)

Selected Abstracts

Error analysis of a standard microwave phase shifter, G. E. Schafer and R. W. Beatty, *J. Research NBS* **64C,** *No. 4, 261 (1960).*

A standard microwave phase shifter has been proposed which utilizes an adjustable short circuit attached to a tunable three-arm waveguide junction. Two classes of errors considered are those due to imperfect tuning of the waveguide junction and those due to inaccuracies in determining the motion of the adjustable short circuit and the width of the waveguide, termed tuning and dimensional errors, respectively. Graphs are presented for estimating the scattering coefficient magnitudes needed to estimate limits of tuning error from observations of amplitude changes during the tuning procedure. Graphs are presented for estimating limits of dimensional error for WR–90 waveguide in the recommended frequency range of 8.2 to 12.4 kMc/s from tolerances of the axial motion of the short circuit and broad dimension of the waveguide.

X-ray attenuation coefficients from 13 to 80 Mev for hydrogen, carbon, water, and aluminum, J. M. Wyckoff and H. W. Koch, *Phys. Rev.* **117,** *No. 5, 1261 (1960).*

The X-ray attenuation coefficients for hydrogen, carbon, water, and aluminum have been measured in the energy range from 13 to 80 Mev by placing varying lengths of attenuators in a 90 Mev bremsstrahlung beam in a good geometry experiment using a large sodium-iodide total-absorption spectrometer as the detector. In the hydrogen case, a difference method employing cyclohexane (C_6H_{12}) and graphite was used. The theoretical attenuation coefficients were calculated using selected Compton and triplet cross sections in addition to the small quasi-deuteron cross sections. A pair cross section increase of 2.25% was required for carbon, water and aluminum to bring the total calculated coefficients into agreement with the measured coefficients in the 60 Mev region. The difference between these calculated cross sections and the measured cross sections in the 13 to 50 Mev region has been ascribed to the giant resonance nuclear absorption. A larger high energy tail to this absorption than predicted by (γ,p) and (γ,n) experiments is indicated.

Forced mixing in boundary layers, G. B. Schubauer and W. G. Spangenberg, *J. Fluid Mech.* **8,** *No. 1, 10 (1960).*

The effect of increasing the rate of mixing in turbulent boundary layers in a region of adverse pressure gradient has been investigated experimentally. Only the two-dimensional case was considered. The boundary layer was formed on a flat wall in a special wind tunnel in which a variety of adverse pressure gradients could be obtained. Speeds were low enough to neglect compressibility. The main objective was to compare the effect of increasing the rate of mixing with the effect of reducing the pressure gradient on boundary-layer development and separation. A variety of mixing schemes was tried, all of them involving fixed devices arranged in a row on the surface in the region of rising pressure. While these differed considerably in effectiveness, they had a generally similar effect on the flow; and, except for effects arising from changes in displacement and momentum thickness introduced at the devices, their effect on the layer was basically equivalent to that of a decrease in pressure gradient. Apart from forced mixing, the shape of the pressure distribution was found to have a significant effect on displacement and momentum thickness, these being minimized and the wall distance decreased for a given pressure rise by a distribution with an initially steep and progressively decreasing gradient.

Flow and stress near an interface between stratified liquids, K. Lofquist, *Phys. of Fluids* **3,** *No. 2, 158 (1960).*

Observations are made of a density current system in which salt water flows turbulently under a pool of fresh water. The density and rate of flow of the salt water are varied, resulting in varying degrees of agitation of the interface. Measurements include the interface slope, the velocity and density profiles and the rate of mixing. Profiles of stress and effective viscosity are developed from the observations and the equation of motion. In the zone of stable stratification the effective viscosity has a minimum equal to or greater than the molecular viscosity depending upon whether the interface is laminar or agitated. Dimensionless relationships between the observed or computed quantities and the given fluid properties and flow characteristics are investigated. The principal independent variables are a Reynolds number and a Froude number. An interfacial stress coefficient is found to depend upon both. With fair accuracy, the velocity profile can be related to the interfacial stress in a manner analogous to that for turbulent flow near a rigid boundary.

Kinetics of the transport of water through silicate glasses at ambient temperatures, W. Haller, *Phys. Chem. of Glass* **1,** *46 (1960).*

The phenomenology of the transport of water constituents into the network of silicate glasses at ambient temperatures is discussed. The geologic hydration of obsidian, the hydration of obsidian artifacts, the water vapor sorption of a high surface area alumino silicate glass, and the water vapor sorption of vitreous silica are compared. It is concluded that, in spite of a wide variety of glass compositions and experimental conditions, the sorption rates are of the order of 10^{-8} $g.cm^{-2}.day^{-1/2}$. The sorption mechanism is interpreted as diffusion of water into the glass, accompanied by an irreversible change in the glass structure.

Heated cell for quantitative infrared spectrophotometry, F. J. Linnig and J. E. Stewart, *Anal. Chem.* **32,** *891 (1960).*

A heated cell is described which is useful for quantitative infrared spectrophotometry. It has been employed for making quantitative measurements on mixtures that are homogeneous only at elevated temperatures. It may be used for obtaining spectra of highly viscous materials and of materials above their melting points, and for quantitatively following chemical reactions at elevated temperatures.

Calibration for carrier operated microphones and other reversible transducers, M. D. Burkhard, E. L. R. Corliss, W. Koidan, and F. Biagi, *J. Acoustical Soc. Am.* **32,** *No. 4, 501 (1960).*

An insert technique described in this paper makes it possible to carry out sound pressure measurements using a microphone operated in a carrier circuit with almost the same accuracy

as can be achieved with more conventional preamplifiers. The carrier system is modified to include a microphone polarizing voltage if the transducer is not self-polarized. Then a calibrating audio-frequency voltage is used to drive the transducer diaphragm to the same displacement amplitude as that generated by the sound pressure. Instead of matching the open-circuit voltage of the microphone, diaphragm motion is matched. A displacement response constant, independent of frequency, is used to determine sound pressure, in contrast to the usual open-circuit response, which depends on frequency.

In a manner analogous to the determination of open-circuit pressure response by the reciprocity technique, the acoustic admittance of the microphone may be evaluated from a series of three voltage ratio measurements and the calculated acoustical transfer admittance of a calibrating coupler. This result can be combined with the open-circuit pressure response determined by the reciprocity technique to give an explicit evaluation of the electromechanical coupling constant.

Accurate microwave wavemeters with convenient calibration tables, H. E. Bussey and A. J. Estin, *Rev. Sci. Instr.* **31,** *410 (1960).*

Accurate and convenient microwave cavity wavemeters are described that are suitable for many precise physical mesaurements. High Q's were attained by refined construction techniques. At 9000 Mc a precision of 0.02 Mc was obtained. The absolute accuracy also may be very high after strains in the metal have stabilized. A calibration table containing 10^4 entries, easily formed by means of a high speed computer, makes the wavemeters convenient to use. The curve fitting method, accurate to one in 10^6, is described.

The nova outburst. V. The temperature and radius of the central exciting star and observation of elements other than hydrogen, S. Pottasch, *Ann. Astrophys J.* **22,** *No. 4, 412 (1959).*

The temperature and radius of the central star (the actual nova) is determined for six novae over the period beginning somewhat after maximum and extending until the nova shell is optically thin to hydrogen ioniozing radiation. During this period the temperature is found to remain roughly constant while the radius appears to decrease. The temperatures are determined using a variation of ZANSTRA's method. The results are shown in Table 2. The energies emitted by stars with these temperatures and radii are computed for the period until the shell becomes optically thin to H ionizing radiation and these energies are compared to the energy found from the light curve and the kinetic energies of the shell.

The extent of the ionized region of the shell can be computed knowing the temperature and radius of the exciting star. This is done and compared with the extent obtained in a different manner in a previous analysis.

Finally the composition of the shell is discussed. For five novae the amounts of hydrogen, helium, oxygen, nitrogen, sulfer, calcium, and neon are determined. The abundance of the last five elements appears to be greater, by a factor of about 5, than the generally accepted cosmic abundance.

Guiding of electromagnetic waves by uniformly rough surfaces—Part I, J. R. Wait, *IRE Trans. Ant. Prop.* **AP–7,** *S–154 (1959).*

A simple derivation is given for the reflection of electromagnetic waves from a perfectly conducting plane surface which has a uniform distribution of hemispherical bosses whose electrical constants are arbitrary. The spacing between the centers of the bosses is taken to be small which is the justification for neglecting the incoherent radiation. An approximate boundary condition is developed which must be satisfied in an average sense by the tangential fields on the reference plane.

The excitation of surface waves on the rough surface is then discussed. It is indicated that to a first order, a rough surface of the kind described here possesses an inductive surface reactance and will support a trapped wave. The effect of finite conductivity of the bosses is to exponentially damp this trapped wave.

Guiding of electromagnetic waves by uniformly rough surfaces—Part II, J. R. Wait, *IRE Trans. Ant. Prop.* **AP–7,** *S—163 (1959).*

Using the model of a single rough surface described in Part I, the influence of curvature is considered. The starting point is a residue-series solution for a vertical dipole over a sphere with an arbitrary surface impedance. It is shown that the curvature has a profound influence on the nature of the surface wave, although it uniformly approaches the conditions for a plane boundary as the radius of curvature approaches infinity.

The propagation between the space bounded by two parallel uniformly rough surfaces is also considered. This is treated first for plane boundaries and then for concentric spherical boundaries. The latter model is useful in explaining certain experimental data on the terrestrial propagation of VLF radio waves.

Normal modes of a lattice of oscillators with many resonances and dipolar coupling, U. Fano, *Phys. Rev.* **118,** *No. 2, 451 (1960).*

The normal modes of a lattice of coupled dipoles are studied as a model of the collective excitations of electrons in condensed materials. Two types of oscillations are found, in which electrostatic coupling has a dominant influence. One of them is analogous to the oscillation of an electron plasma and has a high dipole moment. Other collective oscillations have a low net dipole moment, owing to destructive interference between out-of-phase components. These two types of oscillation occur in systems with a sufficiently high density of oscillator strength in space and in spectrum. A simple estimate indicates that most condensed materials fulfill this condition.

Electron detachment from the negative hydrogen ion by electron impact, S. Geltman, *Proc. Phys. Soc. (London, England)* **LXXV,** *p. 67 (1960).*

The Born-Oppenheimer approximation has been used to evaluate the cross section for the detachment of electrons from H^- by electron impact over an energy range from threshold (0·76 ev) to 75 ev. An empirical correction was then applied to account approximately for the long range Coulomb repulsion between the incident electron and the negative ion. The resulting cross section has a broad maximum of $700\pi a_0^2$ centered at about 45 ev.

Spectra emitted from rare gas-oxygen solids during electron bombardment, L. J. Schoen and H. P. Broida, *J. Chem. Phys.* **32,** *No. 4, 1184 (1960)*

Light emission from rare gas solids containing small amounts of oxygen has been excited by an electron bombardment technique. The Herzberg bands of neutral oxygen and a line group believed to be the $^1S \rightarrow {}^1D$ transition of oxygen atoms from the strongest features of the observed spectra. In a neon matrix, the Second Negative system of O_2^+ has been identified. The effect of the various solids on the vibrational structure of the Herzberg bands is discussed.

Detection and estimation of low concentrations of aldehyde in air, E. E. Hughes and S. G. Lias, *Anal. Chem.* **32,** *No. 6, 708 (1960).*

Aldehyde is adsorbed from an air stream on purified silica gel. The gel is then treated with a solution of p-phenylene diamine and hydrogen peroxide. Oxidation of the p-phenylene diamine is catalyzed by aldehydes and the depth of color produced on the gel by the oxidation products is a measure of the quantity of aldehyde adsorbed. The method is

simple and little equipment is involved. Quantities as low as 10^{-8} mole percent can be easily detected. The method can be readily adapted for field use.

Nonresonant absorption in symmetric-top gases: Dependence of relaxation frequency on temperature, A. A. Maryott, A. Estin, and G. Birnbaum, *J. Chem. Phys.* **32,** *No. 5, 1501 (1960).*

The nonresonant absorption spectra of CHF_3, CH_3F, and $CClF_3$ were obtained in the gaseous state at various temperatures in the range 230° to 360° K. In all cases the maximum value of the dielectric loss per unit pressure varies as T^{-2}, in accordance with the Debye equation. The variation of relaxation frequency (line width) with pressure and temperature is represented by $\Delta\mu \propto p\,T^{-m}$, where m has the following values: 1.59 ± 0.03 for CHF_3, 1.60 ± 0.02 for CH_3F, and 1.27 ± 0.02 for $CClF_3$. Since CHF_3 and CH_3F have rather large dipole moments, the predominant interaction should be of the first-order dipole-dipole type. On this basis Anderson's theory predicts $m=1$. Closer agreement with the experimental data is obtained with an expression derived essentially from dimensional considerations of a torque-impulse model, which gives $m=1.5$. In the case of $CClF_3$, which has a comparatively small dipole moment, the data indicate that molecular reorientation is governed primarily by forces of shorter range.

Electron impact study of the cyanogen halides, J. T. Herron and V. H. Dibeler, *J. Am. Chem. Soc.* **82,** *1555 (1960).*

Mass spectra and appearance potentials are reported for the principal ions of cyanogen chloride, bromide, and iodide. Using these data, the following thermochemical values have been computed: $\triangle H_f CN = 89\pm2$ kcal/mole; $\triangle H_f CN^- = 15\pm4$ kcal/mole, E.A. $(CN) = 74\pm4$ kcal/mole.

The structure of O,O′-diethyl methylphosphonothioate and conjugative properties of the P=S bond, H. Finegold, *J. Am. Chem. Soc.* **82,** *No. 10, 2641 (1960).*

The structure of O, O-diethyl methylphosphonothioate: $CH_3P(S)(OCH_2CH_3)_2$, is shown to include two non-equivalent ethoxy groups. The conclusion was reached by a study of the hyperfine nuclear resonance spectrum resulting from both the H^1 and P^{31} spin resonance transitions. A theory of resonance (mesomeric) stabilization of the molecule involving the P=S bond is proposed to explain the observations. An important inference is that the compound is asymmetric and would be expected to show optical activity.

Analysis of methyl methacrylate copolymers by gas chromatography, J. Strassburger, G. M. Brauer, M. Tryon, and A. F. Forziati, *Anal. Chem.* **32,** *No. 4, 454 (1960).*

Detection, identification, and quantitative determination of copolymers of methyl methacrylate was accomplished by gas chromatographic analysis of the pyrolysis products. The procedure distinguishes between polymer mixtures and copolymers, and detects the presence of 0.2% of copolymer. Composition can be determined quantitatively with a precision of $\pm0.5\%$, from standard curves of the ratio of peak areas at known composition. The analysis takes only a few minutes, can be readily adapted to other copolymers, and is especially useful for cross-linked, insoluble materials.

The black void reactor concept, C. O. Muehlhause, *Nuclear Sci. and Engr.* **7,** *No. 6, 505 (1960).*

The application of heavily loaded cylindrical fuel elements to two principal reactor configurations is considered. The objective of the work is the design of research reactors suitable for radiation effects studies.

The Stokes flow problem for a class of axially symmetric bodies, L. E. Payne and W. H. Pell, *J. Fluid Mech.* **7,** *Pt. 4, 529 (1960).*

This is a continuation of earlier work by the same authors. The methods of the generalized axially symmetric potential theory of A. Weinstein and certain representation theorems of L. Payne for the solution of repeated operator equations are applied to the solution of the Stokes (slow) flow about a spindle-shaped body. The stream function of the flow is found and an expression is given for the drag of the body.

Elastic constants of synthetic single crystal corundum at room temperature, J. B. Wachtman, W. E. Tefft, D. G. Lam, R. P. Stinchfield, *J. Am. Ceram. Soc.* **43,** *No. 6, 334 (1960).*

The six elastic constants (and six elastic compliances) of corundum were determined in the kilocycle/sec frequency range by an accurate, resonance method. The results were checked in the megacycle/sec range with a less accurate, pulse velocity method. The elastic moduli for polycrystalline alumina calculated from the single crystal compliances determined by the resonance method are in good agreement with experimental values obtained on high density polycrystalline alumina. The variation of Young's modulus and of the shear modulus with orientation was calculated from the compliances and the results are shown graphically. The results of the present work do not agree well with previous work on single crystal sapphire. The specification of orientation and the theory used to calculate the elastic constants are given in detail to support the contention that the results of the present work are correct.

Dewar system for low temperature experiments, C. T. Zahn, *Rev. Sci. Instr.* **31,** *No. 3, 328 (1960).*

A special system of glass Dewars for experiments at low temperatures is described in which the liquid nitrogen shield consists of two separate parts, one dipping into the other. The upper shield is constructed with three walls rather than the usual two, since it is open at the bottom. The extra inner wall serves to prevent the liquid nitrogen from flowing through the open bottom. The liquid helium Dewar fits fairly closely inside this extra wall, with a thin air-space between the two, and extends downward into the lower shield. The upper shield is thus mechanically isolated from the liquid helium Dewar. Access to a cold spot of the liquid helium flask is provided by a tube passing upward through the bottom of the lower shield and coupled to the liquid helium flask by means of a spherical ground-glass joint. Various advantages of this system and possible modifications thereof are discussed.

The ionization potential of fluorine, J. T. Herron and V. H. Dibeler, *J. Chem. Phys.* **32,** *No. 6, 1885 (1960).*

The ionization potential of fluorine was found to be 15.83 ev as measured by electron impact. Values for the ionization potentials of Cl_2, Br_2, and the second ionization potentials of Cl_2 and Br_2 are also reported.

Heat of formation of nitrogen trifluoride and the N-F bond energy, G. T. Armstrong, S. Marantz, and C. F. Coyle, *Commun. to Editor, J. Am. Chem. Soc.* **81,** *3798 (1959).*

By igniting mixtures of NF_3 with hydrogen over water and of NF_3 with ammonia, the heats of the following reactions were determined in a bomb calorimeter

$$NF_3(g)+\frac{3}{2}H_2(g)=\frac{1}{2}N_2(g)+3HF\ (aq,\ a=1)$$

$$\Delta H_{25} = -859.0\pm13.4 \text{ kj/mole}$$
$$= -205.3\pm 3.2 \text{ kcal/mole}$$

$$NF_3(g)+4NH_3(g)=3NH_4F(c)+N_2(g)$$

$$\Delta H_{25} = -1085.7\pm4.2 \text{ kj/mole}$$
$$= -\ 259.5\pm1.0 \text{ kcal/mole}$$

The weighted mean heat of formation of NF_3 calculated from the above measurements is -29.7 ± 1.8 kcal/mole and the mean N-F bond energy is 66.4 ± 0.8 kcal/mole.

Microwave spectrum and internal rotation of ethyl cyanide, V. W. Laurie, *J. Chem. Phys.* **31,** *No. 6, 1500 (1959).*

The microwave spectrum of ethyl cyanide has been studied in the region from 17–36 kMc. Both parallel and perpendicular transitions have been assigned. Rotational constants (Mc) for the ground vibrational state are $a_0 = 27663.30$, $b_0 = 4714.14$, $c_0 = 4235.14$, $D_J = 0.0035$, $D_{JK} = -0.0496$. From Stark effects the dipole moment is calculated to be $\mu_a = 3.78$ *D*, $\mu_b = 1.38$ *D*, $\mu = 4.02$ *D*. Hyperfine splittings lead to a value of −3.3 Mc for the quadrupole coupling of the N^{14} nucleus along the a-axis. Rotational transitions of molecules in several excited vibrational states have also been measured. A Coriolis interaction between the torsional mode and the in-plane CCN bend has been found and is discussed. Splittings of transitions of molecules in the first excited torsional state show that the barrier hindering internal rotation of the methyl group is 3.05 kcal/mole.

Microwave spectrum of trans-crotononitrile, V. W. Laurie, *J. Chem. Phys.* **32,** *No. 5, 1588 (1960).*

The microwave spectrum of *trans*−$H_3CCH{=}CHON$ has been investigated in the region from 13–36 kMc. A number of parallel transitions have been measured and fitted with the constants (Mc) $a_0 = 38._2 \times 10^3$, $b_0 = 2297.05$, $c_0 = 2195.22$, $D_J = 0.3_4 \times 10^{-3}$, $D_{JK} = -12.6 \times 10^{-3}$. Failure to resolve splittings from internal rotation of the methyl group implies a lower limit of 2.1 kcal/mole for the internal barrier.

Infrared emission spectra of gaseous B_2O_3 and B_2O_2, D. White, D. E. Mann, P. N. Walsh, and A. Sommer, *J. Chem. Phys.* **32,** *No. 2, 481 (1960).*

The infrared emission spectra of gaseous B_2O_3 and B_2O_2 in the temperature range 1400–1800° K have been studied in the region 700–4000 cm^{-1}. Distinct bands were found for natural B_2O_3 at 2040, 1302, and 742 cm^{-1}, and the $B^{10}-B^{11}$ isotope shifts measured. From the isotope shift data and other considerations the B_2O_3 molecule has been assigned a *V* structure having C_{2v} symmetry. A force constant analysis has been made and a frequency assignment is given from which thermal functions have been computed. The calculated force constants are consistent with the high stability of the molecule. Only one emission band of gaseous B_2O_2, at 1890 cm^{-1}, has been observed. A linear $D_{\infty h}$ structure was assumed and a frequency assignment and thermal functions estimated.

Infrared emission spectrum of gaseous HBO_2, D. White, D. E. Mann, P. N. Walsh, and A. Sommer, *J. Chem. Phys.* **32,** *No. 2, 488 (1960).*

The infrared emission spectrum of the vapor phase of the $B_2O_3(l)-H_2O(g)$ system has been studied at elevated temperatures over the region 700–4000 cm^{-1}. Characteristic bands were found near 3680, 2030, and 1420 cm^{-1}, and approximate $B^{10}-B^{11}$ and H−D isotope shifts measured. It is shown that these bands arise from the molecule HBO_2. The intensity of the 2030 cm^{-1} band was studied as a function of both temperature and water pressure. The intensity *vs* temperature measurements lead to a heat of formation, $\Delta H_0°$, of -135.0 ± 3 kcal/mole for $HBO_2(g)$. The spectroscopic data, considered in the light of our analysis of the $B_2O_3(g)$ infrared spectrum, are compatible with the structure

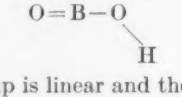

in which the OBO group is linear and the H is off-axis. The force constants are found to resemble those determined for $B_2O_3(g)$. Complete vibrational assignments are given for $HBO_2(g)$ and its trimer $(HBO_2)_3(g)$, a species which has recently been shown to exist in this system. Thermal functions have been computed for both molecules over a wide temperature range.

A demonstration of color perception with abridged color-projection systems, C. S. McCamy, *Photographic Sci. and Engr.* **4,** *No. 3, 155 (1960).*

The way primary colors combine to produce colored pictures was demonstrated. The range of colors perceived when less than three primaries were used was attributed to the known psychological effects of induction by contrast, color constancy by discounting of the illuminant, and memory color, all of which were demonstrated. The reproduction characteristics of two-color systems were demonstrated and a direct comparison was made between a two-color and a three-color reproduction of the same scene.

Other NBS Publications

Journal of Research, Section 64C, No. 4, October–December 1960. 75 cents.

Error analysis of a standard microwave phase shifter. G. E. Schafer and R. W. Beatty. (See above abstract.)

A method of controlling the effect of resistance in the link circuit of the Thomson or Kelvin double bridge. D. Ramaley.

Automatic precise recording of temperature. G. S. Ross and H. D. Dixon.

Gimbal device to minimize the effects of off-center loading on balance pans. H. A. Bowman and L. B. Macurdy.

Response of microchemical balances to changes in relative humidity. H. E. Almer.

Chemical changes occurring during the weathering of two coating-grade asphalts. S. H. Greenfeld.

Characteristics of fifteen coating-grade asphalts. S. H. Greenfeld.

Journal of Research, Section 64D, No. 6, November–December 1960. 70 cents.

URSI National Committee Report:

Commission 1. Radio Measurement Methods and Standards.
Commission 2. Tropospheric Radio Propagation.
Commission 3. Ionospheric Radio Propagation.
Commission 4. Radio Noise of Terrestrial Origin.
Commission 5. Radio Astronomy.
Commission 6. Radio Waves and Circuits.
Commission 7. Radio Electronics.

Temperature-induced stresses in solids of elementary shape, L. H. Adams and R. M. Waxler, NBS Mono. 2 (1960) 25 cents.

Table of wavenumbers, 7000A to 1000μ, C. D. Coleman, W. R. Bozman, and W. F. Meggers, NBS Mono. 3, Vol. II (1960) $6.00.

A method for the dynamic determination of the elastic, dielectric, and piezoelectric constants of quartz, S. A. Basri, NBS Mono. 9 (1960) 15 cents.

The "1958 He^4 Scale of Temperature," H. Van Dijk, M. Durieux, J. R. Clement, J. K. Logan, and F. G. Brickwedde, NBS Mono. 10 (1960) 20 cents.

Mechanical properties of structural materials at low temperatures—A compilation from the literature, R. M. McClintock and H. P. Gibbons, NBS Mono. 13 (1960) $1.50.

Vibration-rotation structure in absorption bands for the calibration of spectrometers from 2 to 16 microns, E. K. Plyler, A. Danti, L. R. Blaine, and E. D. Tidwell, NBS Mono. 16 (1960) 20 cents.

New description of thorium spectra, R. Zalubas, NBS Mono. 17 (1960) 65 cents.

Measurement of neutron flux and spectra for physical and biological applications, NBS Handb. 72 (1960) 35 cents.

Experimental plating of gun bores to retard erosion, V. A. Lamb and J. P. Young, NBS Tech. Note 46 (PB151405) (1960) $2.50.

Magnetic drum directory and programming system for code-sorting letter mail, P. C. Tosini, NBS Tech. Note 50 (PB151409) (1960) $1.75.

Carrier frequency dependence of the basic transmission loss in tropospheric forward scatter propagation, K. A. Norton, NBS Tech. Note 53 (PB161554) (1960) $1.00.

Determination of a general index of effort in sorting mail by conventional methods, S. Henig, NBS Tech. Note 54 (PB161555) (1960) 50 cents.

A bibliography of the physical equilibria and related properties of some cryogenic systems, T. M. Flynn, NBS Tech. Note 56 (PB161557) (1960) $1.75.

Variable capacitor calibration with an inductive voltage divider bridge, T. L. Zapf, NBS Tech. Note 57 (PB161558) (1960) 50 cents.

A survey and bibliography of recent research in the propagation of VLF radio waves, J. R. Wait, NBS Tech. Note 58 (PB161559) (1960) 75 cents.

Measurements and standards in plasma-physics and astrophysics at the National Bureau of Standards, NBS Tech. Note 59 (PB161560) (1960) $1.00.

Proceedings of the 1960 conference on the propagation of E.L.F. radio waves (1960), NBS Tech. Note 61 (PB161562) (1960) 75 cents.

The influence of lowered permissible dose levels on atomic energy operations in the United States, L. S. Taylor, Progr. in Nuclear Energy **1,** 10 (1960).

Optimum antenna height for ionospheric scatter communication, R. G. Merril, IRE Trans. on Communs. Systems **CS–8,** 14 (1960).

Statistical evaluation of interlaboratory cement tests, J. R. Crandall and R. L. Blaine, Am. Soc. Testing Materials Proc. **59,** 1129 (1959).

Measured distributions of the instantaneous envelope amplitude and instantaneous frequency of carriers plus thermal and atmospheric noise, A. D. Watt and R. W. Plush, In Statistical methods of radio wave propagation, Proc. of Symp. University of California, Los Angeles, June 18–20, 1958, p. 233 (Pergamon Press, New York, N.Y., 1960).

Interpretation of some features of low-frequency ionograms, J. M. Watts, J. Atmospheric and Terrest. Phys. **15,** 73 (1959).

Transactions of the Joint Commission for Spectroscopy, Minutes of the Moscow Meeting, August 12–15, 1958 (Abridged), J. Opt. Soc. Am. **50,** No. 4, 396 (1960).

"Ionization" of the hydrogen negative ion, S. Geltman, Proc. 4th Internatl. Conf. on Ionization Phenomena in Gases (North Holland Publishing Co., Amsterdam, The Netherlands), Uppsala 17–21, p. IA19 (1960).

Cryogenic piping system design and installation, R. B. Jacobs, Heating, Piping and Air Conditioning, p. 143 (1960).

Plan for the self-qualification of laboratories, A. T. McPherson, ASTM Bull. No. 246, 17 (1960).

The structure of 0,0′-diethyl methylphosphonothioate and conjugative properties of the P=S bond, H. Finegold, J. Am. Chem. Soc. **82,** No. 10, 2641 (1960).

Effect of notch geometry on tensile properties on annealed titanium at 100°, 25°, −78° and −196° C, G. W. Geil and N. L. Carwile, Am. Soc. Testing Materials Proc. **59,** 985 (1959).

How the method of rating the cooling load for refrigerated trailers has been standardized, P. R. Achenbach, C. W. Phillips, and W. F. Goddard, Am. Soc. Heating, Refgr., Air Cond. Engrs. J. **2,** No. 5, 45 (1960).

The wavefront reversing interferometer, J. B. Saunders, Colloquium on Optics and Metrology, Sponsored by the International Commission of Optics, Brussels, Belgium, May 8–9, 1958, Published in Optics in Metrology, p. 227 (Pergamon Press, New York, N.Y., 1960).

Magnetoresistive effects in indium antimonide and indium arsenide, H. P. R. Frederikse and W. W. Hosler, Vol. 2, Pt. 2, of the book "Solid State Physics in Electronics and Telecommunications," p. 651 (Academic Press, New York, N.Y., 1960).

The NBS meteor burst communication system, R. J. Carpenter and G. R. Ochs, IRE Trans. Communs. Systems **CS–7,** 263 (1959).

Characteristic energy losses of electrons, L. Marton, L. B. Leder, C. Marton, and M. D. Wagner, Proc. 4th Internatl. Conf. on Electron Microscopy, September 1958, p. 281 (Berlin, Germany, 1960).

Radiation patterns of finite-size corner-reflector antennas, A. C. Wilson and H. V. Cottony, IRE Trans. on Ant. Prop. **AP–8,** 144 (1960).

Heat sink method for measuring the cooling loads of refrigerated structures, P. R. Achenbach and C. W. Phillips, Proc. 10th Intern. Congress of Refrigeration, August 1959, Copenhagen, Denmark (1959).

A technique for gripping high-strength fabrics during physical tests, K. F. Plitt and L. A. Dunlap, ASTM Bull. No. 246, 33 (1960).

An analysis of an absolute torsional pendulum viscometer, E. A. Kearsley, Trans. Soc. Rheology **III,** 69 (1959).

Radio echoes from field-aligned ionization above the magnetic equator and their resemblance to auroral echoes, K. L. Bowles, R. Cohen, G. R. Ochs, and B. B. Balsley, Letter J. Geophys. Research **65,** 1853 (1960).

Measurement on the smoothness of paper, T. W. Lashof and M. Mandel, Tappi **43,** No. 5, 385 (1960).

Geomagnetic and solar data, J. V. Lincoln, J. Geophys. Research **65,** 1639 (1960); J. Geophys. Research **65,** 1821 (1960).

The spark of originality, A. T. McPherson, The Chemist **37,** No. 7, 275 (1960).

A simple centering jig and goniometer for punching or drilling spheres for structural models, D. K. Smith, Am. Mineralogist **45,** No. 5–6, 273 (1960).

Propagation of electromagnetic pulses in a homogeneous conducting earth, J. R. Wait, Appl. Sci. Research **B8,** 213 (1960).

Shielded coaxial leads for low temperature electrical measurements, N. L. Brown and R. N. Barfield, Rev. Sci. Instr. **31,** No. 5, 517 (1960).

Rapid impact loading of textile yarns, J. C. Smith, Book, High Speed Testing, Vol. 1, p. 67 (Interscience Pub. Inc., New York, N.Y., 1960).

The absolute zenith intensity of [OI] 5577 at College, Alaska, F. E. Roach and M. H. Rees, J. Geophys. Research **65,** 1489 (1960).

Studies on sudden commencements of geomagnetic storms using IGY data from United States stations, S. Matsushita, J. Geophys. Research **65,** No. 5, 1423 (1960).

Photometric observations of the twilight glow [OI] 5577 and [OI] 6300, L. R. Megill, J. Atmospheric and Terrest. Phys. **17,** 276 (1960).

A study of local geomagnetic influence on the [OI] 5577 nightglow emission at Fritz Peak, J. W. McCaully, F. E. Roach, and S. Matsushita, J. Geophys. Research **65,** No. 5, 1499 (1960).

Local standards laboratories, A. T. McPherson, Handb. of Electrical Measurements, 1960 ed , p. 72 (1960).

A further note on "sweepers," J. M. Watts, J. Atmospheric and Terrest. Phys. **18,** 81 (1960).

The incidence equation $AA^{t}=aA$, K. Goldberg, Am. Math. Mo. **67,** 367 (1960).

Analysis of two-factor classifications with respect to life tests, M. Zelen, Book, Contributions to Probability and Statistics, Paper **42,** p. 508 (Stanford Univ. Press, Stanford, Calif., 1960).

Compressive properties of hard tooth tissues and some restorative materials, J. W. Stanford, K. V. Weigel, G. C. Paffenbarger, and W. T. Sweeney, J. Am. Dental Assoc. **60,** No. 6, 746 (1960).

OH emission in the earth's atmosphere, D. M. Gates and E. Jones, Proc. 2d Natl. Infrared Information Symp. **4,** 145 (1959).

Tropospheric fields and their long-term variability as reported by TASO, P. L. Rice, Proc. IRE **48,** 1021 (1960).

On the power of some rank-order two-sample tests, J. R. Rosenblatt, Book, Contributions to Probability and Statistics," Paper **32,** 358 (Stanford Univ. Press, Stanford, Calif., 1960).

Disc distribution of flares associated with certain radio bursts, C. Warwick, Proc. Symp. Physical Processes in the Sun-Earth Environment, July 20–21, 1959 (Ottawa, Defence Research Telecommunications Establishment), DRTE Pub. No. 1025, 249 (1960).

Effect of tensile properties of reinforcement on the flexural characteristics of beams, R. G. Mathey and D. Watstein, J. Am. Concrete Inst. **31,** No. 12, 1253 (1960).

The intensity of [OI] 5577 in the subauroral region as a function of magnetic activity, F. E. Roach, J. Geophys. Research **65,** No. 5, 1495 (1960).

Valences of the elements in analytical procedures, J. I. Hoffman, Chem. Anal. **49,** No. 1, 30 (1960).

A comparative study of absolute zenith intensities of [OI] 5577, F. E. Roach, J. W. McCaulley, E. Marovich, and C. M. Purdy, J. Geophys. Research **65,** No. 5, 1503 (1960).

Publications for which a price is indicated (except for NBS Technical Notes) are available only from the Superintendent of Documents, U.S. Government Printing Office, Washington 25, D.C. (foreign postage, one-fourth additional). Technical Notes are available only from the Office of Technical Services, U.S. Department of Commerce, Washington 25, D.C. (order by PB number). Reprints from outside journals and the NBS Journal of Research may often be obtained directly from the authors.

INDEX TO VOLUME 64A

January to December 1960

A

Page

Absorption bands for the calibration of spectrometers from 2 to 16 microns, vibration-rotation structure 29
Absorption spectra of some aldopyranosides, conformations of the pyranoid sugars 239
Acid coulometer, silver-perchloric, determination of the value of the faraday 381
Acid dissociation constant and related thermodynamic quantities for triethanolammonium ion in water from 0° to 50° C 343
Acid in the system ethanol-water at 25° C, dissociation constant of anistic (*p*-methoxybenzoic) 351
Aging, some effects of on the surface area of portland cement paste 163
Alditols-*1-t* and alditols-*2-t*. Tritium-labeled compounds VI 433
Aldopyranosides, acetylated, infrared absorption spectra. III. Conformations of the pyranoid sugars 405
Aldopyranosides, infrared absorption spectra of some aldopyranosides, conformations of the pyranoid sugars 239
Aldoses-*1-t* 177
Allen, G. F., R. G. Bates, Acid dissociation constant and related thermodynamic quantities for triethanolammonium ion in water from 0° to 50° C 343
Alumina, hot-pressed, and white sapphire, resistance of to collision with liquid drops 499
Aluminum, determination in precipitation hardening stainless steel and high temperature alloys 181
Aluminum in steel, separation and determination of small quantities 235
Aluminum, titanium, zirconium, and iron, method for the separation of from one another and for their subsequent determination 535
Amalgum, sodium, preparation of in the form of pellets 135
4-Aminopyridinium ion in water from 0° to 50° C, dissociation constant and related thermodynamic quantities 427
Anistic (*p*-methoxybenzoic) acid in the system ethanol-water at 25° C, dissociation constant 351
Armstrong, G. T., R. S. Jessup, Combustion calorimetry with fluorine: constant pressure flame calorimetry 49
Atomic iodine (I II), singly ionized, spectrum 443
Au III, the third spectrum of gold 481

B

Barium borate, vitreaous, radial distribution study 229
Bars, uniform, comparison of experimental and theoretical relations between Young's modulus and the flexural and longitudinal resonance frequencies 147
Bates, R. G., G. F. Allen, Acid dissociation constant and related thermodynamic quantities for triethanolammonium ion in water from 0° to 50° C 343
—*H. B. Hetzer*, Dissociation constant of 4-aminopyridinium ion in water from 0° to 50° C and related thermodynamic quantities 427
Behavior of isolated disturbances superimposed on laminar flow in a rectangular pipe 281
Bell, R. K., and B. B. Bendigo, Separation and determination of small quantities of aluminum in steel 235
Bendigo, B. B., R. K. Bell, Separation and determination of small quantities of aluminum in steel 235
Benzoic acid-7-C^{14} in toluene, for liquid scintillation counters, a carbon-14 beta-ray standard 143
Berman, H. A., E. T. Carlson, Some observations on the calcium aluminate carbonate hydrates 333
Beryllium chromite and other beryllia compounds with R_2O_3 oxides studies 103
Beta-ray standard, carbon-14, benzoic acid-7-C^{14} in toluene, for liquid scintillation counters 143
Bienenstock, A., A. S. Posner, S. Block, Radial distribution study of vitreous barium borate 229
Blaine, I. R., C. M. Hunt, L. A. Tomes, Some effects of aging on the surface area of portland cement paste 163
—, *E. K. Plyler, A. Danti, E. D. Tidwell*, Vibration-rotation structure in absorption bands for the calibration of spectrometers from 2 to 16 microns 29
—, —, *E. D. Tidwell*, Infrared absorption spectrum of methane from 2,470 to 3,200 cm^{-1} 201
Block, S., A. Bienenstock, A. S. Posner, Radial distribution study of vitreous barium borate 229
Borate, vitreous barium, radial distribution study 229
Bower, V. E., R. A. Robinson, M. M. Davis, M. Paabo, Ionization constants of four dinitrophenols in water at 25° C 347
—, *E. E. Sager*, Dissociation constant of anistic (*p*-methoxybenzoic) acid in the system ethanol-water at 25° C 351
Brickwedde, F. G., H. van Dijk, M. Durieux, J. R. Clement, J. K. Logan, The "1958 He^4 scale of temperatures" 1
Brown, D. W., R. E. Florin, L. A. Wall, Gamma irradiation of hexafluorobenzene 269
Burley, G., H. E. Kissinger, Systems silver iodide-sodium iodide and silver and iodide-potassium iodide 403

C

Calcium aluminate carbonate hydrates, some observations 333
Calibration of spectrometers from 2 to 16 microns, vibration-rotation sturcture in absorption bands 29
Calorimetry, combustion with fluorine: constant pressure flame calorimetry 49
Carbon and hydrogen, determination of copolymer composition by combustion analysis 157
Carbon-14 and tritium in films, with a proportional counter, radioassay. Tritium labeled compounds V 363
Carbon-14 beta-ray standard, benzoic acid-7-C^{14} in toluene, for liquid scintillation counters 143
Carlson, E. T., H. A. Berman, Some observations on the calcium aluminate carbonate hydrates 333
Cement paste, portland, some effects of aging on the surface area 163
Clabaugh, W. S., R. Gilchrist, T. J. Murphy, Method for the separation of titanium, zirconium, iron, and aluminum from one another and for their subsequent determination 535
—, *T. J. Murphy, R. Gilchrist*, Preparation of sulfur of high purity 355
Classification of conformers, I. Conformations of the pyranoid sugars 171
Clement, J. R., F. G. Brickwedde, H. van Dijk, M. Durieux, J. K. Logan, The "1958 He^4 scale of temperatures" 1
Coatings and interference filters, tolerances for layer thicknesses in dielectric multilayer 487
Collision with liquid drops and rigid steel spheres, pits in metals 61
Collisions between liquid drops and solids, note on particle velocity 497
Combustion analysis for carbon and hydrogen, determination of copolymer composition 157
Combustion calorimetery with fluorine: constant pressure flame calorimetry 49
Comparison of experimental and theoretical relations between Young's modulus and the flexural and longitudinal resonance frequencies of uniform bars 147
Composition, copolymer, determination by combustion analysis for carbon and hydrogen 157
Conductivity water, ultra low-, by electrophoretic ion exclusion 527
Conformations of the pyranoid sugars:
I. Classification of conformers 171
II. Infrared absorption spectra of some aldopyranosides 239
III. Infrared absorption spectra of some acetylated aldopyranosides 405
Constant of anistic (*p*-methoxybenzoic) acid in the system ethanol-water at 25° C 351
Constant of 2,4,6-trinitro-*m*-cresol in water at 25° C, spectrophotometric determination of ionization 533
Constants, elastic, of synthetic single crystal corundum at room temperature 213
Constants, ionization, of four dinitrophenols in water at 25° C 347
Copolymer composition by combustion analysis for carbon and hydrogen, determination 157
Corliss, C. H., W. C. Martin, The spectrum of singly ionized atomic iodine (I II) 443
Corundum, synthetic single crystal, elastic constants of at room temperature 213
Coulometer, silver-perchloric acid, determination of the value of the faraday 381
Craig, D. N., J. I. Hoffman, C. A. Law, W. J. Hamer, Determination of the value of the faraday with a silver-perchloric acid coulometer 381
—, *C. A. Law, W. J. Hamer*, Stability of silver and Pyrex in perchloric acid-silver perchlorate solutions and in conductivity water 127
Cresol (2,4,6-trinitro-*m*-), in water at 25° C, spectrophotometric determination of ionization constant 533
Crystal, single, elastic constants of synthetic corundum at room temperature 213
Crystals, polymer, formation of with folded chains in dilute solution, theory 73
Cuthill, J. R., W. D. Hayes, P. E. Seebold, Nitriding phenomena in titanium and the 6Al-4V titanium alloy 119

D

Danti, A., E. K. Plyler, L. R. Blaine, E. D. Tidwell, Vibration-rotation structure in absorption bands for the calibration of spectrometers from 2 to 16 microns 29
Davis, M. M., M. Paabo, Spectrophotometric determination of the ionization constant of 2,4,6-trinitro-*m*-cresol in water at 25° C 533
—, —, *R. A. Robinson*, Spectrophotometric determination of the ionization constant of dimethylpicric acid (2,4,6-trinitro-3,5-xylenol) in water at 25° C 531
—, —, —, *V. E. Bower*, Ionization constants of four dinitrophenols in water at 25° C 347
Decaborane, heat of formation 521
Determination of aluminum in precipitation hardening stainless steel and high temperature alloys 181
Determination of copolymer composition by combustion analysis for carbon and hydrogen 157
Determination of the value of the faraday with a silver-perchloric acid coulometer 381
Determination, spectrophotometric, of the ionization constant of dimethylpicric acid (2,4,6-trinitro-3,5-xylenol), in water at 25° C 531
Determination, spectrophotometric, of the ionization constant of 2,4,6-trinitro-*m*-cresol in water at 25° C 533
D-glucose-*6-t*, D-xylose-*5-t*, and D-mannitol-*1-t*, tritium-labeled compounds IV 359
Dielectric multilayer coatings and interference filters, tolerances for layer thicknesses 487
Dimethylpicric acid (2,4,6-trinitro-3,5-xylenol) in water at 25° C, spectrophotometric determination of the ionization constant 531
Dinitrophenols, four, ionization constants in water at 25° C 347
Disturbances superimposed on laminar flow in a rectangular pipe 281
Dissociation constant, acid and related thermodynamic quantities for triethanolammonium ion in water from 0° to 50° C 343
Dissociation constant of 4-aminopyridinium ion in water from 0° to 50° C and related thermodynamic quantities 427
Dissociation constant of anistic (*p*-methoxybenzoic) acid in the system ethanol-water at 25° C 351

Page

D-mannitol-*1-t*, D-glucose-*6-t*, and D-xylose-*5-t*, tritium-labeled compounds IV ... 359
Drops, liquid, and solids, note on particle velocity in collisions ... 497
Duecker, H. C., W. Haller, Ultra low-conductivity water by electrophoretic ion exclusion ... 527
Durieux, M., F. G. Brickwedde, H. van Dijk, J. R. Clement, J. K. Logan, The "1958 He^4 scale of temperatures" ... 1
D-xylose-*5-t*, D-mannitol-*1-t*, and D-glucose-*6-t*, tritium-labeled compounds IV ... 359

E

Effects of aging on the surface area of portland cement paste ... 163
Elastic constants of synthetic single crystal corundum at room temperature ... 213
Electrophoretic ion exclusion, ultra low-conductivity water ...
Energy levels and spectrum of neutral helium (He I) ... 19
Engel, O. G., Note on particle velocity in collisions between liquid drops and solids ... 497
—, Pits in metals caused by collision with liquid drops and rigid steel spheres ... 61
—, Resistance of white sapphire and hot-pressed alumina to collision with liquid drops ... 499
Ethanol-water at 25° C, dissociation constant of anistic (*p*-methoxybenzoic) acid in the system ... 351

F

Fabry-Perot interferometry, phase shift effects ... 191
Faraday, determination of the value with a silver-perchloric acid coulometer ... 381
Fatiadi, A. J., H. L. Frush, H. S. Isbell, Tritium-labeled compounds VI. Alditols-*1-t* and alditols-*2-t* ... 433
Fickle, D. P., J. J. Park, Uranium-platinum system ... 107
Filters, interference, and dielectric multilayer coatings, tolerances for layer thicknesses ... 487
First-order reaction, thermal degradation of polytetrafluoroethylene ... 513
Flame calorimetry, constant pressure: combustion calorimetry with fluorine ... 49
Florin, R. E., L. A. Wall, D. W. Brown, Gamma irradiation of hexafluorobenzene ... 269
Fluorine, combustion calorimetry: constant pressure flame calorimetry ... 49
Formation of decaborane, heat ... 521
Formation of polymer crystals with folded chains in dilute solution, theory ... 73
Formation of titanium trichloride, heat ... 515
Frush, H. L., H. S. Isbell, A. J. Fatiadi, Tritium-labeled compounds VI. Alditols-*1-t* and alditols-*2-t* ... 433
—, —, *N. B. Holt*, Note on the preparation of sodium amalgam in the form of pellets ... 135
—, —, —, Tritium-labeled compounds V. Radioassay of both carbon-14 and tritium in films, with a proportional counter ... 363
—, —, —, *J. D. Moyer*, Tritium-labeled compounds III. Aldoses-*1-t* ... 177
—, —, *J. D. Moyer*, Tritium-labeled compounds IV. D-glucose-*6-t*, D-xylose-*5-t*, and D-mannitol-*1-t* ... 359

G

Gamma irradiation of hexafluorobenzene ... 269
Gamma rays, photovoltaic effect produced in silicon solar cells ... 297
Gilchrist, R., T. J. Murphy, W. S. Clabaugh, Method for the separation of titanium, zirconium, iron, and aluminum from one another and for their subsequent determination ... 535
—, —, —, Preparation of sulfur of high purity ... 355
Gilliland, A. A., E. J. Prosen, W. H. Johnson, Heat of formation of titanium trichloride ... 515
Gold (Au III), the third spectrum ... 481

H

Hague, J. L., L. A. Machlan, E. J. Meros, Determination of aluminum in precipitation hardening stainless steel and high temperature alloys ... 181
Halbach, E. W., R. Stair, R. G. Johnston, Standard of spectral radiance for the region of 0.25 to 2.6 microns ... 291
Haller, W., H. C. Duecker, Ultra low-conductivity water by electrophoretic ion exclusion ... 527
Hamer, W. J., D. N. Craig, J. I. Hoffman, C. A. Law, Determination of the value of the faraday with a silver-perchloric acid coulometer ... 381
—, —, *C. A. Law*, Stability of silver and Pyrex in perchloric acid-silver perchlorate solutions in conductivity water ... 127
Hayes, W. D., J. R. Cuthill, R. E. Seebold, Nitriding phenomena in titanium and the 6Al-4V titanium alloy ... 119
"He^4 scale of temperatures, 1958" ... 1
He^4, vapor pressure of liquid, 1.0° to 5.2° K ... 1
Heat of formation of decaborane ... 521
Heat of formation of titanium trichloride ... 515
Helium (He I), energy levels and spectrum ... 19
Helim, vapor pressure of liquid, 1.0° to 5.2° K ... 1
Hetzer, H. B., R. G. Bates, Dissociation constant of 4-aminopyridinium ion in water from 0° to 50° C and related thermodynamic quantities ... 427
Hexafluorobenzene, gamma irradiation ... 269
High temperature alloys and stainless steels, determination of aluminum in precipitation hardening ... 181
Hoffman, J. D., J. I. Lauritzen, Jr., Theory of formation of polymer crystals with folded chains in dilute solution ... 73
Hoffman, J. I., C. A. Law, W. J. Hamer, D. N. Craig, Determination of the value of the faraday with a silver-perchloric acid coulometer ... 381
Holt, N. B., H. S. Isbell, H. L. Frush, Note on the preparation of sodium amalgam in the form of pellets ... 135
—, —, —, Tritium-labeled compounds V. Radioassay of both carbon-14 and tritium in films, with a proportional counter ... 363
—, —, —, *J. D. Moyer*, Tritium-labeled compounds III. Aldoses-*1-t* ... 177
Hunt, C. M., L. A. Tomes, P. L. Blaine, Some effects of aging on the surface area of portland cement paste ... 163
Hydrates, some observations on the calcium aluminate carbonate ... 333
Hydrobromic acid, infrared spectrum ... 377
Hydrogen and carbon, determination of copolymer composition by combustion analysis ... 157

I

Page

Iglesias, L., The third spectrum of gold (Au III) ... 481
Infrared absorption spectra of some aldopyranosides. II. Conformations of the pyranoid sugars ... 239
Infrared absorption spectra of some acetylated aldopyranosides. III. Conformations of the pyranoid sugars ... 405
Infrared absorption spectrum of methane from 2,470 to 3,200 cm^{-1} ... 201
Interferometry, Fabry-Perot, phase shift effects ... 191
Iodine (I II), spectrum of singly ionized atomic ... 443
Iodide-sodium iodide and silver iodide-potassium iodide, systems silver ... 403
Ionization constant of dimethylpicric acid (2,4,6-trinitro-3,5-xylenol), spectrophotometric determination in water at 25° C ... 531
Ionization constant of 2,4,6-trinitro-*m*-cresol in water at 25° C, spectrophotometric determination ... 533
Ionization constants of four dinitrophenols in water at 25° C ... 347
Iron, titanium, zirconium, and aluminum, method for the separation of from one another and for their subsequent determination ... 535
Isbell, H. S., H. L. Frush, A. J. Fatiadi, Tritium-labeled compounds VI. Alditols-*1-t* and alditols-*2-t* ... 433
—, —, *N. B. Holt*, Note on the preparation of sodium amalgam in the form of pellets ... 135
—, —, —, Tritium-labeled compounds V. Radioassay of both carbon-14 and tritium in films, with a proportional counter ... 363
—, —, —, *J. D. Moyer*, Tritium-labeled compounds III. Aldoses-*1-t* ... 177
—, —, *J. D. Moyer*, Tritium-labeled compounds IV. D-glucose-*6-t*, D-xylose-*5-t*, and D-mannitol-*1-t* ... 359
—, *R. S. Tipson*, Conformations of the pyranoid sugars:
I. Classification of conformers ... 171
II. Infrared absorption spectra of some aldopyranosides ... 239
III. Infrared absorption spectra of some acetylated aldopyranosides ... 405

J

Jessup, R. S., G. T. Armstrong, Combustion calorimetry with fluorine: constant pressure flame calorimetry ... 49
Johnson, W. H., A. A. Gilliland, E. J. Prosen, Heat of formation of titanium trichloride ... 515
—, *M. V. Kilday, E. J. Prosen*, Heat of formation of decarborane ... 521
Johnston, R. G., R. Stair, E. W. Halbach, Standard of spectral radiance for the region of 0.25 to 2.6 microns ... 291

K

Kilday, M. V., E. J. Prosen, W. H. Johnson, Heat of formation of decaborane ... 521
Kissinger, H. E., G. Rurlen, Systems silver iodide-sodium iodide and silver and iodide-potassium iodide ... 403
Koester, C. J., Phase shift effects in Fabry-Perot interferometry ... 191

L

Lam, D. C., Jr., J. B. Wachtman, Jr., W. E. Tefft, R. P. Stinchfield, Elastic constants of synthetic single crystal corundum at room temperature ... 213
Laminar flow in a rectangular pipe, behavior of isolated disturbances superimposed ... 281
Lauritzen, J. I., Jr., J. D. Hoffman, Theory of formation of polymer crystals with folded chains in dilute solution ... 73
Law, C. A., D. N. Craig, W. J. Hamer, Stability of silver and Pyrex in perchloric acid-silver perchlorate solutions and in conductivity water ... 127
—, —, —, *J. I. Hoffman*, Determination of the value of the faraday with a silver-perchloric acid coulometer ... 381
Liquid drops and rigid steel spheres, pits in metals caused by collision ... 61
Liquid drops and solids, note on particle velocity in collisions ... 497
Liquid drops, resistance of white sapphire and hot-pressed alumina to collision ... 499
Liquid scintillation counters, carbon-14 beta-ray standard, benzoic acid-7-C^{14} in toluene ... 143
Logan, J. K., F. G. Brickwedde, H. van Dijk, M. Durieux, J. R. Clement, The "1958 He^4 scale of temperatures" ... 1

M

Machlan, L. A., J. L. Hague, E. J. Meros, Determination of aluminum in precipitation hardening stainless steel and high temperature alloys ... 181
Madorsky, S. L., S. Straus, Note on the thermal degradation of polytetrafluoroethylene as a first-order reaction ... 513
Madorsky, I., L. A. Wood, P. A. Paulson, Determination of copolymer composition by combustion analysis for carbon and hydrogen ... 157
Marlow, W. F., P. W. Medlock, Carbon-14 beta-ray standard, benzoic acid-7-C^{14} in toluene, for liquid scintillation counters ... 143
Martin, W. C., Energy levels and spectrum of neutral helium (He I) ... 19
—, *C. H. Corliss*, The spectrum of singly ionized atomic iodine (I II) ... 443
Medlock, P. W., W. F. Marlow, Carbon-14 beta-ray standard, benzoic acid-7-C^{14} in toluene, for liquid scintillation counters ... 143
Meros, E. J., L. A. Machlan, J. L. Hague, Determination of aluminum in precipitation hardening stainless steel and high temperature alloys ... 181
Metals, pits in caused by collision with liquid drops and rigid steel spheres ... 61
Methane from 2,470 to 3,200 cm^{-1}, infrared absorption spectrum ... 201
Method for the separation of titanium, zirconium, iron, and aluminum from one another and for their subsequent determination ... 535
Methylpicric acid in water at 25° C, spectrophotometric determination of the ionization constant ... 533
Mielenz, K. D., Tolerances for layer thicknesses in dielectric multilayer coatings and interference filters ... 487
Moyer, J. D., H. S. Isbell, H. L. Frush, Tritium-labeled compounds IV. D-glucose-*6-t*, D-xylose-*5-t*, and D-mannitol-*1-t* ... 359
—, —, —, *N. B. Holt*, Tritium-labeled compounds III. Aldoses-*1-t* ... 177
Murphy, T. J., W. S. Clabaugh, R. Gilchrist, Method for the separation of titanium, zirconium, iron, and aluminum from one another and for their subsequent determination ... 535
—, —, —, Preparation of sulfur of high purity ... 355

N

Page

Nitriding phenomena in titanium and the 6Al-4V titanium alloy ... 119
Note on particle velocity in collisions between liquid drops and solids ... 497
Note on the preparation of sodium amalgam in the form of pellets ... 135
Note on the thermal degradation of polytetrafluorethylene as a first-order reaction ... 513

O

Oxides, rare-earth, phase equilibria in systems involving:
Part I. Polymorphism of the oxides of the trivalent rare-earth ions ... 309
Part II. Solid state reactions in trivalent rare-earth oxide systems ... 317
Oxides with R_2O_3, studies of beryllium chromite and other beryllia compounds ... 103

P

Paabo, M., M. M. Davis, Spectrophotometric determination of the ionization constant of 2,4,6-trinitro-*m*-cresol in water at 25° C ... 533
—, —, *R. A. Robinson,* Spectrophotometric determination of the ionization constant dimethylpicric acid (2,4,6-trinitro-3,5,xylenol) in water at 25° C ... 531
—, —, —, *V. E. Bower,* Ionization constants of four dinitrophenols in water at 25° C ... 347
Park, J. J., D. P. Fickle, Uranium-platinum system ... 107
Particle velocity in collisions between liquid drops and solids, note ... 497
Paulson, P. A., L. A. Wood, I. Madorsky, Determination of copolymer composition by combustion analysis for carbon and hydrogen ... 157
Pellets, preparation of sodium amalgam in the form ... 135
Perchloric acid-silver perchlorate solutions and conductivity water, stability of silver and Pyrex ... 127
Perfluoroheptane, gamma irradiation ... 269
Phase diagram, uranium-platinum system ... 107
Phase equilibria in systems involving the rare-earth oxides:
Part I. Polymorphism of the oxides of the trivalent rare-earth ions ... 309
Part II. Solid state reactions in trivalent rare-earth oxide systems ... 317
Phase shift effects in Fabry-Perot interferometry ... 191
Photovoltaic effect produced in silicon solar cells by X- and gamma rays ... 297
Pits in metals caused by collision with liquid drops and rigid steel spheres ... 61
Platinum-uranium system ... 107
Plyler, E. K., Infrared spectrum of hydrobromic acid ... 377
—, *A. Danti, L. R. Blaine, E. D. Tidwell,* Vibration-rotation structure in absorption bands for the calibration of spectrometers from 2 to 16 microns ... 29
—, *E. D. Tidwell, L. R. Blaine,* Infrared absorption spectrum of methane from 2,470 to 3,200 cm^{-1} ... 201
Polymer crystals with folded chains in dilute solution, theory of formation ... 73
Polymorphism of the oxides of the trivalent rare-earth ions. Part I. Phase equilibria in systems involving the rare-earth oxides ... 309
Polytetrafluoroethylene, thermal degradation as first-order reaction ... 513
Portland cement paste, some effects of aging on the surface area ... 163
Posner, A. S., A. Bienenstock, S. Plock, Radial distribution study of vitreous barium borate ... 229
Potassium iodide, systems silver iodide-sodium iodide and silver iodide ... 403
Preparation of sulfur of high purity ... 355
Prosen, E. J., W. H. Johnson, A. A. Gilliland, Heat of formation of titanium trichloride ... 515
—, —, *M. V. Kilday,* Heat of formation of decaborane ... 521
Pyranoid sugars, conformations of:
I. Classifications of conformers ... 171
II. Infrared absorption spectra of some aldopyranosides ... 239
III. Infrared absorption spectra of some acetylated aldopyranosides ... 405
Pyrex and silver, stability in perchloric acid-silver perchlorate solutions and in conductivity water ... 127

R

Radial distribution study of vitreous barium borate ... 229
Radioassay of both carbon-14 and tritium in films, with a proportional counter. Tritium-labeled compounds V ... 363
Rare-earth oxides, phase equilibria in systems involving:
Part I. Polymorphism of the oxides of the trivalent rare-earth ions ... 309
Part II. Solid state reactions in trivalent rare-earth oxide systems ... 317
Reichard, T. W., S. Spinner, W. E. Tefft, A comparison of experimental and theoretical relations between Young's modulus and the flexural and longitudinal resonance frequencies of uniform bars ... 147
Resistance of white sapphire and hot-pressed alumina to collision with liquid drops ... 499
Resonance frequencies, flexural and longitudinal, of uniform bars, comparison of experimental and theoretical relations between Young's modulus ... 147
Robinson, P. A., M. M. Davis, M. Paabo, V. E. Bower, Ionization constants of four dinitrophenols in water at 25° C ... 347
—, *M. Paabo, M. M. Davis,* Spectrophotometric determination of the ionization constant dimethylpicric acid (2,4,6-trinitro-3,5-xylenol) in water at 25° C ... 531
Roth, P. S., S. J. Schneider, Phase equilibria in systems involving the rare-earth oxides:
Part. I. Polymorphism of the oxides of the trivalent rare-earth ions ... 309
Part II. Solid state reactions in trivalent rare-earth oxide systems ... 317

S

Sager, E. E., V. E. Bower, Dissociation constant of anistic (*p*-methoxybenzoic) acid in the system ethanol-water at 25° C ... 351
Sapphire, resistance of white, and hot-pressed alumina to collision with liquid drops ... 499
Scharf, K., Photovoltaic effect produced in silicon solar cells by X- and gamma rays ... 297
Schneider, S. J., P. S. Roth, Phase equilibria in systems involving the rare-earth oxides:
Part I. Polymorphism of the oxides of the trivalent rare-earth ions ... 309
Part II. Solid state reactions in trivalent rare-earth oxide systems ... 317
Seebold, P. E., J. P. Cuthill, W. D. Hayes, Nitriding phenomena in titanium and the 6Al-4V titanium alloy ... 119

Page

Separation and determination of small quantities of aluminum in steel ... 235
Sherlin, G. C., Behavior of isolated disturbances superimposed on laminar flow in a rectangular pipe ... 281
Silicon solar cells, photovoltaic effect produced by X- and gamma rays ... 297
Silver and Pyrex, stability in perchloric acid-silver perchlorate solutions and in conductivity water ... 127
Silver iodide-sodium iodide and silver iodide-potassium iodide, systems ... 403
Silver-perchloric acid coulometer, determination of the value of the faraday ... 381
Sodium amalgam in the form of pellets, preparation ... 135
Sodium iodide and silver iodide-potassium iodide, systems silver iodide ... 403
Solids and liquid drops, note on particle velocity in collisions ... 497
Some observations on the calcium aluminate carbonate hydrates ... 333
Spectral radiance, standard for region of 0.25 to 2.6 microns ... 291
Spectrophotometric determination of the ionization constant of dimethylpicric acid (2, 4, 6-trinitro-3,5-xylenol) in water at 25° C ... 531
Spectrophotometric determination of the ionization constant of 2,4,6-trinitro-*m*-cresol in water at 25° C ... 533
Spectrum and energy levels of neutral helium (^{4}He I) ... 19
Spectrum, infrared, of hydrobromic acid ... 377
Spectrum of methane from 2,470 to 3,200 cm^{-1}, infrared absorption ... 201
Spectrum of singly ionized atomic iodine (I II) ... 443
Spectrum, third, of gold (Au III) ... 481
Spinner, S., T. W. Reichard, W. E. Tefft, A comparison of experimental and theoretical relations between Young's modulus and the flexural and longitudinal resonance frequencies of uniform bars ... 147
Stability of silver and Pyrex in perchloric acid-silver perchlorate solutions and in conductivity water ... 127
Stainless steel and high temperature alloys, determination of aluminum in precipitation hardening ... 181
Stair, R., R. G. Johnston, E. W. Halbach, Standard of spectral radiance for the region of 0.25 to 2.6 microns ... 291
Standard of spectral radiance for the region of 0.25 to 2.6 microns ... 291
Steel, separation and determination of small quantities of aluminum ... 235
Stinchfield, R. P., J. P. Wachtman, Jr., W. E. Tefft, D. G. Lam, Jr., Elastic constants of synthetic single crystal corundum at room temperature ... 213
Straus, S., S. L. Madorsky, Note on the thermal degradation of polytetrafluoroethylene as a first-order reaction ... 513
Studies of beryllium chromite and other beryllia compounds with R_2O_3 oxides ... 103
Sugars, pyranoid conformations:
I. Classification of conformers ... 171
II. Infrared absorption spectra of some aldopyranosides ... 239
III. Infrared absorption spectra of some acetylated aldopyranosides ... 405
Sugars, tritium-labeled ... 177
Sulfur, preparation of high purity ... 355
Surface area of portland cement paste, some effects of aging ... 163
Synthetic single crystal corundum, elastic constants of at room temperature ... 213
Systems silver iodide-sodium iodide and silver iodide-potassium iodide ... 403

T

Tefft, W. E., S. Spinner, T. W. Reichard, A comparison of experimental and theoretical relations between Young's modulus and the flexural and longitudinal resonance frequencies of uniform bars ... 147
—, *J. P. Wachtman, Jr., D. G. Lam, Jr., R. P. Stinchfield,* Elastic constants of synthetic single crystal corundum at room temperature ... 213
Temperatures, 1958 He^4 scale ... 1
The "1958 He^4 scale of temperatures" ... 1
Theory of formation of polymer crystals with folded chains in dilute solution ... 73
Thermal degradation of polytetrafluoroethylene as first-order reaction, note ... 513
Thermodynamic quantities and acid dissociation constant for triethanolammonium ion in water from 0° to 50° C ... 343
Thermodynamic quantities and related dissociation constant of 4-aminopyridinium ion in water from 0° to 50° C ... 427
Thermodynamics: vapor pressure of liquid He^4, 1.0° to 5.2° K ... 1
Third spectrum of gold (Au III) ... 481
Tidwell, E. D., E. K. Plyler, L. R. Blaine, Infrared absorption spectrum of methane from 2,470 to 3,200 cm^{-1} ... 201
—, —, *A. Danti, L. R. Blaine,* Vibration-rotation structure in absorption bands for the calibration of spectrometers from 2 to 16 microns ... 29
Tipson, R. S., H. S. Isbell, Conformations of the pyranoid sugars:
I. Classification of conformers ... 171
II. Infrared absorption spectra of some aldopyranosides ... 239
III. Infrared absorption spectra of some acetylated aldopyranosides ... 405
Titanium and the 6Al-4V titanium alloy, nitriding phenomena ... 119
Titanium trichloride, heat of formation ... 515
Titanium, zirconium, iron, and aluminum, method for the separation of from one another and for their subsequent determination ... 535
Tolerances for layer thicknesses in dielectric multilayer coatings and interferences filters ... 487
Tomes, L. A., C. M. Hunt, R. L. Blaine, Some effects of aging on the surface area of portland cement paste ... 163
Transition: behavior of isolated disturbances superimposed on laminar flow in a rectangular pipe ... 281
Trichloride, titanium, heat of formation ... 515
Triethanolammonium ion in water from 0° to 50° C, acid dissociation constant and related thermodynamic quantities ... 343
2,4,6-Trinitro-*m*-cresol in water at 25° C, spectrophotometric determination of the ionization constant ... 533
(2,4,6-Trinitro-3,5-xylenol) in water at 25° C, spectrophotometric determination of the ionization constant of dimethylpicric acid ... 531
Tritium-labeled compounds:
III. Aldoses-*1-t* ... 177
IV. D-glucose-*6-t*, D-xylose-*5-t*, and D-mannitol-*1-t* ... 359
V. Radioassay of both carbon-14 and tritium in films, with a proportional counter ... 363
VI. Alditols-*1-t* and alditols-*2-t* ... 433

U

Ultra low-conductivity water by electrophoretic ion exclusion ... 527
Uranium-platinum system ... 107
van Dijk, H., F. G. Brickwedde, M. Durieux, J. R. Clement, J. K. Logan, The "1958 He^4 scale of temperatures" ... 1

V

Page

Van Valkenburg, A., C. E. Weir, Studies of beryllium chromite and other beryllia compounds with R_2O_3 oxides 103
Vapor pressure of liquid He^4, 1.0° to 5.2° K 1
Velocity, particle, in collisions between liquid drops and solids, note 497
Vibration-rotation structure in absorption bands for the calibration of spectrometers from 2 to 16 microns 29

W

Wachtman, J. B., Jr., W. E. Tefft, D. G. Lam, Jr., R. P. Stinchfield, Elastic constants of synethetic single crystal corundum at room temperature 213
Wall, L. A., R. E. Florin, D. W. Brown, Gamma irradiation of hexafluorobenzene 269
Water, ultra low-conductivity, by electrophoretic ion exclusion 527
Weir, C. E., A. Van Valkenburg, Studies of beryllium chromite and other beryllia compounds with R_2O_3 oxides 103

Page

Wood, L. A., I. Madorsky, F. A. Paulson, Determination of copolymer composition by combustion analysis for carbon and hydrogen 157

X

X-ray, photovoltaic effect produced in silicon solar cells 297

Y

Young's modulus and the flexural and longitudinal resonance frequencies of uniform bars, comparison of experimental and theoretical relations 147

Z

Zirconium, iron, aluminum, and titanium, method for the separation of from one another and for their subsequent determination 535

UNITED STATES
GOVERNMENT PRINTING OFFICE
DIVISION OF PUBLIC DOCUMENTS
WASHINGTON 25, D.C.

OFFICIAL BUSINESS

PENALTY FOR PRIVATE USE TO AVOID PAYMENT OF POSTAGE, $300 (GPO)

JOURNAL OF RESEARCH of the National Bureau of Standards Vol. 64A, No. 6 November–December 1960
A. Physics and Chemistry

Contents

Page

The spectrum of singly ionized atomic iodine (I II). William C. Martin and Charles H. Corliss. 443

The third spectrum of gold (Au III). Laura Iglesias. 481

Tolerances for layer thicknesses in dielectric multilayer coatings and interference filters. Klaus D. Mielenz. 487

Note on particle velocity in collisions between liquid drops and solids. Olive G. Engel. 497

Resistance of white sapphire and hot-pressed alumina to collision with liquid drops. Olive G. Engel. 499

Note on the thermal degradation of polytetrafluoroethylene as a first-order reaction. S. L. Madorsky and S. Straus. 513

Heat of formation of titanium trichloride. Walter H. Johnson, Alexis A. Gilliland, and Edward J. Prosen. 515

Heat of formation of decaborane. Walter H. Johnson, Marthada V. Kilday, and Edward J. Prosen. 521

Ultra low-conductivity water by electrophoretic ion exclusion. Wolfgang Haller and H. C. Duecker. 527

Spectrophotometric determination of the ionization constant of dimethylpicric acid (2,4,6-trinitro-3,5-xylenol) in water at 25 °C. Marion Maclean Davis, Maya Paabo, and Robert A. Robinson. 531

Spectrophotometric determination of the ionization constant of 2,4,6-trinitro-*m*-cresol in water at 25 °C. Marion Maclean Davis and Maya Paabo. 533

Method for the separation of titanium, zirconium, iron, and aluminum from one another and for their subsequent determination. Thomas J. Murphy, W. Stanley Clabaugh, and Raleigh Gilchrist. 535

Publications of the National Bureau of Standards. 543

Index to volume 64A. 549

For sale by the Superintendent of Documents, U.S. Government Printing Office, Washington 25, D.C. Price 70 cents (single copy). Subscription price: $4.00 a year; $0.75 additional for foreign mailing.

UNITED STATES GOVERNMENT PRINTING OFFICE, WASHINGTON : 1960